

© 2023 by Amanda M. Bachmann. All rights reserved.

INVESTIGATION OF THE IMPACTS OF DEPLOYING REACTORS FUELED BY HIGH-ASSAY LOW  
ENRICHED URANIUM

BY

AMANDA M. BACHMANN

DISSERTATION

Submitted in partial fulfillment of the requirements  
for the degree of Doctor of Philosophy in Nuclear, Plasma, and Radiological Engineering  
in the Graduate College of the  
University of Illinois Urbana-Champaign, 2023

Urbana, Illinois

Doctoral Committee:

Dr. Madicken Munk, Chair  
Professor John R. Abelson  
Dr. Bo Feng, Argonne National Laboratory  
Associate Professor Tomasz Kozlowski  
Professor James F. Stubbins

# Abstract

The United States is considering the deployment of advanced reactors that require uranium enriched between 5-20%  $^{235}\text{U}$ , often referred to as High Assay Low Enriched Uranium (HALEU). At the present, there are no commercial facilities in the US to produce HALEU, prompting questions of how to create a dependable supply chain of HALEU to support these reactors. HALEU can be produced through two primary methods: downblending High Enriched Uranium (HEU) and enriching natural uranium. The amount of HEU available and impurities present in the HEU limit downblending capabilities. The Separative Work Unit (SWU) capacity and amount of natural uranium available limit enriching natural uranium capabilities. To understand the resources necessary to commercially produce HALEU with each of these methods, one can quantify the material requirements of transitioning to HALEU-fueled reactors.

In this dissertation, we model the transition from Light Water Reactors to different advanced reactors, considering once-through and closed fuel cycles to determine material requirements for supporting these fuel cycles. Material requirements of interest across this work include the mass of enriched uranium, mass of HALEU, feed uranium, SWU capacity, and the mass of used fuel sent for disposal. We use CYCLUS and publicly-available information about Light Water Reactors, the X-energy Xe-100, the Ultra Safe Nuclear Corporation Micro Modular Reactor, and the NuScale VOYGR to model potential transition scenarios and demonstrate the methodologies developed in this work. To more accurately model the closed fuel cycles, we develop a new CYCLUS archetype, called OpenMCyclus, that couples with OpenMC to dynamically model fuel depletion in a reactor and provide more accurate used fuel compositions. The results of this transition analysis show how the characteristics of the advanced reactors deployed drive the materials required to support the fuel cycle. Closing the fuel cycle reduces the materials required, but the reduction in materials is driven by the amount of material available for reprocessing.

To gain more insight into how transition parameters not considered in the transition analysis affect material requirements, we perform sensitivity analysis on one of the once-through transitions by coupling CYCLUS with Dakota. The results of the sensitivity analysis highlight some of the trade-offs between different reactor designs. One such tradeoff is the increased HALEU demand but decreased used fuel discharged when increasing the Xe-100 deployment and decreasing the VOYGR deployment. Additionally, these results identify the Xe-100 discharge

burnup as consistently being one of the most impactful input parameters for this transition, because of how the deployment scheme in this work affects the number of Xe-100s built no matter which advanced reactor build share is specified.

To identify potential transitions that minimize material requirements, we then use the CYCLUS-Dakota to optimize a once-through transition using the genetic algorithms in Dakota. In single-objective problems to minimize the SWU capacity required to produce HALEU and minimize the amount of used nuclear fuel, the algorithm finds solutions that are consistent with the results of the sensitivity analysis. The results cannot be taken at face value, because the algorithm did not fully converge and the genetic algorithms do not enforce the applied linear constraint for the advanced reactor build shares to sum to 100%. However, the results provide guidance on how to adjust the input parameters to optimize the transition for a minimal HALEU SWU or the used fuel mass. Parameter adjustments include maximizing the number of Light Water Reactors that receive license extensions to operate for 80 years. Similar results occur when using this method for a multi-objective problem to minimize both the HALEU SWU capacity and the used fuel mass.

Finally, we use neutronics models of the Xe-100 and Micro Modular Reactor reactor designs to evaluate the steady-state reactor physics performance of downblended HEU in these two designs. We compare the performance of the downblended HEU to nominally enriched fuel, based on the  $k_{eff}$ ,  $\beta_{eff}$ , energy- and spatially-dependent neutron fluxes, as well as the fuel, moderator, coolant, and total reactivity temperature feedback coefficients. The differences in the fuel compositions leads to differences in each of the metrics. However, these differences are within error of the results of the nominally enriched fuel, or would not prevent the reactor from meeting stated design specifications or operating in a safe state.

The work completed in this dissertation develops and demonstrates a methodology for modeling fuel cycle transitions and understanding the effects of deploying HALEU-fueled reactors in the US. The effects investigated in these example scenarios include various materials and resources required to support these reactors, and how the parameters of the transition affect these requirements. The information generated from this new methodology can be used to develop the necessary infrastructure and supply chains for support a transition to HALEU-fueled reactors. Furthermore, this work explores how the HALEU production method (enriching compared with downblending) affects reactor performance.

# Acknowledgments

This dissertation would not have been possible without the support of numerous people, as this dissertation embodies the phrase “it takes a village”. I would first like to thank my PhD advisor and committee chair, Dr. Madicken Munk. You helped me in many capacities, including technical mentorship, time management, and professional development opportunities to help prepare me for the next stages of my career. Without you, my PhD experience would not have been as enriching and rewarding. I would also like to thank my committee members: Prof. Jim Stubbins, Prof. Tomasz Kozlowski, Prof. John Abelson, and Dr. Bo Feng for their time and guidance on my dissertation.

In addition to those on my committee, I received substantial mentorship from many others. I am grateful to Dr. Scott Richards for his mentorship while I was at Argonne National Laboratory. Without him, I would have been in graduate school for twice as long. I am also grateful for the other members of the Reactors and Fuel Cycle Analysis (RFCA) group members, Drs. Kalin Kiesling, Tingzhou Fei, Yan Cao, Roger Blomquist, and Hansol Park, for their mentorship, support, and for being wonderful colleagues during my time at Argonne.

I am also grateful to the CYCLUS community, namely Prof. Paul P.H. Wilson, Dr. Baptiste Mouginot, and Jin Whan Bae, for their warm welcome to the CYCLUS community and their support in helping me learn about fuel cycle simulators. I would also like to thank the OpenMC community for their help and guidance in learning about OpenMC. Additionally, I am eternally grateful to Prof. Kathryn Huff, with whom I began my PhD journey. You helped me sculpt my dissertation and pushed me to learn new skills and explore new things. I would not be the researcher I am if I didn’t have your initial guidance.

I am incredibly thankful to all of the members of the Advanced Reactors and Fuel Cycles (ARFC) Research group for all of their guidance, support, and friendship – Gwendolyn Chee, Nathan Ryan, Sam Dotson, Sun Myung Park, Zoë Richter, Luke Seifert, Olek Yardas, Roberto Fairhurst-Agosta, Nataly Panczyk, Lu Kissinger, Nicholas Yeung, Ceser Zambrano, Nathan Glaser, and Elijah Capps. A special thank you to Nathan Ryan, Nataly Panczyk, Ceser Zambrano, and Nathan Glaser for their proof-reading of this document and the others I wrote during my time in ARFC. I would also like to acknowledge and thank all of the other UIUC NPRE students and communities that were part of my journey, as you all made grad school much more bearable, especially as we went through the COVID-19

pandemic. Furthermore, to my friends across the country that supported me through graduate school, I am forever grateful to you.

Finally, I would like to thank my family, Kyle Anderson, and Little R for the love and support each of you gave me throughout my journey.

This material is based upon work supported under an Integrated University Program Graduate Fellowship. Any opinions, findings, conclusions or recommendations expressed in this publication are those of the author(s) and do not necessarily reflect the views of the Department of Energy Office of Nuclear Energy. This work was also partially funded through a SURGE Fellowship from the Grainger College of Engineering at the University of Illinois Urbana-Champaign.

# Table of Contents

<b>List of Tables . . . . .</b>	<b>ix</b>
<b>List of Figures . . . . .</b>	<b>xi</b>
<b>Chapter 1 Introduction . . . . .</b>	<b>1</b>
1.1 Motivation . . . . .	1
1.2 Research Goals . . . . .	3
<b>Chapter 2 Background &amp; Literature Review . . . . .</b>	<b>6</b>
2.1 The nuclear fuel cycle . . . . .	6
2.1.1 Once-through fuel cycle . . . . .	8
2.1.2 Recycling fuel cycle . . . . .	8
2.2 Uranium enrichment . . . . .	11
2.3 Fuel cycle simulators . . . . .	13
2.3.1 CYCLUS . . . . .	14
2.3.2 Fuel depletion . . . . .	16
2.3.3 Verification and use of fuel cycle simulators . . . . .	19
2.4 Sensitivity analysis and optimization . . . . .	20
2.4.1 One-at-a-time Analysis . . . . .	21
2.4.2 Synergistic Analysis . . . . .	22
2.4.3 Global Sensitivity Analysis . . . . .	23
2.4.4 Optimization . . . . .	24
2.4.5 Dakota . . . . .	25
2.5 HALEU . . . . .	26
2.5.1 Production Methods . . . . .	26
2.5.2 Fuel forms . . . . .	27
2.5.3 Expected Demand . . . . .	28
2.5.4 HALEU in reactors . . . . .	29
<b>Chapter 3 Fuel cycle modeling methodology . . . . .</b>	<b>31</b>
3.1 Advanced reactor modeling . . . . .	32
3.2 Once-through fuel cycle scenarios . . . . .	34
3.3 Recycling fuel cycle scenarios . . . . .	37
3.3.1 Limited recycle scenarios . . . . .	38
3.3.2 Continuous recycle scenarios . . . . .	40
3.4 Calculation of results . . . . .	42
3.5 OpenMCyclus . . . . .	44
3.5.1 Fuel depletion and transmutation . . . . .	44
3.5.2 Material handling . . . . .	46
3.5.3 Comparison with CYCLOM Reactor . . . . .	47

<b>Chapter 4 Once-through transition results . . . . .</b>	<b>53</b>
4.1 Scenario 1: LWRs only . . . . .	53
4.2 Energy Generated . . . . .	58
4.2.1 No growth scenarios . . . . .	58
4.2.2 1% growth scenarios . . . . .	59
4.3 Reactor deployment . . . . .	60
4.3.1 No growth scenarios . . . . .	60
4.3.2 1% growth scenarios . . . . .	62
4.4 Uranium resources . . . . .	63
4.4.1 No growth scenarios . . . . .	64
4.4.2 1% growth scenarios . . . . .	69
4.5 SWU capacity . . . . .	72
4.5.1 No growth scenarios . . . . .	72
4.5.2 1% growth scenarios . . . . .	73
4.6 Used nuclear fuel . . . . .	74
4.6.1 No growth scenarios . . . . .	75
4.6.2 1% growth scenarios . . . . .	76
<b>Chapter 5 Recycling transition results . . . . .</b>	<b>79</b>
5.1 Uranium resources . . . . .	79
5.1.1 No growth scenarios . . . . .	80
5.1.2 1% growth scenarios . . . . .	85
5.2 SWU capacity . . . . .	90
5.2.1 No growth scenarios . . . . .	90
5.2.2 1% growth scenarios . . . . .	91
5.3 Separated actinide mass . . . . .	92
5.3.1 No growth scenarios . . . . .	92
5.3.2 1% growth scenarios . . . . .	94
5.4 Used nuclear fuel and high level waste . . . . .	95
5.4.1 No growth scenarios . . . . .	95
5.4.2 1% growth scenarios . . . . .	98
<b>Chapter 6 Sensitivity analysis . . . . .</b>	<b>101</b>
6.1 Methodology . . . . .	101
6.2 One-at-a-time . . . . .	103
6.2.1 Transition start time . . . . .	104
6.2.2 LWR lifetimes . . . . .	105
6.2.3 Xe-100 build share . . . . .	107
6.2.4 MMR build share . . . . .	108
6.2.5 VOYGR build share . . . . .	110
6.2.6 Xe-100 burnup . . . . .	111
6.2.7 MMR burnup . . . . .	111
6.2.8 Burnup variations with a common build share . . . . .	113
6.3 Synergistic . . . . .	114
6.3.1 LWR lifetime and VOYGR build share . . . . .	114
6.3.2 Xe-100 build share and Xe-100 burnup . . . . .	114
6.3.3 MMR build share and Xe-100 burnup . . . . .	116
6.3.4 Transition start and Xe-100 build share . . . . .	117
6.4 Global . . . . .	118
6.4.1 Xe-100 build share . . . . .	121
6.4.2 MMR build share . . . . .	125
6.4.3 VOYGR build share . . . . .	126

<b>Chapter 7 Optimization</b> . . . . .	<b>131</b>
7.1 Methodology . . . . .	131
7.1.1 Single-objective hyperparameter tuning . . . . .	133
7.1.2 Multi-objective hyperparamter tuning . . . . .	137
7.2 Single-objective optimization . . . . .	141
7.2.1 Minimize HALEU SWU . . . . .	142
7.2.2 Minimize waste mass . . . . .	143
7.3 Multi-objective optimization . . . . .	144
<b>Chapter 8 Effects of uranium impurities</b> . . . . .	<b>146</b>
8.1 Methodology . . . . .	146
8.1.1 Xe-100-like model . . . . .	146
8.1.2 MMR-like model . . . . .	148
8.1.3 Temperature variations and feedbacks . . . . .	149
8.1.4 Fuel compositions . . . . .	150
8.2 Results . . . . .	150
8.2.1 Xe-100 reactor metric comparisons . . . . .	152
8.2.2 MMR reactor . . . . .	160
<b>Chapter 9 Conclusions</b> . . . . .	<b>168</b>
9.1 Limitations and Future Work . . . . .	172
<b>References</b> . . . . .	<b>175</b>
<b>Appendix A: Synergistic sensitivity analysis</b> . . . . .	<b>185</b>

# List of Tables

2.1	Definitions for variables used to describe throughput and capacity for an enrichment facility. . . . .	12
2.2	Categories of uranium enrichment by weight fraction of uranium-235. . . . .	26
2.3	Fuel form required by select advanced reactors that will require HALEU. Reactor designs listed here are all of US origin, and information was obtained from [5] unless otherwise specified. . . . .	27
3.1	Design specifications of advanced reactors used in transition analysis. . . . .	32
3.2	Summary of the once-through fuel cycle transition scenarios. . . . .	35
3.3	Summary of the recycle fuel cycle transition scenarios. . . . .	37
3.4	Fast reactor design specification. . . . .	41
4.1	Summary of material needs for Scenario 1. Averages listed are for the duration that Light Water Reactors (LWRs) are deployed (1967-2055). . . . .	58
4.2	Maximum undersupply and oversupply of energy in Scenarios 2-7. . . . .	59
4.3	Maximum undersupply and oversupply of energy in Scenarios 8-13. . . . .	60
4.4	Maximum number of reactors deployed at one time in Scenarios 2-7. . . . .	61
4.5	Maximum number of reactors added to the simulation at a single time step in Scenarios 2-7. . . . .	62
4.6	Maximum number of advanced reactors deployed in Scenarios 8-13. . . . .	63
4.7	Maximum number of advanced reactors deployed in a single time step for Scenarios 8-13. . . . .	63
4.8	Metrics for enriched uranium sent to advanced reactors between 2025-2090 in Scenarios 2-7. . . . .	64
4.9	Cumulative HALEU needs by 2050 for Scenarios 2-7. . . . .	66
4.10	Metrics for feed uranium required by advanced reactors between 2025-2090 in Scenarios 2-7. . . . .	67
4.11	Metrics for enriched uranium required by advanced reactors between 2025-2090 in Scenarios 8-13. . . . .	70
4.12	Metrics for feed uranium required by advanced reactors between 2025-2090 in Scenarios 8-13. . . . .	71
4.13	Metrics for SWU capacity to enrich uranium for advanced reactors between 2025-2090 in Scenarios 2-7. . . . .	73
4.14	Metrics for SWU capacity to enrich uranium for advanced reactors between 2025-2090 in Scenarios 8-13. . . . .	74
4.15	Metrics for waste discharged from advanced reactors between 2025-2090 in Scenarios 2-7. The “Average HALEU” is the average mass of used nuclear fuel (UNF) from HALEU-fueled reactors. . . . .	75
4.16	Metrics for waste discharged from advanced reactors between 2025-2090 in Scenarios 8-13. The “Average HALEU” is the average mass of UNF from HALEU-fueled reactors. . . . .	77
5.1	Metrics for enriched uranium required to fuel reactors in Scenarios 14-16. . . . .	81
5.2	Metrics for plutonium-based fuels required to fuel reactors in Scenarios 14-16. . . . .	83
5.3	Metrics for feed uranium required to produce uranium-based fuels in Scenarios 14-16. . . . .	83
5.4	Metrics for natural uranium required to produce plutonium-based fuels in Scenarios 14-16. . . . .	85
5.5	Metrics of enriched uranium fuel between 2025-2090 in Scenarios 17-19. . . . .	86
5.6	Metrics of plutonium-based fuel between 2025-2090 in Scenarios 17-19. . . . .	87
5.7	Metrics of feed uranium to produce enriched uranium between 2025-2090 in Scenarios 17-19. . . . .	89
5.8	Metrics of natural uranium required to produce plutonium-based fuel between 2025-2090 in Scenarios 17-19. . . . .	89
5.9	Metrics for SWU capacity required to produce enriched uranium in Scenarios 14-16. . . . .	91
5.10	Metrics for SWU capacity required to produce enriched uranium in Scenarios 17-19. . . . .	92

5.11 Metrics of separated actinide masses of between 2020-2090 in Scenarios 14-16. . . . .	93
5.12 Mass of separated plutonium between 2020-2090 in Scenarios 17-19. . . . .	94
5.13 Mass of UNF disposed of between 2025-2090 in Scenarios 14-16. . . . .	96
5.14 Mass of HLW disposed of between 2025-2090 in Scenarios 14-16. . . . .	97
5.15 Mass of UNF disposed of between 2025-2090 in Scenarios 17-19. . . . .	99
5.16 Mass of HLW disposed of between 2025-2090 in Scenarios 17-19. . . . .	99
 6.1 Minimum, average, and maximum value of each metric caused by the variation of each parameter. . . . .	104
6.2 Ranges of the input parameters considered for generating surrogate models in the global sensitivity analysis. The Xe-100 burnup was constrained to 16 different values within the given range, while the other variables were free to vary within the defined range. . . . .	121
6.3 Sobol' indices for the Gaussian model when varying the Xe-100 build share. The first value is the main index, the second value is the total index. Highlighted values indicate a total Sobol' indices of above 0.5.123	
6.4 Sobol' indices for the quadratic model when varying the Xe-100 build share. The first number is the main index, the second is the total index. Highlighted values indicate a total Sobol' indices of above 0.5.124	
6.5 Sobol' indices for the Gaussian model when varying the MMR build share. The first number is the main index, the second is the total index. Highlighted values indicate a total Sobol' indices of above 0.5.126	
6.6 Sobol' indices for the quadratic model when varying the MMR build share. The first number is the main index, the second is the total index. Highlighted values indicate a total Sobol' indices of above 0.5.127	
6.7 Sobol' indices for the Gaussian model when varying the VOYGR build share. The first number is the main index, the second is the total index. Highlighted values indicate a total Sobol' indices of above 0.5.128	
6.8 Sobol' indices for the quadratic model when varying the VOYGR build share. The first number is the main index, the second is the total index. Highlighted values indicate a total Sobol' indices of above 0.5.130	
 7.1 Hyperparameters and values considered in tuning. If a range of values is provided, then the hyperparameter a random value in that range was selected. . . . .	134
7.2 Hyperparameter and model parameter values from the five best performing tuning cases for the single-objective problems. . . . .	137
7.3 Hyperparameters selected for single-objective optimization. . . . .	137
7.4 Values of each hyperparameter considered in the multi-objective hyperparameter tuning. . . . .	138
7.5 Hyperparameter values selected for multi-objective optimization problems based on tuning. . . . .	141
7.6 Values resulting in a minimum HALEU SWU capacity for a once-through transition scenario. . . . .	142
7.7 Values resulting in a minimum waste mass disposed of for a once-through transition scenario. . . . .	143
 8.1 Atom fraction of uranium isotopes in each HALEU composition. Uranium fractions are provided, without the oxygen and/or carbon fractions defined. Therefore, the totals in each column for a reactor model do not sum to one. . . . .	151
8.2 $k_{eff}$ values for the Xe-100-like reactor model for each fuel composition. . . . .	152
8.3 $\beta_{eff}$ value from using each fuel type. . . . .	153
8.4 Reactivity temperature feedback coefficients for each material type in the Xe-100-like model for each fuel type. . . . .	160
8.5 Reactivity temperature feedback coefficient maximum and minimum values reported by Mulder and Boyes for the Xe-100 between 100-900 °C [138]. . . . .	160
8.6 $k_{eff}$ in the Micro Modular Reactor (MMR)-like model at select burnup steps and different HALEU compositions. . . . .	160
8.7 $\beta_{eff}$ value in the MMR-like model at select burnup steps. . . . .	161
8.8 Reactivity feedback coefficients (pcm/K) for different materials at different burnup steps in the MMR-like reactor model. . . . .	167

# List of Figures

2.1	A complete view of options available for a once-through and a recycling nuclear fuel cycle. Reproduced from [31]. . . . .	7
2.2	Diagram of material flow through an enrichment facility cascade. The lines and arrows shown are the product stream from each unit, and the tails stream is not shown. Each box represents a single centrifuge, or unit. How the units comprise a stage, each vertical column, and the cascade, the entire configuration, are identified. Figure recreated from [40]. . . . .	13
3.1	Fuel cycle facilities and material flow between facilities in the once-through fuel cycles modeled. Facilities in blue are used in all once-through scenarios, the facilities in red are added in at the transition start time in the transition scenarios. . . . .	34
3.2	Example of how advanced reactors are deployed in Scenario 7 to meet a theoretical demand of 530 MWe. . . . .	36
3.3	Fuel cycle facilities and material flow between facilities for modeling the transition to advanced reactors with a limited recycle fuel cycle. Before 2025 a once-through fuel cycle is used with the facilities in blue. Facilities in red are deployed starting in 2025. In all limited recycling scenarios the spent UOX from the VOYGRs is sent from the red Cooling Pool to the Separations facility. In Scenarios 14 and 17 the spent UOX fuel from the Xe-100 and MMR are also sent from the red Cooling Pool to the Separations facility, but they are sent directly from the red Cooling Pool to the Repository and are not reprocessed in Scenarios 15 and 18. . . . .	38
3.4	Fuel cycle facilities and material flow between facilities for modeling the transition to advanced reactors with a continuous recycle fuel cycle. Before 2020 a once-through fuel cycle is used with the facilities in blue. The fast reactors are deployed starting in 2025, but the other facilities in red are deployed in 2020 to develop a supply of reprocessed fuel for the fast reactors. . . . .	41
3.5	Full and zoomed in OpenMC models of the PRISM reactor, based on information in [108, 109]. The gold material is the sodium coolant and the different colors of the fuel assemblies correspond to different batches of inner and outer fuel assemblies. . . . .	42
3.6	Material handling pathways between different material inventories in OpenMCyclus and the dynamic resource exchange (DRE) of CYCLUS. Depletion occurs to material in the core, just before it moves to the spent fuel inventory. . . . .	47
3.7	Fuel cycle facilities and material flow between facilities for the sample fuel cycle scenarios used to compare the results of the CYCMORE Reactor and OpenMCyclus DepleteReactor archetypes. . . . .	48
3.8	Comparison of power provided from reactor prototypes when comparing the CYCMORE Reactor and OpenMCyclus DepleteReactor archetypes. . . . .	49
3.9	Transactions of the fresh fuel commodities to the reactor facilities when defined with each archetype and setting. . . . .	50
3.10	Transactions of the used fuel commodities from the reactor facilities when defined with each archetype and setting. . . . .	51
3.11	Transactions of the separated plutonium from the separation facility to the fuel fabrication facility, based on the archetype to define the reactor facilities. . . . .	51
3.12	Transactions of the separated plutonium from the separation facility to the fuel fabrication facility, based on the archetype to define the reactor facilities. . . . .	52

4.1	Energy supplied by LWRs in Scenario 1 during each year of the simulation compared to the number of reactors deployed. . . . .	54
4.2	Mass of enriched uranium supplied to the LWRs in Scenario 1 at each time step. . . . .	55
4.3	Mass of natural uranium required to produce fuel for the LWRs at each time step in Scenario 1. . . . .	56
4.4	SWU capacity required to enrich the uranium sent to LWRs at each time step in Scenario 1. . . . .	57
4.5	Mass of used fuel discharged from the reactors in Scenario 1 as a function of time. . . . .	57
4.6	Annual energy produced compared to demand in Scenarios 2-7. . . . .	58
4.7	Annual energy produced compared to demand in Scenarios 8-13. . . . .	59
4.8	Number of advanced reactors deployed at each time step for Scenarios 2-7. The figures begin at 2025, because no advanced reactors are deployed before then. In the right figure Scenario 2 is removed to highlight the trends in the other scenarios. . . . .	61
4.9	Number of advanced reactors deployed at each time step for Scenarios 8-13. The figures begin at 2025, because no advanced reactors are deployed before then. In the right figure Scenario 8 is removed to help highlight the trends in the other scenarios. . . . .	62
4.10	Mass of enriched uranium required by reactors in Scenarios 2-7. . . . .	65
4.11	Mass of feed uranium required to produce enriched uranium in Scenarios 2-7. . . . .	68
4.12	Mass of enriched uranium required by reactors in Scenarios 8-13. . . . .	69
4.13	Mass of feed uranium required to produce enriched uranium at each time step in Scenarios 8-13. . .	71
4.14	SWU capacity required to produce enriched uranium for reactors in Scenarios 2-7. . . . .	72
4.15	SWU capacity required to produce enriched uranium for reactors in Scenarios 8-13. . . . .	74
4.16	Mass of fuel discharged from reactors as a function of time for Scenarios 2-7. . . . .	76
4.17	Mass of fuel discharged from reactors as a function of time for Scenarios 8-13. . . . .	77
5.1	Mass of enriched uranium required by reactors in Scenarios 14-16. . . . .	81
5.2	Mass of plutonium-based fuel required by reactors in Scenarios 14-16. . . . .	82
5.3	Mass of feed uranium required by reactors in Scenarios 14-16. . . . .	84
5.4	Mass of natural uranium for plutonium-based fuel required by reactors in Scenarios 14-16. . . . .	84
5.5	Mass of enriched uranium required by reactors in Scenarios 17-19. . . . .	86
5.6	Masses of heavy metal in plutonium-based fuel sent to advanced reactors in Scenarios 17-19. . . . .	87
5.7	Masses of feed uranium required by reactors in Scenarios 17-19. . . . .	88
5.8	Mass of natural uranium required by reactors in plutonium-based fuels in Scenarios 17-19. . . . .	89
5.9	SWU capacity required to support reactors in Scenarios 14-16. . . . .	90
5.10	SWU capacity required to support reactors in Scenarios 14-16. . . . .	91
5.11	Mass of separated actinides sent from the separations facility to fuel fabrication in Scenarios 14-16. .	93
5.12	Separated plutonium masses in Scenarios 17-19. . . . .	94
5.13	Separated plutonium masses in the limited recycle fuel cycles, Scenarios 14, 15, 17,18. . . . .	95
5.14	Used nuclear fuel disposed of in Scenarios 14-16. . . . .	96
5.15	Mass of high level waste (HLW) disposed of in Scenarios 14-16. . . . .	97
5.16	Used nuclear fuel disposed of in Scenarios 17-19. . . . .	98
5.17	HLW disposed of in Scenarios 17-19. . . . .	99
6.1	Demonstration of the adjusted advanced reactor deployment scheme to meet a demand of 530 MWe and a VOYGR build share of 50%. . . . .	102
6.2	Change in each metric as a function of transition start time, relative to a transition start in January 2025.105	105
6.3	Change in each metric as a function of percent of LWR fleet operating for 80 years, relative to 0%. . . . .	106
6.4	Change in each metric as a function of Xe-100 build share, relative to a build share of 0%. . . . .	107
6.5	Number of Xe-100s (top left), MMRs (top right), and VOYGRs (bottom left) as a function of Xe-100 build share. . . . .	108
6.6	Change in each metric as a function of MMR build share, relative to a build share of 0%. . . . .	109
6.7	Number of Xe-100s (top left), MMRs (top right), and VOYGRs (bottom left) deployed as a function of time and MMR build share. . . . .	109
6.8	Change in each metric as a function of VOYGR build share, relative to a build share of 0%. . . . .	110
6.9	Number of Xe-100s (top left), MMRs (top right), and VOYGRs (bottom left) deployed as a function of time and VOYGR build share. . . . .	111

6.10 Change in metrics from varying the burnup of fuel discharged from Xe-100, relative to a burnup of 168 MWd/kgU. . . . .	112
6.11 Change in metrics from varying the burnup of fuel discharged from the MMR, relative to a burnup of 82 MWd/kgU. . . . .	112
6.12 Relative changes in the metrics caused by changes in the discharge burnup of the HALEU-fueled advanced reactors, assuming a constant 20% build share for the Xe-100 and MMR. . . . .	113
6.13 Effect of the LWR lifetime and VOYGR build share on the HALEU mass. . . . .	115
6.14 Effect of the LWR lifetime and VOYGR build share on the total enriched uranium mass. . . . .	115
6.15 Effect of Xe-100 discharge burnup and Xe-100 build share on HALEU mass. . . . .	116
6.16 Effect of Xe-100 discharge burnup and Xe-100 build share on total fuel mass. . . . .	117
6.17 Effect of Xe-100 discharge burnup and MMR build share on total fuel mass. . . . .	118
6.18 Effect of transition start time and Xe-100 build share on total fuel mass. . . . .	119
6.19 Effect of transition start time and Xe-100 build share on total fuel mass. . . . .	120
6.20 Comparison of the input data and the results of the Gaussian surrogate model when varying the Xe-100 build share. . . . .	122
6.21 Comparison of the input data and the results of the quadratic surrogate model when varying the Xe-100 build share. . . . .	124
6.22 Comparison of the input data and the results of the Gaussian surrogate model when varying the MMR build share. . . . .	125
6.23 Comparison of the input data and the results of the quadratic surrogate model when varying the MMR build share. . . . .	127
6.24 Comparison of the input data and the results of the Gaussian surrogate model when varying the VOYGR build share. . . . .	128
6.25 Comparison of the input data and the results of the quadratic surrogate model when varying the VOYGR build share. . . . .	129
7.1 Results of coarse tuning for the single-objective optimization. The purple line in the bottom row (total build share at each hyperparameter) identifies a 100% total build share. . . . .	135
7.2 Results of fine tuning for the single-objective optimization. . . . .	136
7.3 Statistics of the hypervolumes resulting from each crossover rate value considered in the MOGA Tuning. . . . .	139
7.4 Statistics of the hypervolumes resulting from each population size considered in the MOGA Tuning. . . . .	140
7.5 Statistics of the hypervolumes resulting from each mutation rate considered in the MOGA Tuning. . . . .	141
7.6 Pareto front resulting from the multi-objective optimization of the once-through transition. . . . .	145
8.1 Xe-100-like core model made in Serpent. . . . .	147
8.2 Geometry of USNC MMR-like core model in Serpent. The light blue represents channels helium, dark blue are fuel channels with Fully Ceramic Microencapsulated (FCM) pellets, and the bright pink is graphite in the core. . . . .	149
8.3 238-group flux in the Xe-100-like reactor model in the active region of the core (top). The absolute difference from the flux from the pure HALEU fuel (bottom). The purple lines denote the delineation of the thermal and fast energy groups used in this work. . . . .	154
8.4 Thermal flux (below 0.625 eV) in the Xe-100-like Sangamon200 reactor model in the radial direction, across the x-axis (top). The absolute difference from the flux from the pure HALEU fuel with $1\sigma$ error shown by the shading (bottom). . . . .	155
8.5 Fast flux (above 0.625 eV) in the Xe-100-like Sangamon200 reactor model in the radial direction, across the x-axis (top). The absolute difference from the flux from the pure HALEU fuel with $1\sigma$ error shown by the shading (bottom). . . . .	156
8.6 Thermal flux (below 0.625 eV) in the Xe-100-like Sangamon200 reactor model in the axial direction (top). The absolute difference from the flux from the pure HALEU fuel with $1\sigma$ error shown by the shading (bottom). 0 cm is the midpoint of the core. . . . .	157
8.7 Thermal flux (below 0.625 eV) in the Xe-100-like Sangamon200 reactor model in the axial direction when the locations of the pebbles are shuffled when using the Y-12 fuel composition (top). The absolute difference from the flux from the pure HALEU fuel with $1\sigma$ error shown by the shading (bottom). . . . .	158

8.8	Fast flux (above 0.625 eV) in the Xe-100-like Sangamon200 reactor model in the axial direction (top). The absolute difference from the flux from the pure HALEU fuel with $1\sigma$ error shown by the shading (bottom).	159
8.9	Top: Flux energy spectrum for each fuel composition at a burnup of 0 MWd/kgU in the active region of the core. The purple line shows the delineation between the fast and thermal neutron energy groups used in other results of this work. Bottom: Difference between the flux from the pure fuel and each of the impure fuels in each energy group. The purple line shows the delineation between the fast and thermal energy groups (0.625 eV).	162
8.10	Radial and axial flux for each energy group when using each fuel composition in the MMR-like model at the beginning of life. The thermal flux encompasses energies below 0.625 eV, and the fast flux encompasses energies above 0.625 eV.	163
8.11	Radial and axial flux for each energy group when using each fuel composition in the MMR-like model at middle of the operation cycle. The thermal flux encompasses energies below 0.625 eV, and the fast flux encompasses energies above 0.625 eV.	165
8.12	Radial and axial flux for each energy group when using each fuel composition in the MMR-like model at the end of life. The thermal flux encompasses energies below 0.625 eV, and the fast flux encompasses energies above 0.625 eV.	166
A.1	Change in metrics resulting from variations in the transition start time and LWR lifetimes.	186
A.1	(cont.) Change in metrics resulting from variations in the transition start time and LWR lifetimes.	187
A.2	Change in metrics resulting from variations in the transition start time and Xe-100 build share.	188
A.3	Change in metrics resulting from variations in the transition start time and MMR build share.	189
A.3	(cont.) Change in metrics resulting from variations in the transition start time and MMR build share.	190
A.4	Change in metrics resulting from variations in the transition start time and VOYGR build share.	190
A.4	(cont.) Change in metrics resulting from variations in the transition start time and VOYGR build share.	191
A.5	Change in metrics resulting from variations in the transition start time and Xe-100 burnup.	192
A.5	(cont.) Change in metrics resulting from variations in the transition start time and Xe-100 burnup.	193
A.6	Change in metrics resulting from variations in the transition start time and MMR burnup.	193
A.6	(cont.) Change in metrics resulting from variations in the transition start time and MMR burnup.	194
A.7	Change in metrics resulting from variations in the LWR lifetimes and Xe-100 build share.	196
A.7	(cont.) Change in metrics resulting from variations in the LWR lifetimes and Xe-100 build share.	197
A.8	Change in metrics resulting from variations in the LWR lifetimes and MMR build share.	197
A.8	(cont.) Change in metrics resulting from variations in the LWR lifetimes and MMR build share.	198
A.9	Change in metrics resulting from variations in the LWR lifetimes and VOYGR build share.	199
A.10	Change in metrics resulting from variations in the LWR lifetimes and the Xe-100 discharge burnup	200
A.10	(cont.) Change in metrics resulting from variations in the LWR lifetimes and the Xe-100 discharge burnup	201
A.11	Change in metrics resulting from variations in the LWR lifetimes and MMR discharge burnup.	201
A.11	(cont.) Change in metrics resulting from variations in the LWR lifetimes and MMR discharge burnup.	202
A.12	Change in metrics resulting from variations in the MMR build share and Xe-100 discharge burnup.	203
A.12	(cont.) Change in metrics resulting from variations in the MMR build share and Xe-100 discharge burnup.	204
A.13	Change in metrics resulting from variations in the MMR build share and MMR discharge burnup.	205
A.13	(cont.) Change in metrics resulting from variations in the MMR build share and MMR discharge burnup.	206
A.14	Change in metrics resulting from variations in the Xe-100 build share and Xe-100 discharge burnup.	207
A.15	Change in metrics resulting from variations in the Xe-100 build share and MMR discharge burnup	208
A.15	(cont.) Change in metrics resulting from variations in the Xe-100 build share and MMR discharge burnup	209
A.16	Change in metrics resulting from variations in the VOYGR build share and Xe-100 discharge burnup.	210
A.16	(cont.) Change in metrics resulting from variations in the VOYGR build share and Xe-100 discharge burnup.	211
A.17	Change in metrics resulting from variations in the VOYGR build share and MMR discharge burnup.	211

A.17 (cont.) Change in metrics resulting from variations in the VOYGR build share and MMR discharge burnup. . . . .	212
---	-----

# **Chapter 1**

## **Introduction**

### **1.1 Motivation**

In the US, the current fleet of nuclear reactors is comprised of two LWR designs: Pressurized Water Reactors (PWRs) and Boiling Water Reactors (BWRs). Both designs use uranium dioxide pellets as fuel, with the uranium enriched to no more than 5%  $^{235}\text{U}$ , and supply about 700-1000 MW of power. These types of reactors have commercially operated in the US since 1957. This fleet of reactors supplied about 19% of all energy and over 50% of all carbon-free energy in the US in 2021 [1], making nuclear energy the third largest producer of energy and the largest producer of carbon-free energy in the United States. Because of nuclear power's ability to produce large-scale carbon-free energy, it is expected to play a role in meeting carbon emission and climate change goals [2]. The LWRs currently deployed in the US have license expiration dates within the next 35 years, with the last license expiring in 2055 [3]. Therefore, if nuclear energy is to continue to produce energy in the US and assist in meeting carbon emission goals after 2050, we must extend current reactor licenses, build new reactors, or some combination of the two.

Multiple countries around the world are building new LWRs [4] and developing new reactor designs [5], often called advanced reactors, to replace or expand the current fleet of reactors. Advanced reactors cover a large swath of design space, with wider ranges in: energy output, fuel form, and cycle length. The variations in reactor designs allow advanced reactors to achieve higher fuel burnup, improved safety performance, and better economic competitiveness than the LWR fleet. In the US, the Department of Energy (DOE) established the Advanced Reactors Demonstration Program (ARDP) [6] to “speed the demonstration of advanced reactors” [6] by developing a cost-sharing program with private companies. The goal of ARDP is to leverage this cost-sharing program to build first-of-a-kind advanced reactors, which will assist in their licensing and understanding challenges and opportunities in the construction process. The reactors built through this program are planned to be operational by the late 2020’s.

One important question that has arisen from the ARDP is how to develop supply chains to support the nuclear fuel cycles of advanced reactors. One design parameter that is different from LWRs and almost every advanced reactor is the fuel form. LWRs use a ceramic uranium dioxide fuel, while advanced reactors typically use fuel forms such as Tristructural Isotropic (TRISO) fuel kernels with uranium oxycarbide, uranium dissolved in molten salts,

and metallic alloy fuels [5]. Additionally, many advanced reactor designs require High Assay Low Enriched Uranium (HALEU), which is uranium enriched between 5% and 20%  $^{235}\text{U}$ , compared with the 3-5%  $^{235}\text{U}$  that is used in LWR fuel. There is presently no commercial supply of HALEU in the US that can provide fuel for the ARDP projects or for a potential future fleet of advanced reactors. Recent international events limit the possibility of obtaining HALEU from abroad. Therefore, the DOE is investigating how to develop a supply chain and Nuclear Fuel Cycle (NFC) for uranium enriched to this increased level [7, 8].

There are two methods to produce HALEU: enrich natural uranium up to the required level or downblend High Enriched Uranium (HEU) to the required enrichment level. The current US nuclear commercial fuel cycle relies on enrichment of natural uranium to create fuel for LWRs, but does not have the capability to enrich natural uranium to produce HALEU [9]. HALEU production through enrichment is limited by the amount of available natural uranium and facility capacities, such as the material throughputs and Separative Work Unit (SWU) capacity. There are three potential sources of HEU that can be downblended to produce HALEU: the used Experimental Breeder Reactor II (EBR-II) fuel at Idaho National Laboratory (INL) [10], inventory at Savannah River Site (SRS) [7], and inventory at Y-12 National Security Complex [11]. The size of each stockpile limits the amount of HALEU produced through downblending, and the first two stockpiles are capable of producing no more than 20 MT of HALEU [7]. Additionally, two of the potential stockpiles of HEU to downblend contain impurities that potentially affect reactor performance [12, 13]. These impurities may limit the amount of downblended HEU that a reactor a reactor can use at once. Currently, there is only one facility in the US commercially licensed to downblend HEU, the BWXT Nuclear Fuel Services Inc. facility in Erwin, TN, which is expected to have the capacity to downblend 1-2 MT of HEU, producing up to 10 MT of HALEU each year [14]. Therefore, meeting HALEU demand through downblending may require the development and licensing of additional facilities to downblend HEU if the BWXT facility does not have enough capacity.

The production of fuels needed for deploying advanced reactors is expected to have numerous impacts on the NFC, stemming from the different materials and enrichment levels needed for advanced reactor fuels. To assist in understanding the impacts from deploying HALEU-fueled reactors, modeling the NFC can provide the material requirements of potential transition scenarios. The technology employed in the NFC often defines the fuel cycle type, and a transition in the nuclear fuel cycle occurs when introducing new fuel types or other fuel cycle technologies. Modeling a NFC, typically aided by a fuel cycle simulator, includes modeling the deployment and decommissioning of facilities in the NFC, such as mines or reactors, and modeling the materials traded between facilities. NFC simulators have been used to model a variety of NFC transitions [15, 16, 17] and quantify the resource requirements of NFCs transitions [18]. Therefore, using NFC simulators to model the transition from the US fleet of LWRs to potential fleets of advanced reactors can inform DOE, researchers, companies, and other key stakeholders

of potential HALEU needs for future advanced reactor deployment. Estimates on potential needs can then inform strategies to develop material supply chains to fuel advanced reactors.

When modeling the NFC to assist in answering questions about HALEU demand and other resources required to meet the demand, there is a large array of input parameters that must be considered, such as when to start a transition, the speed of the transition, and the advanced reactors to deploy. Many times, modelers make assumptions about transition parameters [15, 19] and others use energy projections to determine the parameters [8]. Both are valid methods to determine transition parameters, but only considering a select set of parameters may not capture all of the possible material demands of a transition. Therefore, fuel cycle modelers often perform sensitivity analysis on the transition to understand the potential range of material requirements and how their assumptions affect demand. Sensitivity analysis involves modeling a fuel cycle with small perturbations in various input parameters and analyzing the variance or spread of select output metrics. Sensitivity analysis has been used in multiple NFC analyses [20, 21, 22, 23] to identify the model parameter or parameters that have the greatest impact on specific model outputs or material requirements. Sensitivity analysis can also reveal underlying information about a system that is not necessarily intuitive, such as how much the modeling methodology affects the results. Understanding the material requirements of a NFC coupled with sensitivity analysis aids in understanding key model parameters and optimizing the NFC based on given criteria, such as minimizing the amount of HALEU required. Various optimization schemes have been applied to NFCs to optimize the fuel cycle based on minimizing certain criteria: fuel requirements [24], waste production [25], and combinations of these metrics in multi-objective problems [26]. By combining NFC transition analysis with sensitivity analysis and optimization, one obtains a deep understanding of potential HALEU demand, potential supply chain requirements, and how to alter reactor deployment to aid in developing the supply chain.

## 1.2 Research Goals

The goal of this work is to investigate the impacts of deploying reactors fueled by HALEU in the United States, including the impacts that the reactors have on the NFC and the impacts the NFC has on the reactors. The results of this work are intended to aid and guide policy makers and key stakeholders on how to best establish a fuel cycle to support the deployment of HALEU-fueled reactors. Within this primary goal, there are three specific objectives:

1. **Quantify potential material requirements for the transition from LWRs to advanced reactors in open and closed fuel cycles.** This objective aims at understanding how large-scale decisions in fuel cycle modeling (e.g., the reactors deployed and the type of fuel cycle) impact the material requirements. Material requirements considered for this objective include the mass of HALEU, the feed uranium and SWU capacity required to

produce enriched uranium for advanced reactors, and the amount of UNF that requires disposal.

2. **Understand the impacts of fuel cycle parameters on the material requirements and design optimized transition scenarios.** This objective aims at understanding the effects of small-scale decisions in fuel cycle modeling (e.g., reactor burnup and transition start time) on material requirements, and how this information can be used by decision makers to develop optimal fuel cycle transitions. Fuel cycle parameters of interest include the transition start time, the build share of different advanced reactors, and the discharge burnup of advanced reactors. Optimized transitions scenarios are scenarios in which one or multiple material requirements are minimized, which would make it simpler to establish the fuel cycle.
3. **Identify potential limitations in using downblended HEU on reactor performance.** This objective aims at understanding how this HALEU production method may affect reactor operation and limit the use of this method in supporting the transition to HALEU-fueled reactors. The performance of the reactor is based on reactor physics parameters. Potential limitations include the impact of residual uranium isotopes from the downblending process impacting reactor physics performance.

These goals will be met by completing the following steps:

1. **Model the transition from LWRs to advanced reactors.** Example transition scenarios to multiple fuel cycles with HALEU-fueled reactors will be modeled using the NFC simulator CYCLUS [27]. Multiple transitions will be modeled, with each one varying based on the type of advanced reactors deployed, energy demand, and fuel cycle option (open or closed). This step will quantify and compare the material requirements of each transition scenario to understand how the reactors deployed, energy demand, and fuel cycle options affect material requirements. This step also includes the development of OpenMCYclus, a coupling between CYCLUS and OpenMC, to provide dynamic modeling of fuel depletion within a fuel cycle model.
2. **Perform sensitivity analysis and optimize select transition scenarios.** Sensitivity analysis will be performed on one of the transition scenarios modeled by coupling CYCLUS with Dakota [28], a program for uncertainty quantification and sensitivity analysis. This step will identify the most impactful model parameters on the material requirements of the transition. These results will then be used to determine optimized transition scenarios to minimize specific material requirements, thereby demonstrating an effective application of this methodology.
3. **Neutronics analysis of HALEU created from impure HEU.** The neutronics of the HALEU-fueled reactors in the transition scenarios will be modeled to identify potential effects of using HALEU produced from downblended HEU with known impurities. This step will investigate potential limitations in using this HALEU

production method and how different HALEU production methods affect reactor operation and key safety parameters, such as neutron multiplication, delayed neutron fractions, and reactivity coefficients.

The subsequent chapters of this dissertation present the work done to complete each of these steps and accomplish each objective. Chapter 2 provides necessary background information and a literature review on the nuclear fuel cycle, nuclear fuel cycle modeling efforts, and the use of HALEU in reactors. Chapter 3 discusses the methodology for modeling the transition to advanced reactors in once-through and closed fuel cycles. This chapter includes descriptions of the scenarios modeled, information on the reactors included in the transitions, and the flow of material in each scenario. The scenarios modeled vary based on the advanced reactors deployed, the energy demand of the scenario, and the type of fuel cycle (open or closed). This chapter also includes discussion of the development of OpenMCYclus, a code that couples CYCLUS with OpenMC [29] to provide fuel depletion during a fuel cycle simulation.

Chapter 4 presents and discusses the results of the once-through fuel cycle transition scenarios. Chapter 5 presents and discusses the results of the closed fuel cycle transitions. For each of the transition scenarios modeled, we compared them based on the number of reactors deployed and material requirements, such as the total mass of enriched uranium, mass of HALEU, feed mass to enrich uranium, the SWU capacity required to enrich uranium, and the mass of UNF discharged from the reactors.

Chapter 6 provides results and analysis of the sensitivity analysis performed for select once-through and closed fuel cycle transition scenarios. Model parameters considered for the sensitivity analysis include the transition start time, the percent of LWRs that receive license extensions, the build share of each advanced reactor, and the discharge fuel burnup of the HALEU-fueled advanced reactors. The analysis considers each model parameters effect and their combined effects from varying multiple parameters on the same material requirements considered in Chapters 4 and 5.

Chapter 7 provides results and discussion of the optimization of select once-through and closed fuel cycle transitions. The fuel cycles are optimized for minimizing the SWU capacity required to produce HALEU, minimize the mass of UNF disposed, and both in a multi-objective problem. This portion of the work is done by coupling CYCLUS with Dakota, and the discussion includes analysis of the results and the performance of this methodology for optimizing NFCs.

Chapter 8 provides the methodology and results of evaluating the performance of downblended HEU in the HALEU-fueled advanced reactors. Metrics considered for the reactor performance include the  $k_{eff}$ ,  $\beta_{eff}$ , energy- and spatially-dependent neutron flux, and the fuel, coolant, moderator, and total reactivity temperature feedback coefficients. Finally, Chapter 9 concludes this dissertation by summarizing the main results of the work, identifying gaps in the work, and proposing future work to address the gaps and build upon this work.

# **Chapter 2**

## **Background & Literature Review**

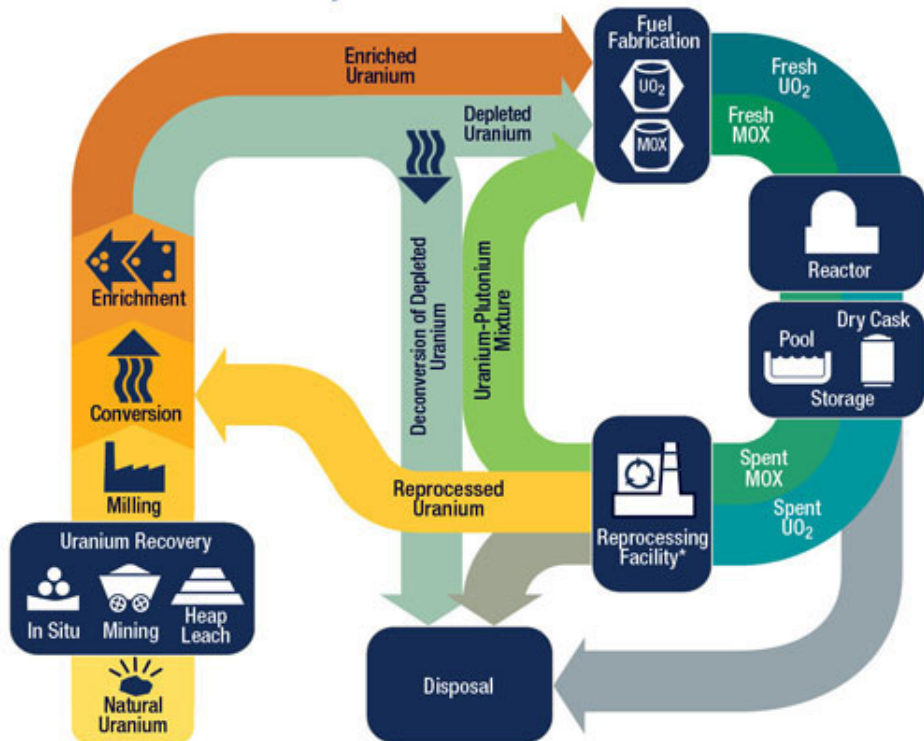
This chapter provides background information and a literature review of topics related to the work completed in this dissertation. The first section provides background information on the Nuclear Fuel Cycle (NFC), and the second section provides more information about the enrichment process. The third section provides a review of different fuel cycle simulators, with special attention paid to CYCLUS (the simulator used in this work), different depletion methods in fuel cycle simulators, and the verification and use of these tools. The fourth section provides background information on sensitivity analysis and optimization, with a focus on how others have applied these methods to the NFC. This section also provides information about Dakota, the tool this work uses to perform sensitivity analysis and optimization. Finally, the fifth section provides more information about HALEU, including production methods, different fuel forms required for advanced reactors, potential demands in HALEU from others' work, and analysis of HALEU performance in different reactor designs.

### **2.1 The nuclear fuel cycle**

The nuclear fuel cycle encompasses the activities and processes for the use of fissile materials in fission nuclear reactors [30]. Uranium, thorium, or plutonium can be used as fuel for a reactor, with this work and most reactor designs focusing on a uranium-based fuel cycle. The nuclear fuel cycle begins with the mining of uranium ores from the earth and ends with the final disposal of the radioactive waste produced [30]. A fuel cycle can vary based on the design of the reactor(s) deployed, such as if enrichment is required to produce the fuel. Figure 2.1 shows an example of the major steps in a nuclear fuel cycle.

The Nuclear Fuel Cycle (NFC) has two primary sections: the front-end and the back-end. The front end encompasses the steps before the fuel arrives at a reactor and the back-end encompasses the steps after the fuel is discharged from the reactor [32]. The front-end of the fuel cycle includes the mining, milling, conversion, and enrichment of uranium, as well as fuel fabrication. The mining step is the physical extraction of uranium ore from the earth's crust. Milling removes the non-uranium containing parts of the ore to purify the ore into yellow-cake uranium ( $\text{U}_3\text{O}_8$ ). The conversion step changes the chemical state of uranium compound for the next step in

## The Nuclear Fuel Cycle



\* Reprocessing of spent nuclear fuel, including mixed-oxide (MOX) fuel, is not practiced in the United States.  
Note: The NRC has no regulatory role in mining uranium.

As of January 2019



Figure 2.1: A complete view of options available for a once-through and a recycling nuclear fuel cycle. Reproduced from [31].

the fuel cycle. If enrichment is present, conversion changes the yellow-cake uranium to  $\text{UF}_6$ . If enrichment is not needed, then the uranium is converted to whatever chemical compound is needed for the fuel fabrication process. Enrichment modifies the relative abundance of different isotopes in the uranium, specifically to increase the abundance of  $^{235}\text{U}$  compared with  $^{238}\text{U}$ . Fuel fabrication then converts the (enriched) uranium to the chemical form required by the reactor(s) deployed. For LWRs, fuel fabrication converts the enriched uranium into a  $\text{UO}_2$  ceramic pellet. Other reactor designs may require that fuel fabrication produce a UCO TRISO pebble, a molten salt, or a metallic fuel.

The front-end of the NFC is often independent of the back-end, but the back-end of the NFC is highly dependent on the front-end and the reactor type because they govern the form and composition of the discharged spent nuclear fuel (SNF). The back-end of the NFC encompasses the processes and activities performed after fuel is discharged from a reactor. Steps commonly included in the back-end of the NFC include storage of UNF, reprocessing, and final disposal of UNF. The back-end of the fuel cycle can also vary, primarily based on if used fuel is reprocessed before final disposal. Whether or not reprocessing is included determines the name for the fuel cycle: a once-through fuel cycle if it does not include and a recycling, twice-through, or closed fuel cycle if it does [30].

### **2.1.1 Once-through fuel cycle**

A once-through fuel cycle is characterized by UNF disposal after discharge from a reactor, and a lack of the UNF undergoing any chemical processes or treatments before disposal [32]. The gray line from the storage to disposal in Figure 2.1 represents the back-end of a once-through fuel cycle. This fuel cycle does not include any of the material flows from the “Reprocessing Facility” in Figure 2.1. This is the fuel cycle option currently employed in the United States.

Once-through NFCs use interim storage and final disposal schemes such as *in situ* pools, dry cask storage, and geological repository [32]. UNF storage in an *in situ* storage pool can last between 3-10 years after reactor discharge [32] and provides active cooling. Dry cask storage can be located on-site or at a centralized location and provides passive cooling to the UNF after active cooling in a pool. Final disposal in a geologic repository, is the ultimate disposal of UNF and is needed in both a once-through and recycling fuel cycle. The US has currently identified Yucca Mountain as a geologic repository site, but the site is currently not operating.

### **2.1.2 Recycling fuel cycle**

A recycling fuel cycle is characterized by UNF undergoing chemical processes to separate out uranium, plutonium, and other actinides from the fuel for subsequent use in a reactor [32]. Reuse of UNF is possible because the metal in the fuel consists of 95-97% uranium and plutonium [32], which can fission and produce energy in a nuclear

reactor. The reuse of UNF in reactors is shown by the arrows from the “Reprocessing Facility” node in Figure 2.1. There are two types of recycling fuel cycle options: a limited recycle scheme and a continuous recycle scheme [33]. A limited recycling scheme involves fuel being reprocessed and burned in a reactor for a finite number of times before final disposal. This fuel cycle scheme is sometimes referred to as a “modified open cycle” because of the disposal of both UNF and HLW [34]. A continuous recycle scheme, sometimes referred to as a “full recycle” fuel cycle scheme, involves actinides from UNF being repeatedly reprocessed and burned in a reactor. Disposal in this fuel cycle only includes fission products and no UNF [34]. The difference in the number of times actinides and UNF are reprocessed in each recycling scheme leads to differences in the amount of new resources (uranium) that must be acquired and the amount of material sent for final disposal in a repository.

There are two primary methods to reprocess UNF: aqueous reprocessing and pyroprocessing. Aqueous reprocessing relies on redox reactions of select actinides (typically uranium and plutonium) to move the actinides from an aqueous phase to an organic phase, while the non-desired materials in the UNF remain in the aqueous phase [32]. There are a variety of methods to perform aqueous reprocessing, with each method removing different combinations of elements from the UNF, but the primary method is the PUREX process. The separated uranium and plutonium from aqueous reprocessing are then fabricated into mixed oxide (MOX) fuel for use in a thermal-spectrum reactor. MOX fuel can go through a limited number passes in a thermal reactor before disposal [32]. Pyroprocessing uses electric potentials to pull actinides (uranium and transuranics (TRUs)) onto a cathode from a molten salt bath, while the fission products remain in the molten salt bath or on the anode. The separated U/TRU material from pyroprocessing can then be fabricated into metallic fuel for use in a fast-spectrum reactor. The UNF from the fast reactor can be reprocessed multiple times and continuously put back into a reactor. Although this technique has a smaller separation factor than aqueous reprocessing, fast-spectrum reactors are less sensitive to impurities in the fuel and can readily use fuel fabricated after pyroprocessing [32]. Aqueous reprocessing is commercially available, and used in France, but pyroprocessing is not commercially available [32, 35]. The type of reprocessing is more dependent on the reactor designs used in the fuel cycle than the fuel cycle option. For example, pyroprocessing is more appropriate in fuel cycles that use metallic fuel, because the electrorefining step requires the UNF to be in a metallic form.

Reprocessing UNF improves resource utilization, compared with a once-through fuel cycle. One estimate reports that uranium ore requirements would decrease by 25% annually if UNF is reprocessed to create MOX fuel for LWRs [36]. Although this decrease in uranium ore requirements may improve the sustainability of the nuclear fuel cycle, current estimates of uranium reserves are expected to last for another 50-100 years [36]. Therefore, reducing natural uranium usage is only of concern if there is an increase in the price of uranium ore. Another known benefit of reprocessing is the reduction in the volume and radioactivity of waste sent to a final repository. Reprocessing can

reduce the waste volume by a factor of four [36], reducing the capacity of a repository required to store all the waste. The radioactivity of the disposed waste decreases to about 10% of the initial amount [32] when employing recycling. Recycling UNF reduces the concentration of actinides that are disposed of, which are the primary contributor to the long-term radioactivity of waste.

Despite these benefits, recycling has known disadvantages compared to a once-through fuel cycle. The amount of low level waste (LLW) generated greatly increases by using reprocessing [36]. The LLW generated from reprocessing includes any solvents or materials used for the process and must be disposed of in accordance with regulations, but not necessarily in a deep geologic repository. Pyroprocessing reduces the amount of LLW compared with a once-through fuel cycle more than aqueous reprocessing because the molten salt bath used in pyroprocessing can be cleaned and re-used. The LLW generated demonstrates how the reprocessing technology employed affects the performance of the fuel cycle. Another disadvantage of reprocessing is the increased proliferation risk. Aqueous reprocessing creates a material stream of pure plutonium [36], which introduces concerns of material diversion to create a nuclear weapon. This concern led to the development of new methods to reprocess UNF, such as the NUEX and COEX reprocessing methods, which do not create a plutonium material stream [36]. Pyroprocessing has a reduced proliferation risk compared with aqueous reprocessing because a plutonium material stream is never created. The extracted plutonium is always mixed with uranium and other TRU material [35]. Additionally, reprocessing UNF is expected to cost more than using a once-through fuel cycle [32, 36]. The estimated leveled cost of electricity (LCOE) are \$30-75/MWh for a once-through fuel cycle, with an average of about \$47/MWh, and \$35-81/MWh for a fuel cycle with reprocessing, with an average of about \$52/MWh [36]. The ranges in the LCOE come from differences in assumptions in determining the costs. Based on these estimates, there is no current economic incentive to reprocess and recycle UNF

Each reprocessing method has advantages and disadvantages. A comparison of fuel cycle options for the Republic of Korea showed that a fuel cycle with pyroprocessing and Sodium-Cooled Fast Reactors (SFRs) required less natural uranium than a once-through fuel cycle or a closed fuel cycle using aqueous reprocessing and PWRs to produce the same amount of energy [37]. Both methods of reprocessing reduced the amount of UNF for disposal, but using pyroprocessing with a fast reactor produced no UNF for disposal. The separated material from pyroprocessing that cannot be recycled in a reactor is assumed to be disposed of as LLW in the analysis. This assumption holds true, such that this waste stream is no longer UNF, but the material would likely be disposed of as HLW in the US. One disadvantage of reprocessing identified by Park et al. [37] is the increase in LLW produced when using aqueous reprocessing and thermal reactors. This result is consistent with the analysis by [36], which showed a decrease in LLW mass when using a fuel cycle with pyroprocessing and fast reactors, compared with a once-through fuel cycle [37].

## 2.2 Uranium enrichment

In the NFC, enrichment increases the relative abundance of  $^{235}\text{U}$  compared with  $^{238}\text{U}$  in the fuel, increasing the relative abundance of fissile material required for operating most reactor designs. There are multiple technologies and processes that can enrich uranium: gaseous diffusion, calutrons, gaseous centrifuges, and laser separation technologies. The US currently employs gaseous centrifuges to enrich uranium for commercial supplies. Gaseous centrifuges are currently used at the Urenco site in New Mexico [38] and planned for the Centrus facility in Piketon, Ohio [39]. Gaseous centrifuges are rotating canisters, relying on the speed of the rotation to move heavier materials to the outside of the canister. Because of this preferential movement, a greater concentration of the lighter material ( $^{235}\text{U}$ ) accumulates near the middle of the canister [40]. To ensure that only the mass difference in the uranium isotopes causes this preferential separation, the uranium is sequestered in  $\text{UF}_6$  gas, because fluorine only has one naturally occurring isotope and thus does not contribute to any mass differences between molecules of  $^{235}\text{UF}_6$  and  $^{238}\text{UF}_6$ .

Multiple quantities govern the capacity of an enrichment facility [30], defined in Table 2.1. The enrichment facility separates the feed material (typically natural uranium) into product and tails streams. The product stream is material at the desired enrichment level and the tails stream is material at enrichment levels lower than that of the feed material. Each of these material streams have a defined assay or weight fraction of  $^{235}\text{U}$ . The Separative Work Unit (SWU) capacity is the physical work required to put into the system to provide the separation needed to meet the product stream demand. It is also related to the amount of energy the facility requires [30]. Each of the quantities in Table 2.1 can be related using the following equations:

$$F = P + T \quad (2.1\text{a})$$

$$x_f F = x_p P + x_t T \quad (2.1\text{b})$$

$$SWU = [P * V(x_p) + T * V(x_t) - F * V(x_f)] * t \quad (2.1\text{c})$$

in which:

$$V(x_i) = (2x_i - 1) * \ln\left(\frac{x_i}{1 - x_i}\right) \quad (2.1\text{d})$$

The subequations comprising Eq. 2.1 show that as the desired enrichment level of the product feed increases, the feed mass must also increase, assuming everything else is held constant. The equations also show that as the desired product enrichment level increases, the amount of SWU capacity needed also increases. However, if

Table 2.1: Definitions for variables used to describe throughput and capacity for an enrichment facility.

Variable	Description	Units
F	Mass of feed material per unit time	kg
P	Mass of product material per unit time	kg
T	Mass of tails material per unit time	kg
$x_f$	weight fraction of $^{235}\text{U}$ in the feed stream	-
$x_p$	weight fraction of $^{235}\text{U}$ in the product stream	-
$x_t$	weight fraction of $^{235}\text{U}$ in the tails stream	-
SWU	the physical work required to separate the isotopes	kg-SWU
t	time step	d
V	Separation Potential	-
$x_i$	weight fraction of $^{235}\text{U}$ in the $i$ stream	-

the product mass decreases, then the required SWU capacity also decreases. Therefore, changes to the product enrichment level and mass throughput have similar effects on the amount of feed material and required SWU capacity. Opposing changes to both quantities (i.e., an increase in one and a decrease in the other) will not lead to a clear expectation for the change in feed material or the SWU capacity. The effect on these variables will depend on the magnitude of the changes.

The separation needed to enrich uranium cannot be performed in a single separation step because of the small separation efficiency of gas centrifuges. Therefore, centrifuges at a facility are placed into cascades, as shown in Figure 2.2. Each cascade is designed with multiple separation stages in series, with multiple centrifuge units in parallel comprising each stage [40]. Each stage outputs a product enriched to a certain amount (less than the final product of the cascade), then the product from one stage becomes the feed material for the next stage in the cascade to produce a greater enrichment level. The tails material from each stage is combined with feed material for the previous stage, to help strip out any  $^{235}\text{U}$  that is left in the tails. Figure 2.2 does not show the use of tails from each stage as feed for the previous step. Using the tails in the previous stage develops the cascade into a counter-current cascade [40] and helps to improve the efficiency of the entire cascade. Depending on the mass of product material needed, an enrichment facility may have multiple cascades, with each cascade housing multiple centrifuges. Changing the product stream assay (the  $^{235}\text{U}$  weight fraction) requires a change in the cascade configuration of a facility, even if the required SWU capacity is the same. Therefore, understanding the product stream assay, SWU capacity needed, and the amount of product needed aids in designing facilities to meet potential demand of HALEU.

The design parameters for a cascade are optimized based on the separation factor achieved in the centrifuges, the  $\text{UF}_6$  flow rate, and the material assays. The required product assay and the separation factor of each stage govern the number of stages required in a cascade [41]. Therefore, to achieve a higher product assay either more stages need to be added or each stage needs to achieve a greater separation factor. The product flow rate governs

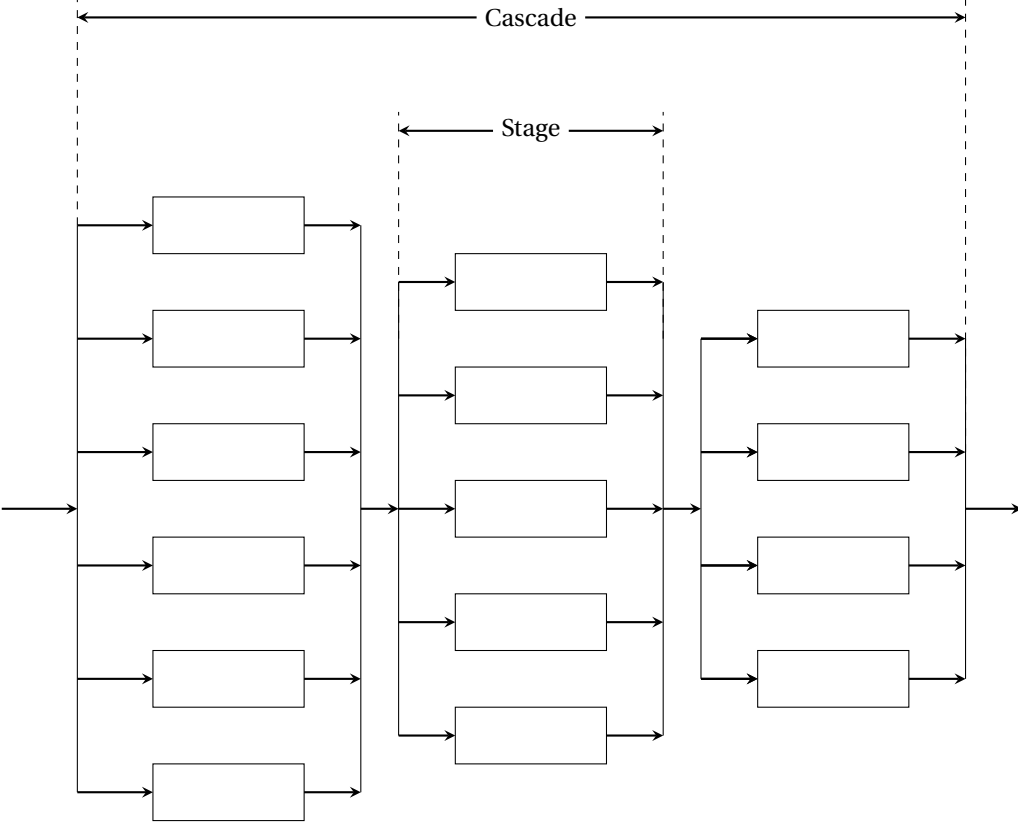


Figure 2.2: Diagram of material flow through an enrichment facility cascade. The lines and arrows shown are the product stream from each unit, and the tails stream is not shown. Each box represents a single centrifuge, or unit. How the units comprise a stage, each vertical column, and the cascade, the entire configuration, are identified. Figure recreated from [40].

the number of centrifuges in each stage [41]. As the flow rate increases, so do the number of centrifuges per stage.

## 2.3 Fuel cycle simulators

NFC simulators are computational tools to model the flow of materials and the commissioning and decommissioning of facilities for a fuel cycle. NFC simulators can evaluate the transition between fuel cycle options (e.g., from a once-through to a recycling fuel cycle), the performance of one fuel cycle with a growth in the demand of nuclear power, and the effect of perturbations on the material and facility requirements for a fuel cycle [17]. NFC simulators include multiple functionalities and capabilities: material flow tracking, facility deployment and retirement, timing, facility capacities, and external fissile material sources (e.g., mines) [42]. Each of the features listed here are considered “foundational capabilities” by Brown et al. [42]. Each of these features can then be expanded upon through “integral” or “exemplary” features to expand the foundational capabilities. Examples of integral features include strategic deployment of facilities to meet a specified material demand or material

prioritization. Examples of exemplary features include modeling radioactive decay of materials or calculations of fuel depletion in a reactor [42].

A variety of fuel cycle simulators have been developed, often to focus on specific areas of the NFC [43]. Some of the NFC simulators developed include Dynamic Model of Nuclear Development (DYMOND) [21, 44], the Verifiable Fuel Cycle Simulation Model (VISION) [45], ORION [46], COSI6 [47], and Nuclear Fuel Cycle Simulator (NFCsim) [48]. Another NFC simulator is CYCLUS, an open-source, agent-based NFC simulator [27]. The next section describes CYCLUS more in-depth because it is the simulator chosen for this work. DYMOND is a fuel cycle simulator developed by Argonne National Laboratory (ANL) initially for the Gen IV Fuel Cycle Crosscut Group. This simulator combines multiple modeling paradigms, including system dynamics, discrete events, and agent-based modeling [44, 21]. DYMOND accepts inputs of reactor and fuel characteristics, fuel cycle facility properties, the facilities that use each fuel type, and an energy demand to output the reactor fleet composition [44]. VISION was developed primarily to meet the program objectives of the Advanced Fuel Cycle Initiative (AFCI) and is based on DYMOND [45]. VISION was initially developed to be US-focused, but has been modified to be more generalized in its capabilities [44]. VISION dynamically models the mass flow of material through the entire fuel cycle and calculates metrics based on the AFCI program objectives. New functionalities added to VISION, compared with DYMOND, include estimating economic costs and modeling isotope decay. VISION has multiple modules to model the mass flow, calculate metrics, perform control, or integration. Both DYMOND and VISION model the fuel cycle at a fleet level, instead of a facility level [44]. The UK National Nuclear Laboratory developed ORION, which tracks up to 2500 nuclides as they move through a nuclear fuel cycle [46]. ORION models facilities as individual objects, it models the decay and irradiation of the tracked nuclides [44]. COSI6 was developed by Commissariat à l'Énergie Atomique et aux Énergies Alternatives (CEA) to study different evolutions of reactors and fuel cycles and provide technical information to decision makers [47]. COSI6 simulates a fuel cycle in a chronological order based on user-provided inputs, and does not provide any decision making. NFCsim was developed by Los Alamos National Laboratory (LANL) to address contemporary gaps in the ability of fuel cycle simulators to model transition scenarios or time-dependent information of sensitive material locations [48]. NFCsim applies an object-oriented philosophy to represent each element of a fuel cycle model. Objects are grouped into classes, with classes grouped together to form superclasses.

### 2.3.1 CYCLUS

CYCLUS is a dynamic, open source agent-based fuel cycle simulator. Built in C++, CYCLUS uses only open source and freely available libraries to provide full access to all users and developers. The CYCLUS architecture treats materials and facilities independently, similar to ORION, and allows for variable fidelity levels [27]. These attributes of CYCLUS allow for the software to model any fuel cycle scenario.

**CYCLUS** uses the notion of an *agent* to represent different components in the simulated fuel cycle. Agents are defined using the **CYCLUS** application programming interface (API), which allows users to develop their own suite of agent libraries and use them within **CYCLUS**. The API anticipates the structure on information about a given library required by the core **CYCLUS** kernel, facilitating information sharing between the library and the **CYCLUS** framework. This framework also allows for flexibility in licensing and distribution of the user-developed libraries. Libraries are loaded without changes to the **CYCLUS** kernel and without unwanted transfer of sensitive information, allowing agent library development with export controlled software while still allowing **CYCLUS** to be open-source.

The agent-based modeling paradigm employed by **CYCLUS** allows agent level modeling, as opposed to system level modeling. This paradigm allows different fuel cycle facilities, such as a reactor and a fuel fabrication plant, to be defined independently but still interact with each other in the simulation. There are three main groups of agents within the **CYCLUS** architecture: facilities, institutions, and regions. The agent types are related using a parent-child hierarchy: regions are parents of institutions, and institutions are parents of facilities. Facilities are the individual units in the fuel cycle that implement technologies, such as a fuel fabrication facility or a uranium mine. Institutions manage the facilities, similar to how a company manages facilities, and are responsible for the deployment of facilities. Regions provide geographic and political context for the institutions and regions and can be thought of as similar to individual nations.

The CYCMORE agent library provides a variety of libraries that can be dynamically loaded into **CYCLUS** for use in a simulation [27, 49]. These libraries include multiple facilities, two institutions, and one region as of CYCMORE 1.3 [27]. The two institutions (the DeployInst and ManagerInst) interact with the region (the GrowthRegion) to deploy facilities as needed to meet a commodity demand specified by the region. The DeployInst manually defines the number of each facility to be deployed at each time step. These facilities registered with the GrowthRegion for their contribution to the demand and are decommissioned at the end of their lifetime. The ManagerInst calculates the number of each facility type to deploy to meet the demand given by the GrowthRegion, based on what is not met through facilities deployed by other institutions in the region.

In **CYCLUS**, agents trade materials through the DRE [50, 27]. The DRE defines the supply-demand communication framework and treats facilities as black boxes so the solution strategy is agnostic to the resource types being exchanged. The DRE is a novel concept and unique to **CYCLUS**. It provides a flexible architecture to support supply-demand modeling and dynamic material flows between facilities [27]. There are three steps in the DRE: information gathering, resource exchanges, and trade execution [50]. During the information gathering phase facilities that need materials state their demand for a given material (e.g., a reactor stating a demand for fuel), referred to as requests. Requests from a facility can be more than what is actually required (e.g. a reactor requesting extra fuel assemblies just in case one breaks mid-cycle). Additionally, facilities can state mutual requests, or state

requests for materials in which either of the materials would meet the demand (e.g., a reactor requesting UOX and MOX fuel but only needing one to meet their request), with a preference defined for each material. Requests for materials can have constraints attached, such as quantity limits or if the request is *exclusive*. Exclusive requests mean that it must be met fully from a single response to the request (or bid), as opposed to being met through multiple small bids. Then facilities that produce materials also state the amount of a material they have to trade away (e.g., a fuel fabrication plant stating that they have 3 fuel assemblies), as the or bids. Using the information of the material requests and the bids, the DRE creates an exchange graph. The exchange graph is a bipartite network [50] with nodes for the requests and the responses to the requests.

Once the exchange graph is created, the requesting facilities can apply preferences to possible each potential bid based on the facility making the bid [27]. Preferences can be based on the agent making the bid, the bidding agent's institution, or the bidding agent's region. For example, a reactor agent can prefer to receive fuel assemblies from agent(s) that belong to a specific institution (mimicking but not fully enforcing contracts between companies), or agents in a specific region (mimicking international trade agreements). The addition of preferences of potential bids allows the DRE to more closely mimic supply chain dynamics within a fuel cycle. A solution is found to the exchange graph by matching requests with responses. A feature of CYCLUS is that it is possible for requests to be unmet if there is not enough material in the responses to fully meet the bid. To account for this capability, unconstrained false nodes are defined in the exchange graph to ensure a feasible solution is possible [51]. A solution to the exchange graph is found using a simulation-based heuristic or a mathematical program [50]. Mathematical models to solve the exchange graph include mixed-integer linear program (MILP) and linear program (LP), with MILP required to solve the exchange graph if any of the requests are denoted as exclusive [27]. Once a solution is found to the exchange graph, the materials are traded between the matched facilities in the trade execution phase. In the trade execution phase, the materials are traded between the facilities matched between the requests and bids.

Similar to many of the other fuel cycle simulators developed, material compositions in CYCLUS are defined using recipes. Recipes are typically defined as stagnant compositions at the beginning of a simulation. However, there are instances in which fuel compositions need to be dynamic during a simulation, such as when accounting for fuel depletion. The next section discussed how different fuel cycle simulators address fuel depletion.

### 2.3.2 Fuel depletion

Fuel depletion is an important component of fuel cycle simulations because the composition of used fuel affects the decay heat, amount of fissile material present, and the volume of the used fuel. Each of these fuel properties affects transportation of the UNF, repository storage limits, and how much material is available for reprocessing and recycling. Therefore, fuel cycle simulators must have a way to account for fuel depletion.

One possible way to account for fuel depletion is pre-define compositions of used fuel and update the composition of fuel materials when they are discharged from a reactor. This methodology is used in VISION [52], the CYCAMORE Reactor archetype CYCLUS [49], and is available through ORION [15]. To use this method the used fuel compositions must be known *a priori*, with used fuel compositions typically obtained by using another program to model depletion before modeling the fuel cycle. This method of accounting for fuel depletion provides a fast and simple way to model a fuel cycle. Although it has been used to model closed fuel cycles [53, 19], it is most appropriate for once through fuel cycles [15] because the same compositions for fresh fuel are loaded into a reactor at each refueling, which means that the used fuel compositions do not vary greatly between discharged batches.

Brown et al. consider dynamic modeling of fuel depletion, or modeling depletion during a fuel cycle simulation, to be an “exemplary” quality of a fuel cycle simulator [42], and is available in different simulators. Dynamic depletion modeling allows a fuel cycle simulator to more accurately model the effects of depletion on fuel compositions in a fuel cycle. Some of the fuel cycle simulators that have dynamic fuel depletion capabilities are ORION [44], DYMOND [54], and NFCSim [48]. ORION allows users to define material compositions using recipes or have the program model decay and depletion of the material [15]. ORION has some built-in reactor-specific cross sections for modeling depletion during a fuel cycle simulation, or users can generate and provide their own cross section data customized for the reactors and fuel cycle they are modeling. DYMOND models depletion through a coupling with ORIGEN2, a stand-alone depletion solver, using pre-generated reactor-specific depletion libraries [54]. The coupling of DYMOND with ORIGEN2 provides dynamic updates to used fuel compositions, but it also allows for the code to perform criticality searches to determine fresh fuel compositions based on the used fuel compositions available. This criticality search provides more accurate compositions of the fresh fuel produced than using a recipe to define the composition because it creates a feedback mechanism between the fresh and used fuel compositions [54]. However, the increased accuracy in fuel compositions in DYMOND comes at the cost of increased computational cost [54]. NFCSim is coupled with Los Alamos Criticality Engine (LACE), a criticality and burnup engine developed to couple with NFCSim to model the time-dependent nature of nuclear materials in a fuel cycle simulation [48]. By providing LACE with cross section libraries, it can find fluence-dependent burnups and production and destruction rates for actinides in the fuel materials. This information is then used to develop reactor-specific reactivity models based on the fluence as the independent variable. This coupling with LACE provides a cycle-dependent way to determine used fuel compositions upon discharge from the reactor or at a later time (e.g., after initial cooling or upon entrance to a separations facility).

The core kernel of CYCLUS does not provide a method to dynamically model depletion of fuel. However, the modular nature of CYCLUS means that developers can easily create archetypes that provide this functionality. One such archetype is Cyclus-Based ORiGen (CyBORG), which is a reactor-style archetype that couples CYCLUS with

ORIGEN [55]. CyBORG leverages the validated depletion capabilities in ORIGEN to model fuel depletion during a fuel cycle simulation [55]. User-defined parameters (such as fresh fuel compositions, irradiation time, and power level) are passed to CyBORG, which then produces a problem-specific cross section library. The library is then passed to ORIGEN to perform the depletion calculation. The depleted material compositions are then passed to CYCLUS to update the appropriate material compositions and recipes in a simulation. Use of this archetype requires users to have a license to use ORIGEN, as it is an export-controlled code, which can pose issues in a user being able to use this archetype.

A third-party archetype library developed to account for fuel depletion is Bright-lite [56]. The Bright-lite library contains three different archetypes: `ReactorFacility`, `FuelfabFacility`, `ReprocessingFacility`. This archetype library models depletion by determining fresh and used fuel compositions based on burnup, criticality, and transmutations matrix curves. Bright-lite has two operation modes: forward mode and blending mode [56]. In forward mode, Bright-lite reads in a defined fuel composition and depletes based on the neutron fluence through the material and a target (i.e.  $k_{eff} = 1$ ). In blending mode, Bright-lite connects the `ReactorFacility` and `FuelfabFacility` to mix multiple material streams to create a single stream that meets a specific target: burnup-criticality or burnup-conversion ratio. This archetype library can be used for modeling multiple reactor designs and multiple fuel forms, but requires different cross section libraries for each reactor and fuel type. Bright-lite comes with pre-defined libraries or a user may supply their own library that can be interpolated by Bright-lite. There is little published use of this archetype library in the current literature, suggesting that there are significant barriers to its use or that other archetypes are sufficient to meet the performance of this archetype library.

A third archetype to add dynamic depletion capabilities to CYCLUS is the `ann_pwr` archetype [57]. This archetype attempts to strike a balance between computational cost and depletion accuracy by predicting the used fuel composition based on fuel burnup and initial enrichment using trained neural networks. A similar depletion method was used with the Core Library for Advanced Scenario Simulation (CLASS) NFC simulator to predict core loading and cross section data for a PWR loaded with MOX fuel [58]. The neural networks for the `ann_pwr` archetype were trained on data in the Used Nuclear Fuel Storage, Transportation & Disposal Analysis Resource and Data System (UNFST&DARDS) Unified Database (UDB) [59]. Performance of this archetype is very promising, showing much faster compute times and reduced memory requirements than other depletion methods as well as greater agreement to the data in the UDB than using a standard recipe composition [57]. However, this archetype is very limited in applicability for many fuel cycles. The neural network was trained only on data from PWR assemblies, so a user cannot use this archetype to model depletion in other reactor types. Expansion of this archetype to include other reactor types would require developing separate neural networks for each reactor design, or the develop a new network that accounts for reactor type as an input parameter.

### **2.3.3 Verification and use of fuel cycle simulators**

Verification activities of NFC provides a comparison of the results from different simulators for a defined fuel cycle. These activities are important because each fuel cycle simulator uses a different methodology for defining materials and facilities. These activities also identify different modeler interpretations of the fuel cycle information, and how to translate that into a fuel cycle model. Multi-lab efforts validated some of the NFC simulators discussed here (DYMOND, VISION, ORION, and CYCLUS) using a no growth transition from LWRs to SFRs [44, 53]. Each LWR in the scenario provides 1000 MWe of electricity and each SFR provides 333.3 MWe of electricity. The scenario is simple enough that a spreadsheet could calculate the results, which served as an analytical solution. The results from each NFC simulator were compared to each other and to the spreadsheet solution. Any observed differences were either explained based on modeling implementation or resolved through changes to the necessary code.

The results of the verification efforts showed agreement between each of the codes and the spreadsheet results, but it also identified modeling differences. For example, VISION and DYMOND model continuous reprocessing at each time step, as opposed to the instantaneous reprocessing modeled by the spreadsheet [44]. This difference led to DYMOND reporting lower annual mass flow rates for the SFRs and a small delay in the idle UNF inventory modeled by VISION compared with the spreadsheet solution. Another difference identified is that the CYCAMORE Reactor archetype models each fuel assembly and batch as discrete material [53], as opposed to the other codes assuming continuous fuel discharge. This difference leads to oscillations in the UNF discharged when using CYCLUS, while the other codes results do not have these oscillations. However, this modeling decision in CYCLUS produced results that are closer to reality, because of the cyclic nature of fuel loading and discharge from reactors. Additionally, the CYCAMORE Reactor archetype depletes half of the core of fuel upon decommissioning, while the other NFC simulators deplete the entire core of fuel upon decommissioning. This difference affects the TRU material inventory, and the methodology was temporarily removed to demonstrate that the different methodologies led to the difference in results [53].

A common use of NFC simulators is to evaluate the performance of fuel cycles based on specific criteria. For example, work with DYMOND, Dynamic Analysis of Nuclear Energy System Strategies (DANESS), and NFCsim evaluated how different fuel cycle options could reduce UNF volume in a repository [60]. This work showed how the exclusion of TRUs from material sent to a repository significantly decreases the decay heat of material in the repository. NFC simulators have also evaluated the transition between fuel cycle options. Dynamic simulations of fuel cycle options for the AFCI Campaign in 2005 demonstrate the importance of the magnitude, timing, and rate of deploying facilities for meeting demands of the new fuel cycle option [61]. Furthermore, NFC simulators are used to model the transition between different fuel cycle options or technology. Quantifying the transition between fuel cycle options occurs by studying metrics such as the energy output and resource requirements of the transition [62].

Resource requirements can include the mass of natural uranium, enrichment needs, fuel irradiation, UNF, waste production, and cost.

The use of NFC simulators over the last decade has primarily been guided by the Nuclear Fuel Cycle Evaluation and Screening (E&S) from the U.S. Department of Energy, Office of Nuclear Energy (DOE-NE) [33]. This project categorized multiple fuel cycle options into 40 different Evaluation Groups (EGs) based on characteristics such as the recycling scheme, the type of fuel burned, and the type of reactor (e.g., thermal critical reactor, fast critical reactor). The EGs were compared on their performance at equilibrium on nine evaluation criterion, including nuclear waste management and resource utilization. The results of this project showed that the most benefit comes from fuel cycles that use continuous recycling of U/Pu with new or natural uranium in fast critical reactors (EG 23), continuous recycling of U/TRU with new or natural uranium in fast critical reactors (EG 24), continuous recycling of U/Pu with new or natural uranium in both fast and thermal critical reactors (EG 29), or continuous recycling of U/TRU with new or natural uranium in both fast and critical reactors (EG 30) [33].

Based on the results of the E&S, several efforts modeled the transition to these promising fuel cycle options using fuel cycle simulators [15, 19, 44, 53, 63]. Researchers used ORION to model the transition from a once-through fuel cycle option using enriched uranium in thermal critical reactors to a closed fuel cycle with U/Pu recycling in fast critical reactors (EG 01 to EG 23) [15]. This work demonstrated the importance of new LWRs and license extensions of existing reactors for this transition.

Djokic et al. used CYCLUS to model the transition from EG 01 to EG 23 assuming a 1% growth in power demand [19]. The results from CYCLUS were compared to the results from modeling the same transition scenario with DYMOND. The power generated, reactor entry time, and reactor exit time for the CYCLUS simulation qualitatively matches well with the results of the DYMOND simulation, but the power demand growth could match better to the target 1% by slightly modifying the SFR deployment [19]. Littell [63] also modeled the EG 01 to EG 23 transition in CYCLUS. This work included constraints such as restricting the mass of separated plutonium to less than 100 MT, not allowing reprocessing to begin until at least 2050, and allowing up to 5% surplus or deficit in the energy from compared with the demand. This work found that the separated plutonium constraint could be met, except when reprocessing first begins because of the accumulation of UNF before reprocessing begins [63].

## 2.4 Sensitivity analysis and optimization

Sensitivity analysis identifies and quantifies how each input parameter of a model affects output metrics [22]. Sensitivity analysis is useful in fuel cycle modeling because of the multiple sources of uncertainty in modeling the nuclear fuel cycle, such as facility design parameters, scenario assumptions, and reactor physics calculations [64].

To perform sensitivity analysis, one simulates a fuel cycle multiple times with small perturbations in model inputs between each simulation, with the output metrics observed for any changes caused by each perturbation. Output metrics are presented through three different indicators: the final value, the maximum value, or the cumulative sum [64]. Thiolliere et al. [22] demonstrated a methodology to perform sensitivity analysis, defining the specific input parameters to perturb and the range of values those parameters can take. They defined the range of values based on known technical capabilities, then sampled uniformly across the range of values to build the simulations. Feng et al. [21] used a similar methodology, using random sampling in the identified range of input variable values. Some common parameters varied during sensitivity analysis include the fuel burnup [22, 64], the LWR lifetime [21, 64], and the transition start time or introduction date of new reactor technology [20, 26, 64]. Common model outputs used in sensitivity analysis include natural uranium requirements [54, 64], plutonium inventory [20, 64], and SWU capacity required [54, 64].

There are multiple types of sensitivity analysis, and this work considers one-at-a-time (OAT), synergistic, and global sensitivity analysis. Each type of analysis differs based on the number of parameters varied at once. In OAT analysis, only one parameter is varied, in synergistic analysis, two parameters are varied at once, and in global sensitivity analysis more than two parameters are varied.

#### **2.4.1 One-at-a-time Analysis**

OAT analysis investigates the effects of varying a single input parameter and its effects on a single output metric, providing a relative impact of the input on the metric. There are multiple ways to report the results of OAT, such as a correlation coefficients or sensitivity value. Correlation coefficients are values between 0 and 1 that describes how linearly two variables are related. Closer to 1 indicates a very linear relationship and closer to 0 indicates not a strong linear relationship. Correlation coefficients provide information about linear relationships, but do not provide information about non-linear relationships. The sensitivity value is defined as:

$$q = \frac{p_{ref}(R_{ref} - R_s)}{R_{ref}(p_{ref} - p_s)} \quad (2.2)$$

in which

$p_{ref}$  = reference value for the input parameter

$p_s$  = value for the input parameter

$R_{ref}$  = value for the output metric when the input parameter is  $p_{ref}$

$R_s$  = value of the output metric when the input parameter is  $p_s$

and quantifies the percent change in the output per percent change in the input value [64]. Using this metric requires identifying a reference input parameter value ( $p_{ref}$ ) and the calculation of the output from the reference input value ( $R_{ref}$ ) for comparison. The sensitivity indicator quantifies the percent variation of an output metric based on a 1% change in the input parameter [64]. The sensitivity indicator assumes a linear relationship between the input parameter and the output metric [64], so it is not applicable to all OAT analysis.

OAT analysis has been applied to multiple fuel cycle scenarios and transitions. The Organisation for Economic Cooperation and Development (OECD) conducted OAT analysis for a transition scenario from PWRs to SFRs [64]. They examined the effects of 15 different input parameters (including the energy demand, first year of reprocessing fuel from PWRs, and the enrichment tails assays) on 22 different output metrics (including the cumulative mass of natural uranium required, the SWU capacity required, and the plutonium inventory at various fuel cycle facilities). Their analysis showed that the energy demand and the introduction date of SFRs had the most pronounced effect on many of the output metrics based on the sensitivity indicator. When using the sensitivity indicator, their analysis showed that the SFR introduction date, the energy demand, and the enrichment tails assay had the greatest impacts on the natural uranium consumption and the SWU requirements.

Chee [20] performed OAT analysis on the EG 01 to EG 30 transition (once-through fuel cycle with PWRs fleet transitioning to a closed fuel cycle with MOX fueled PWRs and SFRs). Chee considered the cooling time length for UNF, the fleet share of MOX PWRs to SFRs, and the transition start year as the model input parameters to vary and metrics related to the environmental impact, resource utilization, and how well the reactor deployment matches to the E&S [33] as the output metrics of the OAT analysis. The analysis showed that each of the input parameters primarily impact the proliferation risk output metrics, with some impact on the final mass of HLW.

## 2.4.2 Synergistic Analysis

Synergistic analysis is a multi-parameter approach that varies two different model inputs to investigate their combined impact on output metrics, which provides a more comprehensive view of the impact of the input parameters by evaluating the coupled effects of the parameters. This analysis is performed by sweeping over a range of values for each input parameter, then observing the response in each output metric for each combination. Through this process the input parameters resulting in the maximum or minimum value of the output metric can be found.

Chee [20] also performed synergistic analysis for the EG 01 to EG 30 transition. Their analysis showed how the reactor fleet share and the transition start year affect the maximum plutonium inventory at different facilities, such as how minimizing the MOX-fueled PWR fleet share minimizes the plutonium inventory in the cooling pools. Other work on synergistic sensitivity analysis for NFCs examined the effects of the introduction of both thermal

reprocessing and fast reactor technology for a given NFC on the number of reactors constructed, the LCOE, the mass of enrichment tails, and the SWU capacity [26]. By combining all four output metrics into a single output metric, this analysis showed how the later introduction dates for both thermal reprocessing and fast reactor technology minimizes the combined metric. The work by Passerini et al. [26] and Chee [20] not only describe the combined effect of two different model parameters on output metrics, but they also demonstrate how this analysis can be used for optimization of a NFC.

### 2.4.3 Global Sensitivity Analysis

Global sensitivity analysis varies multiple parameters at a time to investigate their individual and combined effects on the output metrics. Synergistic sensitivity analysis is a sub-set of global sensitivity analysis, in which specifically two input parameters are varied. Global sensitivity analysis can perform many functions such as identifying the input parameter(s) that have the most impact on an output metric and identifying input parameter(s) that have the least or negligible impact on output metrics [22]. One metric used in global sensitivity analysis is the Sobol' indices ( $S_i$ ), which represent the contribution of each input parameter on the variance of the output metric. The indices are broken down into multiple orders based on how many input parameter interactions are considered. For example, a first order index (referred to as a main effect sensitivity index by [28]) describes the portion of the variance in the output metric that the input parameter is solely responsible for. Mathematically the first order index is defined as [28]:

$$S_i = \frac{Var_{x_i}[E(Y|x_i)]}{Var(Y)} \quad (2.3)$$

in which

$Y$  is the output metric

$x_i$  is the input parameter

$Var_{x_i}[E(Y|x_i)]$  is the variance of the conditional expectation

$Var(Y)$  is the total variance of  $Y$

A total index defines the contribution of a single input parameter on the output metric, with all interactions with other inputs considered [28]. It is defined as [28]:

$$S_{TOT} = \frac{E(Var(Y|x_{-i}))}{Var(Y)} = \frac{Var(Y) - Var[E(Y|x_{-i})]}{Var(Y)} \quad (2.4)$$

in which

$$x_{-i} = (x_1, \dots, x_{i-1}, x_{i+1}, \dots, x_m)$$

The Sobol' indices are always less than 1 and will all sum to 1, based on variance decomposition theory. The higher the Sobol' index, the more impact the input variable has on the output metric [22].

Using first order and total Sobol' indices, Thiolliere et al. [22] identified the fraction of MOX fuel in a reactor and the burnup for uranium oxide (UOX) fuel as the most impactful model parameters on the plutonium production and inventory for a transition from PWRs fueled with UOX to PWRs fueled with MOX. Additionally, they identified cooling time of the UOX as contributing to the inventory of minor actinides (MAs), mostly from the americium production. Analysis performed by Richards and Feng [54] showed that the advanced reactor build share had the largest first order and total Sobol' index for the natural uranium consumption, normalized maximum reprocessing capacity required, and the mass of waste produced. The advanced reactor build share and the energy demand growth had similar first order Sobol' indices for the leveled cost of the transition, but the energy demand growth had the largest total Sobol' index for the leveled cost of the transition. These results mean that the advanced reactor build share and energy demand have similar magnitudes of their impact on the metric on their own. However, the energy demand combines with the other parameters to have an even greater impact on the metric.

#### 2.4.4 Optimization

Optimization is the search for a solution of a given problem to meet specific objectives. When applied to fuel cycles, optimization is the determination of which fuel cycle option or facility deployment schedule will meet desired goals. Common factors considered with optimization of a nuclear fuel cycle are natural resource utilization, economics, environmental impacts, and proliferation concerns [26, 33]. Optimizing a fuel cycle can be solved as a single-objective or multi-objective problem.

A variety of algorithms can be used to optimize a given fuel cycle. Linear programming tools have been used for optimization, but have intrinsic issues with solving non-linear problems, such as fuel cycles, as demonstrated by Passerini et al. [26]. Linear programming optimization tools will often find a local minimum, but not the global minimum, one of the limitations in using them to optimize a NFC. Another method explored to optimize fuel cycle options is genetic algorithms, which have been shown to find a global minimum when considering multiple objectives [26].

Examples of optimized fuel cycles with LWRs show that using a once-through fuel cycle minimizes cost, but reprocessing and recycling as much material as possible minimizes the amount of natural uranium required [65].

Both objectives may be desired at the same time, demonstrating how objectives can be met through contradictory actions if a multi-objective approach is taken. The optimization of a fuel cycle can be driven by a variety of parameters, such as prioritizing the type of reactor deployed or prioritizing the waste disposal aspect of the NFC. An example of the latter evaluated fuel cycle options based on radiotoxicity of the UNF and HLW in a repository [62]. These examples demonstrate that fuel cycle optimization is possible, and that there are many ways to define the optimization problem.

#### 2.4.5 Dakota

One tool for performing sensitivity analysis and optimization is Dakota [28]. Developed by Sandia National Laboratory (SNL), Dakota provides a systematic way for scientists and engineers to “obtain improved or optimal designs or understand sensitivity or uncertainty using simulation-based models” [28]. Dakota can easily be coupled with a variety of codes in a “black-box” manner so as to not supply Dakota with any of the other program’s source code. Dakota performs sensitivity analysis by sampling from a given range of values for an input parameter, feeding this value to the code it is coupled to, then reading the output of the code to determine the output metric (the response function) for that input value. Through this method, Dakota does not need any information about the code to which it is coupled. The sampling of the input parameter values can be performed with a variety of methods, including even grid spacing across multiple dimensions, specific intervals along a specific vector, or Latin Hypercube Sampling [28].

Dakota performs optimization through a variety of methods, including gradient-based, multi-objective optimization, and surrogate-based minimization [28]. The optimization problem can be solved by minimizing an objective function based on given constraints. The constraints can be upper and lower bounds for a value or nonlinear equality constraints with a given target value. The optimization methods in Dakota have been applied to a variety of engineering problems, including for the optimization of carbon fiber composites [66] and to compare different multi-objective optimization techniques [67].

Dakota has been coupled with fuel cycle simulators such as DYMOND [54] and CYCLUS [20] to perform sensitivity analysis, previously discussed in Sections 2.4.1 - 2.4.3. Chee [20] used Dakota to perform OAT, synergistic, and global sensitivity analysis on the transition from EG 01 to EG 30 with both CYCLUS and DYMOND. Chee used even multidimensional grid search sampling in Dakota to perform the OAT and synergistic analysis. Richards and Feng [54] coupled Dakota with DYMOND to perform global sensitivity analysis for a sample NFC to demonstrate this capability. This work utilized the Latin Hypercube Sampling method in Dakota to provide random sampling across the input parameter space. Random sampling is necessary for calculating Sobol’ indices because they are based on the variance in the output space.

## 2.5 HALEU

HALEU is uranium that is enriched between 5-20% by mass in  $^{235}\text{U}$ , and is considered a subset of Low Enriched Uranium (LEU). Fuel for LWRs is enriched to no more than 5%  $^{235}\text{U}$ , based on Nuclear Regulatory Commission (NRC) regulations [68]. Table 2.2 provides definitions of some of the main classifications of uranium enrichment.

Table 2.2: Categories of uranium enrichment by weight fraction of uranium-235.

Category	Weight fraction (%)
Depleted	<0.711
Natural	0.711
LEU	0.711-20
HALEU	5-20
HEU	$\geq 20$

### 2.5.1 Production Methods

There are two primary methods for producing HALEU. The first option is to enrich natural uranium up to the required level. There is only one facility in the US currently licensed to enrich uranium, the Urenco LES facility in Eunice, New Mexico [69]. This facility is only licensed to enrich uranium up to 5.5%  $^{235}\text{U}$  [69], which is less than many of the HALEU-fueled reactor designs require. Another enrichment facility is currently under development in Piketon, Ohio which is licensed to enrich uranium up to 20%  $^{235}\text{U}$  [69], however this is only designed to be a demonstration facility producing a total of 600 kg of HALEU [39]. There is the possibility of developing more facilities that could produce up to 12 MTU/year of HALEU [69]. There is the possibility of importing HALEU from other countries, but countries in Western Europe also lack facilities to produce HALEU and there is strategic importance in developing domestic infrastructure [69].

The other HALEU production option is to downblend HEU to the required HALEU level. The DOE is considering multiple sources of HEU to create HALEU [69]. The first is used fuel from EBR-II, which can produce a total of 10 MTU of HALEU at 19.75% enrichment [69]. The next source is the stored HEU solution at SRS from used research reactor fuel. Estimates of the amount of HALEU that can be produced from this stockpile vary from 4 MTU [69] to 20 MTU [7]. These sources of HALEU would certainly be beneficial to fueling reactors, but they are a very limited supply of HALEU that cannot be counted on for long-term support of HALEU reactors.

Before HEU can be downblended, it must first undergo a recovery step. The recovery step helps to purify the fuel before downblending. There are two methods to perform recovery: electrochemical processing or the ZIRCEX process [70]. The electrochemical processing method is better suited for used EBR-II fuel, because it is already in a metallic form, and is expected to produce about 5 MTU of 19.75% HALEU by 2023 [70]. The ZIRCEX process is a solvent extraction system, with an uncertain timeline for a full-scale facility [70]. The Fuel Conditioning Facility at

INL employs the electrochemical processing method to process and downblend HEU from used EBR-II fuel.

## 2.5.2 Fuel forms

The HALEU produced, using natural uranium or HEU, must be fabricated into the appropriate fuel form for the reactor. At present, advanced reactors being designed require HALEU in a variety of fuel forms, as shown in Table 2.3. This dissertation focuses on advanced reactors that require TRISO fuel, so more details about that fuel form are provided.

Table 2.3: Fuel form required by select advanced reactors that will require HALEU. Reactor designs listed here are all of US origin, and information was obtained from [5] unless otherwise specified.

Reactor Name	Company	Fuel form
SC-HTGR	Framatome	UCO TRISO compacts
Xe-100 [71]	X-energy	UCO TRISO pebbles
Mk 1 PB-FHR	UC Berkeley	UCO TRISO pebbles
EM <sup>2</sup>	General Atomics	UC pellet
eVinci	Westinghouse	UO <sub>2</sub> or UN
MMR [72]	Ultra Safe Nuclear Company (USNC)	UCO FCM compact
Natrium	Terrapower	Metallic
Superstar	ANL	U/Pu metallic fuel
Westinghouse Lead Fast Reactor	Westinghouse	UO <sub>2</sub> , potentially UN

TRISO fuel particles contain a small fuel kernel surrounded by four layers of material: a porous carbon buffer layer, and inner pyrolytic carbon layer, a silicon carbide layer, and an outer pyrolytic carbon layer [73]. The fuel kernel in the center contains the uranium fuel, typically in an oxide or oxycarbide form. The porous carbon buffer acts as an attenuator for any recoil fission products and accommodates pressure changes from gas accumulation. The pyrolytic carbon layers protect the silicon carbide layer from any chemical degradation, while the silicon carbide layer maintains the structural integrity of the particle from any stresses and is the primary barrier against fission product gas release. The actual dimensions of each layer depends on the exact manufacturing and design purpose, but the TRISO kernels are typically between 350-600  $\mu\text{m}$  in diameter [73]. TRISO particles have favorable performance at the high temperatures at which many advanced reactors operate [73].

Typically, TRISO kernels are combined into a pebble or cylindrical compact for placement in a graphite block, based on the design of the reactor [73]. Both the pebble and compact forms for TRISO fuel have previously been used in reactors; the High Temperature Engineering Test Reactor (HTTR) uses TRISO particles in cylindrical compacts embedded in a graphite block [74] and the AVR Reactor in Germany used TRISO pebbles as fuel [75]. TRISO particles can also be placed in a silicon-carbide matrix to form FCM fuel. This fuel form performs better in high-burnup applications because of improved stability under neutron irradiation and greater thermal conductivity [76]. The use of FCM fuel in LWRs to burn TRU material from waste has been investigated [76, 77] as an additional application of

this fuel form.

The variety of advanced reactor designs that require TRISO fuel drives a need to develop a TRISO fabrication facility. X-energy is currently developing such a facility to produce the TRISO fuel required by some of the advanced reactor designs [78]. X-energy expects the facility to be operational around 2025. The facility will produce 8 MTU/year, and will expand to 16 MTU/year by the early 2030s [78]. Additionally, INL is investigating how they can use their Materials and Fuels Complex for fabrication of metallic, ceramic, and intermetallic fuels with HALEU [79]. These projects are examples of development of a fuel fabrication facility to accompany the enrichment capabilities to produce HALEU fuel for reactors. However it is unclear if these planned capacities will be sufficient to meet the future demand of HALEU fuel. Modeling potential HALEU and TRISO needs can help in determining if these capacities are sufficient.

### **2.5.3 Expected Demand**

Multiple efforts have been made and are in progress to understand potential HALEU demand over different time frames. Nuclear Energy Institute (NEI) surveyed 10 advanced reactor companies to help understand the anticipated needs for HALEU from the reactor designers [80, 81, 82]. The most recent of these surveys [82] reports a need of up to 613 MTU/year by 2035 and a cumulative need of 2924.3 MTU by 2035. This expected demand is only for uranium enriched between 10-20%  $^{235}\text{U}$ , so the full demand for HALEU may be larger when uranium enriched between 5-10% is considered. Demonstration projects with a site selected (such as the ARDP projects) will need an estimated 20 MTU of HALEU between 2024-2027 [69], with a potential cumulative need for 78.7 MTU of HALEU by 2027 [82]. Refueling these projects will need an estimated 6 MTU/year of HALEU [69]. Based on the estimates of how much HALEU can be produced from available HEU stockpiles, the stockpiles would be used by 2024. Therefore, HALEU production will require enrichment capacities or additional HEU stockpiles to supply these reactors.

Models of reactor deployment to meet current net-zero carbon goals estimate that 520 MTU/year of HALEU will be needed by 2050 [8]. This work assumed that reactors requiring HALEU would be deployed alongside reactors that don't require HALEU, including the deployment of new LWRs and small modular reactors (SMRs). The cumulative need for HALEU by 2050 is about 5350 MTU according to this model, but this varies between 3450-7175 MTU based on the type of advanced reactor deployed. This expected demand is much less than the cumulative needs for LWRs between 2021-2050 (about 78,000 MTU) [8]. An important consideration in this work is that all HALEU is assumed to be at 19.75% enrichment, which is higher than what some advanced reactor designs need.

Demand for HALEU for the ARDP projects is expected to begin in 2024 and other reactor projects anticipate coming online in the mid-2020's [69]. Producing HALEU for these reactors develops the infrastructure to produce HALEU for potential future commercial fleets of HALEU-fueled reactors. HALEU enrichment must begin before

the reactor deployment date to provide enough time for the fuel fabrication process and proper transportation. First core loadings of fuel are needed by 2027 for the ARDP demonstration reactors [8], so the first HALEU must be enriched by 2024 to provide time for the fuel fabrication process [69].

#### 2.5.4 HALEU in reactors

Various studies in literature evaluate the performance of HALEU fuel in reactors. These studies considered the use of HALEU fuel in LWRs and SMRs, comparing the performance of the HALEU to uranium enriched to less than 5%  $^{235}\text{U}$ .

Burns et al. investigated the reactor and fuel cycle performance of an LWR fueled by an enrichment above 5% [83]. Their work showed that increasing the fuel enrichment up to 7% does not largely affect the fuel temperature or the moderator temperature coefficients, but it does decrease the soluble boron coefficient and increase the maximum burnup at the edges of the fuel pellets. The impacts on the fuel cycle include an increase in the amount of natural uranium required, a decrease in the amount of high-level waste disposed of per unit energy, and the radioactivity of the UNF and HLW reduces slightly, 100 years after discharge [83].

Carlsen et al. investigated the use of HALEU in the NuScale SMR design [84]. Increasing the fuel enrichment to 8.34% (compared with the current <5% design) doubled the fuel discharge burnup and the cycle time. Fission product poisons, specifically  $^{149}\text{Sm}$  and  $^{135}\text{Xe}$ , increased in concentration when using HALEU fuel compared with using the base design. This increase impacts the neutron poisons needed during operation and the radioactivity of the fuel after discharge. Using HALEU in the core also led to a reduction in the LCOE of the reactor for certain combinations of enrichment and cycle length [85, 84].

In addition to comparing HALEU to fuel with lower enrichment, previous studies investigated how the uranium isotopic composition affects the performance of the HALEU fuel. Analysis of fuel for the Massachusetts Institute of Technology (MIT) Reactor showed that manufactured fuel had a slightly higher  $^{235}\text{U}$  concentration (19.8% instead of 19.75%) and a slightly higher density than original models accounted for [86]. These changes in the fuel caused a greater  $^{235}\text{U}$  loading in the core, increasing the  $k_{eff}$  by 431 pcm [86]. The differences in modeled and manufactured fuel meant that the modelers had to account for more statistical uncertainty in the reactor performance, which can be computationally intensive. To alleviate potential computational costs, the modelers developed "high reactivity" and "low reactivity" fuel compositions based on uncertainty in the manufactured fuel compositions. This additional analysis of the extra fuel compositions was sufficient to show that the reactor could still meet safety margins with the fuel composition variations [86].

If HALEU fuel is produced by downblending HEU, it is possible the HALEU will contain impurities of minor uranium isotopes [69]. Bounding studies on the uranium isotopic composition of HALEU produced from used fuel

from EBR-II shows the presence of  $^{232}\text{U}$ ,  $^{233}\text{U}$ ,  $^{234}\text{U}$ , and  $^{236}\text{U}$  [12]. HALEU created from downblended HEU at the Y-12 Nuclear Security Complex also has  $^{232}\text{U}$ ,  $^{234}\text{U}$ , and  $^{236}\text{U}$  impurities [13].  $^{233}\text{U}$  is a fissile isotope and is expected to affect the neutron population inside a reactor.  $^{232}\text{U}$ ,  $^{234}\text{U}$ , and  $^{236}\text{U}$  are parasitic neutron absorbers, so their presence is also expected to affect the neutron population. Celikten and Sahin compared the reactor neutronics performance of using HALEU containing  $^{235}\text{U}$  and  $^{238}\text{U}$  with the performance using HALEU from Y-12 with the impurities [87]. By performing burnup dependent Monte Carlo N-Particle code (MCNP) simulations of the potential Replacement Reactor Concept at National Institute of Standards and Technology (NIST), the authors showed that using the HALEU with the HEU impurities showed a decrease in reactivity that led to an 8% reduction in the cycle length. This analysis suggests that these impurities may impact the performance of commercially deployed reactors as well, which warrants further investigation of the reactor performance when using downblended HEU as fuel.

## Chapter 3

# Fuel cycle modeling methodology

Fuel cycle modeling encompasses the modeling of different fuel cycle facilities and processes, and the material sent between facilities to support the facilities and processes. Modeling the transition between different nuclear fuel cycles provides information on the quantity and timing of various materials to meet specific objectives. For example, the amount of fuel required for reactors deployed to meet a prescribed energy demand. This work models introduces and demonstrates a methodology for modeling potential transitions from the current fleet of LWRs in the US to advanced reactors and quantifying the resources required to support the different fuel cycles. This work considers a variety of transition scenarios, grouped into once-through and recycle scenarios. Sections 3.2 and 3.3 describe details specific to each fuel cycle type.

We used CYCLUS [27] to model the transitions, with archetypes from the CYCLOMOR library [49] defining the non-reactor facilities. To model historic and future demand during and after the transition, each scenario models the fuel cycle between 1965-2090 using a time step of one month. The transition from LWRs to advanced reactors begins in January 2025, which leads to the energy demand of each transition to be relative to the energy generated by LWRs in 2025. Many of the current plans for HALEU-fueled reactors do not have these reactors deployed until the late 2020s [88] through ARDP and other programs. Selecting 2025 as the transition start time for this work provides a bounding case for an aggressive deployment of these reactors.

We aimed to make the LWR deployment and operation aspect of the transitions as realistic as possible. Therefore, we used the International Atomic Energy Agency (IAEA) Power Reactor Information System (PRIS) database [89] to obtain the start dates and power outputs (MWe) for all of the LWRs and end dates for select LWRs. The PRIS database only contains end dates for reactors that are shut down before the publication of the database each year. Reactors still operating in December 2020 (the year of the database used for this work) lack an end date in the PRIS database, so we assume they operate until their current operating license expiration date obtained from [3]. This work considers only reactors in the PRIS database with a power level above 400 MWe, to avoid including prototype and research reactors. Approximate fuel masses used in the cores of the LWRs were obtained from literature [90, 91].

To understand the material requirements to support each of the transition scenarios, we consider multiple metrics: the energy produced, the number of reactors deployed, the uranium requirements (both enriched uranium

required for fuel and feed uranium to produce enriched uranium), the SWU capacity required to produce the enriched uranium, and the amount of waste produced. Comparing each of these metrics provides information on the material requirements of the transition, which further informs the capacity and number of facilities required to support the transition. Our use of these metrics to understand the transitions is supported by previous fuel cycle modeling efforts. The natural uranium usage and waste production are two of the metrics used in the Evaluation and Screening (E&S) [33], and the mass of enriched uranium was the primary result of the work by Dixon et al. [8].

### 3.1 Advanced reactor modeling

This work considers three advanced reactors: the USNC MMR, [72, 92], the X-energy Xe-100 [93], and the NuScale VOYGR reactor [94, 95, 96]. We selected these three advanced reactors because of the availability of open-source design information. Table 3.1 provides some design parameters of each of these reactors. The values in this table closely match the design information about each reactor that is available through open-source information. The USNC MMR and X-energy Xe-100 reactors require HALEU, but the NuScale VOYGR requires LEU with a similar enrichment level to current LWR fuel. This work includes the NuScale VOYGR, despite not requiring HALEU fuel, because the NRC granted it design approval [97] and it is the author's opinion that it is very likely to be deployed along-side HALEU-fueled reactors. Including the VOYGR reactor in the transition scenarios provides insight into how the deployment of HALEU-fueled and non-HALEU-fueled advanced reactors in tandem affects the material requirements of the transition.

Table 3.1: Design specifications of advanced reactors used in transition analysis.

Design Criteria	USNC MMR [92]	X-energy Xe-100 [93]	NuScale VOYGR [94, 95, 96]
Reactor type	Modular HTGR	Modular HTGR	SMR
Power Output (MWth)	15	200	250
Capacity Factor	100%	95%	95%
Enrichment (% $^{235}U$ )	19.75	15.5	<4.95
Cycle Length (yrs)	20	online refuel	1.5
Number of cycles	1	6	3
Fuel form	UO <sub>2</sub> FCM compacts	UCO TRISO pebbles	UO <sub>2</sub> pellets
Discharge fuel burnup (GWd/MTU)	82	168	45
Reactor Lifetime (yrs)	20	60	60

The refueling scheme for each reactor includes the cycle length, the refueling time, and the refueling mass. The

enriched uranium mass required by each reactor type was calculated based on the reactor thermal power, cycle length, and burnup:

$$\text{mass [kg]} = \frac{\text{Power [MWth]} * \text{cycle length [d]} * \text{number of cycles}}{\text{burnup [MWd/kg]}} \quad (3.1)$$

To calculate the total mass of the fuel (including the non-heavy metal in the fuel), the enriched uranium mass was divided by the mass fraction of uranium in the fuel form for the reactor. Any non-uranium bonded components of the fuel, such as silicon-carbide in TRISO particles, were not considered in the mass. This methodology assumes that the uranium and uranium-containing fuel components would be the limiting factor in the fuel cycle and other fuel components would be available as needed.

The MMR does not undergo refueling; the initial core burns for the entire lifetime of the reactor [72]. Therefore, the MMR has a cycle length that matches the reactor lifetime. Additionally, the refueling mass for the MMR is zero. The Xe-100 undergoes online refueling operations, with each TRISO pebble passing through the reactor six times before discharge [93]. Every seven months about 1/6th of the pebbles in the core are expected to be discharged. The Xe-100 refueling is modeled as a refueling time of zero months and a replacement of 1/6th of the core mass every seven months. The VOYGR contains 37 fuel assemblies, with three different enrichment levels [94]. Each refueling replaces 13 fuel assemblies, with the middle assembly replaced at every refueling. Therefore, 13/37th of the core mass is replaced at each refueling. The fuel enrichment used is a weighted average of the assembly enrichments presented in [94]. NuScale reports that a refueling outage for the VOYGR will take ten days [98].

Fresh fuel recipes for the advanced reactors are based on the defined fuel form for each reactor using the specified uranium isotope ratio for enrichment. Both the MMR and VOYGR are intended to be built in sets (2 MMR per site [92] and up to 12 VOYGR units per site [95]), but in this study every reactor design is treated on a single unit basis. Therefore, the number of reactors built in each of the transitions does not represent the number of unique sites required to build the reactors. All cores modeled are assumed to be equilibrium cores; this work does not consider start-up cores or the transition to equilibrium.

To properly account for the capacity factor of each reactor, we multiplied the power output (in MWe) of each reactor by the capacity factor and removed explicit modeling of outages. We applied this methodology to the advanced reactors and the LWR fleet. We assumed the LWRs operate with a 92.66% capacity factor based on the last five years of fleet-averaged capacity factors [99]. By removing explicit modeling of outages, the outages do not artificially affect the capacity factors. The operating cycle of the LWRs and VOYGRs was extended by 1 time step, to ensure that these facilities received fuel on the same schedule as if the outages were explicitly modeled. The Xe-100 and MMR already do not have an outage period to model, so we did not make any further changes to the models of these reactors.

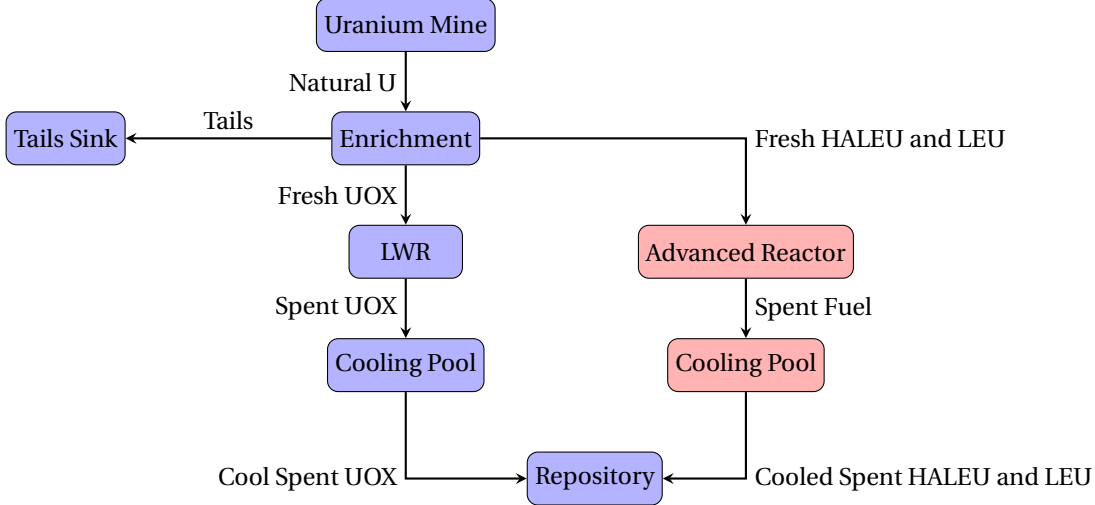


Figure 3.1: Fuel cycle facilities and material flow between facilities in the once-through fuel cycles modeled. Facilities in blue are used in all once-through scenarios, the facilities in red are added in at the transition start time in the transition scenarios.

## 3.2 Once-through fuel cycle scenarios

This section describes the various once-through fuel cycle transitions modeled in this work. A once-through fuel cycle is the current fuel cycle in the US, so modeling these fuel cycles provides insight into changes in material requirements from deploying different reactors and not from changes in the type of fuel cycle. Figure 3.1 shows the flow of material through the modeled once-through fuel cycles. The ‘Advanced Reactor’ node in Figure 3.1 represents any subset of the advanced reactors (Xe-100s, MMRs, and VOYGRs) included in the scenario. This model assumes that all enriched uranium is produced by enriching natural uranium; this work does not consider downblending HEU to produce LEU. This fuel cycle is a simplified version of the modeled fuel cycle in [18], removing steps in the fuel cycle that do not affect the reported results such as milling and fuel fabrication. Removing some of the steps simplified the models from a user standpoint and reduced the size of the CYCLUS output file, facilitating data analysis. The transition from the LWRs to the advanced reactors begins in 2025. Each of the non-reactor facilities have an unlimited capacity to produce or process materials, to prevent material unavailability from influencing the results. The reactor agents in the scenarios, advanced reactors and LWRs, are modeled using the CYCAMORE Reactor archetype.

The once-through scenarios model the current fleet of LWRs in the US and the transition to multiple combinations of the advanced reactors and different energy demand scenarios, summarized in Table 3.2. Scenario 1 models the LWR fleet without the transition to any advanced reactor to provide a comparison with historic needs for a fuel cycle based on enrichments to less than 5%  $^{235}\text{U}$ . The energy demands are based on the energy supplied by the LWRs in 2025 (the start of the transition). A no growth energy demand applies a constant demand for the

energy produced by LWRs in 2025, and a 1% growth demand applies an exponential growth demand starting at the energy produced by LWRs in 2025. A 1% annual growth in demand (Scenarios 8-13) is less than what Dixon et al. [8] modeled (1.2%-2%), but more than the average growth between 2020-2050 in the reference case of the 2022 U.S. Energy Information Administration (EIA) Annual Energy Outlook (0.82%) [100], and provides a middle-ground estimate on material requirements for a growing energy demand.

Table 3.2: Summary of the once-through fuel cycle transition scenarios.

Scenario number	Reactors present	Energy growth model
1	LWRs	N/A
2	LWRs and MMR	No growth
3	LWRs and Xe-100	No growth
4	LWRs, Xe-100, and MMR	No growth
5	LWRs, MMR, and VOYGR	No growth
6	LWRs, Xe-100, and VOYGR	No growth
7	LWRs, Xe-100, MMR, and VOYGR	No growth
8	LWRs and MMR	1% growth
9	LWRs and Xe-100	1% growth
10	LWRs, Xe-100, and MMR	1% growth
11	LWRs, MMR, and VOYGR	1% growth
12	LWRs, Xe-100, and VOYGR	1% growth
13	LWRs, Xe-100, MMR, and VOYGR	1% growth

Another aspect of modeling a fuel cycle transition is the composition of different materials. We use recipes to define all of the material compositions in the once-through transitions. Recipes for LWR fresh and used fuel were found in work by Jacobson et al. [101], assuming a burnup of 51 MWd/kg. Section 3.1 describes how this work determined recipes for fresh fuel in the advanced reactors. Other important recipes in the simulations include natural uranium (0.711% weight fraction  $^{235}\text{U}$ ) and enrichment tails (0.2% weight fraction  $^{235}\text{U}$ ). We obtained used fuel compositions for the Xe-100 and MMR by developing models in Serpent [102] and performing depletion. The models used are described in detail in Section 8.1. We applied the LWR used fuel composition from Jacobson et al. [101] to the VOYGR used fuel, as a simplifying assumption. The LWRs and VOYGR are similar designs, using light water for coolant and moderator, a thermal neutron spectrum, uranium dioxide fuel at similar enrichment levels, and similar burnups, which supports this as a reasonable assumption.

The institutions in the simulations govern the deployment of reactors. A CYCMORE DeployInst institution [27] deploys and decommissions the LWRs according to their start and end dates. A second CYCMORE DeployInst deploys and decommissions the advanced reactors, based on calculations external to the CYCLUS simulations, of when new reactors must be deployed to meet the energy demand. All of the facilities and institutions in the simulation are in the same region, which represents that all facilities are in the same country.

Many of the transition scenarios consider the deployment of multiple advanced reactors. Therefore, we implement a modified greedy algorithm as the advanced reactor deployment scheme to determine the number of

each advanced reactor deployed in each scenario based on the energy demand. The advanced reactor deployment scheme preferentially deploys the advanced reactor with the largest power output in the scenario (e.g., Xe-100s in Scenario 7) until their deployment would create an oversupply of power (i.e., the number of reactors is rounded down). Then the next largest reactor (e.g., VOYGRs in Scenario 7) is deployed until an oversupply of power would be created. Finally, the reactor with the smallest power output in the scenario (e.g., MMRs in Scenario 7) is deployed until the demand is fully met (i.e., the number of reactors needed is rounded up). The demand met by deploying new reactors is the difference between the energy produced by previously deployed reactors and the energy demand at each time step. Figure 3.2 illustrates how the advanced reactors would be deployed in Scenario 7 to meet a fictitious demand of 530 MWe. For this example, 5 Xe-100s, 1 VOYGR, and 1 MMR are deployed, producing a total of 534 MWe. This deployment strategy aims to minimize the number of reactors deployed, minimize power oversupply.

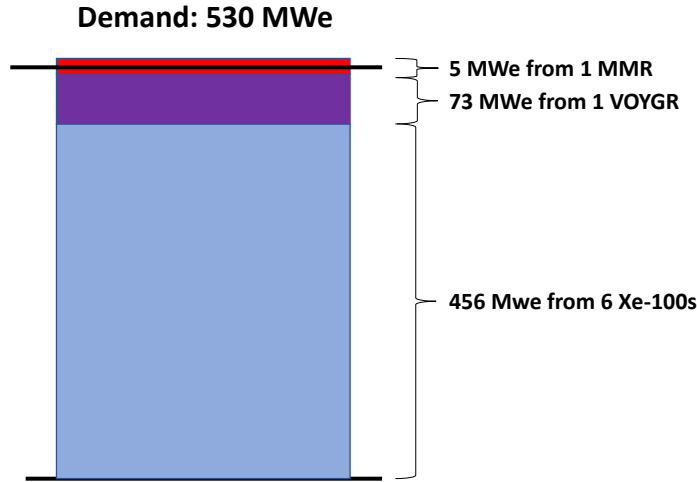


Figure 3.2: Example of how advanced reactors are deployed in Scenario 7 to meet a theoretical demand of 530 MWe.

This deployment strategy is used to deploy advanced reactors when there is unmet demand in energy from the decommissioning of LWRs or when the demand increases (such as in the 1% growth scenarios). When there is unmet demand from the decommissioning of advanced reactors, the advanced reactors are redeployed on almost a one-to-one basis. A slightly smaller number of advanced reactors may be redeployed if there is an oversupply of power greater than the power output of the reactor to be redeployed.

### 3.3 Recycling fuel cycle scenarios

This section describes the closed fuel cycle modeled in this work. We created these transition scenarios to investigate how closing the fuel cycle and the recycling scheme impact material requirements. The recycle scenarios investigated vary by the energy demand of the scenario and the recycling scheme (Table 3.3). Energy demands vary between a no growth and a 1% growth model, using the same demand curves as the once-through fuel cycle models. Variations in the recycling scheme include either a limited or a continuous recycle. Limited recycle scenarios assume that UNF is recycled once and disposed of after a second pass through the reactor. Continuous recycling assumes that all UNF is recycled an unlimited number of times until all fissile material has been used. Both recycling schemes were considered in the Evaluation and Screening (E&S) [33], which led to their inclusion in this work. Another distinction between some of the scenarios is if used TRISO fuel is recycled. Reprocessing TRISO faces many challenges and many of the technologies are at a low technology readiness level [103, 104]. Therefore, by modeling scenarios that do and do not recycle TRISO we can model a variety of potential fuel cycles.

Table 3.3: Summary of the recycle fuel cycle transition scenarios.

Scenario number	Energy growth model	Recycle scheme	Advanced reactors	TRISO recycled?
14	No growth	Limited	Xe-100, MMR, VOYGR	Yes
15	No growth	Limited	Xe-100, MMR, VOYGR	No
16	No growth	Continuous	SFR	N/A
17	1% growth	Limited	Xe-100, MMR, VOYGR	Yes
18	1% growth	Limited	Xe-100, MMR, VOYGR	No
19	1% growth	Continuous	SFR	N/A

All of the scenarios with limited recycling model the transition from the current fleet of LWRs to the X-energy Xe-100, the USNC MMR, and the NuScale VOYGR, the same as in scenarios 7 and 13. Therefore, the advanced reactor deployment schedules for these two scenarios are applied to the limited recycling scenarios for the appropriate energy growth model (i.e., Scenarios 7, 14, and 15 have the same deployment schedule and Scenarios 13, 17, and 18 have the same deployment schedule). We do not consider all advanced reactor combinations considered in the once-through scenarios to limit the scope of the work. Using this deployment combination provides some comparison between the once-through and recycle transition scenarios. Because these scenarios use the same advanced reactor deployment schedule, the number of advanced reactors and the energy supplied are not examined in the results because they will be the same for each of these scenarios. Instead, the results of these scenarios will focus only the material requirements.

Continuous recycle requires a fast reactor, but all of the reactors considered in this work so far have a thermal neutron energy spectrum. Therefore, Scenarios 16 and 19 model the transition from LWRs to a SFR. Section 3.3.2 provides more information about how we modeled a fast reactor for these fuel cycles. The continuous

recycle scenarios (Scenarios 16 and 19) deploy only the fast reactor, and no thermal advanced reactors (i.e., no Xe-100s, VOYGRs, or MMRs). Section 3.3.2 provides more information about the SFR modeled for the continuous reprocessing scenarios.

### 3.3.1 Limited recycle scenarios

Figure 3.3 shows the fuel cycle and material flows for the scenarios with limited recycling (Scenarios 14, 15, 17, and 18). In Scenarios 14 and 17, all used fuel from the advanced reactors is sent to the reprocessing facility. In Scenarios 15 and 18, only the used fuel from the VOYGRs is sent to the reprocessing facility because the VOYGR is the only advanced reactor that does not use TRISO fuel. The Xe-100 and VOYGRs can receive UOX or MOX fuel. The MMRs can only receive UOX, as a modeling assumption stemming from the lack of refueling for this reactor.

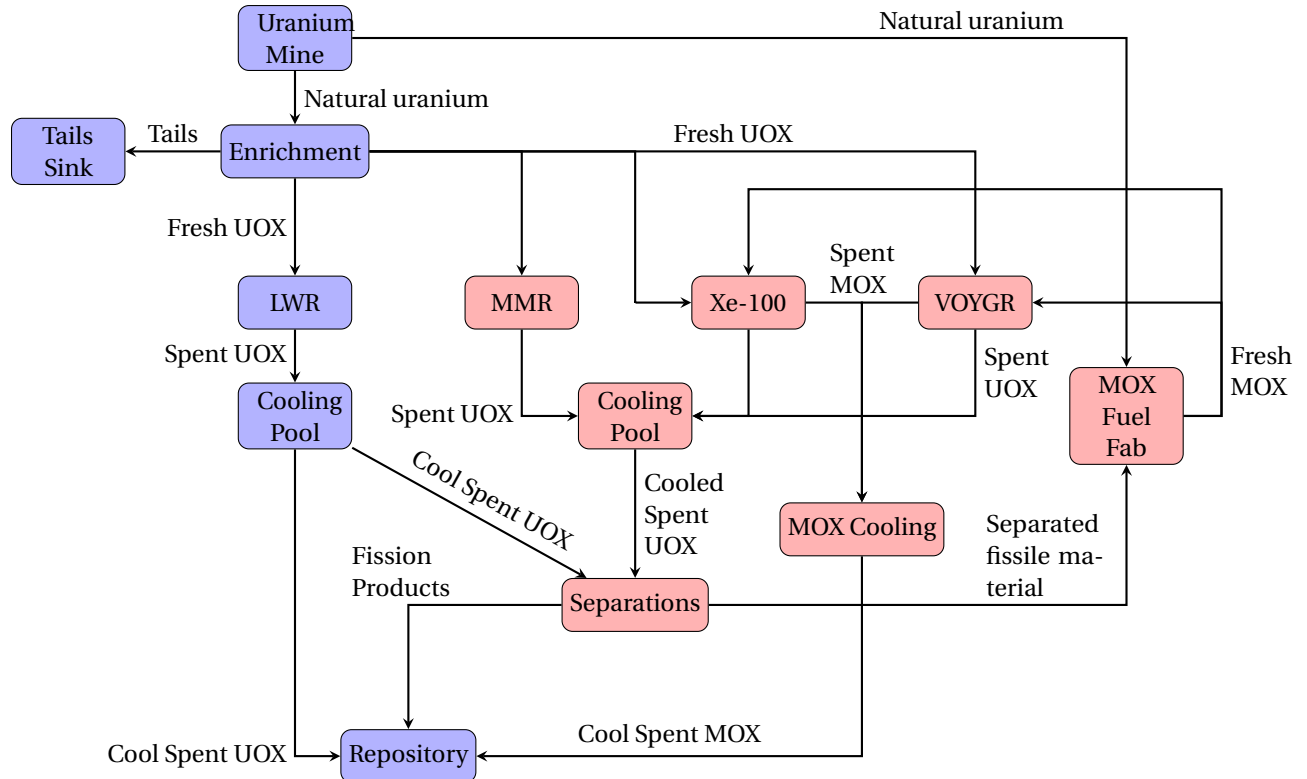


Figure 3.3: Fuel cycle facilities and material flow between facilities for modeling the transition to advanced reactors with a limited recycle fuel cycle. Before 2025 a once-through fuel cycle is used with the facilities in blue. Facilities in red are deployed starting in 2025. In all limited recycling scenarios the spent UOX from the VOYGRs is sent from the red Cooling Pool to the Separations facility. In Scenarios 14 and 17 the spent UOX fuel from the Xe-100 and MMR are also sent from the red Cooling Pool to the Separations facility, but they are sent directly from the red Cooling Pool to the Repository and are not reprocessed in Scenarios 15 and 18.

We model the LWRs and MMR with the CYCAMORE Reactor archetype, because these reactors only receive uranium-based fuel so the used fuel compositions would be consistent between fuelings. Each of these reactors use

the fresh and used fuel recipes that are used for the once-through scenarios. We model the Xe-100 and VOYGR as receiving uranium- and plutonium-based fuel, so the used fuel compositions will vary with different amounts of each fuel type loaded into the reactors which means that the CYCAMORE Reactor archetype will not be the most accurate way to model these reactors. Therefore, we developed a new archetype for CYCLUS called the OpenMCyclus DepleteReactor that couples CYCLUS with OpenMC [29] to dynamically model depletion and provide more accurate used fuel compositions. This archetype expands the capabilities of CYCLUS archetypes to dynamically model fuel depletion during a simulation by providing a coupling to an open-source depletion solver and provide reactor-agnostic depletion. Section 3.5 provides more details on how this archetype works and how it compares to the CYCAMORE Reactor archetype. OpenMCyclus couples with the stand-alone depletion solver in OpenMC [105], so modeling a reactor with this archetype requires information about the refueling scheme for the reactor as well as one-group cross section data to perform the depletion.

For the VOYGR, we generated the one-group cross section data by using the built-in PWR assembly model in OpenMC. We modified this model so that the enrichment level of the fuel matched the core average of the VOYGR modeled in this work. We then used OpenMC to generate the cross section data through the `openmc.deplete.MicroXS` class. For the Xe-100 model, we used the Xe-100-like model described in Section 8.1.1 in Serpent [102] to generate the cross section data. We then post-processed the cross section data from Serpent to match the format required by OpenMC. For both the VOYGR and Xe-100 DepleteReactor models, we used the simplified depletion chain for PWRs from OpenMC (referred to as the CASL chain) [105]. Using this depletion chain results in adequate accuracy to the full depletion chain [105] and reduced run times compared with the full depletion chain.

A separations facility is deployed 5 years before the transition begins (i.e. in January 2020), as this strategy is commonly used for modeling transitions with recycling [26, 54] to ensure that enough fuel can be separated and processed in time for use in advanced reactors. Although this is a non-physical time to begin recycling in the US, using this timeline ensures that there will be enough reprocessed fuel for all of the advanced reactors, and one can observe the maximum benefit of recycling. Additionally by using this timeline, specifically ensuring that advanced reactors are deployed at the same time as when they are deployed in the once-through transition, provides an even comparison between these fuel cycle options. Based on the timeline of the separations facility deployment, only the UNF from the LWRs that is leaves wet storage after 2020 is reprocessed.

The separations facility separates out plutonium from the other materials in the fuel, emulating the aqueous reprocessing method without explicitly modeling the chemistry. The partitioning factor is 99% for plutonium, based on a conservative estimate of stated process losses for aqueous reprocessing [106] and the separation efficiency previously used in previous fuel cycle modeling [33, 15]. The separated material from this facility is then sent to a MOX fuel fabrication facility that produces MOX with a pre-defined composition for the advanced reactors. To

determine the plutonium fraction in the MOX fuel, we calculated the plutonium equivalence of the  $^{235}\text{U}$  based on the cross section data generated for the Xe-100 and VOYGR and Eq. 3.2 [107].

$$N_{\text{Pu}239} = N_{\text{U}235} * \frac{p_{\text{U}235} - p_{\text{U}238}}{p_{\text{Pu}239} - p_{\text{U}238}}, \quad (3.2)$$

in which:

$p_i = v\sigma_f - \sigma_a$  for nuclide  $i$

$N$  is the atom fraction of nuclide  $i$

$v$  is the average number of neutrons per fission

$\sigma_f$  is the fission microscopic cross section for the nuclide

$\sigma_a$  is the absorption microscopic cross section for the nuclide

Using this method helps ensure that the fuel used will allow the reactor to run for the same cycle time and have the same assembly mass despite the different properties of  $^{235}\text{U}$  and  $^{239}\text{Pu}$ . All plutonium in the MOX for the Xe-100 and VOYGR is  $^{239}\text{Pu}$ , as a simplifying assumption, even though fabricated MOX will have other plutonium isotopes present. The separated plutonium is the fissile stream for the MOX fuel fabrication, and natural uranium from the mine is the filler material. The separation step is modeled using the CYCAMORE Separations archetype, and the MOX fuel fabrication is modeled using the CYCAMORE Mixer archetype. The Mixer archetype combines the separated plutonium and natural uranium material streams in the constant ratios of plutonium to uranium of the MOX fuel composition for each reactor.

### 3.3.2 Continuous recycle scenarios

Figure 3.4 shows the facilities and material flow for the continuous recycle scenarios (Scenarios 16 and 19). The fast reactor is modeled based on the PRISM design from GE-Hitachi (GEH) in the UNF Recycle mode [108], because of the availability of open-source information to accurately model the design and fuel compositions. Table 3.4 defines some of the design parameters of the SFR in these scenarios.

We modeled the SFR with the OpenMCyclus DepleteReactor archetype. To generate the one-group cross section data needed for depletion we developed an OpenMC model of the PRISM reactor in an equilibrium state (shown in Figure 3.5). Information about the dimensions and core configuration of the reactor were found in [108, 109]. These sources also provided some information about the fresh fuel composition (the “reprocessed fuel” material in Figure

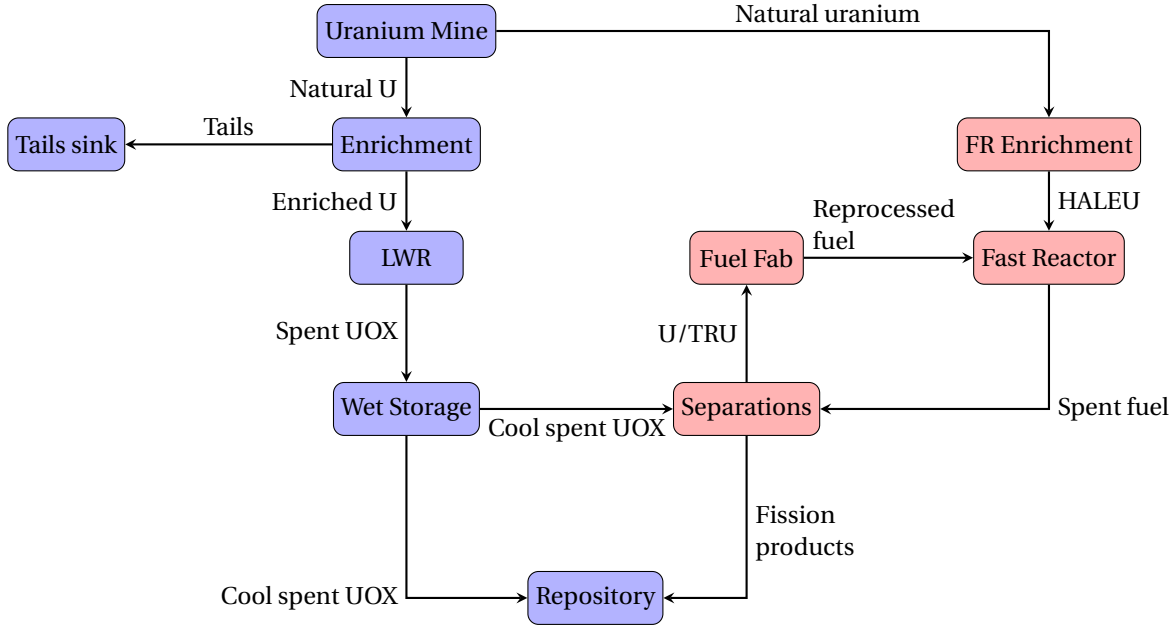


Figure 3.4: Fuel cycle facilities and material flow between facilities for modeling the transition to advanced reactors with a continuous recycle fuel cycle. Before 2020 a once-through fuel cycle is used with the facilities in blue. The fast reactors are deployed starting in 2025, but the other facilities in red are deployed in 2020 to develop a supply of reprocessed fuel for the fast reactors.

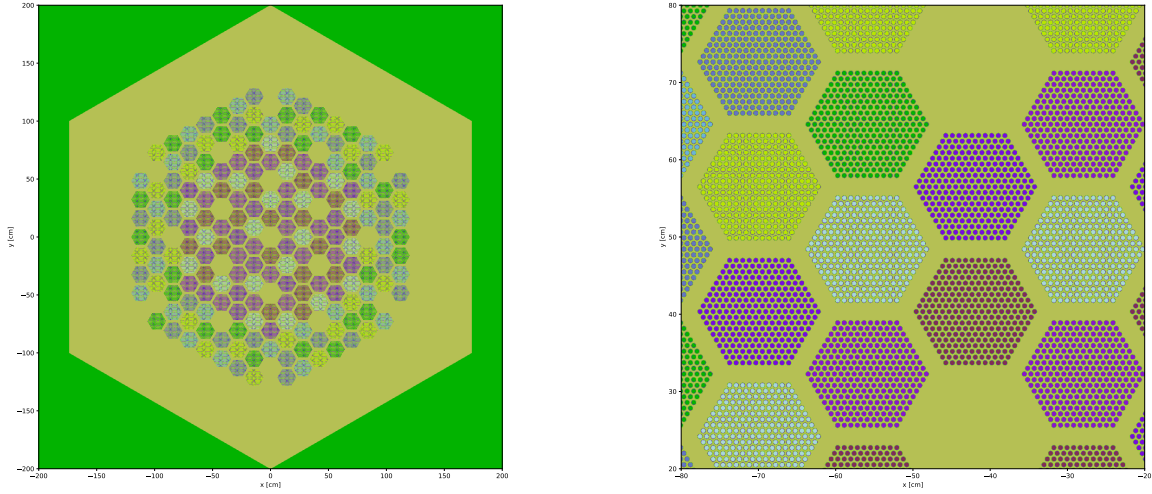
Table 3.4: Fast reactor design specification.

Design Criteria	PRISM [108, 109]
Reactor type	Sodium Fast Reactor
Power Output (MWth)	840
Capacity Factor	90% <sup>1</sup>
Enrichment (wt% fissile Pu)	11.3/13.5 <sup>2</sup>
Cycle Length (yrs)	1
Number of cycles	4
Fuel form	Metallic
Discharge fuel burnup (MWd/kg HM)	87.51
Reactor Lifetime (yrs)	60

<sup>1</sup> Assumed value

<sup>2</sup> The PRISM in UNF Recycle mode has two different driver fuel compositions. We performed a weighted average of the two compositions to determine the fresh fuel composition.

3.4), which we supplemented with the isotopic ratios defined for the S-PRISM reactor (a 1000 MWth SFR of a similar design) in [110]. We then used the transport-coupled depletion solver in OpenMC to obtain compositions for each fuel batch at the beginning of cycle in this reactor. After revising the model to include each of the batch beginning of cycle compositions in the core locations given in [109], we ran the model through OpenMC again to obtain the one-group cross section data for this core in an equilibrium state. We calculated the HALEU composition required for this fuel cycle based on the one-group cross section data and plutonium equivalence in this system (Eq. 3.2).



(a) Radial view of the entire PRISM model.

(b) Detailed view of the assembly lattice for each fuel type.

Figure 3.5: Full and zoomed in OpenMC models of the PRISM reactor, based on information in [108, 109]. The gold material is the sodium coolant and the different colors of the fuel assemblies correspond to different batches of inner and outer fuel assemblies.

To support using reprocessed fuel in the fast reactor, the separations facility is deployed in 2020, consistent with the limited recycling scenarios. For these scenarios, uranium and transuranic elements (neptunium, plutonium, americium) are separated out from the used fuel with 99% efficiency. This change in separated elements allows these fuel cycles to emulate pyroprocessing, which is better suited for reprocessing metallic fuel. If not enough reprocessed fuel is available to support the fast reactor fleet, then HALEU is supplied to fuel the reactors, but the reactors have a preference for reprocessed fuel over HALEU. We calculated the total core mass using Eq. 3.1, and divided as needed for the mass of each assembly in the core. We also calculated the deployment scheme for this reactor using the same methodology described in Section 3.1, based on the applicable demand curve (no growth for Scenario 16 and 1% growth for Scenario 19), the power output of the SFR, and the capacity factor of the SFR.

### 3.4 Calculation of results

The results of the transition scenarios modeled include the energy generated, the number of advanced reactors deployed, the mass of enriched uranium, mass of feed uranium, SWU capacity required to produce the enriched uranium, and the UNF discharged from the reactors. Each of these results are obtained from the CYCLUS output file of the simulation.

The energy generated in each scenario is calculated and reported by CYCLUS. Each reactor facility produces

a commodity called “power”, and the total output of each reactor facility is reported at each time step that they produce it. CYCLUS reports the time step that each facility in the simulation enters (commissions) and exits (decommissions) the simulation. Based on this information, we determine the total number of each type of reactor operating in a given time step.

The other results in this work are calculated based on commodity transactions to and from facilities. The mass of enriched uranium is the mass of fuel traded between the enrichment facility and the reactors, multiplied by the mass fraction of uranium in the fuel form. Multiplying by the mass fraction of uranium means that the other fuel components are not included in this mass. We also use this process to determine the mass of heavy metal in the plutonium-based fuels in the recycle fuel cycle. The reported mass of enriched uranium is used as the product produced by an enrichment facility,  $P$  in Eq. 2.1. This methodology does not account for any losses from fuel fabrication.

The feed uranium masses and SWU capacity are calculated based on the mass of enriched uranium traded to the reactors, using Eq. 2.1. The natural uranium traded to the enrichment facility is not used for this result because the enrichment facility does not have a specified limit on the amount of feed material it can store. Therefore, the enrichment facility continuously requests and receives feed uranium from the uranium mine without consideration for how much it needs to produce the enriched uranium for the reactors. This work does not place a limit on the enrichment facility capacity to ensure that the reactors are fully fueled and prevent other facility limits from influence the reported material demands.

In the recycle fuel cycles, we also consider the mass of separated actinide material, the “separated fissile material” in Figure 3.3 and the “U/TRU” in Figure 3.4. This metric has important implications on the amount of plutonium-based fuel that can be produced in a fuel cycle. To determine this metric, we determine the mass of material traded from the “Separations Facility” to the fuel fabrication facilities for the plutonium-based fuels. The fuel fabrication facilities do not have any capacity limits, so all separated actinide material is traded to the fuel fabrication facilities as soon as it is produced.

Finally, in the once through scenarios the mass of UNF generated is the mass of used fuel that is traded from the reactor facilities to the cooling pools. This mass is the entire fuel form, not just the uranium or heavy metal mass in the used fuel, because the entire fuel form must be considered when determining disposal needs and options. In the recycling scenarios, the used fuel mass is the mass traded from the used fuel cooling facilities to the repository. This change in the calculation of used fuel mass in the recycling scenarios is because not all of the material discharged from the reactors is disposed of in these scenarios, and the inclusion of the waste from reprocessing is captured in this metric. Furthermore, the recycling scenarios also report the mass of HLW sent for disposal. This material is the “Fission products” material in Figures 3.3 and 3.4. This is an important metric, because HLW has similar

disposal requirements to UNF. Therefore, understanding the HLW in these scenarios provides a more complete understanding of the disposal requirements of these facilities.

## 3.5 OpenMCyclus

Current capabilities to model fuel depletion in CYCLUS (Section 2.3.2) either use stagnant recipes (the CYCAMORE Reactor), require export controlled codes (CyBORG [55]), or are reactor design specific (ann\_pwr [57]). Using recipes for fuel compositions is not as accurate as dynamically modeling fuel depletion in a closed fuel cycle [15], and the other capabilities have limited accessibility and applicability in fuel cycle modeling. To address these gaps we developed OpenMCyclus. OpenMCyclus is an archetype library that holds the DepleteReactor archetype, and is open-source and permissively licensed [111]. Currently, OpenMCyclus only holds the DepleteReactor archetype, so the two terms are used interchangeably across this work. OpenMCyclus couples CYCLUS with the stand-alone depletion solver in OpenMC [105] to provide dynamic updates of used fuel composition during a fuel cycle simulation. Dynamically updating used fuel composition is important in modeling closed fuel cycles because of the variations in the fresh fuel placed in the core between cycles [15]. This coupling with OpenMC arose because of the open-source nature of OpenMC and its rich Python API, which both compliment the open-source nature and Python API of CYCLUS. There are two primary components to OpenMCyclus: fuel depletion and transmutation and the material handling.

### 3.5.1 Fuel depletion and transmutation

OpenMCyclus performs fuel depletion through the depletion solver in OpenMC, which solves a system of first-order ODEs that describes the rate of change of each nuclide as a function of production and loss mechanisms [105]. OpenMC applies a Chebyshev rational approximation method (CRAM) solver and multiple time integration methods to solve the system of equations, which has been shown to have good agreement with the depletion solver in Serpent [105]. OpenMC provides this capability in two primary forms: transport dependent and transport independent solvers. To simplify the information needed and reduce run times, OpenMCyclus uses the transport independent solver through the `IndependentOperator` class of the `openmc.deplete` module.

Using this class requires users to provide information including one-group microscopic cross section data, depletion chain data, the number of depletion steps, power level, and material compositions for the fuel. The multi-group cross section data must be provided by the user through a “.csv” file by specifying a path to the file, assumed to be titled “micro\_xs.csv” by the archetype. Users can obtain this data by running a transport calculation of the desired reactor geometry using OpenMC or another transport solver. The depletion chain data is an “.xml”

file that is assumed to be in the same directory as the cross section data, under a filename that is specified by the user. The depletion steps are 30 days each (corresponding to 1 month), with one depletion step for each month of the operating cycle, as defined by the user. The power level is defined by the user, and is converted from MW to W (units assumed by CYCLUS to units assumed by OpenMC). Each of these variables (depletion chain data file name, path to the cross section data and depletion chain data, the number of depletion steps, and the power level) are defined by the user through the CYCLUS input file then passed from the archetype to OpenMC.

There are two different material definitions when using OpenMCyclus: the fresh fuel composition and the OpenMC materials. The fresh fuel compositions are defined as a recipe in the CYCLUS input file. The OpenMC materials are passed to OpenMC for depletion, and are located in an “.xml” file (assumed to be in the same directory as the cross section and depletion chain data, and assumed to be titled “materials.xml”). Information in this file includes the material ID, material name, material volume, material density, and the material composition. The information is read in by CYCLUS and the compositions are updated by the archetype to contain the composition of each assembly in the reactor when depletion is performed. The updated information is then passed to OpenMC for depletion.

To account for multiple batches of fuel in the core, all of the assemblies are depleted and have their compositions updated at the end of each cycle, with the depletion time equaling one cycle length. This methodology differs from the CYCMORE Reactor archetype, which transmutes the composition of only the number of assemblies in a batch, and immediately changes the composition from that of the fresh fuel to that of used fuel at the end of each cycle before the assemblies are discharged. Therefore, by accounting for changes in fresh fuel composition (e.g., UOX to MOX) and multiple batches in a core, OpenMCyclus is expected to be more sensitive to changes in used fuel composition than the CYCMORE Reactor archetype. Additionally, the CYCMORE Reactor assumes that all used fuel has the same composition, so even assemblies that are discharged after only one cycle have the same composition as those that are discharged after the full number of cycles. Furthermore, when a reactor facility is decommissioned, the default behavior of the CYCMORE Reactor archetype is to transmute only half of the assemblies in the core, while the OpenMCyclus archetype transmutes all of the assemblies. This setting in the CYCMORE Reactor (`decom_transmute_all`) can be toggled to True so that both archetypes have the same behavior.

One known limitation of the depletion methodology in this archetype is that the cross section data does not get updated as the fuel compositions change. While this affects the accuracy of the used fuel compositions, this methodology was chosen to provide a balance between fuel composition accuracy and computation resources to run a simulation with this archetype.

### 3.5.2 Material handling

The material handling of the OpenMCyclus DepleteReactor archetype encompasses how material is transferred within different inventories in the archetype, how the archetype interacts with the DRE, and how these interactions are recorded to the database.

The DepleteReactor has three different material inventories that are internal to the archetype: “fresh fuel”, “core”, and “spent fuel”. Each of these inventories are `cyclus.typesystem.ResBufMaterialInv` objects, which means that the material objects (i.e., fuel) can be moved between the different inventories as needed, and each inventory has a defined capacity. Movements between these inventories are not recorded to the database. The fresh fuel inventory represents extra fuel that is kept on site at the facility. The core inventory represents the fuel in the core and used for operating the reactor. The spent fuel inventory represents fuel that is finished in the core, and has been fully transmuted to the used fuel composition. Material requests that are traded into the archetype can be placed in the fresh fuel or core inventories, based on the capacities of each. The material in the spent fuel inventory is used to generate bids for requests, and is traded away to other facilities when the bids are matched with a request by the DRE.

The frequency of material movement between these inventories and the timing of requests and bids in the DRE are based on the user-defined cycle length and refuel time state variables. A reactor agent (a deployed prototype) requests enough fuel assemblies to fill the fresh fuel and core inventories. Each fuel assembly to fill the fresh fuel and core inventories is a separate request, with each request being exclusive (i.e., partial fulfillment of the request by another agent is not allowed). If multiple commodities can meet a request for an assembly (e.g., UOX or MOX assemblies), then all of the possible commodities are requested through mutual requests based on user-defined preferences for each commodity. Materials are requested in quantities to match the user-defined assembly mass size. Information about the materials is recorded to the output database, including the commodity name, material mass, sending prototype, and the receiving prototype. If the agent receives enough fuel and the core inventory is filled, then the agent begins its operating cycle. During the operating cycle, the reactor is recorded as producing the user-defined power each time step of the cycle, and will only request more fuel assemblies if the fresh fuel inventory is not filled. At the end of the operating cycle, the fuel in the core is transmuted as described in Section 3.5.1, and one batch of fuel (a user-defined state variable) is discharged from the core inventory to the spent fuel inventory. If there is any fuel in the fresh fuel inventory, then it is loaded into the core. Then, more fuel for the fresh fuel and the core inventories are requested from other facilities, and the materials in the spent fuel inventory are traded away if requested by other facilities. Before starting the next operating cycle, the facility experiences a refueling period, that lasts as long as the user-defined state variable. During this period, the facility does not produce any power. If the core is not full and within the operating cycle, then it does not produce any power. After the refueling period ends,

the facility enters back into the operating cycle and repeats this process until it is retired or until the simulation ends. Figure 3.6 shows the movement of materials between each of the material inventories of the archetype and the CYCLUS DRE.

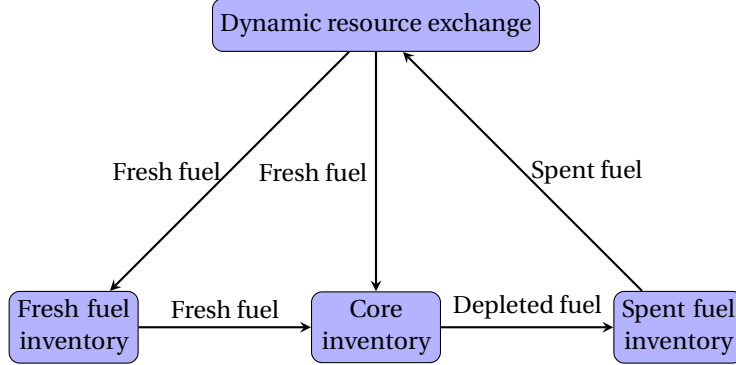


Figure 3.6: Material handling pathways between different material inventories in OpenMCyclus and the DRE of CYCLUS. Depletion occurs to material in the core, just before it moves to the spent fuel inventory.

If the facility reaches the end of its lifetime during a simulation, all of the fuel in the core is transmuted one final time and all of the assemblies are discharged from the core to the spent fuel inventory. If there are any assemblies in the fresh fuel inventory, then they are also moved to the spent fuel inventory to be traded away to other facilities. Once the core and spent fuel are both empty, the facility is decommissioned and exits the simulation.

### 3.5.3 Comparison with CYCMORE Reactor

To compare the results from OpenMCyclus, we created a sample fuel cycle scenario to model with the CYCMORE Reactor archetype and the OpenMCyclus DepleteReactor archetype. All of the code used to define the scenarios, generate data, and the analysis are publicly available [111]. Figure 3.7 shows the fuel cycle for this comparison. Each of the non-reactor facilities are defined using archetypes in the CYCMORE library, with the CYCMORE Mixer defining the “MOX Fuel Fab” agent. The Mixer agent takes in multiple material streams and combines them in a user-defined ratio to produce a final output stream.

The entire simulation is 200 months, in 1-month increments. Reactors are deployed using the CYCMORE DeployInst institution archetype: 2 at time step 1, 1 at time step 50, 1 at time step 100, and 1 at time step 150. The reactors have a lifetime of 60 time steps, cycle length of 12 time steps, refueling length of 1 time step, three batches per core, one assembly per batch, a power output of 195 W, and an assembly size of 0.00602 kg. The reactors prefer MOX over UOX.

To obtain a used fuel composition for the CYCMORE Reactor archetype and cross section data for the DepleteReactor archetype, we used the PWR pin cell example model in OpenMC [112]. Using the pin-cell model is a

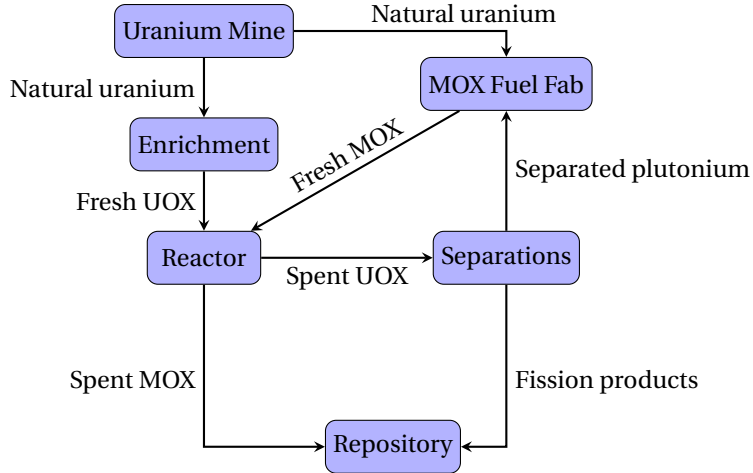


Figure 3.7: Fuel cycle facilities and material flow between facilities for the sample fuel cycle scenarios used to compare the results of the CYCMORE Reactor and OpenMCyclus DepleteReactor archetypes.

simplifying assumption about the size of the reactors to provide a minimal working example, and led to the small power level and assembly mass of the prototypes. We used this model in OpenMC to generate the one-group cross section data required to define the `IndependentOperator` class in OpenMC. Using this cross section data, we depleted the pin cell model using OpenMC to obtain the used UOX and used MOX compositions, with the depletion modeling the entire time that an assembly would be in the the core (i.e., 36 months straight). These compositions were then converted into recipes for use in CYCLUS. The one-group cross section data from OpenMC was then used to run OpenMCyclus, ensuring that the same data is used for both archetypes.

We ran the scenario with the CYCMORE Reactor archetype twice, toggling the `decom_transmute_all` setting between `True` and `False`. Toggling this setting allows us to explore how the different methodologies to handle the fuel upon a facility decommissioning in the CYCMORE Reactor affects the results of the simulation and provide a more comprehensive comparison between the two archetypes. When this setting is `True`, all of the fuel in the archetype is transmuted to the used fuel composition when the facility is decommissioned. When set to `False`, only half (or rounded up if there is an odd number) of the fuel assemblies are transmuted upon decommissioning. The other half of the fuel assemblies remain at the fresh fuel composition. We compared the archetypes based on the energy generated by the reactor prototypes and the transactions of fresh fuel, used fuel, and separated plutonium.

### Comparison results

Comparing the energy provided from the different reactor archetypes is important because many fuel cycle scenarios are designed based on deploying reactors to meet a specific power demand. Therefore, ensuring that the `DepleteReactor` will produce the correct amount of power at the correct times supports its use for modeling fuel

cycle transitions.

Figure 3.8 shows the power provided from the reactor prototypes when using each archetype. There is perfect agreement between the archetypes, even with the different settings for the CYCAMORE Reactor. At the start of the scenario, the prototypes produce 390 W of power, because two reactors are deployed. When the third reactor is deployed at time step 50, the power provided increases to 585 W. When there is only one reactor deployed (e.g., between time steps 63-99) 195 W of power are produced. Every 13th time step after a reactor facility deploys, the facility produced 0 W of power, signifying that it is refueling. All of these results match expectations.

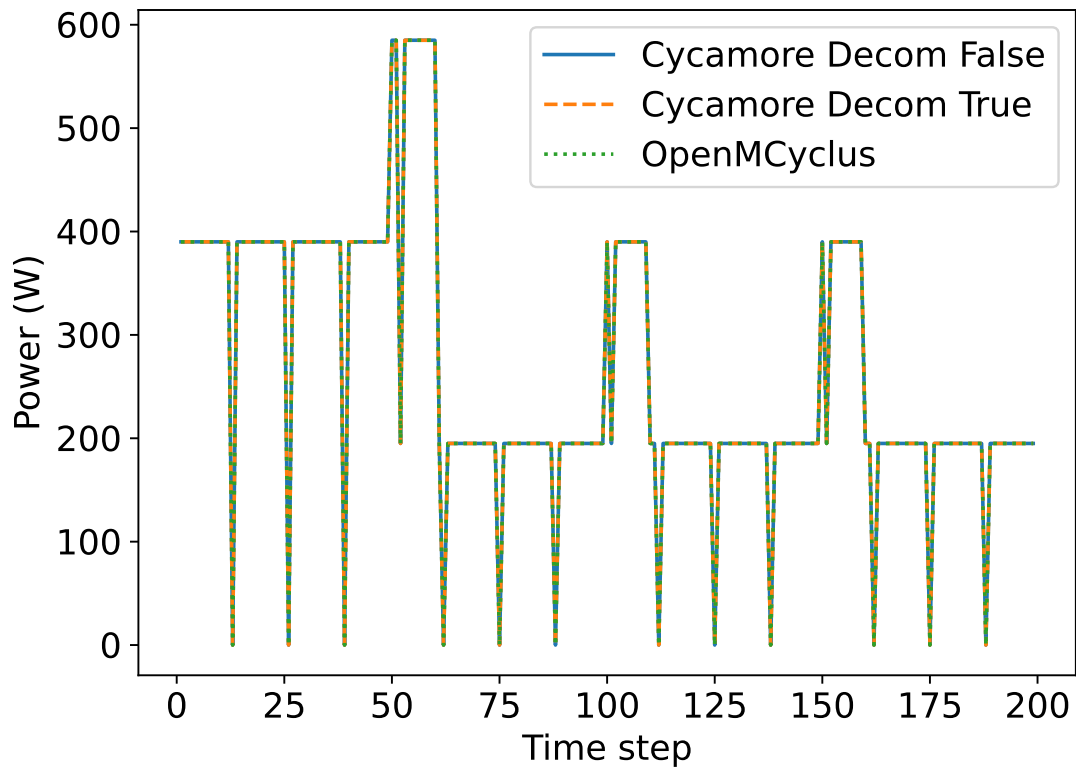


Figure 3.8: Comparison of power provided from reactor prototypes when comparing the CYCAMORE Reactor and OpenMCyclus DepleteReactor archetypes.

Figure 3.9 shows the transactions of fresh UOX and fresh MOX fuel to the facilities when each archetype is used. The total amount of fuel and when any fuel is received is in agreement between all three scenarios. At each time step that a reactor facility is commissioned, a full core's worth of fuel (i.e., three assemblies) are sent to the reactor. The reactors also receive fuel at the expected intervals for refueling (every thirteen months or twelve after deployment because of the lack of refueling period). The differences that arise between the archetypes is in how much of each fuel commodity is received at each time step. Because the MOX fuel is preferred over the UOX fuel, the supply

of plutonium available to create the MOX fuel is the driving factor of this difference and the primary difference between these scenarios.

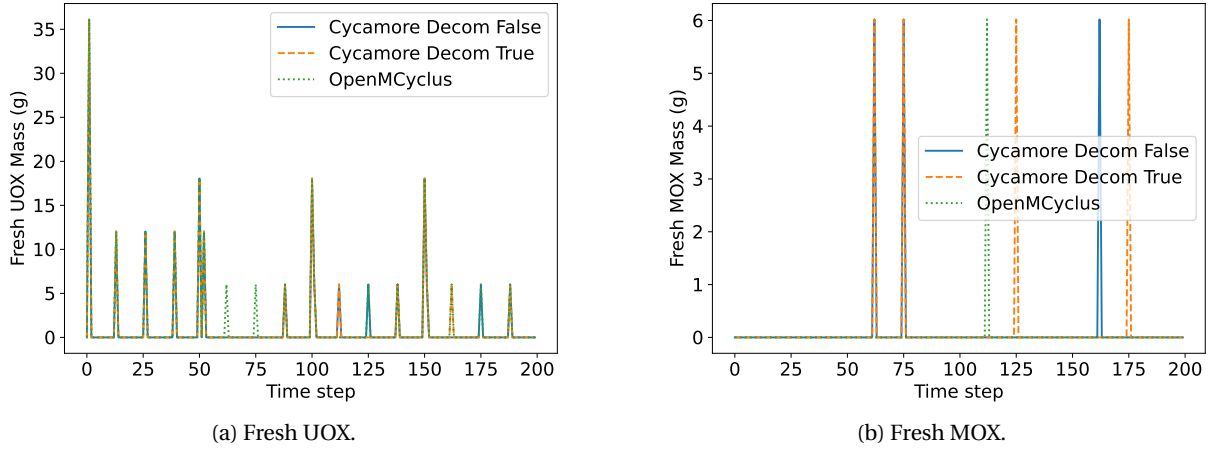


Figure 3.9: Transactions of the fresh fuel commodities to the reactor facilities when defined with each archetype and setting.

Figure 3.10 shows the transactions of used fuel from the reactors to the separations facility in each scenario. There is more variation between the scenarios with the CYCAMORE Reactor archetype and the scenario with OpenMCyclus. The differences in fresh fuel commodities received by the reactor facilities propagate to differences in the used fuel commodity discharged by the reactors in each scenario. The timing and quantity of fuel traded for non-retirement transactions is consistent between all three scenarios, but the commodity type (used UOX or used MOX) may differ. There are differences in the used fuel transactions that correspond to fuel discharged at the retirement of the facilities. The OpenMCyclus archetype discharges all of the assemblies in the same time step that the reactor retires. However, the CYCAMORE Reactor archetype discharges 2/3 of the assemblies in the same time step that the facility retires, and the remaining 1/3 of the assemblies in the next time step. The behavior of the CYCAMORE Reactor upon retirement is consistent regardless of the `decom_transmuted_all` setting. This difference in transactions identifies a methodology difference between the two archetypes. However, it only affects a scenario when a reactor facility is retired, and a one time step difference in when the fuel from the core is traded away is not large. Therefore, this methodology difference is not expected to lead to large differences in the behavior of a scenario.

Finally, Figure 3.11 shows the instantaneous and cumulative masses of separated plutonium traded from the separations facility to the fuel fabrication facility. Because of the large material capacity of the fuel fabrication facility, all of the separated plutonium is traded away in the time step after it is separated, so the separations facility does not accumulate an inventory of separated plutonium. The three different scenarios show consistency in when the separated plutonium is traded: one time step after a used UOX assembly is traded to the separations facility.

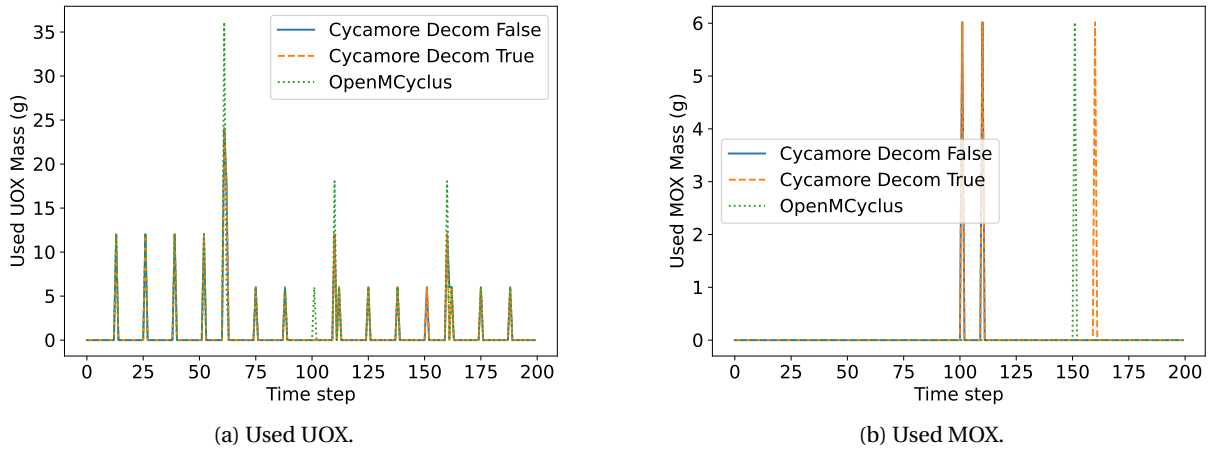


Figure 3.10: Transactions of the used fuel commodities from the reactor facilities when defined with each archetype and setting.

However, the amount of plutonium traded varies between the three scenarios. The two scenarios that use the CYCAMORE Reactor show agreement in the traded plutonium mass until time step 61, when the first two reactors are retired. The disagreement between these two scenarios arises from the `decom_transmute_all` setting. When set to `True`, all of the assemblies in the core are transmuted upon retirement, while when set to `False` only half of the assemblies are transmuted (in this case two of the three assemblies). Therefore, when this setting is `False`, not all of the used fuel assemblies traded away have the used fuel composition, and there is less plutonium in the defined material compositions of the used fuel assemblies than when all of the assemblies are transmuted.

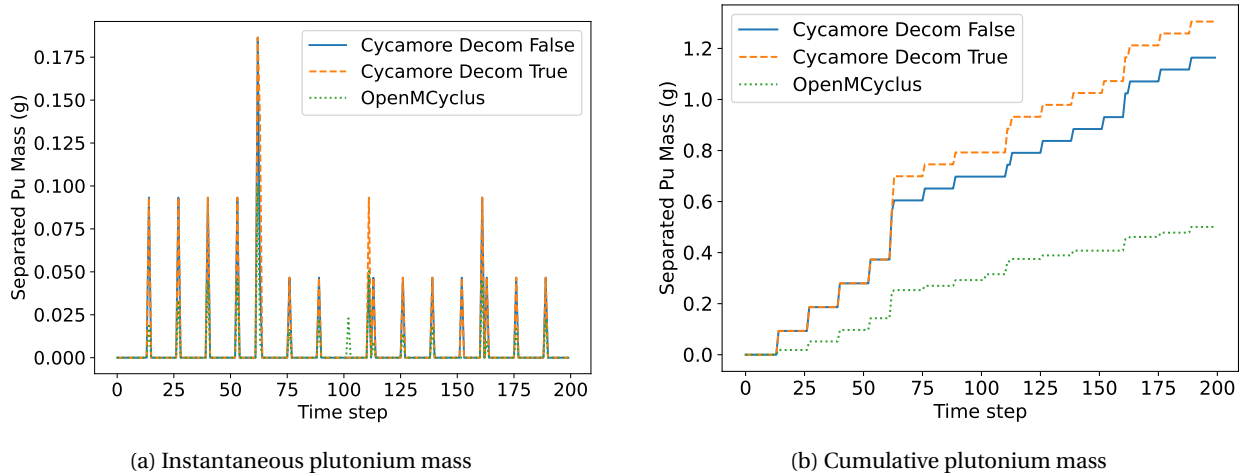


Figure 3.11: Transactions of the separated plutonium from the separation facility to the fuel fabrication facility, based on the archetype to define the reactor facilities.

The differences in traded separated plutonium when using the CYCAMORE Reactor and OpenMCyclus archetype stems primarily from the different methodologies in how the assemblies are transmuted. For the used fuel composi-

tions in the cases with the CYCAMORE Reactor, we depleted an assembly for an entire residence time (36 months continuously). However, in OpenMCyclus the fuel is depleted for a single cycle at a time (12 months in this case). Therefore, the assemblies discharged at the end of the first two cycles by the OpenMCyclus prototypes have not been depleted for the full 36 months like they are with the CYCAMORE Reactor prototype. To confirm that the difference in the time steps of the depletion led to the difference in separated plutonium inventory, we temporarily changed the OpenMCyclus source code to deplete the fuel in a more similar manner to that of the CYCAMORE Reactor: each assembly was depleted for the full 36 month residence time right before being discharged. This modification, shown in red in Figure 3.12, shows that when the assemblies are always depleted for the full 36 month duration the separated plutonium masses are more consistent with those from using the CYCAMORE Reactor archetype. The consistency between the two archetypes when using the modified OpenMCyclus provides confidence in the results of OpenMCyclus when the fuel is depleted each cycle instead of upon discharge. CYCAMORE

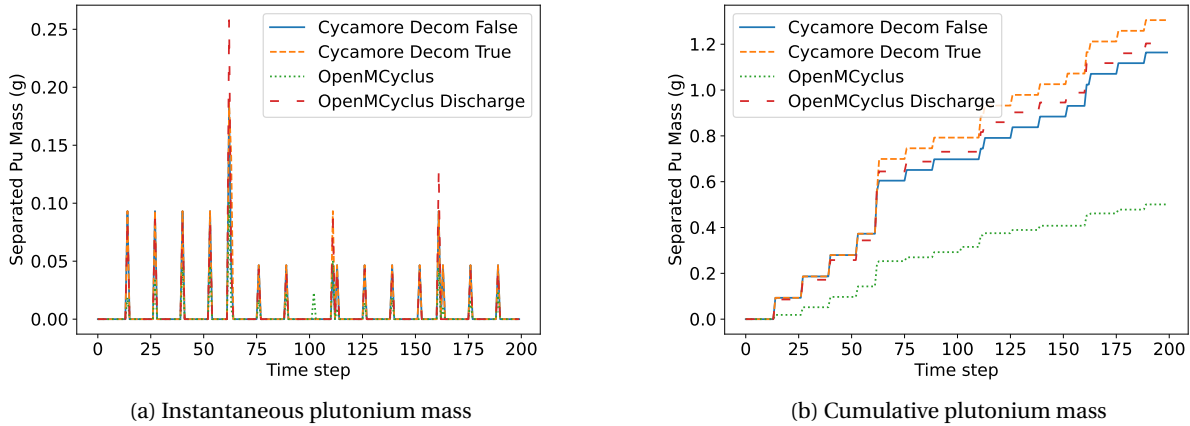


Figure 3.12: Transactions of the separated plutonium from the separation facility to the fuel fabrication facility, based on the archetype to define the reactor facilities.

The transmutation methodologies differences between the archetypes led to the differences in the traded plutonium masses, which then led to the differences in the type of fresh fuel received by the reactors in each scenario. The CYCAMORE Reactor archetype with all of the assemblies transmuted at facility decommissioning resulted in this scenario having the most fresh MOX assemblies sent to the reactors.

# Chapter 4

## Once-through transition results

The once-through transition scenarios are compared on multiple criteria: the energy supplied by the reactors, the number of advanced reactors deployed, the uranium resources required, the amount of SWU capacity required to enrich uranium, and the mass of UNF discharged. Each of these metrics can be used to inform policies and decisions of potential deployment schedules and the fuel cycle infrastructure required to support the deployment schedule.

Bachmann et al. [18] presents a subset of these results for similar scenario definitions, except in that work they assumed the LWRs operate for 60 years if they are not decommissioned before December 2020. This difference in the assumed lifetime of the LWRs impacts the energy demand, the deployment schedule of advanced reactors, and the material requirements of the advanced reactors because a different number of LWRs are operating when the transition begins. The results of Scenario 1 (only LWRs with no transition to advanced reactors) are presented first. Then, each metric for the transition scenarios are presented, first for the no growth scenarios (Scenarios 2-7) then for the 1% growth scenarios (Scenarios 8-13).

### 4.1 Scenario 1: LWRs only

Scenario 1 models only the LWRs deployed in the United States with no prescribed energy demand. This scenario provides insight on historical requirements of the nuclear industry as well as future demands if the US does not deploy any new reactors and decommissions current reactors at their current license expiration. The deployment and material requirements of the LWRs will be the same for each of the other scenarios (Scenarios 2-13). Therefore, analysis of the other scenarios will focus on the requirements of the advanced reactors deployed. The results of Scenarios 2-13 are compared with the results of Scenario 1 to provide a comparison of material requirements between new and current reactors.

Figure 4.1 shows the number of reactors deployed in Scenario 1 as a function of time and the energy produced by the LWRs each year. The energy produced by the LWRs scales with the number of reactors deployed, as one would expect. This scenario deploys a maximum of 109 LWRs at one time, producing between 98.18-99.81 GWe-yr,

and deploys 92 LWRs when the transition begins in January 2025. The first LWR is commissioned in August 1967, and all of the LWRs are decommissioned by October 2055. In 2025, the LWRs produce 87.198 GWe-y of energy, which is the basis of the energy demand for the other scenarios.

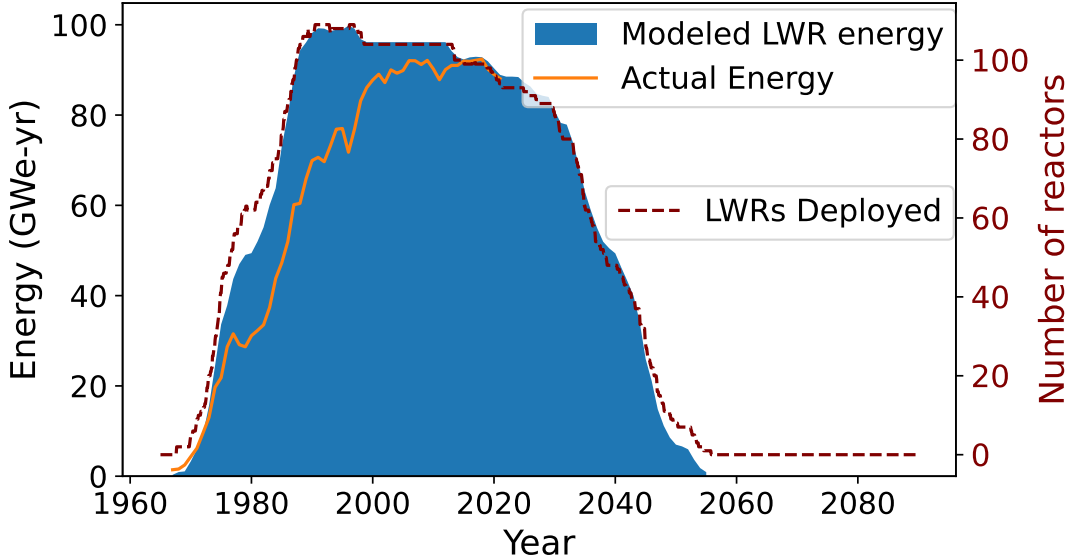


Figure 4.1: Energy supplied by LWRs in Scenario 1 during each year of the simulation compared to the number of reactors deployed.

Figure 4.1 also shows historic data of the energy generated by nuclear reactors in the US [113]. The energy in this simulation does not always match the historic data because of differences in capacity factors. This work assumes that all LWRs operate at a 92.66% capacity factor throughout their operation, but the US nuclear fleet has operated with a wide range of capacity factors because of planned outages that last longer than 1 month and unplanned outages. However, the difference between the simulation and the historic data are minimal during the early 2020's because the capacity factors of the simulation and the industry during this time are very similar.

The mass of enriched uranium sent to the LWRs in this scenario (Figure 4.2) follows the general pattern of the reactor deployment, but with more variation between individual time steps. The increased variation between time steps is because of the staggering of outages for the reactors, or when they receive fuel. Times that receive more fuel correspond with more LWRs undergoing refueling outages. There are also times with large increases in the mass of fuel sent to the reactors, such as in 1996, because these times include the deployment of a new reactor with a full core of fuel instead of the smaller amount required for refueling.

The maximum amount of enriched uranium sent to the LWRs at any one time in this scenario is 480.0 MTU, which occurs in the 1980s. The average mass of enriched uranium sent to LWRs while they are deployed (1967-2055) is 135.65 MTU/month. The average mass of enriched uranium sent to the LWRs between when they are first

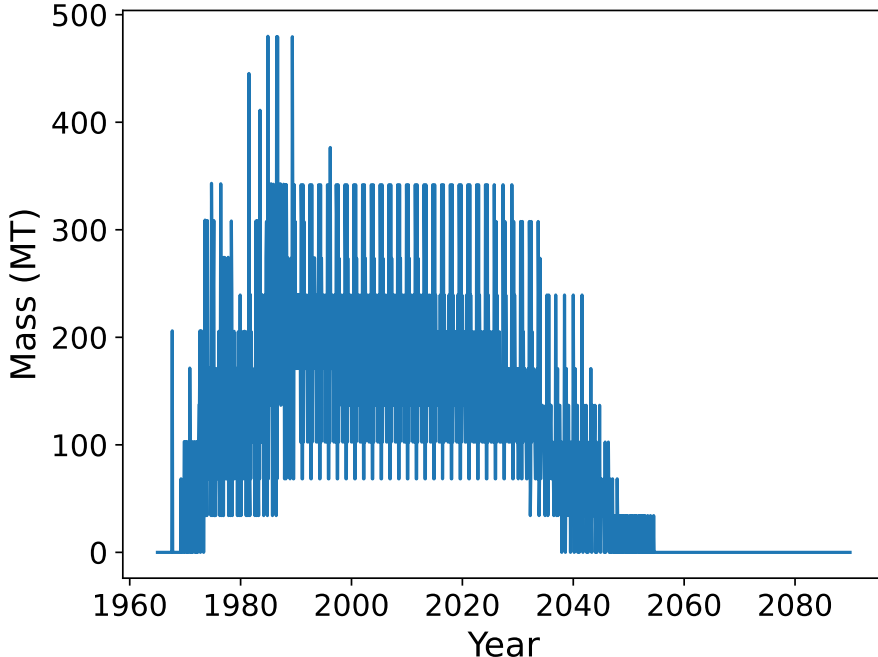


Figure 4.2: Mass of enriched uranium supplied to the LWRs in Scenario 1 at each time step.

deployed and 2025 is 164.57 MTU/month. This average is larger than what is reported in [18] because the average reported by Bachmann et al. accounts for the time before the LWRs are deployed while the average reported here does not. The average mass of uranium sent to LWRs between 2025-2055, from the start of the transition to when they are all decommissioned is 81.48 MTU/month. Comparing the averages shows that the vast majority of enriched uranium is sent to the LWRs before 2025, which matches with the decline in the number of LWRs deployed after 2020. After 2025, a cumulative total of 29,985 MTU is sent to the LWRs, which is less than the cumulative mass reported in [18] because Bachmann et al. assumed that all LWRs would operate for 60 years, which is longer than the assumed operating time for some LWRs in this work. This scenario requires a cumulative total of 143,377 MT of enriched uranium.

The next metric of interest is the mass of natural uranium required as feed material to produce the enriched uranium for the reactors, shown in Figure 4.3. The mass of feed uranium is about an order of magnitude larger than the mass of the enriched uranium. Scenario 1 requires a maximum of 2850 MT of feed uranium at one time and an average of 1,088 MT/month of natural uranium when LWRs are deployed. Before 2025, this scenario requires an average of 1,320 MTU/month of natural uranium, and requires an average of 653.8 MTU/month after 2025. In total, the LWRs require 1,150,385 MT of feed uranium.

Next is the SWU capacity required to produce the enriched uranium for the LWRs, shown in Figure 4.4. This scenario requires a maximum of 3,470 MT-SWU to enrich the uranium sent to the reactors at one time step and an

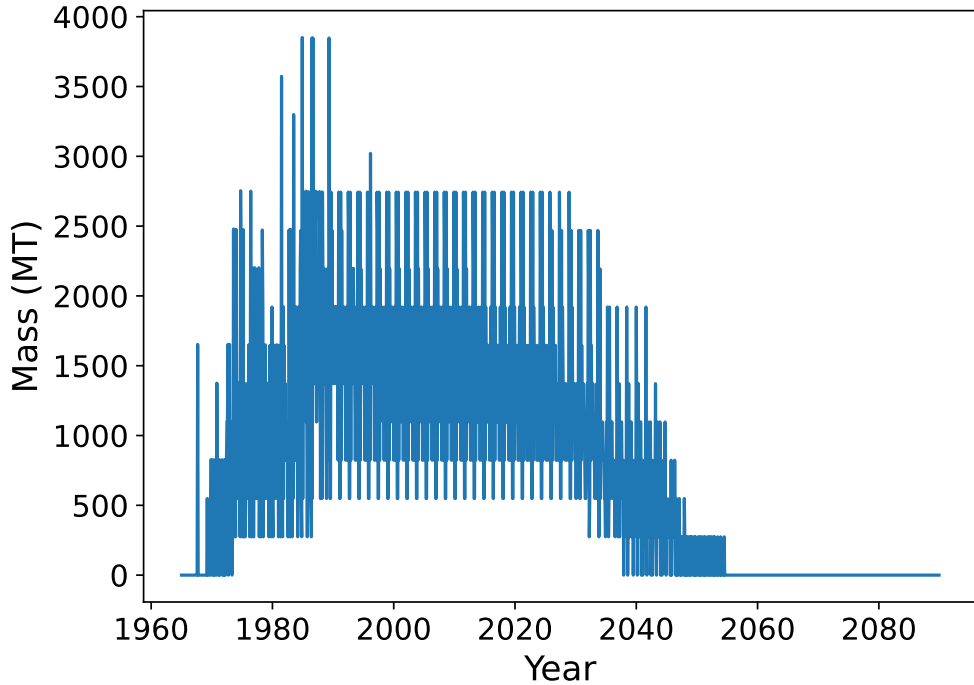


Figure 4.3: Mass of natural uranium required to produce fuel for the LWRs at each time step in Scenario 1.

average of 981 MT-SWU/month to enrich all of the uranium sent to the LWRs when they are deployed. An average of 1189 MT-SWU/month is required to produce the enriched uranium for LWRs between their initial deployment and 2025, and 589.1 MT-SWU/month is needed to produce the enriched uranium sent to LWRs between 2025 and 2055. The values reported here are different than what Bachmann et al. [18] reports for a few different reasons. The first reason is that these results consider only the time steps in which the LWRs are deployed (1967-2055) while Bachmann et al. considers all time steps (1965-2090). The other reason is the use of different enrichment levels for the LWR fuel. Bachmann et al. assumes an enrichment of 4.5% while this work assumes 4.3%  $^{235}\text{U}$  enrichment for LWR fuel.

The last metric is the UNF discharged from the reactors as a function of time (Figure 4.5). The LWRs discharge a maximum of 411.1 MT of used fuel in one time step and an average of 130.0 MT/month when they are deployed. Between the first LWR deployment and 2025 the LWRs discharge an average of 149.1 MTU/month, and an average of 94.27 MT/month between 2025-2055. The LWRs discharge a total of 137,479 MT of UNF in Scenario 1.

Table 4.1 summarizes all of the material needs of Scenario 1.

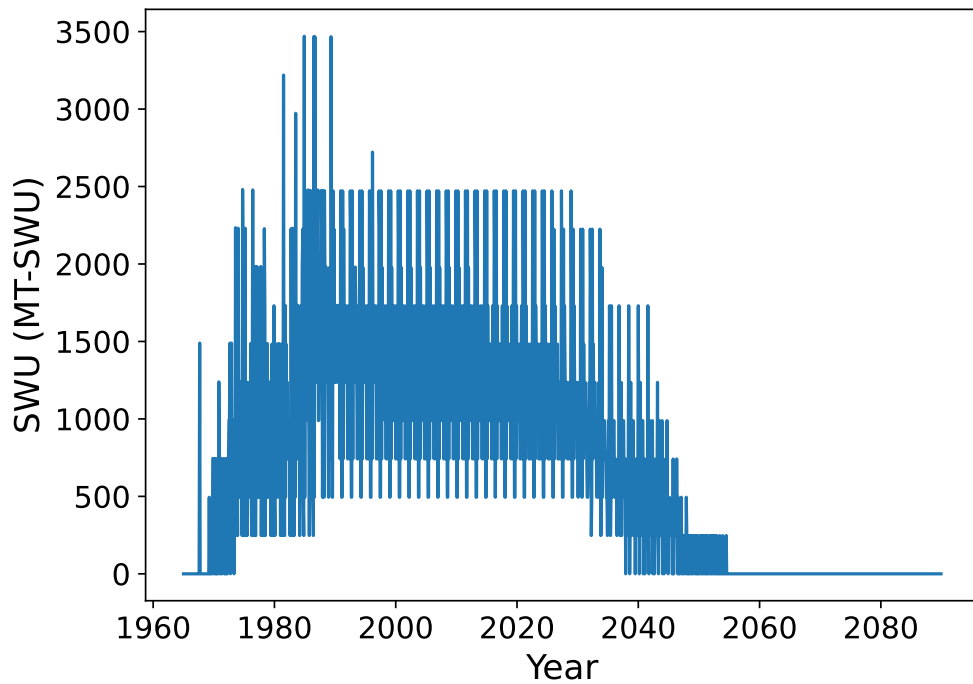


Figure 4.4: SWU capacity required to enrich the uranium sent to LWRs at each time step in Scenario 1.

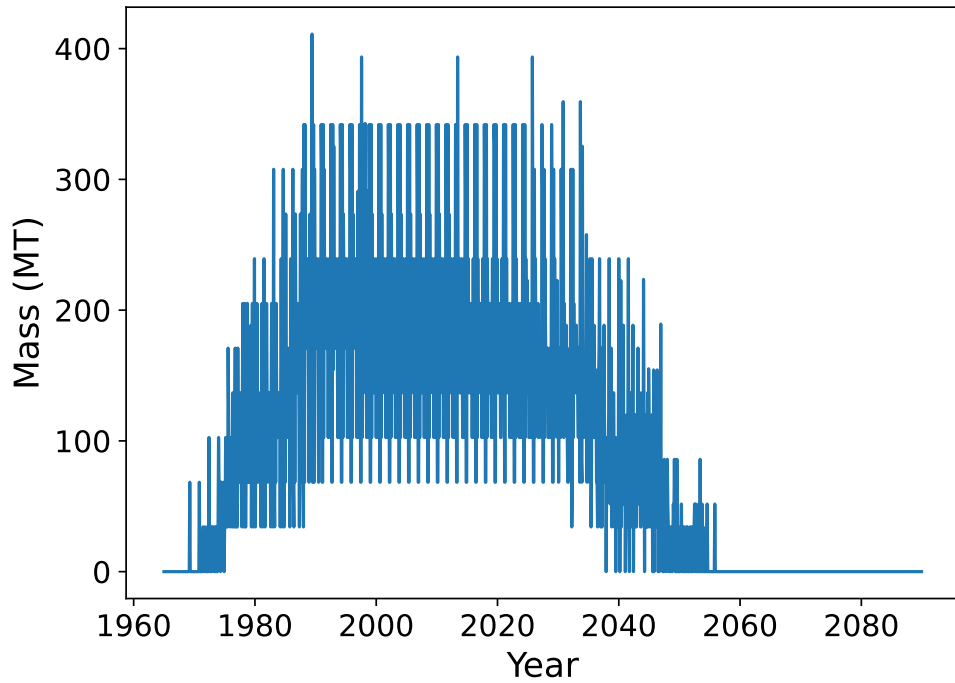


Figure 4.5: Mass of used fuel discharged from the reactors in Scenario 1 as a function of time.

Table 4.1: Summary of material needs for Scenario 1. Averages listed are for the duration that LWRs are deployed (1967-2055).

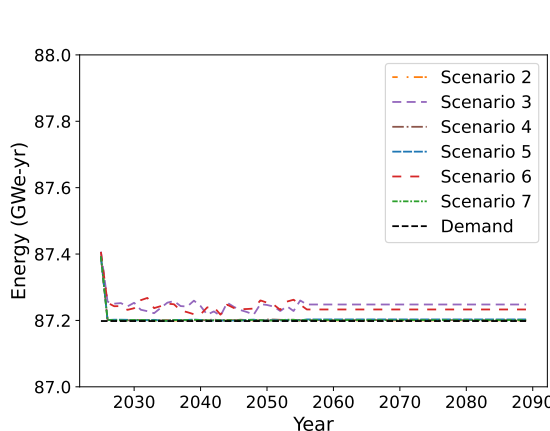
Metric	Average	Cumulative	Maximum	Units
Uranium mass	135.6	143,377	480.0	MT
Feed uranium mass	1088	1,150,385	3850	MT
SWU Capacity	980.7	–	3470	MT-SWU
Waste discharged	130.0	137,479	411	MT

## 4.2 Energy Generated

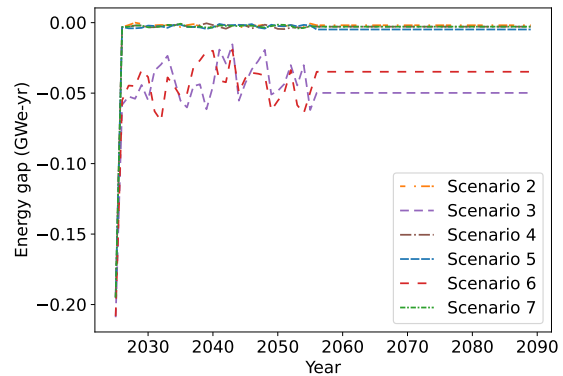
This section reports and compares the energy produced in the no growth and 1% growth transition scenarios to the energy demand. This result considers the energy produced by LWRs and advanced reactors, and compares the different scenarios based on any under- or over-supply of energy present.

### 4.2.1 No growth scenarios

The energy demand in the no growth scenarios (Scenarios 2-7) is a constant 87.198 GWe-yr, based on the energy supplied by the reactors in Scenario 1 in 2025. The energy produced in each of these scenarios meets or exceeds the demand, as Figure 4.6 shows. There is little variation in the amount of energy produced in each of these scenarios because refueling outages are not explicitly modeled. All of the scenarios have an oversupply of power in 2025, up to 0.2 GWe-yr (Table 4.2), before dropping to a value closer to the energy demand. This initial oversupply of 0.2 GWe-yr is a result of the energy demand being set based on the average amount of energy the LWRs supply over 2025. The LWRs provide slightly more than the demand in the first few months of 2025, and the demand is met through LWRs and advanced reactors in the later months of the year.



(a) Annual energy produced compared to demand for Scenarios 2-7 between 2025-2090.



(b) Gap between energy demand and energy produced by reactors in Scenarios 2-7 between 2025-2090. Positive values indicate an undersupply of energy and negative values represent an oversupply of energy.

Figure 4.6: Annual energy produced compared to demand in Scenarios 2-7.

Table 4.2: Maximum undersupply and oversupply of energy in Scenarios 2-7.

Scenario	Maximum oversupply (GWe-yr)	Maximum undersupply (GWe-yr)
2	0.195	0.000
3	0.209	0.000
4	0.195	0.000
5	0.195	0.000
6	0.208	0.000
7	0.195	0.000

Scenarios 3 and 6 produce an oversupply of energy because these scenarios only deploy the Xe-100 and VOYGR, which have a larger power output than the MMR. Therefore, their deployment can't be used to fine-tune meeting an energy demand. The oversupply of energy in each of these scenarios ranges between 15-69 MWe-yr, which is less than the power output of the Xe-100 and VOYGR and demonstrates the round-up aspect of the deployment scheme in this work.

#### 4.2.2 1% growth scenarios

In the 1% growth scenarios, the energy demand is always met or exceeded, as shown in Figure 4.7. There is an initial oversupply of energy, which is consistent with the results energy produced in the no growth scenarios. The maximum oversupply of energy among the 1% growth scenarios (Table 4.3) is 0.436 GWe-yr, which is more than the maximum oversupply of energy in the no growth scenarios.

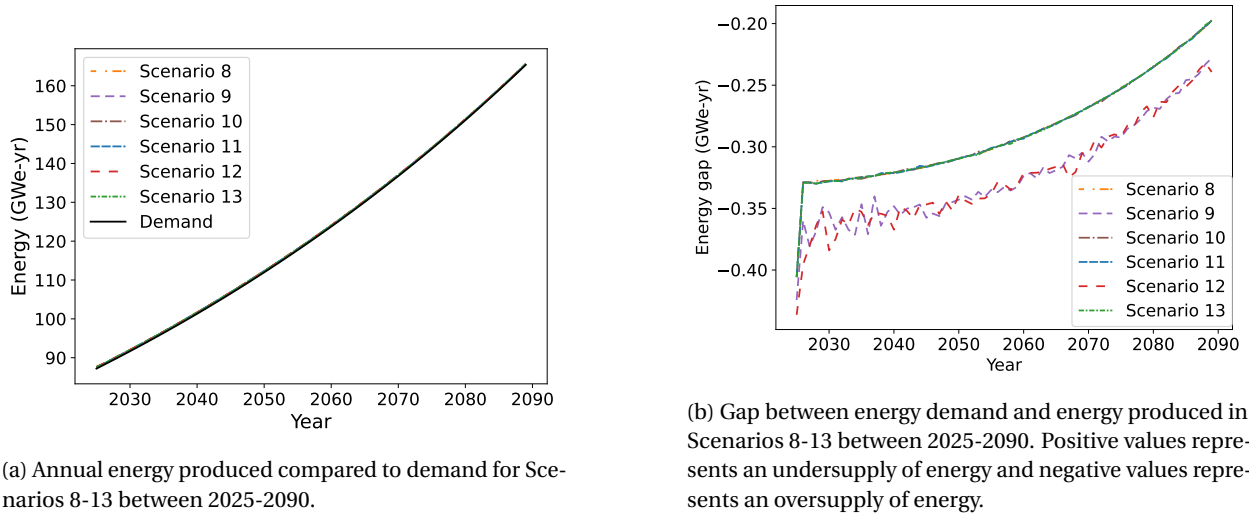


Figure 4.7: Annual energy produced compared to demand in Scenarios 8-13.

There is consistency in the amount of energy oversupply between scenarios that deploy similar reactors. All of the scenarios that deploy MMRs (Scenarios 8, 10, 11, and 13) have the same over maximum oversupply of energy, and the other two scenarios have similar maximum oversupplies of energy. This consistency is a result of the

Table 4.3: Maximum undersupply and oversupply of energy in Scenarios 8-13.

Scenario	Maximum oversupply (GWe-yr)	Maximum undersupply (GWe-yr)
8	0.406	0.000
9	0.424	0.000
10	0.406	0.000
11	0.406	0.000
12	0.436	0.000
13	0.406	0.000

deployment scheme deploying the reactor with the smallest power output last to meet any remaining demand.

## 4.3 Reactor deployment

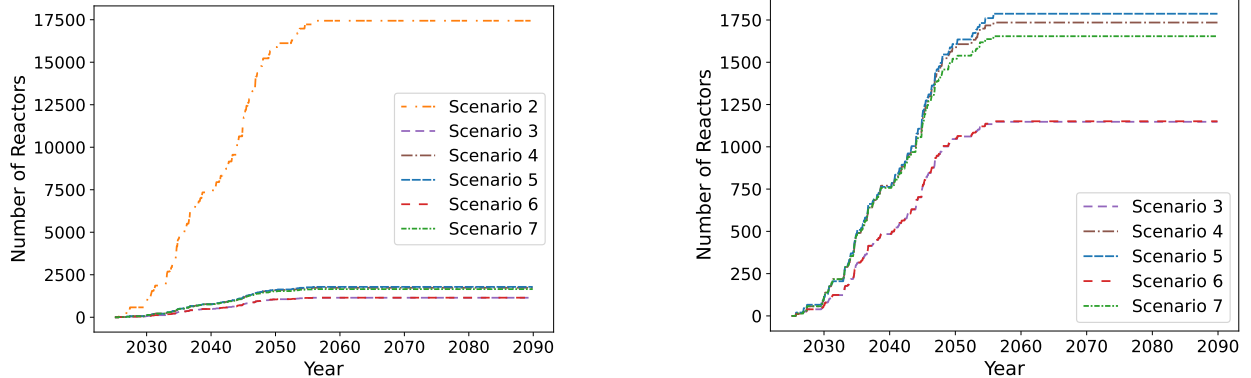
The different power output of each advanced reactor leads to different requirements in the number of advanced reactors deployed in each transition scenario. This section compares the scenarios on the number of advanced reactors built. This metric takes two different forms: the number of reactors that are in the simulation at one time and the number of reactors that are built (enter the simulation) in a single time step. These metrics combined provide insight into the number of reactors needed and the rate at which to build them.

### 4.3.1 No growth scenarios

Advanced reactors are first deployed in September 2025 for Scenario 2-7, 9 months after the transition start time. The advanced reactor initial deployment time is more than six years earlier than the initial deployment time reported for no growth scenarios in the work by Bachmann et al. [18]. The differences in deployment times results from different deployment schemes (Bachmann et al. used the CYCMORE ManagerInst institution to deploy advanced reactors to match installed capacity to a demand in energy generation), different power output from the MMR and Xe-100, and a different energy demand (resulting from different assumptions of how long LWRs operate).

The number of reactors deployed varies based on the reactors deployed in each scenario and scales with the power output of each type of reactor, as shown in Figure 4.8. Scenario 2 requires the most reactors, requiring 17,440 reactors at one time, because the MMR has the smallest power output of the reactors considered in this work. Scenario 3 requires the fewest advanced reactors (1148) because this scenario only deploys the Xe-100, which has the largest power output.

All of the scenarios have a constant number of advanced reactors deployed starting in October 2055 because all of the LWRs are decommissioned by this time and the deployment scheme replaces advanced reactors with a reactor of the same design. The number of Xe-100s and VOYGRs combined in each scenario is similar, about 1,100, because these two reactor designs have similar power outputs (80 MWe and 77 MWe, respectively). Therefore, the



(a) Total number of advanced reactors deployed at each time step in Scenarios 2-7 between 2025-2090.

(b) Total number of advanced reactors deployed at each time step in Scenario 3-7 between 2025-2090.

Figure 4.8: Number of advanced reactors deployed at each time step for Scenarios 2-7. The figures begin at 2025, because no advanced reactors are deployed before then. In the right figure Scenario 2 is removed to highlight the trends in the other scenarios.

Table 4.4: Maximum number of reactors deployed at one time in Scenarios 2-7.

Scenario	MMRs [#]	Xe-100s [#]	VOYGRs [#]	Total [#]
2	17,440	-	-	17,440
3	-	1,148	-	1,148
4	629	1,106	-	1,735
5	636	-	1,151	1,787
6	-	1,070	81	1,151
7	542	1,105	7	1,654

deployment of one over the other does not greatly affect the total number of reactors deployed to meet the energy demand. However, deploying them in tandem reduces the number of MMRs deployed (Scenarios 4 and 5 compared with Scenario 7).

Scenarios 4, 6, and 7 primarily deploy Xe-100s and Scenario 5 primarily deploys VOYGRs as a result of the deployment scheme used in this work. The Xe-100 and VOYGR have the largest power output of the reactors deployed in each of those scenarios, and are therefore preferentially deployed in each of these scenarios. This preferential deployment leads to these reactors supplying most of the energy in each scenario.

In addition to the total number of advanced reactors deployed at each time, the maximum number of each advanced reactor deployed in a single time step is reported in Table 4.5. This information provides insight into the speed at which new reactors must be built. For scenarios with multiple advanced reactors, the numbers reported do not necessarily occur in the same time step. Scenario 2 requires the largest number of reactors to be deployed at a single time, because the MMR has the smallest power output. Scenarios 3 and 6 deploy the fewest reactors in a single time step, based on the total column of Table 4.5, because of the large power output from the Xe-100 and VOYGR.

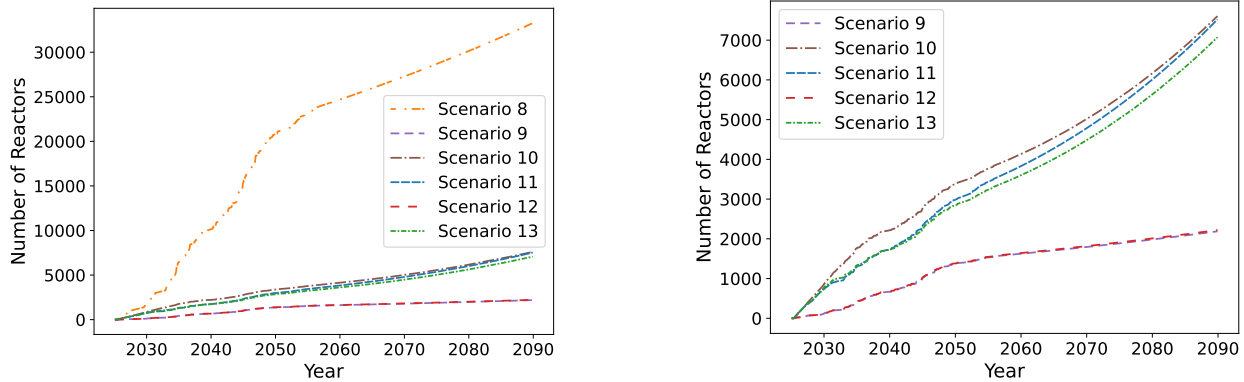
Table 4.5: Maximum number of reactors added to the simulation at a single time step in Scenarios 2-7.

Scenario	MMRs [#]	Xe-100s [#]	VOYGRs [#]	Total[#]
2	856	-	-	856
3	-	46	-	46
4	16	46	-	52
5	24	-	47	66
6	-	45	1	46
7	16	46	1	52

### 4.3.2 1% growth scenarios

All of the 1% growth scenarios deploy advanced reactors beginning in May 2027, which is 32 months (almost three years) before their initial deployment reported by Bachmann et al. for a 1% growth transition [18].

Transitioning to only the MMR (Scenario 8) requires the largest number of reactors, and transitioning to only the Xe-100 (Scenario 9) requires the fewest number of advanced reactors (Figure 4.9, Table 4.6). Scenarios 10 and 13 have similar numbers of reactors deployed, as do Scenarios 9 and 12, because these pairing differ by the inclusion of the VOYGR which has a similar power output to the Xe-100. Compared with the no growth scenarios, MMRs are a greater fraction of the total number of reactors deployed when they are deployed with the other reactors (Scenarios 10, 11, and 13). This increase is because early in the transition, the growth of the energy demand changes in increments smaller than the power output of the Xe-100 and VOYGR. Therefore, the deployment scheme of this work dictates the deployment of MMRs to fulfill the unmet demand.



(a) Total number of advanced reactors deployed at each time step in Scenarios 8-13 between 2025-2090.

(b) Total number of advanced reactors deployed at each time step in Scenario 9-13 between 2025-2090.

Figure 4.9: Number of advanced reactors deployed at each time step for Scenarios 8-13. The figures begin at 2025, because no advanced reactors are deployed before then. In the right figure Scenario 8 is removed to help highlight the trends in the other scenarios.

The number of reactors deployed in the simulation increases with time, partly because of the growth in the energy demand and partly because of the deployment scheme. The deployment scheme dictates that the largest

Table 4.6: Maximum number of advanced reactors deployed in Scenarios 8-13.

Scenario	MMRs [#]	Xe-100s [#]	VOYGRs [#]	Total [#]
8	33,265	-	-	33,265
9	-	2,189	-	2,189
10	5,798	1,807	-	7,605
11	5,627	-	1,893	7,520
12	-	1,420	801	2,221
13	5,228	1,809	37	7,704

Table 4.7: Maximum number of advanced reactors deployed in a single time step for Scenarios 8-13.

Scenario	MMRs [#]	Xe-100s [#]	VOYGRs [#]	Total [#]
8	936	-	-	936
9	-	47	-	47
10	49	47	-	56
11	49	-	49	56
12	-	47	3	48
13	46	47	1	58

reactor is preferentially deployed to meet unmet energy demand. This unmet energy demand is determined after decommissioned advanced reactors are replaced with an equal number of the same type of advanced reactor. The MMR has the shortest lifetime, in addition to the smallest power output. Therefore, the MMRs in the scenarios are replaced with more MMRs, instead of potentially being replaced with a larger reactor if there is enough unmet demand in the time step from MMR decommissioning or demand growth. This aspect of the deployment scheme artificially inflates the number of MMRs deployed in each scenario, which leads to the MMRs having a larger effect on the material requirements of each scenario.

Regarding the rate of reactor deployment, Scenario 8 deploys the most reactors in a single time step (Table 4.7), with 936 MMRs deployed at once. Scenario 13 requires the next largest number of reactors deployed in a single time step, 58 total advanced reactors built. The maximum number of Xe-100s and VOYGRs deployed in a single time step in the 1% growth scenarios are similar to the numbers required for the no growth scenarios. But the number of MMRs deployed for a single time step are at least twice the numbers for the no growth scenarios. The increase in the number of MMRs highlights to MMRs providing an inflated share of the energy demand in the 1% growth scenarios.

## 4.4 Uranium resources

This metric considers both the mass of enriched uranium and the mass of natural uranium feed required by each scenario. The feed uranium masses considered are the masses needed at an enrichment facility, and does not account for any process losses during a milling process or the grade of the uranium ore. Therefore, the values reported are not the same as what would need to be mined. Additionally, the enriched uranium masses reported

do not account for any fuel fabrication losses, which others have previously assumed to be 0.1% [33]. Using these assumptions still yields reasonable estimates of the uranium resources required in each scenario.

The masses of uranium resources are divided into four different metrics: the average monthly mass of uranium to supply all advanced reactors, the average monthly mass of HALEU, the maximum mass of uranium required by all advanced reactors in a single time step, and the cumulative mass required by advanced reactors in the scenario. Each of these metrics provide information on how to design facilities, such as the average facility capacity required to meet the average demand and peaks in demand. The monthly averages are calculated beginning in January 2025, when the transition begins but not when the advanced reactors are first deployed. Therefore, the reported averages are slightly lower than if they were calculated starting at the advanced reactor deployment time. This reporting methodology provides an average for if facilities are built to support the front-end of the NFC starting in January 2025. Additionally, these metrics do not account for any extra fuel assemblies or TRISO pebbles kept on site as reserve fuel.

#### 4.4.1 No growth scenarios

##### Enriched uranium

The mass of enriched uranium sent to reactors (Fig. 4.10) varies based on the advanced reactors deployed in the scenario. Scenario 5 has the largest average mass of enriched uranium sent to reactors each month, followed by Scenario 2 (Table 4.8). Scenario 2 also requires the largest mass of enriched uranium sent to advanced reactors at one time, followed by Scenario 5. Scenario 3 requires the smallest average mass of enriched uranium. Scenarios 3, 4, and 7 have similar monthly averages for enriched uranium mass. All of the scenarios require a smaller average mass of enriched uranium than the LWRs before 2025.

Table 4.8: Metrics for enriched uranium sent to advanced reactors between 2025-2090 in Scenarios 2-7.

Scenario	Average (MT/month)	HALEU Average (MT/month)	Maximum (MT)	Cumulative (MT)
2	88.16	88.16	1,139	68,674
3	32.96	32.96	90.50	25,676
4	34.94	34.94	95.41	27,222
5	166.5	3.198	568.1	129,704
6	42.36	30.69	106.2	33,000
7	35.39	34.50	95.41	27,572

The uranium usage of each advanced reactor dictates the uranium requirements of each scenario. The MMR has the smallest specific power (thermal power per unit mass) for a single core mass and the Xe-100 has the largest specific power. This metric means that to meet the same thermal power output, the Xe-100 will require the least uranium mass, followed by the VOYGR then the MMR. However, this does not include any fuel needed for refueling.

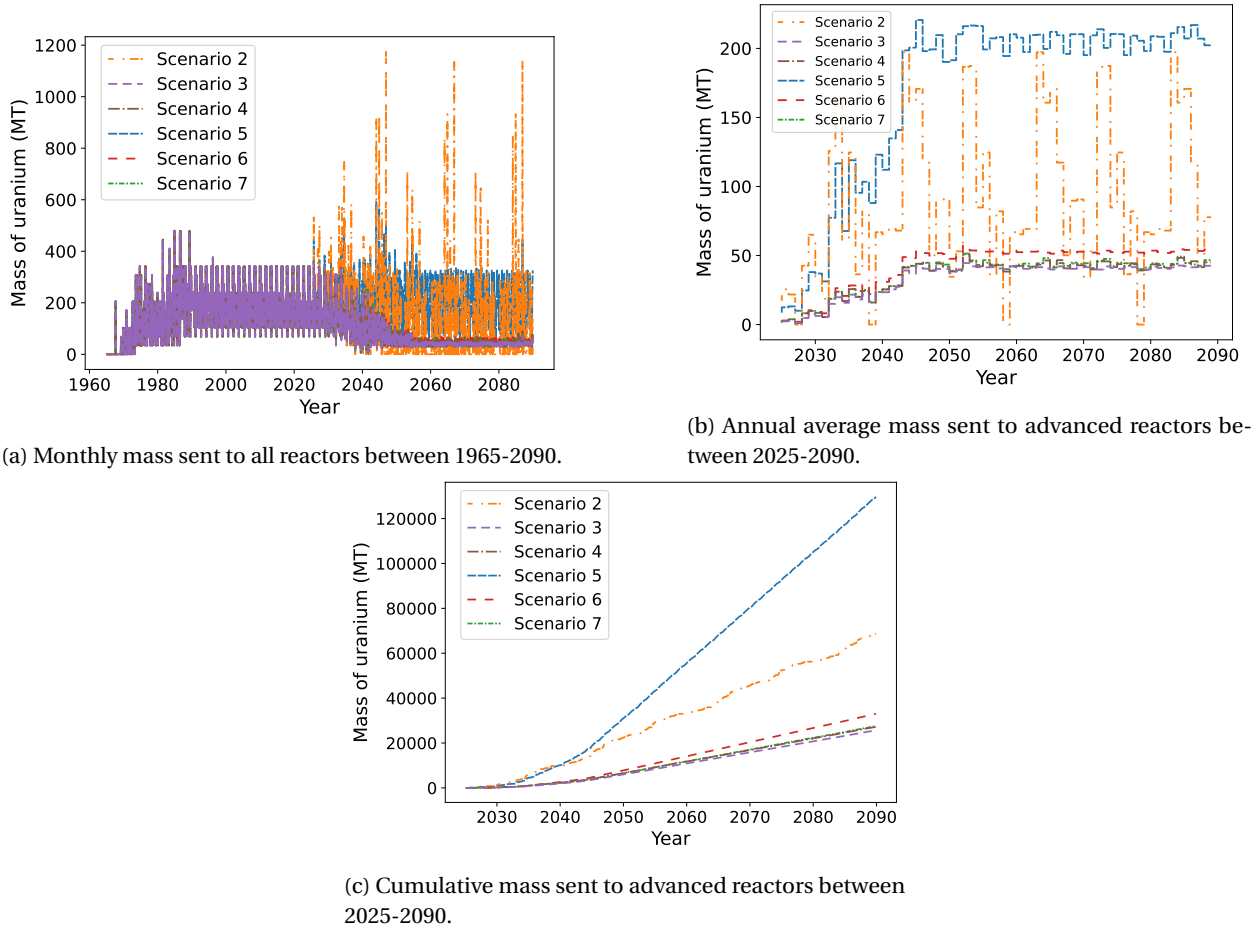


Figure 4.10: Mass of enriched uranium required by reactors in Scenarios 2-7.

The MMR does not need any uranium for refueling, but the Xe-100 and VOYGR do. The Xe-100 requires a smaller mass for each refueling than the VOYGR and a smaller mass over the same amount of time. Therefore, the VOYGR requires the most mass over a given period of time to produce a certain amount of power (accounting for refueling schemes and power output). This larger mass requirement of the VOYGR leads to the masses required by Scenario 5, which primarily deploys VOYGRs, and contributes to the larger mass of enriched uranium in Scenario 6, compared with Scenario 7.

Comparing the MMR and Xe-100, the Xe-100 requires less uranium than the MMR, and the least of all three advanced reactors, over a given period of time to produce a given amount of power. The reduced uranium mass results from the high burnup of the Xe-100, so the reactor gets more energy out of each mass of fuel and has a larger power output. This reduced uranium mass required by the Xe-100 leads to Scenario 3 requiring the least enriched uranium by deploying only Xe-100s. Scenarios 4, 6, and 7 require similar masses of uranium because Xe-100s constitute a majority of the advanced reactors deployed and largely control the uranium required.

Scenario 2 requires the largest average mass of HALEU, because of the large number of MMRs deployed in this scenario. Scenario 5 requires the smallest average mass of HALEU, despite requiring the largest average mass of enriched uranium, because most of the reactors in Scenario 5 are VOYGRs which do not require HALEU. All of the other scenarios (Scenarios 3, 4, 6, and 7) require similar average masses of uranium and HALEU because they deploy similar numbers for each type of reactor.

Scenarios 2 and 5 require the largest mass of enriched uranium at a single time step. For Scenario 2, the large difference between the average and maximum amount of uranium is because of the refueling scheme for the MMR. The MMR only requires fuel when it is first being commissioned, therefore they do not require uranium at time periods in which new reactors are not deployed. Additionally, the MMR refueling scheme causes the variation in the monthly requirements and annual averages of enriched uranium masses observed in Figure 4.10. The large difference between the monthly average and the maximum presents challenges in designing enrichment and fuel fabrication facilities to meet the demand. Designing such facilities would have to consider the material demands and lead times while also limiting the amount of stockpiled enriched uranium at each the facility, as idle stockpiles of enriched uranium poses a proliferation risk.

Finally, Scenario 5 requires the largest cumulative mass of enriched uranium for the no growth scenarios, because the VOYGR requires more uranium than the other two reactors and this scenario primarily deploys VOYGRs. Scenario 3 requires the smallest cumulative mass of enriched uranium, because the Xe-100 requires the smallest mass of uranium of the advanced reactors. The advanced reactors in all of these scenarios require a smaller cumulative mass of fuel than the LWRs. Additionally, deploying the VOYGR in tandem with the other advanced reactors results in an increase in the cumulative mass of enriched uranium needed (e.g., Scenario 3 compared with Scenario 6). This trend suggests that deploying VOYGRs increases the enriched uranium needs of the fuel cycle, even if it decreases the amount of HALEU needed.

The cumulative HALEU need by 2050 for each scenario (Table 4.9) is similar to the mass reported by Dixon et al. [8], 5350 MTU, with the exception of Scenarios 2 and 5. Scenario 2 requires a greater cumulative mass of HALEU because of the large number of MMRs deployed. Scenario 5 requires a much lower mass of HALEU because this scenario primarily deploys VOYGRs.

Table 4.9: Cumulative HALEU needs by 2050 for Scenarios 2-7.

Scenario	Cumulative mass (MT)
2	22,223
3	5,936
4	6,529
5	798
6	5,509
7	6,430

## Feed uranium

For the mass of feed uranium, Scenario 2 requires the largest average mass to supply the advanced reactors (Figure 4.11, Table 4.10). Scenario 2 requires the most feed uranium because it requires more enriched uranium than most of the other no growth scenarios and it requires the highest product assay. As shown by Eq. 2.1b, as the product assay increases, the mass of feed uranium increases, assuming all other variables are constant. Therefore, the combination of an increased product mass and an increased product assay results in a large increase in the feed mass required. Scenario 5 requires the next largest average mass of feed uranium. This scenario requires less feed uranium than Scenario 2 because most of the product uranium for this scenario is for the VOYGRs, which require a lower enrichment assay than the MMRs. Based on Eq. 2.1b, a lower product assay results in a lower mass of feed material required. The decrease in the product assay overpowers the increase in feed required by the increased product mass. Scenario 5 still requires more feed material than the other scenarios because the average product mass required is much larger than the other scenarios, which offsets some of the decrease in feed material from the decrease in the product assay.

Table 4.10: Metrics for feed uranium required by advanced reactors between 2025-2090 in Scenarios 2-7.

Scenario	Average (MT/month)	HALEU Average (MT/month)	Maximum (MT)	Cumulative (MT)
2	3,372	3,372	43,612	2,627,374
3	986.9	986.9	2,710	768,793
4	1,073	1,073	2,912	835,887
5	1,365	122.4	4,896	1,063,737
6	1,008	918.9	2,768	785,020
7	1,063	1,056	2,912	828,036

When comparing the feed material to create HALEU in each scenario, Scenario 2 requires the most feed material because this scenario requires the largest average mass of HALEU and HALEU at the highest product assay. Scenario 5 requires the least feed material for HALEU because the majority of the reactors in this scenario are VOYGRs. Additionally, fueling the Xe-100 requires less feed uranium than fueling the MMR because the Xe-100 requires a lower product assay and a smaller product mass per core. Scenarios 3, 4, and 7 require similar feed uranium masses (about 1,000 MTU/month). Deploying VOYGRs alongside the other advanced reactors (e.g., between Scenarios 3 and 6) decreases the average mass of feed uranium to create HALEU. Deploying VOYGRs decreases the average of all feed uranium if MMRs are also deployed, because the decrease in product assay between these reactors offsets the increase in total product mass when calculating the feed mass.

The maximum feed uranium required by each scenario poses some challenge in facility design. The maximum feed uranium required varies between 2.7-12.9 times larger than the average feed material, which means facilities that produce feed uranium will likely need to be designed with a larger capacity than the average feed uranium

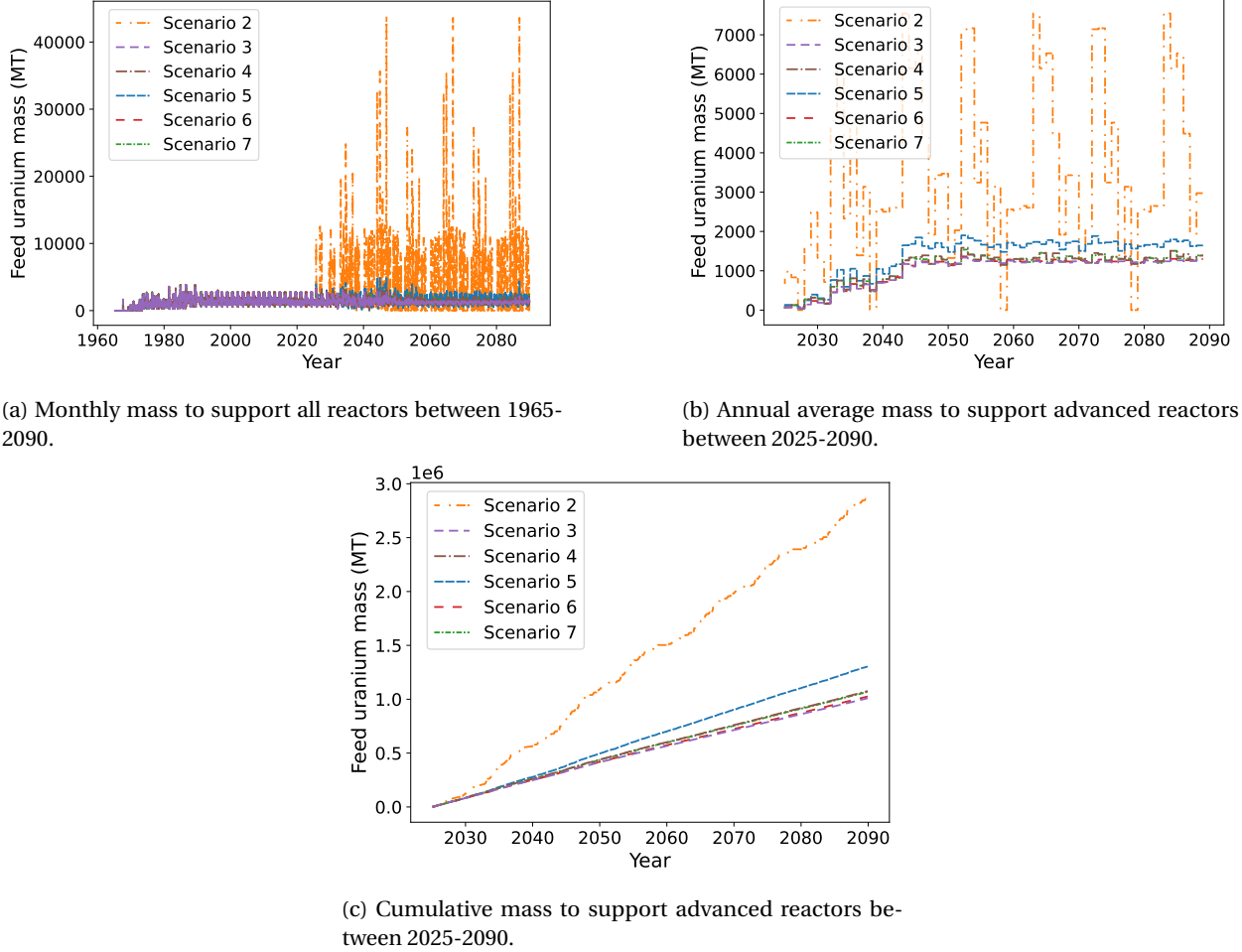


Figure 4.11: Mass of feed uranium required to produce enriched uranium in Scenarios 2-7.

required to meet the peaks. The cumulative mass of feed uranium required by each scenario ranges between 737,000-978,000 MT for every scenario except Scenario 2. Scenario 2 requires over 2.64 million MT, which is more feed uranium than what is required by the LWRs. The EIA reports about 176,000 MT of  $\text{U}_3\text{O}_8$  reserves in the US available at up to \$100/pound at the end of 2019 [114], or about 149,000 MT of uranium, which is smaller than the cumulative needs for all of these scenarios. Therefore, the US would have to consider either uranium from international sources or uranium reserves at increased prices to meet the cumulative demand of feed uranium for each of these scenarios.

#### 4.4.2 1% growth scenarios

##### Enriched uranium

The trends observed in the 1% growth scenarios match the trends observed with the no growth scenarios that deploy the same reactor types (i.e., Scenarios 2 and 8), as shown in Figure 4.12 and Table 4.11. Scenario 11 requires the largest average mass of enriched uranium, and Scenario 8 requires the next largest average. Scenario 8 requires the largest average mass of HALEU, while Scenario 11 requires the least. Scenario 8 requires an average of 141.8 MT of HALEU per month, Scenario 9 requires the smallest monthly average of enriched uranium, because this scenario deploys the least number of reactors, and the Xe-100 requires the smallest mass of fuel in the core.

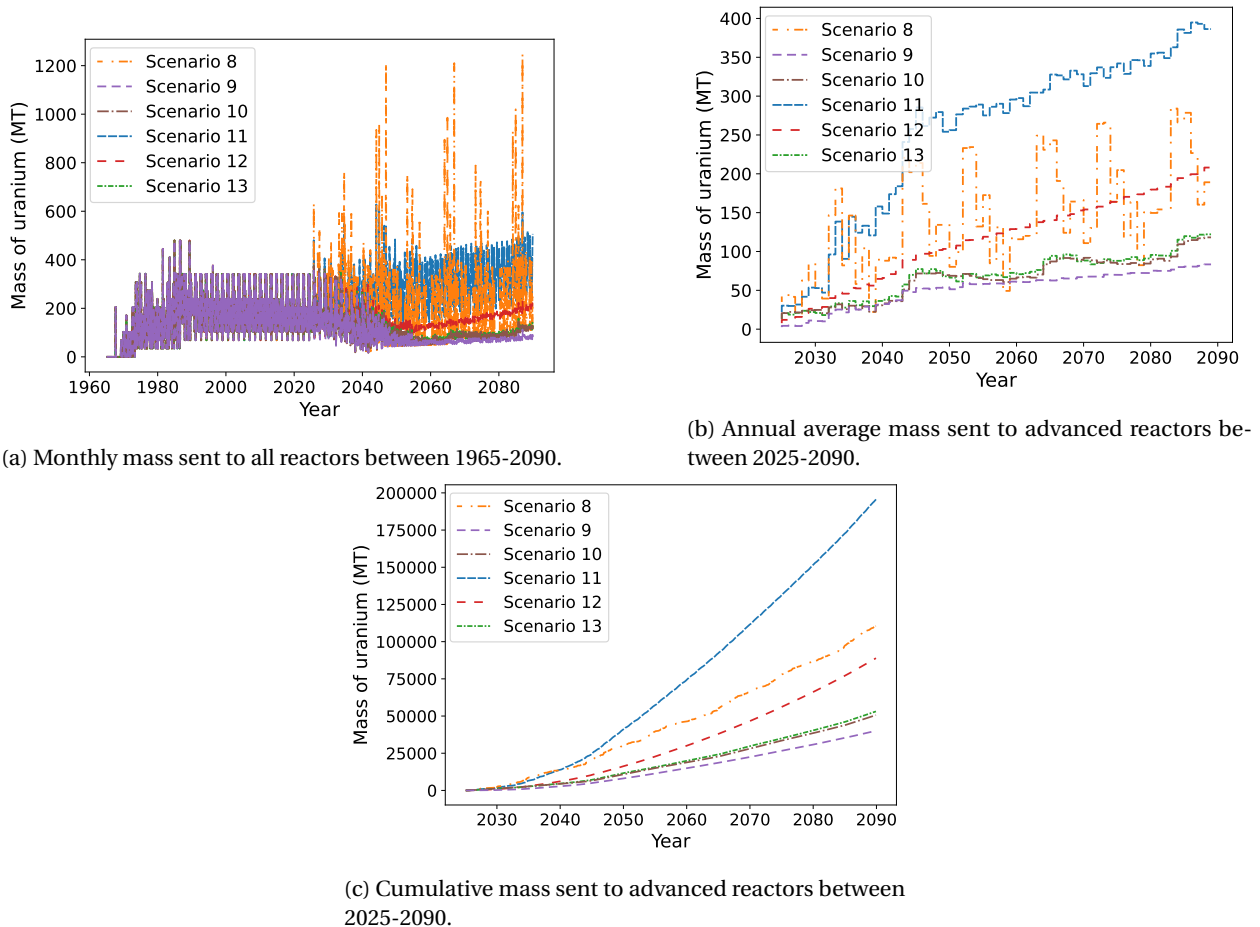


Figure 4.12: Mass of enriched uranium required by reactors in Scenarios 8-13.

Scenario 12 requires a larger monthly average mass of enriched uranium than Scenarios 9, 10, and 13. The no growth scenarios exhibit this result as well, but it is more pronounced in the 1% growth scenarios (comparing Figures 4.10 and 4.12). The more pronounced result in the 1% growth scenarios is a result of the difference in energy demand and the deployment scheme. Scenarios 6 and 12 deploy the Xe-100 and the VOYGR. The increase in energy

Table 4.11: Metrics for enriched uranium required by advanced reactors between 2025-2090 in Scenarios 8-13.

Scenario	Average (MT/month)	HALEU Average (MT/month)	Maximum (MT)	Cumulative (MT)
8	141.8	141.8	1,246	110,486
9	51.47	51.47	112.50	40,097
10	65.01	65.01	145.6	50,643
11	251.1	18.93	606.2	195,645
12	114.1	36.42	237.7	88,910
13	68.19	61.98	157.8	53,118

demand in Scenario 12 results in more VOYGRs deployed relative to the number of Xe-100s deployed. The VOYGR meeting more of the energy demand in Scenario 12 and the VOYGR requiring more enriched uranium than the Xe-100 lead to more enriched uranium needed for Scenario 12, relative to other scenarios that deploy Xe-100s.

The maximum mass of enriched uranium required in each scenario ranges between 2.2-8.8 times the average monthly mass, which is a smaller ratio than for the no growth scenarios. The increase between the average and the maximum is smaller for the 1% growth scenarios because the averages increase more than the maximums for the scenarios deploying the same reactors (e.g., between Scenarios 2 and 8). The cumulative mass of enriched uranium required has a similar pattern to the average mass; Scenario 11 requires the most mass, followed by Scenario 8. Scenario 9 requires the smallest cumulative mass. The advanced reactors in Scenario 11 require more enriched uranium than the LWRs, but the other scenarios require less than the LWRs.

### Feed uranium

The trends of the mass of feed uranium required by Scenarios 8-13 (Figure 4.13, Table 4.12) are consistent with trends of the feed requirements of the no growth scenarios. Scenario 8 requires the most feed uranium based on any of the metrics in Table 4.12, because of the larger number of reactors deployed than the other scenarios and all of the reactors deployed require HALEU. The larger product assay of HALEU, compared with the product assay for LWRs or VOYGRs, means that more feed uranium is needed to produce the same product mass (Eq. 2.1b). Scenario 11 requires the next largest amount of feed uranium, with most of the feed uranium used to produce enriched uranium for the VOYGRs. The other scenarios require similar monthly averages of feed uranium, with Scenario 9 requiring the least amount of feed uranium. The similarity in feed uranium required by Scenarios 9, 10, 12, and 13 is a result of the Xe-100 and VOYGR requiring similar feed uranium masses and the deployment scheme primarily deploying the Xe-100 and VOYGR in each of these scenarios. Scenarios 10, 11, and 13 require more feed uranium than Scenarios 9 and 12, because of the deployment of MMRs in Scenarios 10, 11, and 13 and the MMR requiring more feed uranium than the Xe-100 and VOYGR. To produce HALEU, Scenario 8 requires the most feed uranium and Scenario 11 requires the least.

The maximum feed uranium required varies between 2.2-8.8 times the monthly average of all feed uranium,

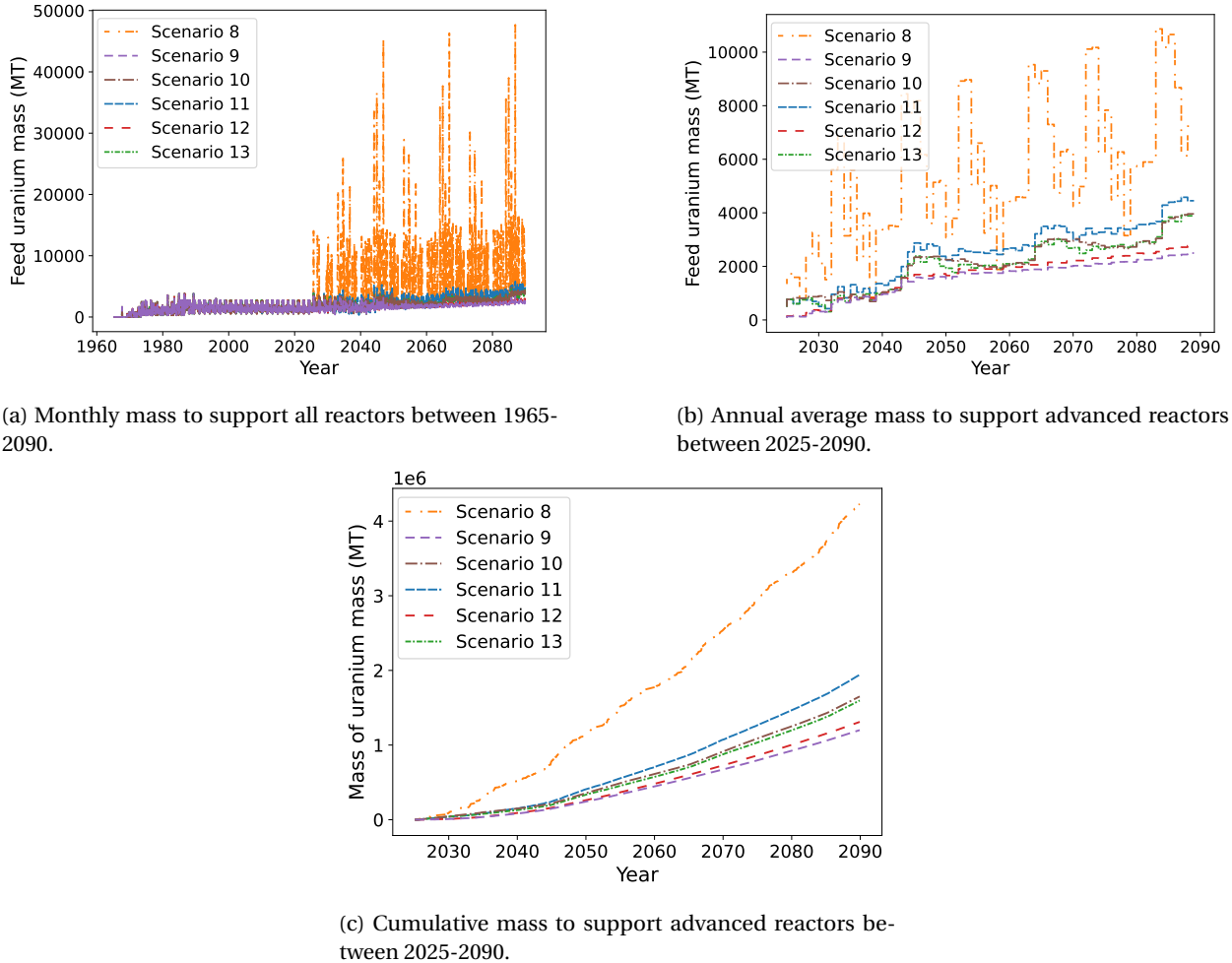


Figure 4.13: Mass of feed uranium required to produce enriched uranium at each time step in Scenarios 8-13.

Table 4.12: Metrics for feed uranium required by advanced reactors between 2025-2090 in Scenarios 8-13.

Scenario	Average (MT/month)	HALEU Average (MT/month)	Maximum (MT)	Cumulative (MT)
8	5,426	5,426	47,689	4,226,992
9	1,541	1,541	3,368	1,200,546
10	2,119	2,119	4,813	1,651,029
11	2,491	724.2	5,801	1,941,265
12	1,682	1,090	3,679	1,310,418
13	2,050	2,003	4,987	1,597,312

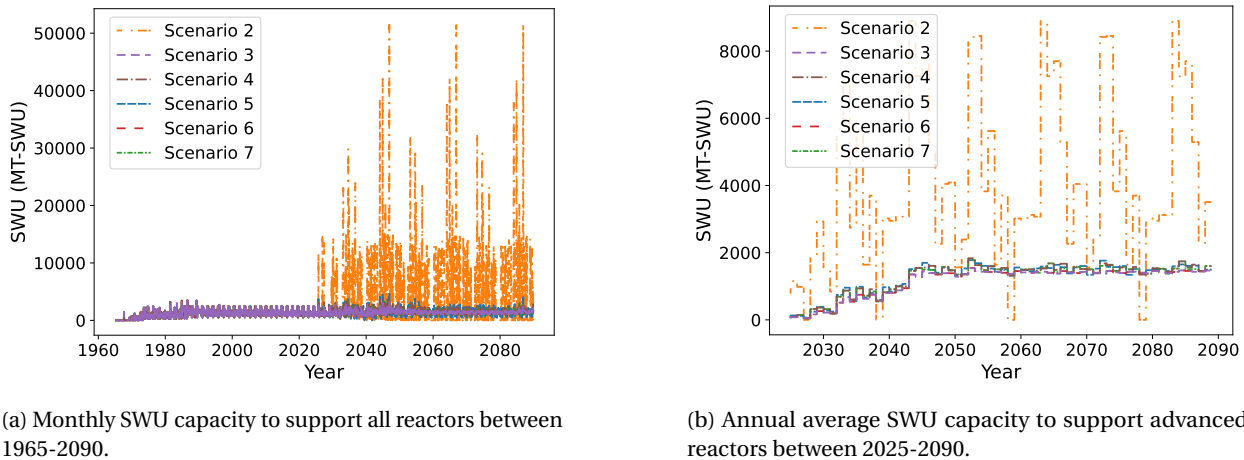
which is similar to the ratios of the maximum and average masses required for enriched uranium. Scenario 8 requires the largest maximum peak of feed uranium, corresponding to the deployment of 936 MMRs. Because of the large number of reactors and the large mass of feed uranium required in Scenario 8, the cumulative mass of feed uranium quickly diverges from the cumulative mass of the other scenarios after the transition start time.

## 4.5 SWU capacity

This section reports the results of the SWU capacity required to support the advanced reactors in the transition scenarios. The SWU requirements were calculated using Eq. 2.1, the mass of enriched uranium, the feed uranium required, and the assay of each material stream (feed, tails, and product) in each scenario. This metric relates to the facility capacity and design required to enrich natural uranium and produce enriched uranium for each scenario. Understanding this metric, and specifically how much SWU capacity is required to produce HALEU is vital to developing infrastructure to produce HALEU. Unless specified as SWU capacity to produce HALEU, the reported SWU capacities are required to produce any enriched uranium less than 20%  $^{235}\text{U}$ .

### 4.5.1 No growth scenarios

The SWU capacity required to produce the enriched uranium for the no growth scenarios follows a similar pattern as the feed uranium required by each scenario (Figure 4.14, Table 4.13). Scenario 2 requires the largest average monthly capacity, average monthly capacity to produce HALEU, and maximum capacity needed. Scenario 3 requires the smallest average for the total SWU capacity, and Scenario 5 requires the smallest average SWU capacity to produce HALEU. Scenario 3 requires the least SWU capacity because it only deploys Xe-100s, which require the smallest SWU capacity to produce a core-load of fuel. Scenario 6 requires a very similar SWU capacity to support all of the advanced reactors because the Xe-100 and VOYGR (which are both deployed in Scenario 6) require similar SWU capacity. The increased product assay required by the Xe-100, compared with the VOYGR, evens out with the decrease in product mass to result in similar SWU requirements to produce enriched uranium for these two reactors. Scenario 2 requires a larger average SWU capacity than the LWRs before 2025 because of the greater product assay required by the MMR.



(a) Monthly SWU capacity to support all reactors between 1965-2090.

(b) Annual average SWU capacity to support advanced reactors between 2025-2090.

Figure 4.14: SWU capacity required to produce enriched uranium for reactors in Scenarios 2-7.

Table 4.13: Metrics for SWU capacity to enrich uranium for advanced reactors between 2025-2090 in Scenarios 2-7.

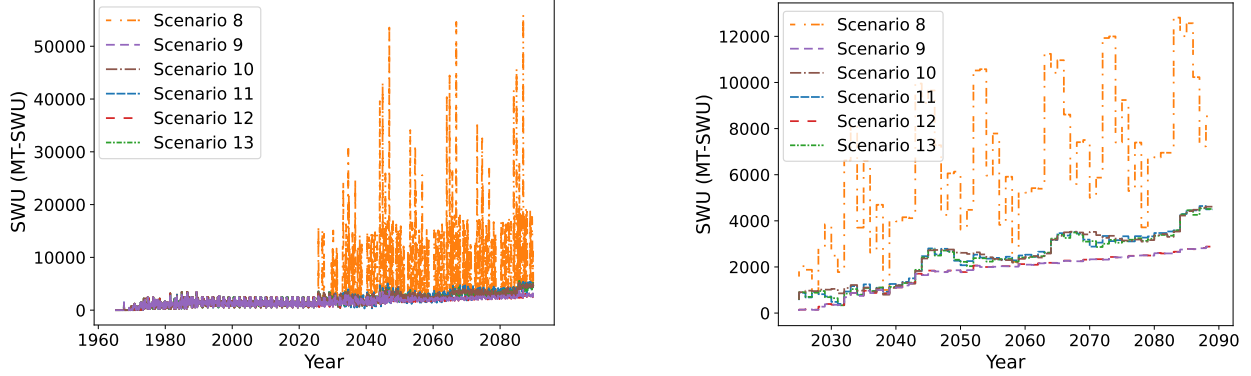
Scenario	Average (MT-SWU/month)	Average for HALEU (MT-SWU/month)	Maximum (MT-SWU)
2	3,978	3,978	51,433
3	1,136	1,136	3,119
4	1,238	1,238	3,360
5	1,246	144.3	4,550
6	1,137	1,058	3,149
7	1,224	1,218	3,360

The SWU capacity required to produce HALEU decreases when deploying the VOYGR along with the other reactors, with the exception of deploying the VOYGR with both HALEU-fueled reactors, as noted with the feed uranium requirements. Scenario 5 requires the least SWU capacity to produce HALEU because most of the enriched uranium in this scenario is for VOYGRs which don't require HALEU. However, this scenario requires a similar average SWU capacity as most of the other scenarios because of the off-setting effect of the increase in product mass and decrease in product assay between the Xe-100 and VOYGR.

The maximum SWU capacity required to meet enriched uranium demand varies between 2.7-12.9 times the monthly average for all SWU. The magnitude differences between the average and the maximum pose potential problems for facility design and nonproliferation safeguards. Facilities will likely need to be built at a capacity greater than the average monthly requirement in order to produce enough enriched uranium to meet the peak demands. However, such a design may result in idle enrichment capacity during time periods in which the additional capacity is not needed to meet peaks, which poses a proliferation risk. Additionally, the SWU requirements reported here do not account for different centrifuge cascade designs required to produce enriched uranium for each advanced reactor. Cascade designs will differ based on the amount of material needed (more material means more centrifuges in parallel) and the product assay (higher product assay means more stages), and understanding how to establish the cascades to support these transition scenarios would require additional exploration.

#### 4.5.2 1% growth scenarios

The SWU capacity required to meet the enriched uranium demand of the 1% growth scenarios follows similar patterns as the SWU capacity required in the no growth scenarios (Figure 4.15, Table 4.14). Scenario 8 requires the largest average SWU capacity and the largest SWU capacity to create HALEU, Scenario 9 requires the smallest average SWU capacity to enrich uranium for all advanced reactors, and Scenario 11 requires the smallest average SWU capacity to create HALEU. Comparing the monthly average capacity and the monthly average capacity to produce HALEU shows that most or all of the SWU capacity needed is to produce HALEU, except in Scenario 11. The maximum SWU capacity required ranges between 2.2-8.9 times the average SWU capacity required by each scenario. All of these scenarios require more SWU capacity than the LWRs before 2025.



(a) Monthly SWU capacity to support all reactors between 1965-2090.

(b) Annual average SWU capacity to support advanced reactors between 2025-2090.

Figure 4.15: SWU capacity required to produce enriched uranium for reactors in Scenarios 8-13.

Table 4.14: Metrics for SWU capacity to enrich uranium for advanced reactors between 2025-2090 in Scenarios 8-13.

Scenario	Average (t-SWU/month)	Average for HALEU (t-SWU/month)	Maximum (t-SWU)
8	6,339	6,339	56,239
9	1,774	1,774	3,878
10	2,462	2,462	5,600
11	2,421	854.1	5,605
12	1,780	1,256	3,926
13	2,367	2,325	5,784

Scenarios 9 and 12 require very similar SWU capacities, and Scenarios 10, 11, and 13 require similar SWU capacities. The feed uranium requirements had the same scenario groupings. The difference between these scenario groupings is the deployment of MMRs; Scenarios 9 and 12 do not deploy MMRs but Scenarios 10, 11, and 13 deploy MMRs. Producing enriched uranium for the MMR requires more SWU capacity than providing enriched uranium for the Xe-100 and VOYGR, with the Xe-100 and VOYGR requiring similar SWU capacities. Combined with the inflated number of MMRs deployed as a result of the deployment scheme, Scenarios 10, 11, and 13 require more SWU capacity to produce all enriched uranium for advanced reactors by 2090 than Scenarios 9 and 12.

## 4.6 Used nuclear fuel

The final metric of interest for the once-through transition scenarios is the amount of UNF that must be disposed of. UNF produced in a NFC has implications on the options to treat and store the waste. A once-through fuel cycle will dispose of all of the UNF discharged from the reactors, although the timing is affected by the duration in wet storage. The masses reported here are the masses discharged from the reactors, which matches the capacity needs for disposal in a dry storage system or a geologic repository, but not necessarily the timing of the disposal. The masses presented here are the masses of all materials in the UNF, not just the uranium discharged, because all

materials in the UNF must be disposed of. UNF characteristics other than mass will affect repository and material handling needs, such as decay heat, UNF volume, and criticality safety. However, reporting the mass of UNF is common in fuel cycle analysis [15, 44, 53], which lead to the use of reporting the UNF mass in this work.

#### 4.6.1 No growth scenarios

The magnitude of discharged UNF from the advanced reactors (Figure 4.16) follows the same pattern as the enriched uranium masses, but with delayed timing. This pattern matches expectations, but the values are different from the masses of enriched uranium. This difference arises for two reasons: first, the UNF masses include any carbon or oxygen in the fuel forms (UCO and UO<sub>2</sub>), which are not included in the enriched uranium masses; second, the fuel in the reactors at the end of the simulation are not included in these calculations because they are not traded to the cooling pool facility. Scenario 5 experiences the largest average mass of UNF discharged but the smallest average mass of UNF discharged from HALEU-fueled reactors. Scenario 3 discharges the smallest average and cumulative mass of UNF. These trends are consistent with the mass of enriched uranium required in each scenario and the design characteristics of the advanced reactors deployed in each scenario. For example, Scenario 5 discharges the largest average mass of UNF because it primarily deploys VOYGRs, which have a lower specific power than the Xe-100 and require more fuel per unit power than the Xe-100 and MMR. The average mass of UNF discharged by advanced reactors is less than the average discharged by LWRs before 2025.

Table 4.15: Metrics for waste discharged from advanced reactors between 2025-2090 in Scenarios 2-7. The “Average HALEU” is the average mass of UNF from HALEU-fueled reactors.

Scenario	Average (MT/month)	Average HALEU (MT/month)	Maximum (MT)	Cumulative (MT)
2	66.19	66.19	1,293	51,560
3	34.29	34.29	68.13	26,712
4	35.44	35.44	83.37	27,605
5	159.2	2.395	406.3	124,016
6	43.14	31.93	82.71	33,608
7	35.95	35.10	83.37	28,008

The first UNF discharged from advanced reactors is in June 2030 for Scenarios 3, 4, 6, and 7, June 2031 in Scenario 5, and December 2049 in Scenario 2. The differences in timing of first UNF discharge from advanced reactors is a result of the refueling scheme of each type of reactor. Xe-100s, deployed in Scenarios 3, 4, 6, and 7, utilize online refueling and discharge UNF every 7 months, which results in the first discharge soon after their initial deployment. VOYGRs, deployed in Scenarios 4, 5, 6, and 7, have an 18-month refueling cycle, so the first UNF discharge for these reactors occurs 18 months after deployment. MMRs, deployed in Scenarios 2, 4, 5, and 7, do not undergo refueling, so the first UNF discharge occurs 20 years after first deployment. The shortest refueling time of the reactors deployed in a scenario governs when first UNF discharge in that scenario. Thus, the Xe-100 drives the

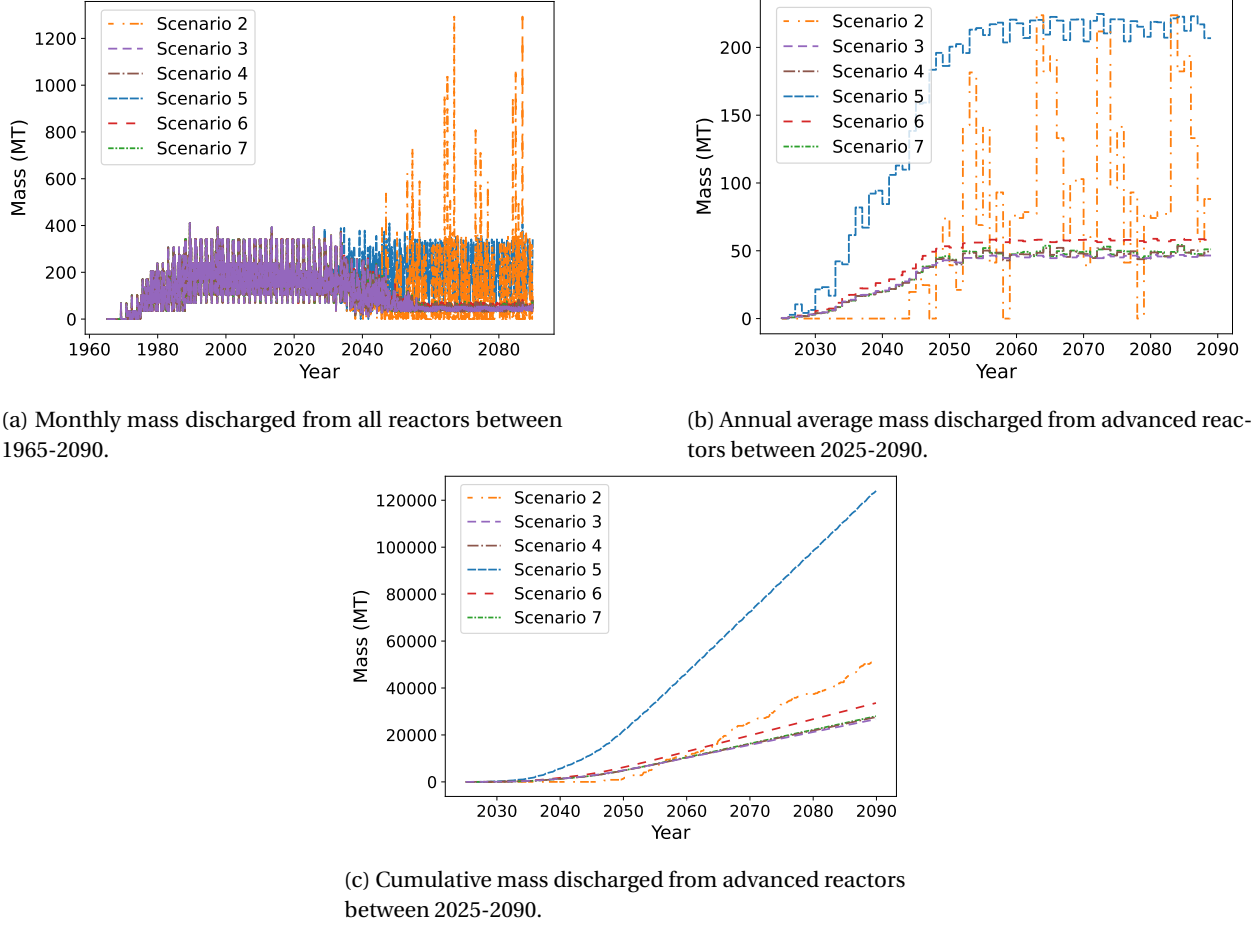


Figure 4.16: Mass of fuel discharged from reactors as a function of time for Scenarios 2-7.

first UNF discharge in Scenarios 3, 4, 6, and 7, the VOYGR drives the first UNF discharge in Scenario 5, and the MMR drives the first UNF discharge in Scenario 2.

The advanced reactors in all of the scenarios discharge less UNF than the LWRs. The 1982 Nuclear Waste Policy Act [115] requires an initial repository in the US to have a capacity of 70,000 MTHM. Based on this capacity, a geologic repository could store all of the waste produced from advanced reactors except for Scenario 5. To store all of the waste from advanced reactors in Scenario 5, either the repository capacity would need to be expanded or a second repository must be sited.

#### 4.6.2 1% growth scenarios

For the 1% growth scenarios, similar patterns are observed to the no growth scenarios. Scenario 11 discharges the largest average mass of UNF while also discharging the smallest average mass of UNF from HALEU-fueled reactors, as shown by Figure 4.17 and Table 4.16. Scenario 9 discharges the smallest average mass of UNF. The first UNF

discharge is in November 2027 in Scenarios 9, 10, 12, and 13, in November 2028 in Scenario 11, and May 2047 in Scenario 8. These initial disposal dates are consistent with the shortest cycle time of the reactors deployed in each scenario (20 years in Scenario 8, 18 months in Scenario 11, and 6 month in Scenarios 9, 10, 12, and 13) and an initial deployment in May 2027.

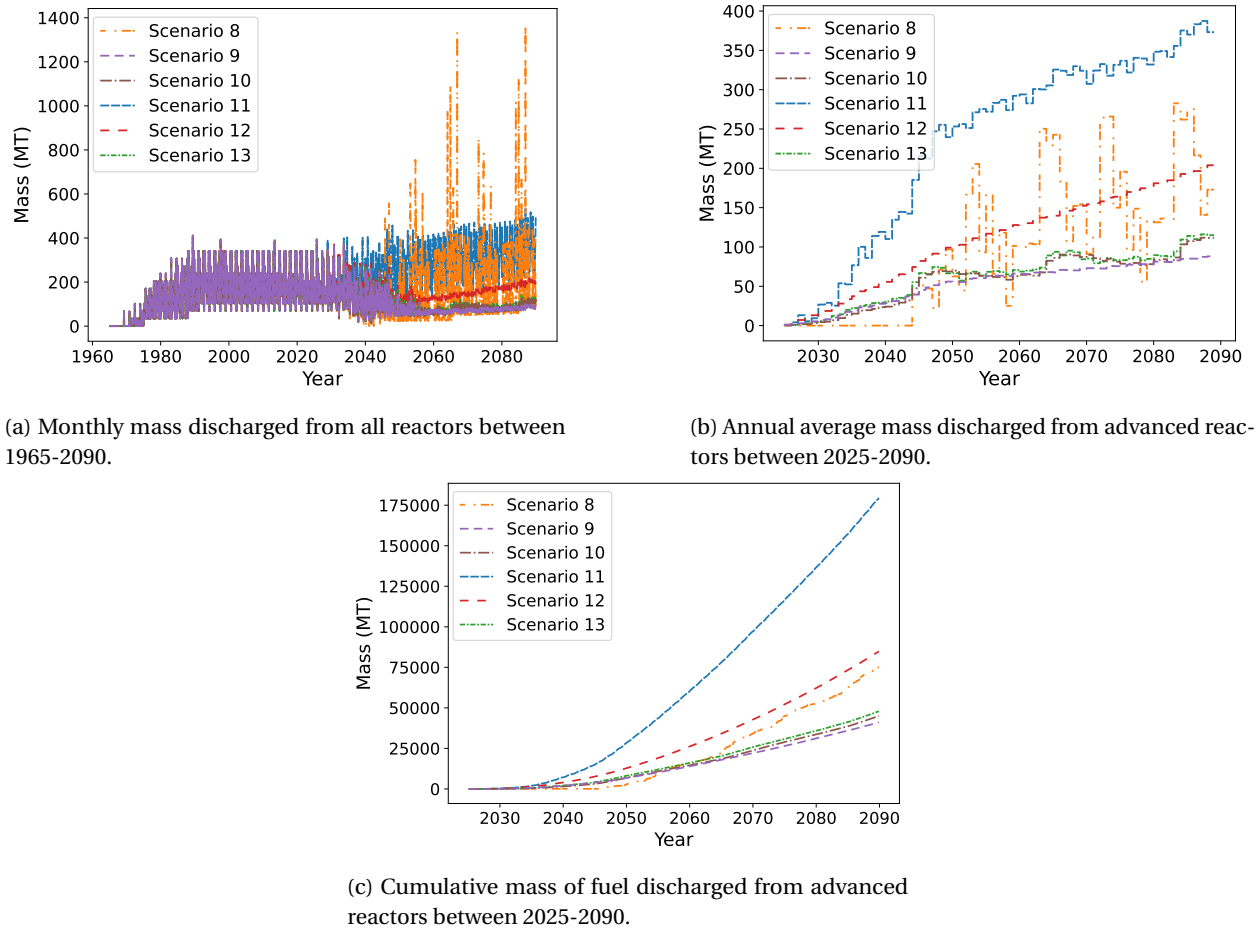


Figure 4.17: Mass of fuel discharged from reactors as a function of time for Scenarios 8-13.

Table 4.16: Metrics for waste discharged from advanced reactors between 2025-2090 in Scenarios 8-13. The “Average HALEU” is the average mass of UNF from HALEU-fueled reactors.

Scenario	Average (MT/month)	Average of HALEU (MT/month)	Maximum (MT)	Cumulative (MT)
8	96.39	96.39	1,373	75,085
9	52.67	52.67	108.9	41,026
10	57.79	57.79	133.6	45,014
11	230.5	10.56	533.1	179,534
12	109.0	37.57	226.9	84,880
13	61.47	55.45	145.0	47,884

Based on the cumulative masses, the proposed 70,000 MTHM capacity of a geologic repository in the US would

only store the UNF discharged from advanced reactors in Scenarios 8, 9, 10, and 13. Additional repositories or an expanded capacity of the repository would be required to dispose of the waste from Scenarios 11 and 12. The cumulative UNF discharged from advanced reactors is less than the cumulative mass discharged from the LWRs in all scenarios except Scenario 11. Scenario 11 discharges more UNF because of the large number of VOYGRs it deploys to meet the increasing energy demand.

# **Chapter 5**

## **Recycling transition results**

This chapter reports the results for the recycle fuel cycle scenarios (Scenarios 14-19) described in Section 3.3. The primary results considered for these fuel cycle transitions are the uranium resources needed, the SWU capacity required, the separated plutonium masses, and the mass of disposed material. This chapter does not focus on the number of reactors or the energy supplied by the reactors because most of the scenarios use the same deployment scheme as Scenarios 7 or 13 (depending on the energy demand curve of the scenario). For the two scenarios that deploy the SFR instead of the other advanced reactors (Scenarios 16 and 19), the maximum number of SFRs deployed in each scenario is 312 and 595, respectively. These scenarios require far fewer reactors than the other scenarios because the SFR has a larger power output than the other advanced reactors (311 MWe compared with 80 MWe for the Xe-100).

We model most of the advanced reactors (the Xe-100, VOYGR, and SFR) using the OpenMCyclus archetype (Section 3.5). This archetype provides the dynamic fuel depletion on a per cycle basis for this work, increasing the accuracy of the used fuel compositions and the amount of plutonium-based fuel that can be produced and used to fuel the advanced reactors.

### **5.1 Uranium resources**

We divide the uranium resources described here into two primary components: the heavy metal mass and the natural uranium required to produce fuel. We further divide the heavy metal mass into two parts: the enriched uranium and the heavy metals in plutonium-based fuel (MOX or U/TRU fuel). Enriched uranium is in the HALEU, UOX, and UCO fuels. Heavy metals in plutonium-based fuels include the natural uranium, plutonium, and transuranic elements in the MOX and U/TRU fuels. We separate these metrics because of the different processes and resources needed to produce each fuel type. We also divide the natural uranium masses into two parts: the feed uranium to produce enriched uranium and the natural uranium required to produce plutonium-based fuel. Dividing this metric provides more details on the resources needed to support these fuel cycles.

### **5.1.1 No growth scenarios**

This section presents the results of the uranium resources required in the no growth, closed fuel cycle scenarios (Scenarios 14-16). We divide these results into the heavy metal masses (enriched uranium and heavy metals in plutonium-based fuel) and the natural uranium masses (feed uranium and natural uranium to produce plutonium-based fuels). We compare each of these material requirements based on monthly averages, maximum values, and cumulative masses. We also compare the enriched uranium and feed uranium masses based on the monthly average for HALEU.

#### **Heavy metal masses**

Figure 5.1 shows the mass of enriched uranium required by Scenarios 14-16. Scenario 15 requires the most enriched uranium, followed by Scenario 14, then Scenario 16. Scenario 15 requires the most enriched uranium because less material is available for reprocessing (no TRISO used fuel gets reprocessed), leading to less separated plutonium and less plutonium-based fuel available. The advanced reactors in these scenarios prefer plutonium-based fuel over uranium-based fuel, meaning that they will accept as much plutonium-based fuel that is available. Therefore, a larger supply of plutonium-based fuel means than less uranium-based fuel is needed to support these reactors. The annual average mass of enriched uranium (Figure 5.1b) in Scenarios 14 and 15 increases in 2043 because the plutonium-based fuel stockpiled up from reprocessed LWR UNF is used up and there is not as much plutonium from the advanced reactor UNF to produce more plutonium-based fuel.

Scenario 16 does not require any uranium-based fuel to support the advanced reactors. This result stems from a few key differences between Scenario 16 and the other no growth closed fuel cycle scenarios. The first difference is that all of the advanced reactors in Scenario 16 can accept reprocessed fuel, while the MMRs in Scenarios 14 and 15 will only accept UOX. This modeling decision for the MMR means that any fuel cycle that deploys the MMR will always require some amount of uranium-based fuel. Therefore, the lack of MMR deployment in Scenario 16 allows the possibility for this scenario to not require enriched uranium if there is enough plutonium-based fuel to fuel the advanced reactors. The second difference is the reprocessing scheme. In Scenario 16, the used fuel can be reprocessed an infinite number of times while in Scenarios 14 and 15 the used uranium-based fuel can only be reprocessed once and the plutonium-based fuel can not be reprocessed. This difference is inherent to the type of fuel cycle (limited vs. continuous recycle), and increases the amount of UNF available for reprocessing. Additionally, the reprocessing step in Scenario 16 removes the uranium, neptunium, plutonium, and americium from the used fuel, compared with only plutonium being separated out in Scenarios 14 and 15. Allowing more material to be separated out of the UNF in Scenario 16 leads to more separated actinide material to create the plutonium-based fuel.

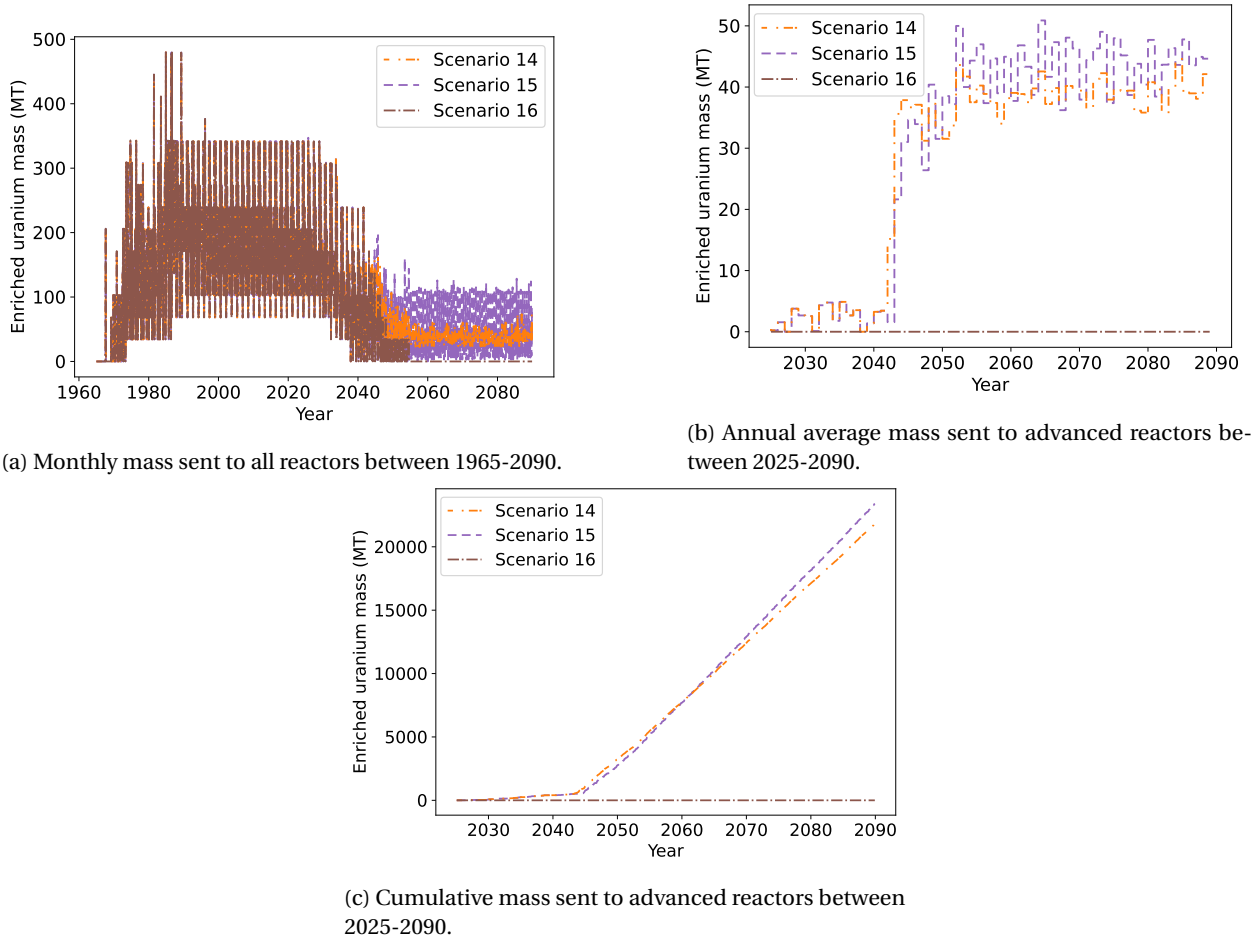


Figure 5.1: Mass of enriched uranium required by reactors in Scenarios 14-16.

Table 5.1 reports the average enriched uranium mass, average HALEU mass, maximum enriched uranium mass, and cumulative enriched uranium mass required in Scenarios 14-16. Scenario 14 requires less enriched uranium than Scenario 7, despite having the same advanced reactor deployment schedule, because of the change in the fuel cycle. By reprocessing used fuel, the average HALEU mass required drops by 21.3%. A similar decrease in cumulative HALEU needs is seen in Scenario 15. However, the removal of TRISO reprocessing results in a smaller decrease (15.1% decrease). By reprocessing the TRISO-based fuels in Scenario 14, the reactors in this scenario needs 6.35% less cumulative enriched uranium than the reactors in Scenario 15.

Table 5.1: Metrics for enriched uranium required to fuel reactors in Scenarios 14-16.

Scenario	Average (MT/month)	HALEU Average (MT/month)	Maximum (MT)	Cumulative (MT)
14	28.01	27.16	87.01	21,920
15	30.05	29.20	143.8	23,407
16	0	0	0	0

Scenarios 14, 15, and 16 require a cumulative enriched uranium mass of 3,162 MT, 2,667 MT, and 0 MT,

respectively, by 2050. These values are smaller than the needs of the once-through fuel cycles (Table 4.9) and the estimated 5,350 MT in a once-through fuel cycle from Dixon et al. [8]. The closed fuel cycle scenarios require less HALEU than the once-through fuel cycles because of the inclusion of reprocessing and use of plutonium-based fuel in the advanced reactors.

In addition to the enriched uranium, the advanced reactors receive heavy metals for the plutonium-based fuels. Figure 5.2 shows that Scenario 16 requires more plutonium-based fuel than the other scenarios. This result is consistent with the reactors in Scenarios 16 not receiving any enriched uranium. Scenario 14 uses the next largest mass of heavy metals for plutonium-based fuel, followed by Scenario 15.

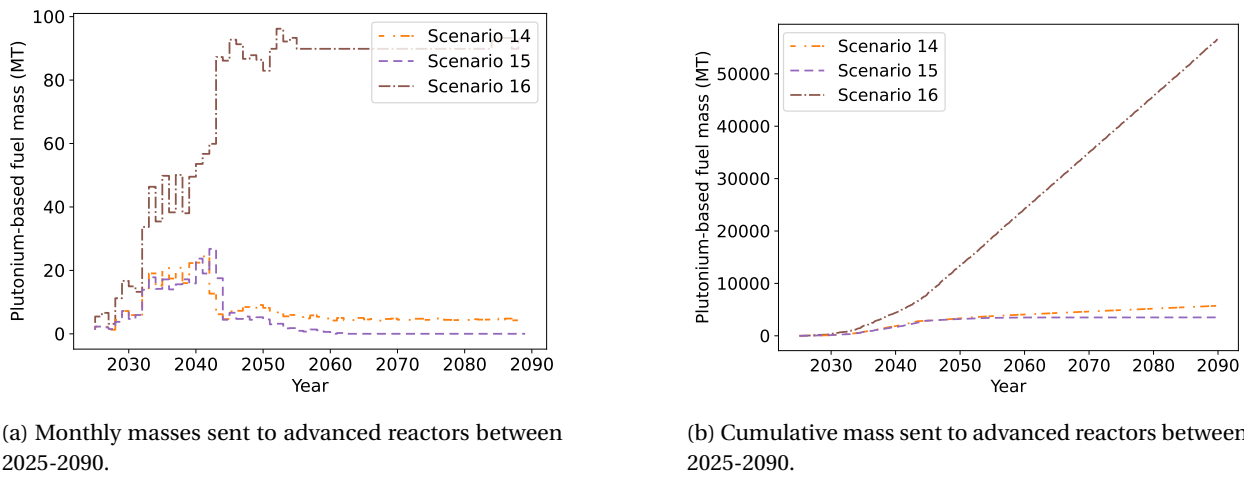


Figure 5.2: Mass of plutonium-based fuel required by reactors in Scenarios 14-16.

As Table 5.2 reports, the average and cumulative masses of plutonium-based fuel heavy metals in Scenario 16 are an order of magnitude greater than the masses in Scenario 14-15. This large difference is a result of the different reprocessing schemes, as previously described. Scenario 16 needs a monthly average of plutonium-based fuel heavy metal that is more than the maximum mass needed in Scenario 14. More heavy metal for plutonium-based fuel is sent to advanced reactors in Scenario 14 than in Scenario 15 because the reprocessing of TRISO fuel in Scenario 14 increases the availability of plutonium-based fuel. The heavy metals for plutonium fuels in Scenarios 14 and 15 show a decrease in 2043, corresponding to the increase in enriched uranium sent to reactors in these scenarios. After the initial stock of plutonium-based fuel from LWR used fuel is used in Scenarios 14 and 15, these scenarios use an average of 5.26 MT/month and 1.49 MT/month of plutonium-based fuel, respectively. These values are both smaller than the average values reported in Table 5.2, highlighting the importance of a stockpile of plutonium-based fuel from LWR used fuel in providing plutonium-based fuel for advanced reactors in these fuel cycles.

When comparing the total cumulative mass of heavy metal (enriched uranium and heavy metal in plutonium-based fuel) required by each scenario, Scenario 16 needs the most material of these three scenarios. This result

Table 5.2: Metrics for plutonium-based fuels required to fuel reactors in Scenarios 14-16.

Scenario	Average (MT/month)	Maximum (MT)	Cumulative (MT)
14	7.351	53.81	5,727
15	4.506	81.59	3,510
16	72.70	241.9	56,630

stems from the different discharge burnups of the reactors. The SFR has a burnup of 87.51 MWd/kg HM and the Xe-100 (the reactor that meets most of the demand in Scenarios 14 and 15) has a burnup of 168 MWd/kg U. The Xe-100 gets more energy out the fuel per unit mass, which leads to Scenarios 14 and 15 requiring less fuel than Scenario 16. Scenario 16 is most similar to Scenario 2 in the amount of heavy metals required, because the SFR and MMR have similar discharge burnups (87.51 MWd/kg compared with 82.6 MWd/kg).

### Natural uranium

Figure 5.3 shows the natural uranium required as feed uranium to produce enriched uranium fuel for advanced reactors in Scenarios 14-16. Scenario 15 requires the most feed uranium, followed by Scenarios 14 and 16. This pattern follows with the enriched uranium mass in each scenario, because the enriched uranium mass dictates the amount of feed uranium needed. Scenario 15 requires the most feed mass because less UNF is available for reprocessing, leading to more enriched uranium required. Scenario 16 does not require any feed uranium because it does not require any enriched uranium.

Table 5.3 reports the metrics for the feed uranium required in Scenarios 14-16. The cumulative feed uranium needed in Scenarios 14 and 15 are both less than the cumulative feed uranium needed in Scenario 7. The decrease in feed uranium needed demonstrates how using a closed fuel cycle can reduce the feed uranium needs in addition to reducing the fuel mass needs.

Table 5.3: Metrics for feed uranium required to produce uranium-based fuels in Scenarios 14-16.

Scenario	Average (MT/month)	HALEU Average (MT/month)	Maximum (MT)	Cumulative (MT)
14	842.9	836.4	2,628	656,582
15	903.9	897.4	4,450	704,106
16	0	0	0	0

Next, Figure 5.4 shows the natural uranium required for the plutonium-based fuels in Scenarios 14-16. These results follow the same pattern as the heavy metal for plutonium-based fuels in these scenarios (Figure 5.2). However, the natural uranium mass is less than the total heavy metal mass, because the uranium is only a part of the total heavy metal mass in plutonium-based fuel. Scenario 16 requires the most natural uranium because the reactors in this scenario only receive the U/TRU fuel. Scenario 15 requires the least natural uranium, because this scenario results in the least plutonium-based fuel.

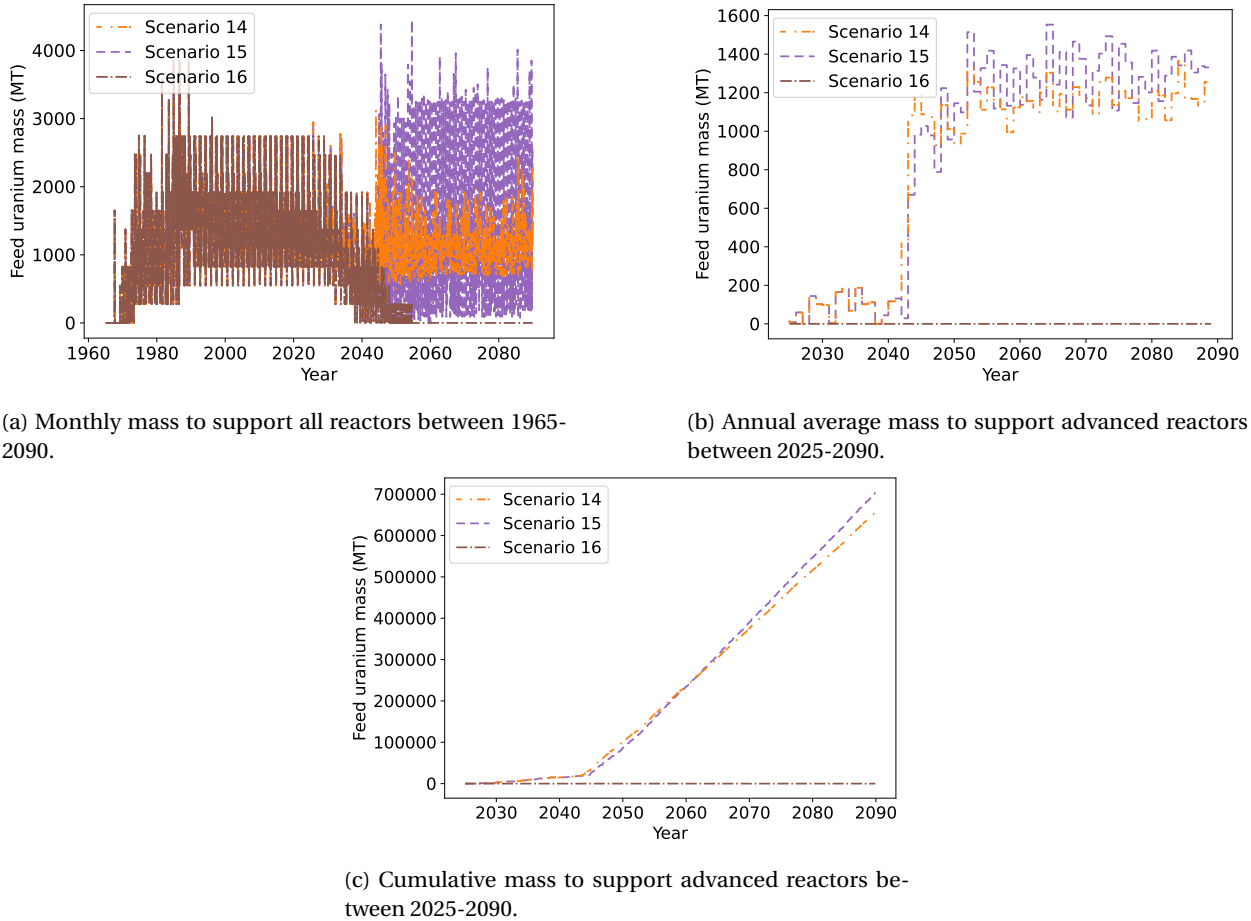


Figure 5.3: Mass of feed uranium required by reactors in Scenarios 14-16.

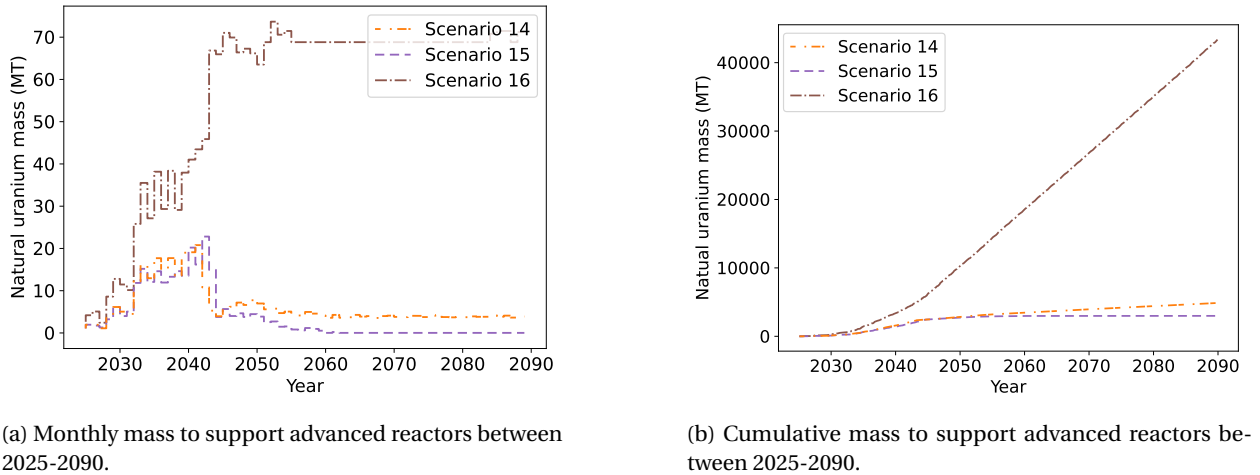


Figure 5.4: Mass of natural uranium for plutonium-based fuel required by reactors in Scenarios 14-16.

Table 5.4 reports the metrics for the natural uranium required for Scenarios 14-16. The metrics for Scenario 16 are one order of magnitude greater than the metrics for Scenarios 14-15, the same as the metrics of the plutonium-

based fuel heavy metal. The cumulative natural uranium mass needed by Scenario 16 is more than one order of magnitude smaller than the cumulative feed uranium masses in Scenarios 14 and 15, because of the difference in process losses in each use of natural uranium. Using natural uranium as fill material in plutonium-based fuel has relatively small process losses because the material is used in its direct form. However, using natural uranium as feed for enrichment has large material losses (referred to as the tails material stream) because of the low enrichment of natural uranium (0.711%). Based on Eq. 2.1, the process losses increase with increased product mass demand and with increased product assay. The different masses of natural uranium for use in plutonium-based fuel and for enrichment suggests that fuel cycle that maximizes the amount of plutonium-based fuel and minimizes the amount of enriched uranium required helps to minimize natural uranium requirements.

Table 5.4: Metrics for natural uranium required to produce plutonium-based fuels in Scenarios 14-16.

Scenario	Average (MT/month)	Maximum (MT)	Cumulative (MT)
14	6.256	45.80	4,874
15	3.835	69.44	2,987
16	55.68	185.3	43,372

### 5.1.2 1% growth scenarios

This section presents the results of the uranium resources required in the 1% growth, closed fuel cycle scenarios (Scenarios 17-19). We divide these results into the fuel masses (enriched uranium and heavy metals in plutonium-based fuel) and the natural uranium masses (feed uranium and natural uranium to produce plutonium-based fuels).

#### Fuel masses

The first fuel mass considered is the enriched uranium mass, shown in Figure 5.5. These results show the same pattern as this metric for the no growth scenarios: Scenario 18 requires the most enriched uranium and Scenario 19 does not require any enriched uranium. In Scenarios 17 and 18 the increase in enriched uranium need occurs closer to 2040 and is a more gradual increase than the observed increase in Scenarios 14-15. These results stem from differences in the growth in energy demand, and subsequent differences in reactor deployment, leading to the stockpile of plutonium-based fuel from LWR UNF to be used up sooner. The differences in energy demand and reactor deployment lead to different proportions of the advanced reactors, specifically the artificially inflated number of MMR deployed in these scenarios described in Section 4.3.2. These differences lead to the more gradual increase in the enriched uranium needs because of the slow increase in the number of MMRs deployed.

Table 5.5 reports the metrics for the enriched uranium masses for Scenarios 17-19. The cumulative enriched

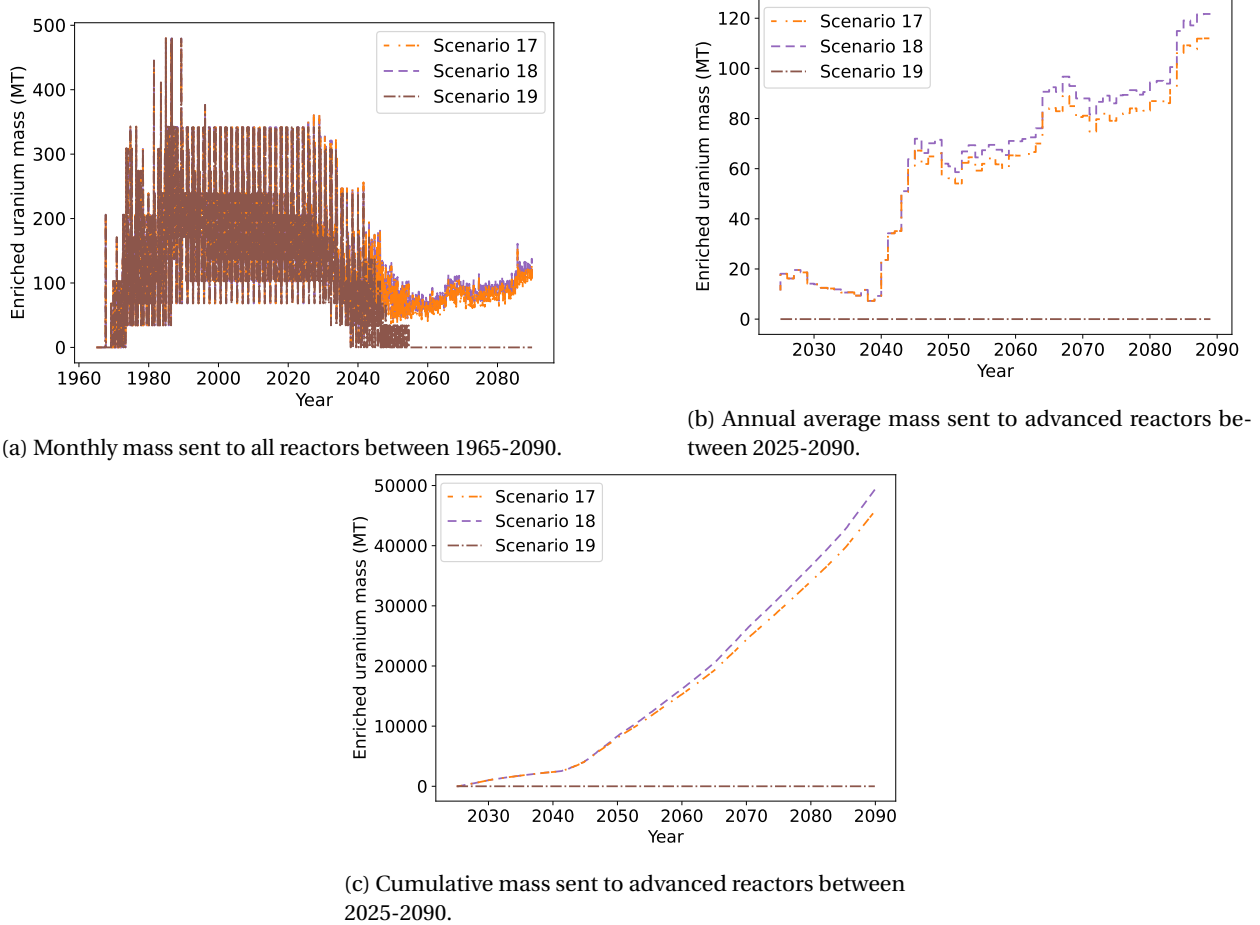


Figure 5.5: Mass of enriched uranium required by reactors in Scenarios 17-19.

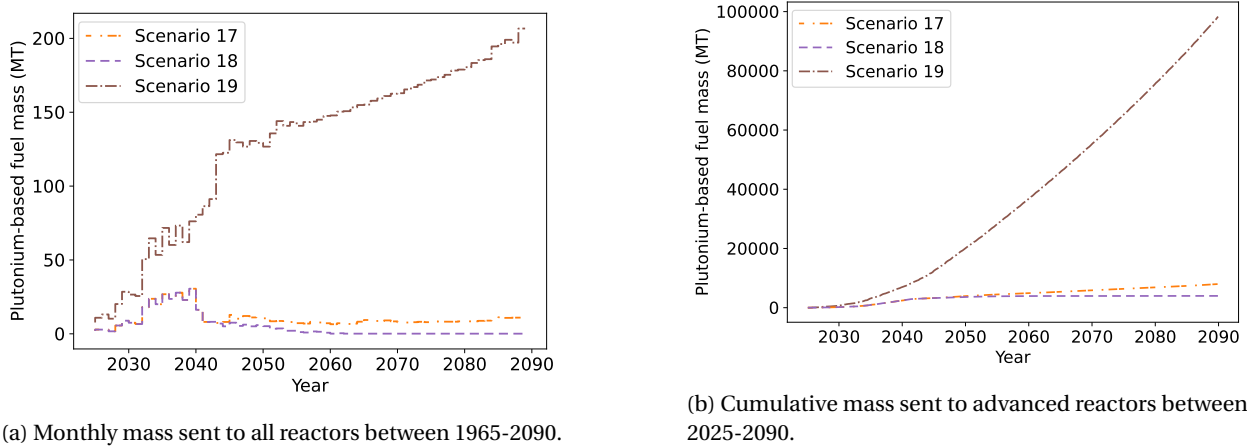
uranium in Scenarios 17 and 18 are less than the cumulative enriched uranium required by Scenario 13. However, the cumulative mass for Scenario 18 is larger than the cumulative in Scenario 9. These results highlight how reprocessing can reduce enriched uranium needs, but the reactors deployed and their fuel usage is still an important factor in how much enriched uranium is needed.

Table 5.5: Metrics of enriched uranium fuel between 2025-2090 in Scenarios 17-19.

Scenario	Average (MT/month)	Average HALEU (MT/month)	Maximum (MT)	Cumulative (MT)
17	58.72	52.81	152.2	45,742
18	63.32	57.42	160.9	49,329
19	0	0	0	0

Next is the mass of plutonium-based fuels sent to the advanced reactors in Scenarios 17-19, shown in Figure 5.6. Similar to the patterns of the no growth scenarios, Scenario 19 requires the most plutonium-based fuel of the three scenarios and Scenario 17 requires more than Scenario 18. Scenarios 17 and 18 show the initial stockpile of plutonium-based fuel from LWR UNF that gets used by 2040. The plutonium-based fuel mass in Scenario 18

drops to near zero after 2060, because all of the used fuel from the LWRs has been processed and used to create plutonium-based fuel, and there are so few VOYGRs (the only advanced reactor used fuel reprocessed in this scenario) to produce more separated plutonium and more MOX. The differences in the plutonium-based fuel heavy metal masses in these three scenarios is primarily a function of the reprocessing scheme of each scenario.



(a) Monthly mass sent to all reactors between 1965-2090.

(b) Cumulative mass sent to advanced reactors between 2025-2090.

Figure 5.6: Masses of heavy metal in plutonium-based fuel sent to advanced reactors in Scenarios 17-19.

Table 5.6 reports the metrics for the heavy metals in plutonium-based fuels required in Scenarios 17-19. Scenario 19 uses the largest heavy metal mass, followed by Scenario 17, then 18. Scenario 19 requires more total heavy metal (in enriched uranium and plutonium-based fuels) than Scenarios 17 and 18, as well as Scenarios 9, 10, 12, and 13. Scenario 19 uses the most similar cumulative mass of heavy metal as Scenario 8, because the MMR and SFR have the most similar burnups of the advanced reactors considered. However, Scenario 19 requires less heavy metal than Scenario 8 because the SFR has a higher burnup than the MMR. These results emphasize how the reactors deployed play an important role in determining how much fuel is required for a fuel cycle.

Table 5.6: Metrics of plutonium-based fuel between 2025-2090 in Scenarios 17-19.

Scenario	Average (MT/month)	Maximum (MT)	Cumulative (MT)
17	10.25	62.56	7,987
18	5.109	62.56	3,979
19	126.2	318.7	98,323

## Natural uranium

The next two metrics are related to the natural uranium requirements of Scenarios 17-19. The first of these two metrics is the natural uranium needed as feed material for enrichment, shown in Figure 5.7. The feed uranium masses follow with the enriched uranium masses in these scenarios, because of the relationship between these two metrics. Scenario 18 requires the most feed uranium, and Scenario 19 requires no feed uranium. There is increased

demand for feed uranium with time in Scenarios 17 and 18, resulting from the increased energy demand and the increased demand of uranium-based fuel in the scenarios.

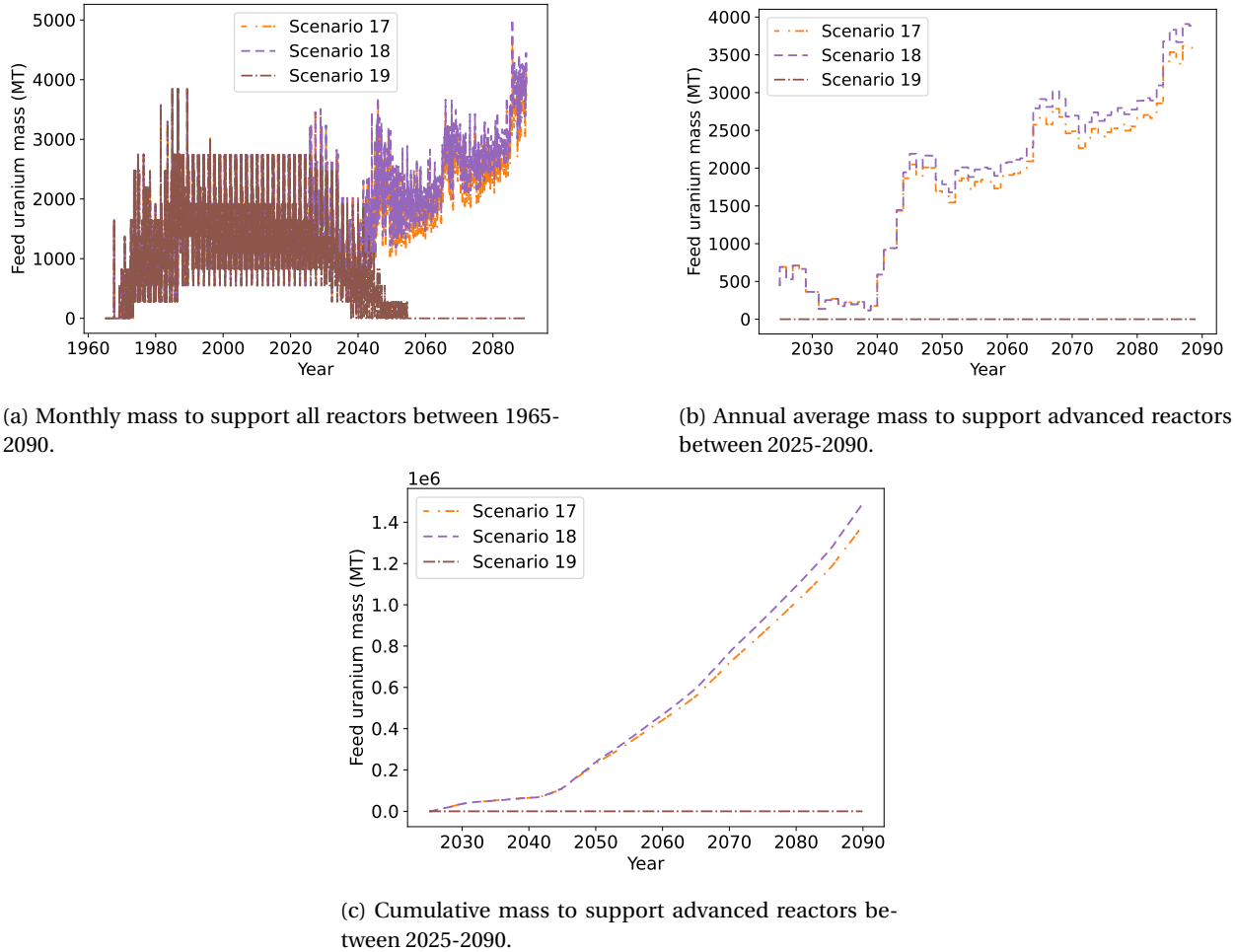


Figure 5.7: Masses of feed uranium required by reactors in Scenarios 17-19.

Table 5.7 reports the metrics for the feed uranium in Scenarios 17-19. Scenarios 17 and 18 need more feed uranium than Scenarios 9 and 12. Scenarios 9 and 12 primarily deploy the Xe-100, while Scenarios 17 and 18 deploy an inflated number of MMRs, because of the direct replacement of MMRs in the deployment scheme. The inflated number of MMRs increases the feed uranium requirements because the MMRs only accept HALEU fuel in these scenarios, and the MMR requires more feed uranium per unit energy than the Xe-100. Scenario 19 does not require any feed uranium because the SFRs in this scenario only receive plutonium-based fuel.

Finally, Figure 5.8 shows the natural uranium required to produce plutonium-based fuels in Scenarios 17-19. Scenario 19 requires the most natural uranium for plutonium-based fuels, followed by Scenario 17, then Scenario 18. The masses of plutonium-based fuel drives the demand for this natural uranium, therefore these results follow the same patterns seen in Figure 5.6. Scenario 19 requires the most natural uranium for plutonium-based fuels

Table 5.7: Metrics of feed uranium to produce enriched uranium between 2025-2090 in Scenarios 17-19.

Scenario	Average (MT/month)	HALEU Average (MT/month)	Maximum (MT)	Cumulative (MT)
17	1,774	1,728	4,750	1,381,600
18	1,866	1,911	5,014	1,489,022
19	0	0	0	0

because the advanced reactors in this scenario only receive plutonium-based fuel, and the SFR requires more fuel than the Xe-100.

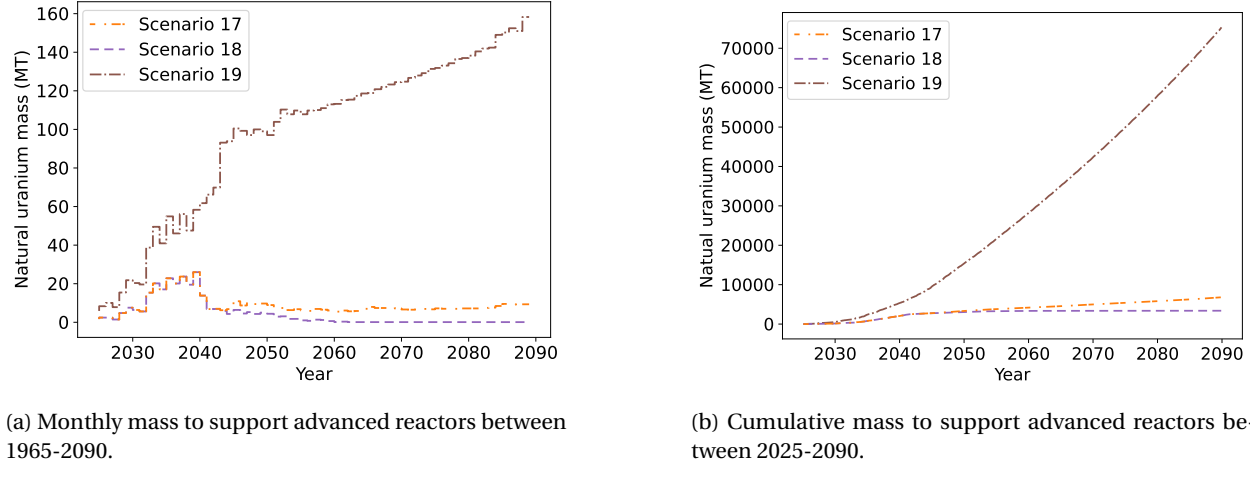


Figure 5.8: Mass of natural uranium required by reactors in plutonium-based fuels in Scenarios 17-19.

Table 5.8 reports the metrics for the natural uranium for plutonium-based fuels in Scenarios 17-19. These metric follow the same pattern observed for the no growth scenarios (Scenarios 14-16). Despite Scenario 19 requiring the most natural uranium for plutonium-based fuels, this total is still less than the cumulative feed uranium masses required in Scenarios 17 and 18 by almost a factor of two. The decreased total natural uranium mass in Scenario 19, compared with Scenarios 17 and 18, is a result of the lack of (or minimal) material loss in using natural uranium for plutonium-based fuel, compared with the losses from using natural uranium as feed material for enrichment.

Table 5.8: Metrics of natural uranium required to produce plutonium-based fuel between 2025-2090 in Scenarios 17-19.

Scenario	Average (MT/month)	Maximum (MT)	Cumulative (MT)
17	8.726	53.24	6,797
18	4.348	53.24	3,387
19	96.67	244.1	75,303

## 5.2 SWU capacity

The next category of metrics of interest is the SWU capacity required to produce the enriched uranium in each of the scenarios. The SWU capacity has important implications on the design and capacities of enrichment facilities required to support these fuel cycles.

### 5.2.1 No growth scenarios

Figure 5.9 shows SWU capacity required in Scenarios 14-16. For Scenarios 14 and 15 the required SWU capacity for the advanced reactors is relatively small, then increases around 2043, corresponding with the increased need for enriched uranium for reactors observed in Figure 5.1. Scenario 16 does not require any SWU capacity because the advanced reactors in this scenario do not receive any enriched uranium.

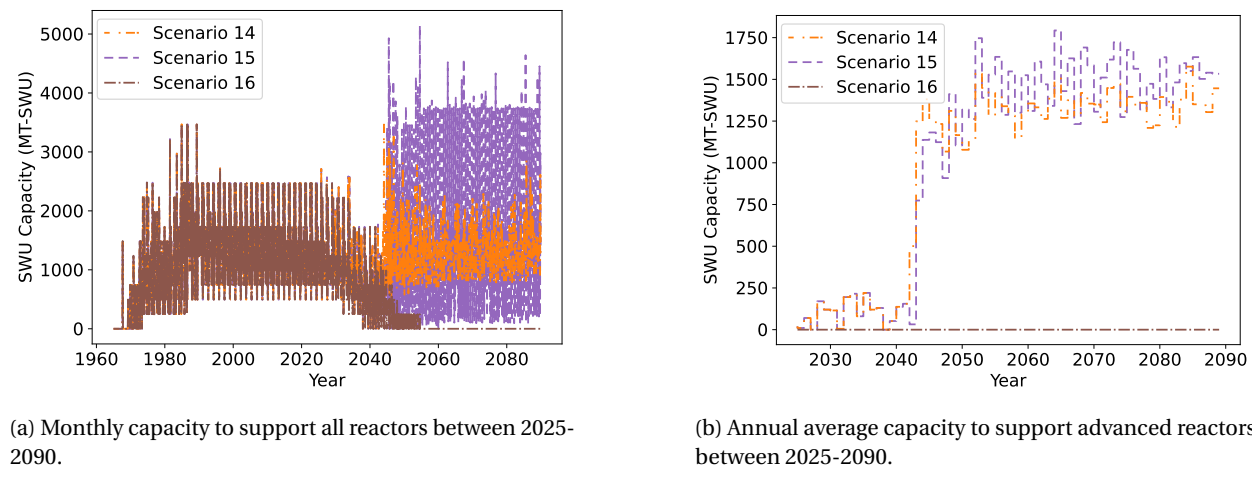


Figure 5.9: SWU capacity required to support reactors in Scenarios 14-16.

Table 5.9 reports the metrics of required SWU capacity in Scenarios 14-16. Scenarios 14 and 15 require smaller average SWU capacities than Scenarios 2-7, and require a smaller average SWU capacity to produce HALEU than Scenarios 2, 3, 4, 6, and 7. Scenario 5 requires less SWU capacity to produce HALEU because this scenario primarily deploys VOYGRs and requires less HALEU than any of the no growth scenarios that require HALEU. The differences in the SWU capacity needed by these scenarios is a function of the reactors deployed and the amount of material available for reprocessing. These parameters drive the amount of enriched uranium needed in each scenario, which drives the needed SWU capacity.

The results of these scenarios identify recycling UNF as a way to reduce the SWU capacity required in a fuel cycle. Additionally, increasing the amount of UNF available for reprocessing further reduces the SWU capacity required. The lack of needed SWU capacity in Scenario 16 indicates that developing this fuel cycle would not require any new enrichment capacity to be developed in the US. However, the US does not have any facilities for reprocessing

Table 5.9: Metrics for SWU capacity required to produce enriched uranium in Scenarios 14-16.

Scenario	Average (MT-SWU/month)	HALEU Average (MT-SWU/month)	Maximum (MT-SWU)
14	971.6	965.9	3,032
15	1,042	1,036	5,142
16	0	0	0

commercial fuel. Therefore, reprocessing fuel does not assist in meeting initial HALEU demand because the US would need to develop new infrastructure to support any of these transitions, whether it is enrichment facilities, reprocessing facilities, or both. Advanced reactors in Scenarios 14 and 15 require enriched uranium fuel, including HALEU. These scenarios require a smaller HALEU SWU capacity than the once-through scenarios, but the US would need to develop HALEU enrichment and reprocessing facilities to support these transitions.

### 5.2.2 1% growth scenarios

Figure 5.10 shows the SWU capacity required to enrich uranium in Scenarios 17-19. Similar to the feed uranium masses, the mass of enriched uranium drives the required SWU capacity. Scenario 18 requires the most SWU capacity, followed by Scenario 17, and Scenario 19 does not need any SWU capacity to support the advanced reactors.

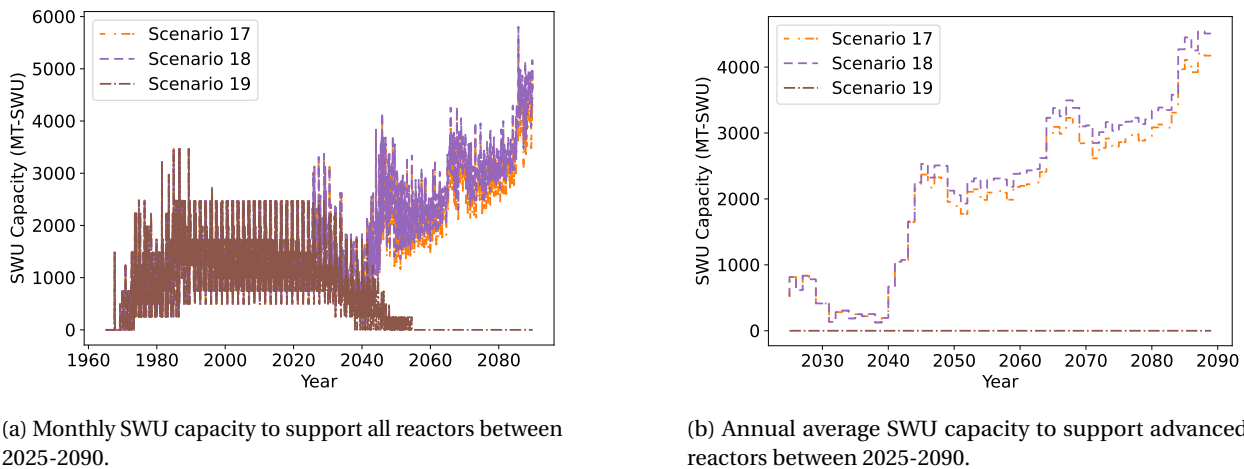


Figure 5.10: SWU capacity required to support reactors in Scenarios 14-16.

Table 5.10 reports the metrics for the SWU capacities required in Scenarios 17-19. Scenarios 17 and 18 require less SWU capacity than Scenario 13, because the use of reprocessing and plutonium-based fuel decreases the need for enriched uranium. Scenarios 17 and 18 require more SWU capacity than Scenarios 9 and 12, because of the difference in the advanced reactors deployed between these scenarios. These results vary from the results of the no growth scenarios, in which the average SWU of the closed fuel cycles were smaller than the average capacity

in the once-through fuel cycles. This difference between the energy demand curves is a result of the deployment scheme artificially inflating the number of MMRs built. This extra deployment of MMRs in the 1% growth scenarios that deploy the MMR increases the SWU capacity because the MMR requires more enriched uranium and a higher enrichment level than the Xe-100 and VOYGR. Therefore, the deployment scheme of the reactors affects the metrics of the transition when changing the energy demand.

Table 5.10: Metrics for SWU capacity required to produce enriched uranium in Scenarios 17-19.

Scenario	Average (MT-SWU/month)	HALEU Average (MT-SWU/month)	Maximum (MT-SWU)
17	2,049	2,009	5,504
18	2,207	2,168	5,806
19	0	0	0

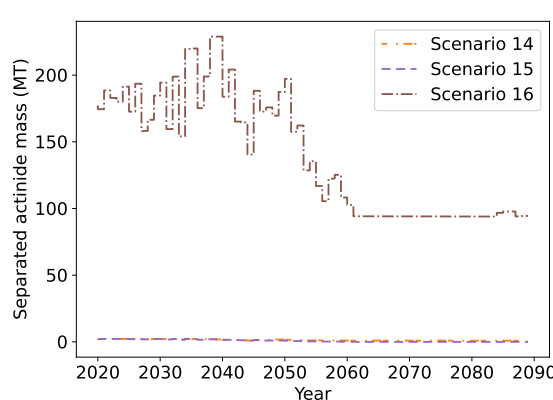
## 5.3 Separated actinide mass

The next metric of interest is the separated actinide mass sent from the separations facility to the fuel fabrication facility. The separated actinide masses include any actinides separated from UNF (i.e., uranium, neptunium, plutonium, and americium). This metric provides context on how much material is available for producing plutonium-based fuels, and has implications on separations and fabrication facility size needs. Separations facilities are deployed starting in 2020, so these results begin in 2020 instead of 2025 like the other results.

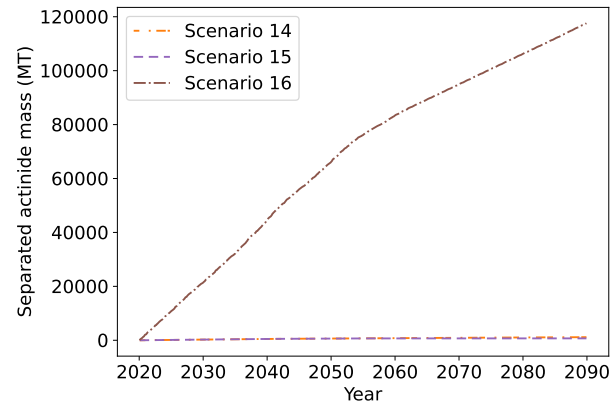
### 5.3.1 No growth scenarios

Figure 5.11 shows the separated plutonium masses in Scenarios 14-16. Scenario 16 has the most separated plutonium of the three scenarios, which is consistent with the other results of these scenarios. Scenarios 14 and 15 have very little separated plutonium compared with Scenario 16. The primary reason for this large difference is the elements separated out in each scenario. In Scenario 16, four different actinide elements are separated out from the fission products (uranium, neptunium, plutonium, and americium), but in Scenarios 14 and 15 only plutonium is separated out. The inclusion of other elements to separate out in Scenario 16 (primarily the uranium, which consists of up to 93% of UNF), increases the mass of material separated out from the UNF.

Table 5.11 reports the metrics of the separated actinide masses in Scenarios 14-16. All three scenarios experience a maximum amount of separated actinides at the same time, in November 2031. This timing corresponds with UNF discharged from LWRs in November 2025 and fuel from advanced reactors discharged in October 2031. This consistency in the maximum for these three scenarios emphasizes the importance of reprocessing the UNF from LWRs in these metrics.



(a) Monthly mass between 2020-2090.



(b) Cumulative mass between 2020-2090.

Figure 5.11: Mass of separated actinides sent from the separations facility to fuel fabrication in Scenarios 14-16.

Table 5.11: Metrics of separated actinide masses of between 2020-2090 in Scenarios 14-16.

Scenario	Average (MT/month)	Maximum (MT)	Cumulative (MT)
14	1.372	4.735	1,150
15	0.840	4.735	705.0
16	140.1	454.3	117,584

From the metrics in Table 5.11, the metrics for the separated actinide masses in Scenario 16 are two orders of magnitude greater than the metrics in Scenarios 14 and 15. The metrics for Scenario 16 are also larger than the plutonium-based fuel metrics for the scenario in Table 5.2. The larger mass of separated actinide material than plutonium-based fuels required by the reactors drives the lack of enriched uranium to support these reactors. The difference between the two material streams stems from the reprocessing of uranium from LWR fuel, which constitutes about 93% of the LWR UNF. Therefore, reprocessing uranium from LWR UNF plays an important role in supporting this fuel cycle. Between 2060-2090 (after all used fuel from LWRs is processed) the SFRs require an average of 90.3 MT/month of U/TRU fuel, and an average of 95.2 MT/month of separated actinides. Therefore, the SFR could still sustain producing enough plutonium-based fuel from reprocessing SFR UNF.

Scenario 16 models the reprocessed uranium as being part of the fresh reprocessed fuel. Therefore, it is likely that fabricating the reprocessed fuel would not need the natural uranium masses defined in Table 5.4. If this production method is possible, then the natural uranium needs of the fuel cycle would drop to near-zero, further emphasizing how a closed fuel cycle can help minimize natural uranium needs.

In these fuel cycles, we model the Xe-100, VOYGR, and SFR through the OpenMCyclus archetype, instead of using the CYCMORE Reactor like in the once-through scenarios. The comparison between OpenMCyclus and the CYCMORE Reactor (Section 3.5.3) shows that the CYCMORE Reactor yields larger separated plutonium masses than OpenMCyclus. Therefore, using the CYCMORE Reactor would potentially overestimate the amount

of separated actinide material, which would overestimate the amount of plutonium-based fuel for the advanced reactors. Therefore, by using OpenMCyclus for the reactors that receive plutonium-based fuel in the closed fuel cycles, we can expect that the separated actinide and plutonium-based fuel masses are more accurate than if we used the CYCMORE Reactor archetype.

### 5.3.2 1% growth scenarios

Figure 5.12 shows the mass of separated actinide material in Scenarios 17-19. Similar to the no growth scenarios, Scenario 19 has a much greater mass of separated actinide material than Scenarios 17 and 18. The greater mass in Scenario 19 is a result of multiple actinide elements being separated out from the UNF, compared with only plutonium separated in Scenarios 17 and 18, as well as more fuel being reprocessed in Scenario 19.

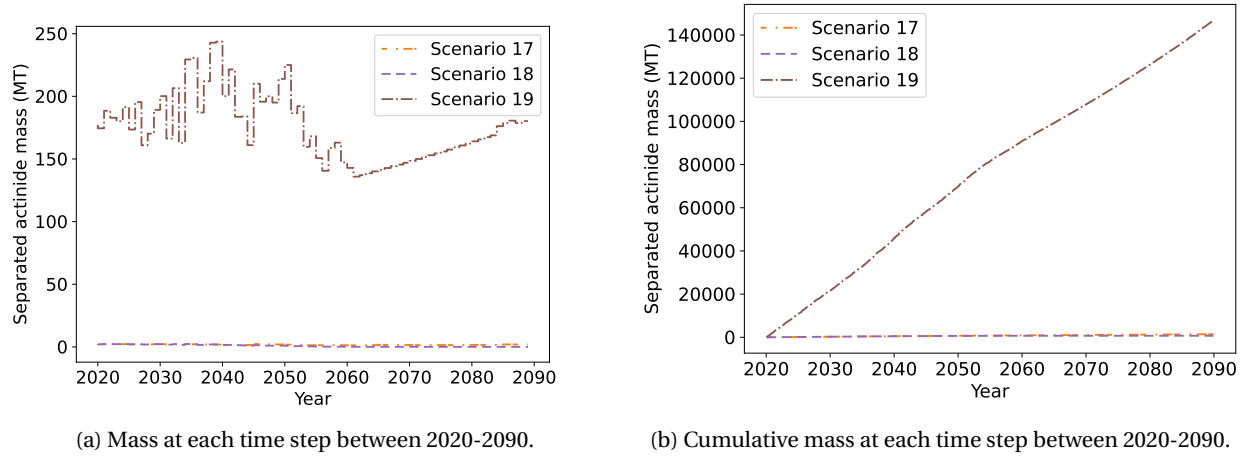


Figure 5.12: Separated plutonium masses in Scenarios 17-19.

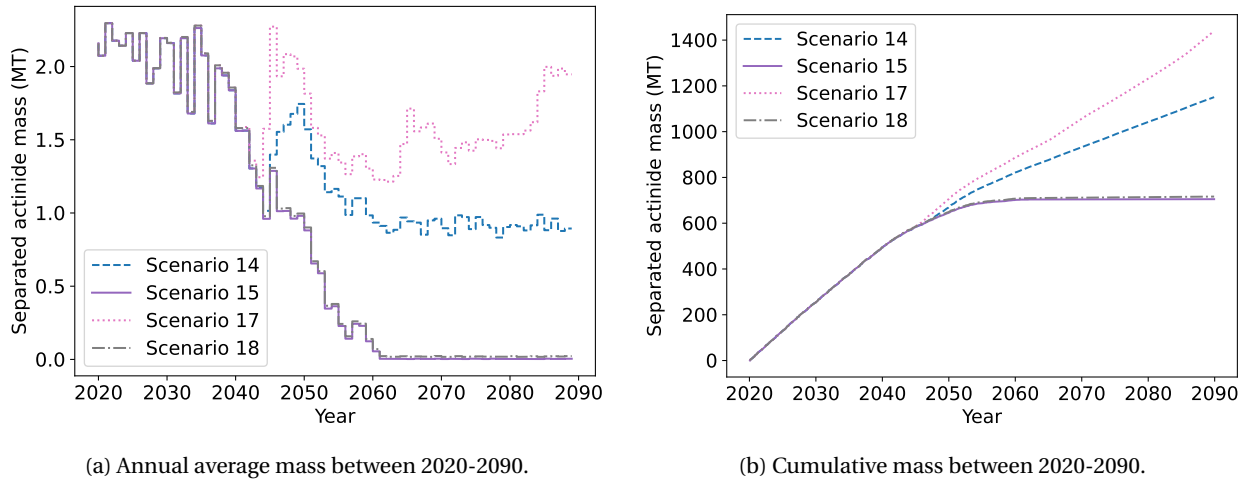
Table 5.12 reports the metrics of the separated actinide masses on Scenarios 17-19. Scenarios 17 and 18 have the maximum separated plutonium mass in November 2031, the same time as the maximum in Scenarios 14 and 15. The consistency in the maximum separated actinide mass in all four of the limited recycle scenarios emphasizes the importance of reprocessing the LWR UNF in these scenarios.

Table 5.12: Mass of separated plutonium between 2020-2090 in Scenarios 17-19.

Scenario	Average (MT/month)	Maximum (MT)	Cumulative (MT)
17	1.715	4.735	1,439
18	0.854	4.735	716.4
19	175.0	500.0	146,837

Figure 5.13 shows the annual average and cumulative separated actinide mass in Scenarios 14, 15, 17, and 18. All four of these scenarios have the same separated actinide masses until November 2028, Scenarios 14 and 15 have

the same separated actinide mass until November 2041, and Scenarios 17 and 18 have the same separated actinide mass until February 2042. The similarities between these four scenarios is a result of the LWR UNF driving the amount of available separated actinide material, and the use of the same advanced reactor build share for scenarios of the same growth. However, the fuel considered for reprocessing has a greater impact on the amount of separated actinide material available than the energy demand. Scenarios 15 and 18 differ by a maximum of 41 kg of separated actinide material for a single time step, while Scenarios 14 and 17 differ by a maximum of 1.4 MT in a single time step.



(a) Annual average mass between 2020-2090.

(b) Cumulative mass between 2020-2090.

Figure 5.13: Separated plutonium masses in the limited recycle fuel cycles, Scenarios 14, 15, 17, 18.

## 5.4 Used nuclear fuel and high level waste

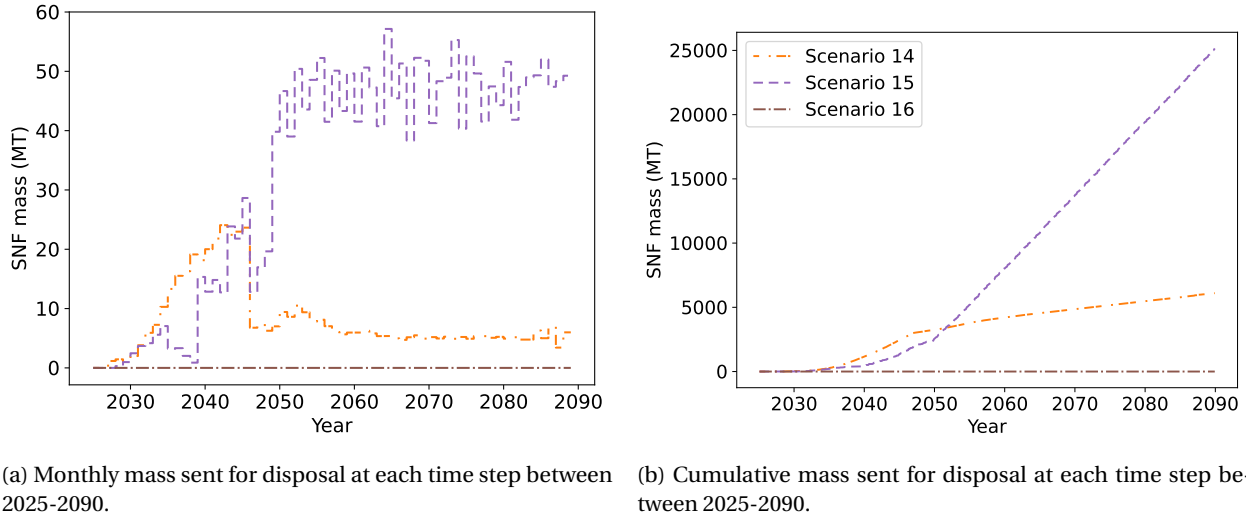
This section provides the results of the UNF and HLW sent to disposal in the closed fuel cycles. The once-through scenario results only defined the UNF sent for disposal because all of the materials needing disposal in those scenarios are UNF. With the addition of the separation step, the UNF discharged from reactors gets separated into two different material streams, one of the separated plutonium and one of HLW that is sent for disposal. UNF is the used fuel from each of the reactors that is disposed with reprocessing. HLW is the waste (e.g., fission products) separated out from the reprocessed UNF.

### 5.4.1 No growth scenarios

This section presents the results of the UNF and HLW masses that are sent for disposal in a material sink in the no growth recycle scenarios.

## Used nuclear fuel

Figure 5.14 shows the masses of advanced reactor UNF disposed of in Scenarios 14-16. In Scenario 14 only the used MOX fuel is disposed of, in Scenario 15 the used MOX as well as the used TRISO-based MMR and Xe-100 fuels are disposed of, and no UNF is disposed of in Scenario 16. The disposal of MMR UNF in Scenario 15 leads to the single times with larger disposal masses, because of the single-batch fueling scheme of the MMR. The additional fuel that is disposed of in Scenario 15, compared with Scenarios 14 and 16, increases the amount of UNF disposed.



(a) Monthly mass sent for disposal at each time step between 2025-2090. (b) Cumulative mass sent for disposal at each time step between 2025-2090.

Figure 5.14: Used nuclear fuel disposed of in Scenarios 14-16.

Table 5.13 reports the metrics for the UNF disposal in Scenarios 14-16. The values in this table are smaller than the UNF masses in the once-through scenarios (Table 4.15). This decrease in UNF disposal is a result of the reprocessing in Scenarios 14-16, and is an advantage of a closed fuel cycle.

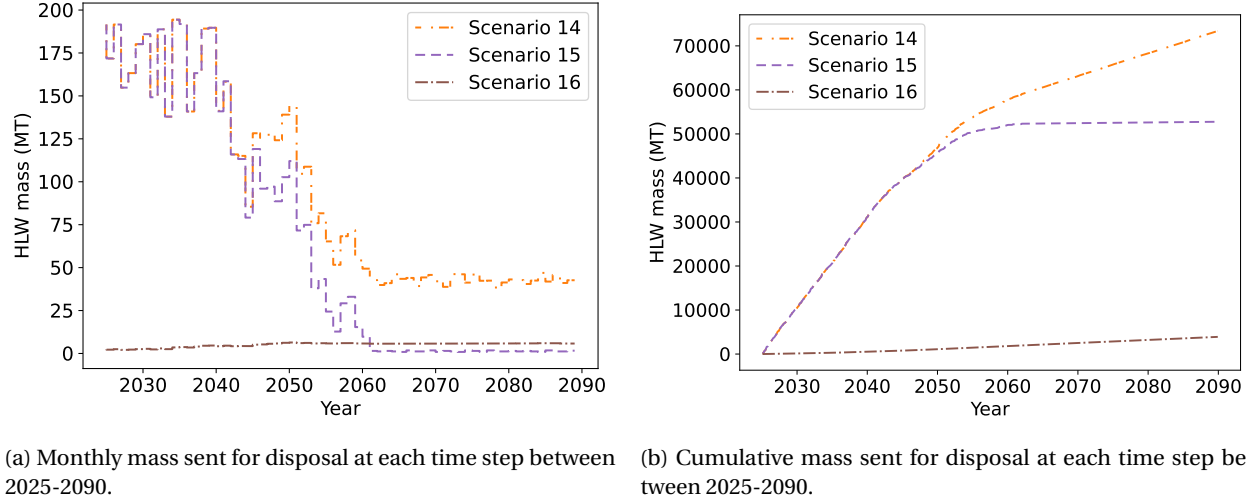
Table 5.13: Mass of UNF disposed of between 2025-2090 in Scenarios 14-16.

Scenario	Average (MT/month)	Maximum (MT)	Cumulative (MT)
14	7.835	41.33	6,103
15	32.29	145.4	25,153
16	0	0	0

Based on these values and the results in Figure 5.14, including more fuel for reprocessing can greatly reduce the mass of UNF. All three of these scenarios have a cumulative UNF mass smaller than that of all of the once-through scenarios. Additionally, the UNF from advanced reactors in all three of these scenarios is less than the 70,000 MT limit for Yucca Mountain. The reduction in UNF mass compared with the once-through scenarios highlights an advantage of closed fuel cycles.

## High level waste

Figure 5.15 shows the HLW masses for disposal in Scenarios 14-16. Scenario 14 results in the most HLW, because more material is reprocessed in this scenario than in Scenario 15, and less actinide material is separated out than in Scenario 16. The HLW mass in Scenario 15 reaches a near-zero level around 2060, because all of the LWR UNF is reprocessed by this time which leaves only the VOYGR UNF available for reprocessing. A maximum of 7 VOYGRs are deployed at a time in Scenario 15, so there is very little UNF reprocessed and little HLW generated after 2060.



(a) Monthly mass sent for disposal at each time step between 2025-2090. (b) Cumulative mass sent for disposal at each time step between 2025-2090.

Figure 5.15: Mass of HLW disposed of in Scenarios 14-16.

Table 5.14 reports the metrics for the HLW in Scenarios 14-16. Scenario 16 generates very little HLW because the actinide material separated out comprises most of the mass of the UNF. The HLW masses for Scenarios 14 and 15 are larger than the UNF masses for these scenarios, and are larger than the UNF masses of the no growth, once-through scenarios, except Scenario 5. The increase comes from the inclusion of LWR UNF for reprocessing in these scenarios. Including this UNF increases the disposed material mass because this metric is not solely focused on material from the advanced reactors like it was for the once-through scenarios. The average for Scenario 14 is similar to the average UNF disposed of between 2025-2055 in Scenario 1 (94.27 MT/month).

Table 5.14: Mass of HLW disposed of between 2025-2090 in Scenarios 14-16.

Scenario	Average (MT/month)	Maximum (MT)	Cumulative (MT)
14	94.21	440.2	73,389
15	67.73	440.2	52,764
16	5.011	10.09	3,903

The HLW in each of these scenarios has a different composition than the UNF, but both waste streams still require a geologic repository for final disposal. Therefore, both the UNF and HLW masses must be considered for evaluating repository capacities. The HLW in Scenario 14 is more than the 70,000 MT limit of Yucca Mountain, so a

second repository would be needed to disposal of both waste streams. The UNF and HLW materials in Scenario 15 sum to 77,917 MT, meaning that a second repository would be needed to support this scenario as well. These material streams sum to 3,903 MT in Scenario 16, which means that the Yucca Mountain limit of 70,000 MT would be sufficient to support this scenario.

### 5.4.2 1% growth scenarios

This section presents the results of the UNF and HLW masses that are sent for disposal in a material sink in the 1% growth recycle scenarios.

#### Used nuclear fuel

Figure 5.14 shows the mass of UNF disposed of in Scenarios 17-19. These results follow a similar pattern to the no growth scenarios; Scenario 18 disposes of the most UNF, followed by Scenario 17, and Scenario 19 does not have any UNF disposed of. This pattern emerges because of the material available for reprocessing in each scenario. The more UNF reprocessed, the less UNF disposed.

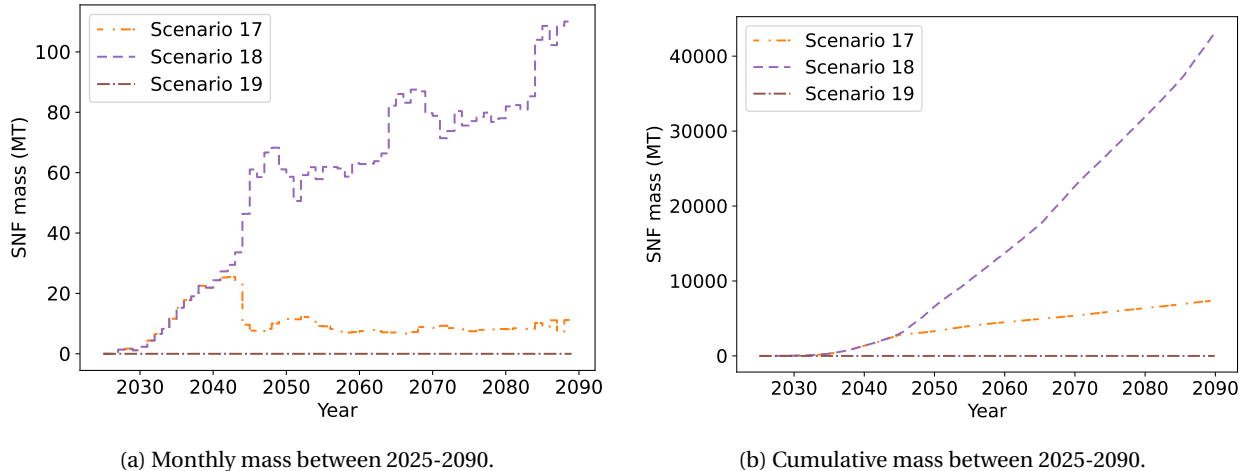


Figure 5.16: Used nuclear fuel disposed of in Scenarios 17-19.

Table 5.15 reports the metrics of the UNF disposed of in Scenarios 17-19. Scenarios 17 and 19 dispose of less UNF than Scenarios 8-13, but Scenario 18 disposes of more UNF than Scenario 9. Scenario 9 only deploys the Xe-100, while Scenario 18 has an artificially inflated number of MMRs deployed, and the Xe-100 uses less fuel than the MMR. We observe this effect in Scenario 18 and not Scenario 17, because MMR UNF is reprocessed in Scenario 17 but not in Scenario 18. Therefore the MMR UNF in Scenario 17 get split between the HLW and plutonium-based fuel material streams. The UNF mass comparisons between the closed and once-through fuel cycles are consistent with the other results: reprocessing fuel reduces material metrics, but the reactors deployed are the primary driver

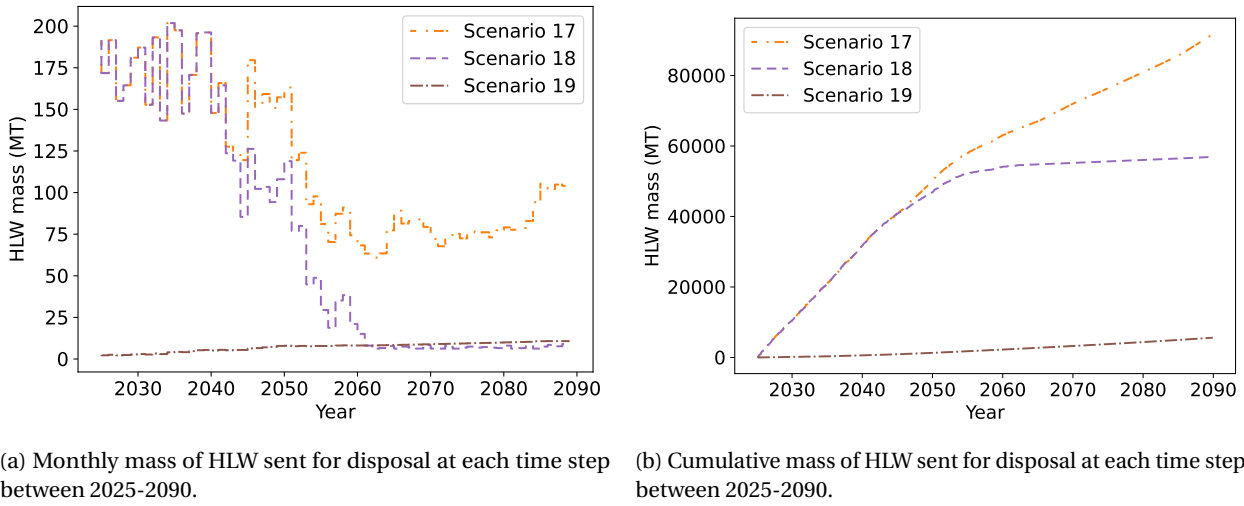
of the metrics.

Table 5.15: Mass of UNF disposed of between 2025-2090 in Scenarios 17-19.

Scenario	Average (MT/month)	Maximum (MT)	Cumulative (MT)
17	9.542	35.47	7,433
18	55.34	157.4	43,113
19	0	0	0

### High level waste

Finally, Figure 5.17 shows the HLW mass disposed of in Scenarios 17-19. These results are similar to the results from the no growth closed fuel cycle scenarios; Scenario 17 has the most HLW mass, followed by Scenario 18, and Scenario 19.



(a) Monthly mass of HLW sent for disposal at each time step between 2025-2090. (b) Cumulative mass of HLW sent for disposal at each time step between 2025-2090.

Figure 5.17: HLW disposed of in Scenarios 17-19.

Table 5.16 reports the metrics for the HLW mass in Scenarios 17-19. These values are almost all larger than the values for the no growth fuel cycles (Table 5.14), but Scenarios 17 and 18 have the same maximum value as Scenarios 14 and 15. The consistency in the maximum value in these four scenarios corresponds to LWR UNF reprocessing, and emphasizes the impact that LWR UNF has on the material availability and requirements of these fuel cycles.

Table 5.16: Mass of HLW disposed of between 2025-2090 in Scenarios 17-19.

Scenario	Average (MT/month)	Maximum (MT)	Cumulative (MT)
17	117.7	440.2	91,670
18	73.06	440.2	56,915
19	7.195	15.29	5,604

The cumulative HLW mass in Scenario 17 is larger than the 70,000 MT limit for Yucca Mountain. The cumulative HLW mass in Scenario 18 is less than the 70,000 MT limit, but combining this with the 43,113 MT of UNF pushes the total waste over the 70,000 MT limit. Therefore, a second repository would be needed to support material disposal in these scenarios. The total HLW and UNF masses in Scenario 19 are less than the 70,000 MT limit, which means that Yucca Mountain would be sufficient to support the disposal needs of this scenario.

# Chapter 6

## Sensitivity analysis

Sensitivity analysis identifies how and the extent to which variations in model input parameters affect select performance metrics of the fuel cycle. Additionally, it reveals the combined effect of varying multiple parameters on an output metric. This information can then be used to design an optimized transition scenario by identifying which input parameters will affect the results the most, and how these parameters should be changed to obtain desired results (e.g., minimizing HALEU requirements of a transition).

### 6.1 Methodology

We performed sensitivity analysis on Scenario 7 (once-through fuel cycle transition to Xe-100, VOYGR, and MMR with a no growth energy demand) using a coupling between CYCLUS with Dakota [28], an open-source code developed by Sandia National Laboratory (SNL) for uncertainty quantification, sensitivity analysis, and optimization. This coupling mirrors the scripts in the `dewrapper` GitHub repository [116]. We performed three different types of sensitivity analysis: one-at-a-time (OAT), synergistic, and global. OAT analysis varies a single input parameter to investigate the effect of each parameter individually. In the context of this work, synergistic analysis varies two input parameters at once to investigate how the interaction of the two parameters affects the results. Finally, the global sensitivity analysis varies more than two input parameters to provide a holistic view of how multiple parameters interact and affect the output metrics. For this work, we considered variations in the transition start time, the build share of each type of advanced reactor, the LWR lifetimes, and the discharge burnup of fuel from the HALEU-fueled reactors.

The transition start time ranges from January 2025 to January 2040 in three-month intervals, but the same energy demand is specified for all perturbations (87.20 GWe-yr). We consider this parameter to provide a relaxation of the aggressive 2025 transition start date used in the transition analysis of Chapters 4 and 5.

We consider three iterations of the build share, once for each advanced reactor, with build share percentages ranging from 0-50% in increments of 5%. To account for the build share of an advanced reactor, we adjusted the deployment scheme described in Section 3.2. Instead of the reactor type with the largest power output deployed

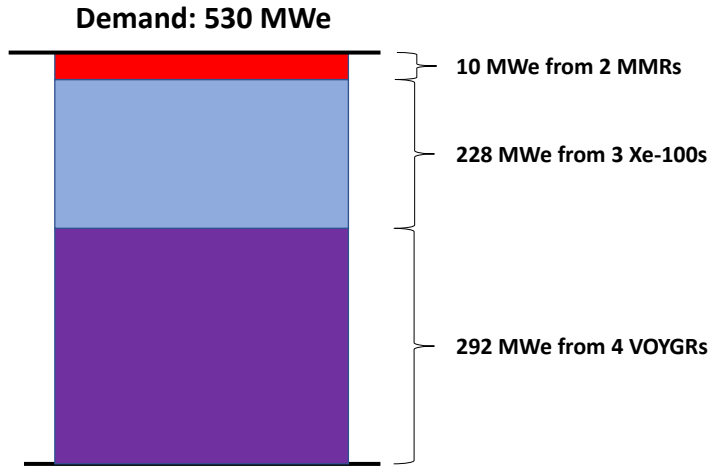


Figure 6.1: Demonstration of the adjusted advanced reactor deployment scheme to meet a demand of 530 MWe and a VOYGR build share of 50%.

first, the reactor with the specified build share is deployed first until the build share is met. Then the remaining two advanced reactor types are deployed in the manner described in Section 3.2, with the larger of the two remaining reactors preferentially deployed and the smaller reactor deployed last to meet or exceed the power demand. Figure 6.1 illustrates how we applied this deployment scheme to meet a fictional demand of 530 MWe and a VOYGR build share of 50%. We vary this parameter of the transition because of the large effect of the advanced reactors deployed in each of the transition scenarios. Unless an advanced reactor build share is specified, this analysis applies the same advanced reactor deployment schedule as Scenario 7 (see Section 4.3.1).

The LWR lifetimes are varied based on the percent of the fleet that operate for 80 years. This variable varies between 0-50%, in increments of 5%, of the LWR fleet operating for 80 years, while the other LWRs operate for 60 years. This input parameter reflects the effects of different numbers of LWRs receiving license extensions to 80 years. Various utilities are exploring and pursuing license extensions for LWRs, so including this parameter reflects this occurrence. The LWRs do not all start operation at the same time, so the selection of the LWRs that operate for 80 years affects the results, even if the number is the same. Therefore, reactors are prioritized based on their power outputs for the lifetime extensions, reflecting the greater likelihood of larger units receiving a license extension. Previous sensitivity analysis of fuel cycle transitions considered the impact of the transition start time and the LWR lifetimes [20, 21], which provides some basis for why these input parameters were selected for this work.

Finally, we varied the discharge burnup of the two HALEU-fueled reactors in this work (the Xe-100 and MMR) because these two reactors are reaching burnup levels larger than the NRC-approved 62 MWd/kgHM [117]. There-

fore, it is possible that these reactors would need to be operated under different conditions until higher burnups are approved by the NRC. Therefore, inclusion of this variable explores the impact on resource needs if these reactors are prohibited from achieving their reported burnup values. This analysis is not performed for the VOYGR because this design aims to achieve a burnup that is within the NRC limit.

To vary the burnup of the Xe-100, we considered two difference approaches. The first approach was to vary the number of passes through the core for each pebble while keeping the length of each pass and the total mass of uranium in the core constant (i.e., reducing the number of batches). Varying the number of passes between one and six results in discharge burnup values of 28, 56, 84, 112, 140, and 168 MWd/kgU, using Eq. 3.1. This approach provides a coarse grid for the burnup values that reflects possible changes to meet current NRC regulations. The second approach varies the length of each pass by one month, while keeping the number of passes and the total mass of uranium constant. This approach provides a more fine grid around the declared burnup value, reflecting potential small variations in reactor operation. The second approach results in burnup values of 151 and 185 MWd/kgU, which are about  $\pm 10\%$  of the stated discharge burnup of 168 MWd/kgU.

To vary the MMR burnup, we varied the cycle time (and thus lifetime) of the reactor while the total mass of uranium was held constant. Cycle times of 10, 15, and 20 years were considered, resulting in burnup values of 41, 62, and 82 MWd/kgU. Additionally, the lifetime was varied to result in burnup values  $\pm 10\%$  and  $\pm 5\%$  around the stated burnup of 82 MWd/kg, resulting in burnup values of 74, 78, 86, and 90 MWd/kgU.

The sensitivity analysis focuses on the effects of these input parameters on the following metrics: the amount of waste generated that must be sent to a repository (UNF mass), the mass of enriched uranium, the mass of HALEU, the amount of SWU capacity required to produce all enriched uranium, the SWU capacity required to produce HALEU, and the feed uranium required to produce HALEU. We considered each of these metrics within the transition analysis, allowing for comparison between Chapters 4, 5, and this chapter. We compare each metric based on the cumulative sum required, starting at the transition start time.

## 6.2 One-at-a-time

This section discusses the results of the OAT sensitivity analysis as applied to Scenario 7. A subset of this analysis is presented in [118], but the analysis presented here has an expanded scope and updated methodology to address the non-consistent replacement of advanced reactors in the previously published work. The results in this subsection focus on the relative change in each metric for each parameter varied, because of the large range of the metric values. To that end, Table 6.1 reports the minimum, average, and maximum value for each metric.

Table 6.1: Minimum, average, and maximum value of each metric caused by the variation of each parameter.

Parameter	Metric	Minimum	Average	Maximum	Units
Transition Start	Fuel Mass	2.832e+07	3.001e+07	3.086e+07	kg
	HALEU Mass	2.777e+07	2.931e+07	3.005e+07	kg
	Total SWU	9.727e+08	1.036e+09	1.068e+09	kg-SWU
	HALEU SWU	9.690e+08	1.031e+09	1.062e+09	kg-SWU
	UNF	2.600e+07	2.744e+07	2.813e+07	kg
	HALEU Feed	8.406e+08	8.936e+08	9.204e+08	kg
LWR Lifetimes	Fuel Mass	2.226e+07	2.574e+07	2.934e+07	kg
	HALEU Mass	2.186e+07	2.528e+07	2.885e+07	kg
	Total SWU	7.780e+08	8.973e+08	1.021e+09	kg-SWU
	HALEU SWU	7.753e+08	8.941e+08	1.018e+09	kg-SWU
	UNF	1.956e+07	2.305e+07	2.669e+07	kg
	HALEU Feed	6.716e+08	7.746e+08	8.820e+08	kg
Xe-100 Build Share	Fuel Mass	8.230e+07	1.130e+08	1.471e+08	kg
	HALEU Mass	2.827e+06	1.078e+07	1.804e+07	kg
	Total SWU	1.083e+09	1.090e+09	1.102e+09	kg-SWU
	HALEU SWU	1.275e+08	3.999e+08	6.501e+08	kg-SWU
	UNF	7.511e+07	1.032e+08	1.344e+08	kg
	HALEU Feed	1.081e+08	3.448e+08	5.622e+08	kg
MMR Build Share	Fuel Mass	3.702e+07	4.918e+07	6.134e+07	kg
	HALEU Mass	2.670e+07	3.852e+07	5.039e+07	kg
	Total SWU	9.901e+08	1.600e+09	2.212e+09	kg-SWU
	HALEU SWU	9.205e+08	1.528e+09	2.138e+09	kg-SWU
	UNF	3.440e+07	4.066e+07	4.689e+07	kg
	HALEU Feed	7.995e+08	1.310e+09	1.822e+09	kg
VOYGR Build Share	Fuel Mass	3.045e+07	6.436e+07	9.510e+07	kg
	HALEU Mass	1.516e+07	2.233e+07	3.045e+07	kg
	Total SWU	1.077e+09	1.082e+09	1.092e+09	kg-SWU
	HALEU SWU	5.528e+08	7.988e+08	1.080e+09	kg-SWU
	UNF	2.765e+07	5.870e+07	8.679e+07	kg
	HALEU Feed	4.775e+08	6.913e+08	9.353e+08	kg
Xe-100 Burnup	Fuel Mass	2.761e+07	5.888e+07	1.591e+08	kg
	HALEU Mass	2.681e+07	5.809e+07	1.583e+08	kg
	Total SWU	9.559e+08	2.034e+09	5.489e+09	kg-SWU
	HALEU SWU	9.505e+08	2.029e+09	5.484e+09	kg-SWU
	UNF	2.486e+07	5.614e+07	1.564e+08	kg
	HALEU Feed	8.233e+08	1.760e+09	4.761e+09	kg
MMR Burnup	Fuel Mass	3.065e+07	3.124e+07	3.293e+07	kg
	HALEU Mass	2.986e+07	3.045e+07	3.214e+07	kg
	Total SWU	1.059e+09	1.085e+09	1.162e+09	kg-SWU
	HALEU SWU	1.054e+09	1.080e+09	1.156e+09	kg-SWU
	UNF	2.791e+07	2.850e+07	3.019e+07	kg
	HALEU Feed	9.128e+08	9.354e+08	1.000e+09	kg

### 6.2.1 Transition start time

Delays in the transition start time generally decrease all of the output metrics, as shown in Figure 6.2. This result matches expectations, because if the advanced reactors are deployed for less time, then they require fewer resources. However, there are some oscillations in the output metrics between individual time steps. For example, a transition

start time of October 2029 increases the fuel mass and UNF mass relative to July 2029, the start time previous. This increase results from changes in the number of each advanced reactor deployed, because of differences in the gap between energy produced and energy demand that must initially be filled when advanced reactors are deployed. By waiting until October 2029, more VOYGRs are deployed than when the transition starts in July 2029. As discussed in Chapter 4, the VOYGR needs a larger fuel mass, and thus discharges more UNF than the Xe-100 and MMR. Therefore, these two metrics increase for this particular transition start time.

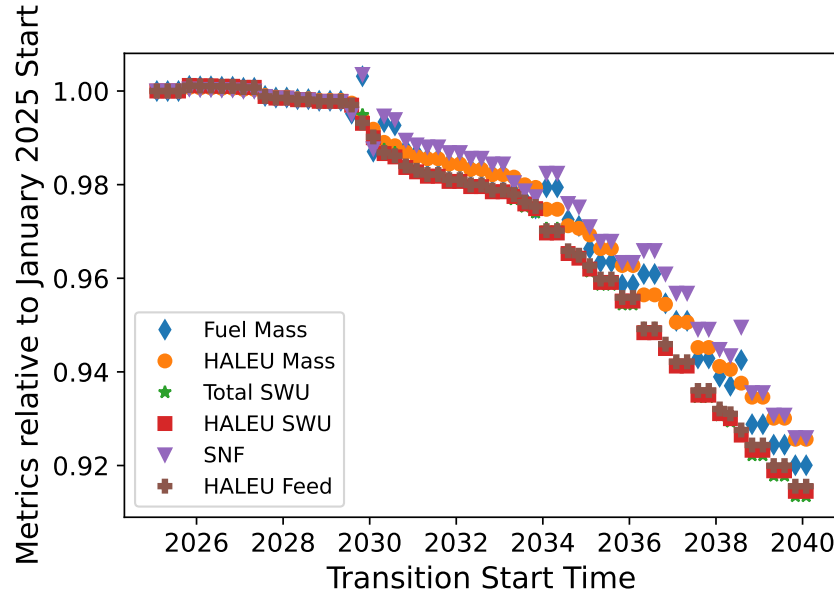


Figure 6.2: Change in each metric as a function of transition start time, relative to a transition start in January 2025.

One of the disadvantages in delaying the transition start time is the increasing gap between energy supplied and energy demand as the transition start time is delayed. All of these scenarios have a constant demand of 87.20 GWe-yr beginning in January 2025. By delaying the transition start time to after September 2025 (the observed initial deployment time of advanced reactors in Section 4.3.1), there is a difference between the energy supplied and the energy demand. The largest gap observed is 36.7 GWe-yr, when reactors are deployed starting in January 2040. Therefore, delaying the transition start time is not an ideal method of potentially reducing materials to support advanced reactors.

### 6.2.2 LWR lifetimes

The next metric varied is the percent of the LWRs that operate for 80 years, reflecting the effect license extensions in the LWR fleet. Figure 6.3 shows that the percent of the LWR fleet operating for 80 years increases, all of the metrics decrease. All of the metrics decrease linearly and by a similar magnitude, with some variation because of changes in

the number of each advanced reactor deployed, as discussed in Chapter 4. The UNF mass decreases more than the other metrics across this parameter space, ranging between 19.5-26.7 MTU.

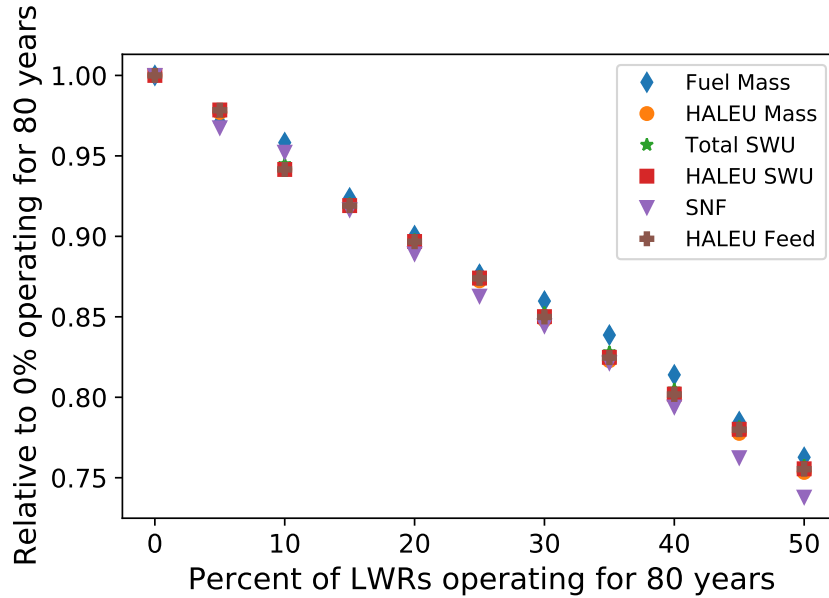


Figure 6.3: Change in each metric as a function of percent of LWR fleet operating for 80 years, relative to 0%.

Across this parameter space, the metrics decrease by a greater fraction than when varying the transition start time. The increased impact on the metrics is partly because of a small modeling change. When varying the transition start time, the LWRs are assumed to have the same lifetime as the ones used in the transition analysis. Almost all of these lifetimes are 60 years but there are a select few (such as Watts Bar Unit 2) that are currently licensed for 40 years. A simplifying assumption for modeling the effects of extending the LWR lifetimes is that they operate for either 60 or 80 years, giving those select few reactors an artificial lifetime extension from 40 to 60 years, compared with the previous analysis. This modeling difference does not have a large impact on the results as evidenced by the maximum HALEU mass when varying the LWR lifetimes being only 4.9% lower than the maximum HALEU mass when varying the transition start time. Therefore, we can attribute most of the change in the metrics to the change in the LWR lifetimes and not the artificial increase in lifetimes from 40 to 60 years. Additionally, extending the LWR lifetimes inherently delays the start time of the transition, or at least decreases the speed of the transition, because the LWRs are sufficient to meet the energy demand for a longer period of time. In addition to causing greater change in the metrics, the energy demand is always met when varying the LWR lifetimes, which suggests that extending the lifetimes of the LWRs is a preferable parameter to vary if one wishes to decrease material requirements of this transition.

### 6.2.3 Xe-100 build share

Figure 6.4 shows that as the Xe-100 build share increases, the HALEU-related metrics increase while the total UNF and total fuel mass decrease and the total SWU capacity stays relatively constant. Figure 6.5 shows that as the Xe-100 build share increases, the number of MMRs is relatively constant and the number of VOYGRs decreases. These results show that as the Xe-100 build share increases, the Xe-100s are primarily replacing power that is supplied by the VOYGRs, instead of a portion of both of the other advanced reactors. This replacement of VOYGRs is because of the deployment scheme used in this work, as the VOYGR has the largest power output between the VOYGR and MMR. Therefore, VOYGR deployment is maximized when the Xe-100 build share is 0%. This effect of the deployment scheme indicates that varying this parameter highlights trade-offs between the Xe-100 and VOYGR reactors.

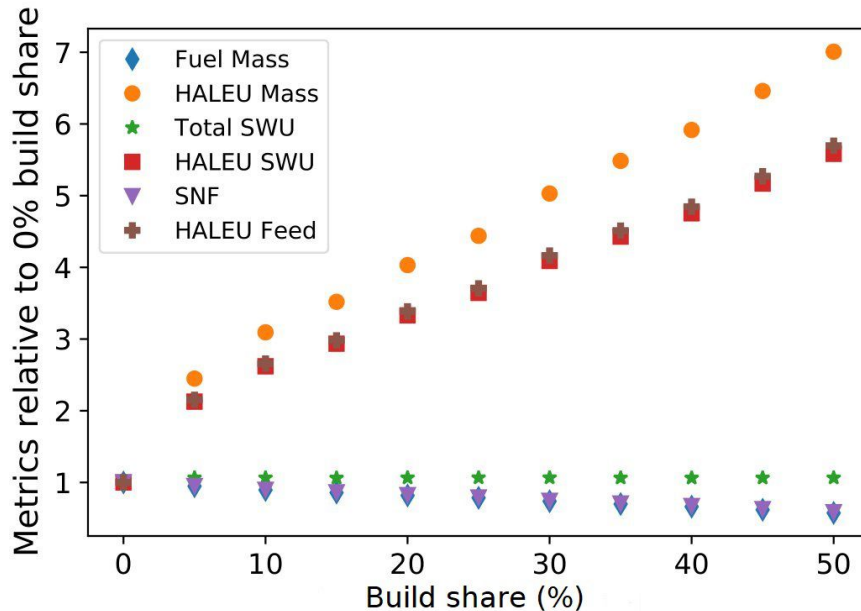


Figure 6.4: Change in each metric as a function of Xe-100 build share, relative to a build share of 0%.

The HALEU-related metrics increase with Xe-100 build share because more of the demand is met through advanced reactors requiring HALEU. The total fuel mass and UNF mass decrease because the Xe-100 requires less fuel per unit time and energy than the VOYGR, as discussed in Chapter 4. The total SWU capacity required is relatively constant, decreasing between 0.3–1.7% compared to the SWU capacity required for a 0% Xe-100 build share. This stagnant behavior of the total SWU capacity is consistent with the similar SWU capacity required by Scenarios 3–7 in Section 4.5.1, when either the Xe-100 or VOYGR are primarily deployed. These results highlight the trade-off between the HALEU-related metrics and the total fuel mass and UNF mass in deploying the Xe-100 versus the VOYGR. Both reactors require similar SWU capacities but because of the different product assays required, the

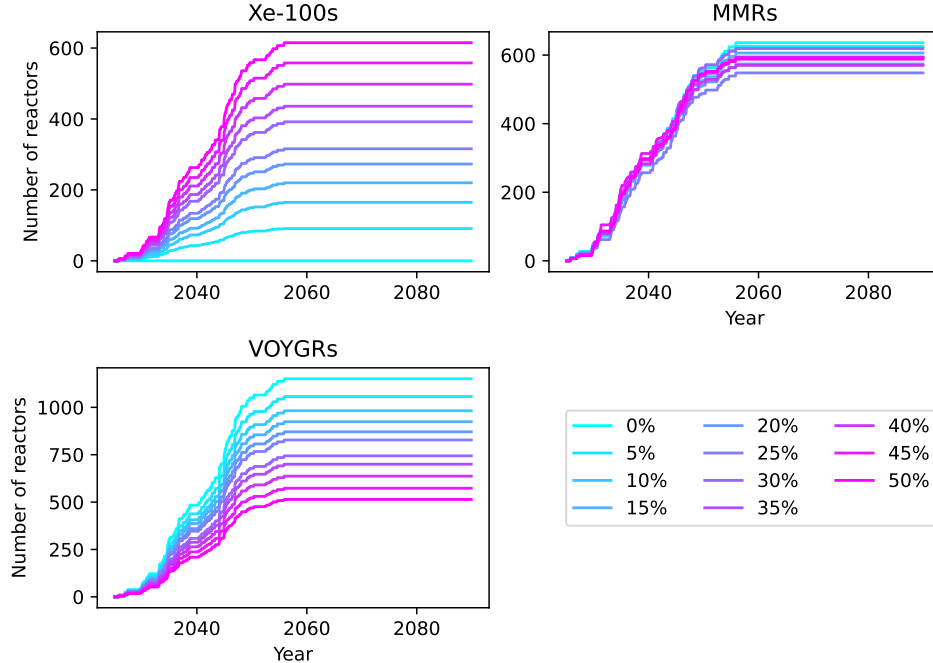


Figure 6.5: Number of Xe-100s (top left), MMRs (top right), and VOYGRs (bottom left) as a function of Xe-100 build share.

cascade configuration will vary. The HALEU-related metrics increase up to 638% of the mass required for a 0% Xe-100 build share. The total fuel mass and UNF mass decrease to up to 44.11% of the mass required for 1 0% Xe-100 build share.

#### 6.2.4 MMR build share

All of the metrics increase with increasing MMR share, as shown in Figure 6.6. As the MMR build share increases, the total SWU, HALEU SWU, and HALEU feed have the greatest relative increase because more of the advanced reactor fleet uses the highest enrichment level of the three advanced reactors. The HALEU mass increases with the MMR build share MMRs replace Xe-100s as the build share increases, shown in Figure 6.7. The MMR requires a greater fuel mass than the Xe-100, causing the increase in the HALEU mass as MMRs replace Xe-100s. The larger fuel mass required by the MMR, compared with the Xe-100, compounds with the higher enrichment required by the MMR to cause the greater relative increase in the total SWU, HALEU SWU, and HALEU feed.

The UNF mass does not experience the same relative increase as the total fuel mass because any fuel that is still in a reactor core at the end of the simulation is not accounted for in the UNF mass. Therefore, as the MMR build share increases, more of the enriched uranium sent to reactors is still in a reactor core at the end of the simulation because of the long cycle time of the MMR. Based on the replacement of Xe-100s with MMRs as the MMR build share increases, these results highlight the effects of deploying the MMR over the Xe-100.

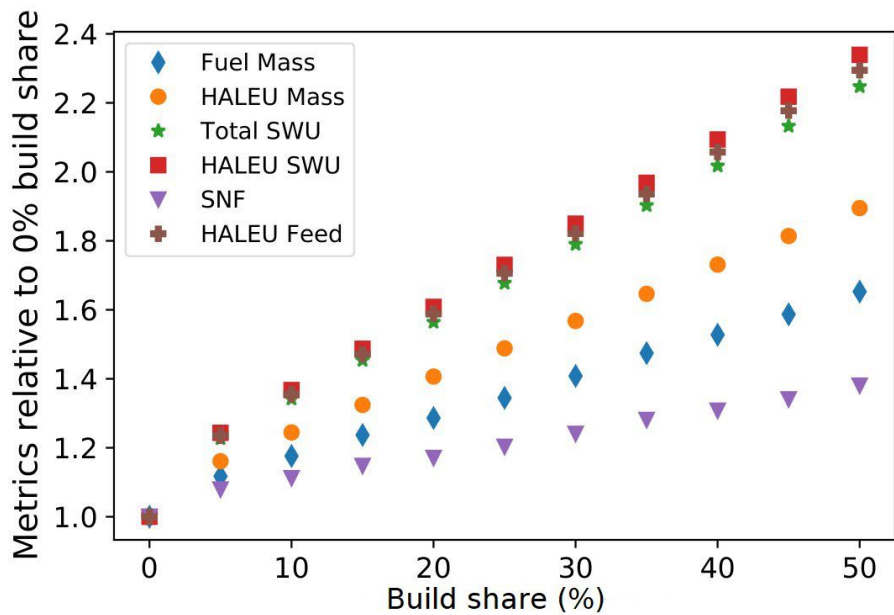


Figure 6.6: Change in each metric as a function of MMR build share, relative to a build share of 0%.

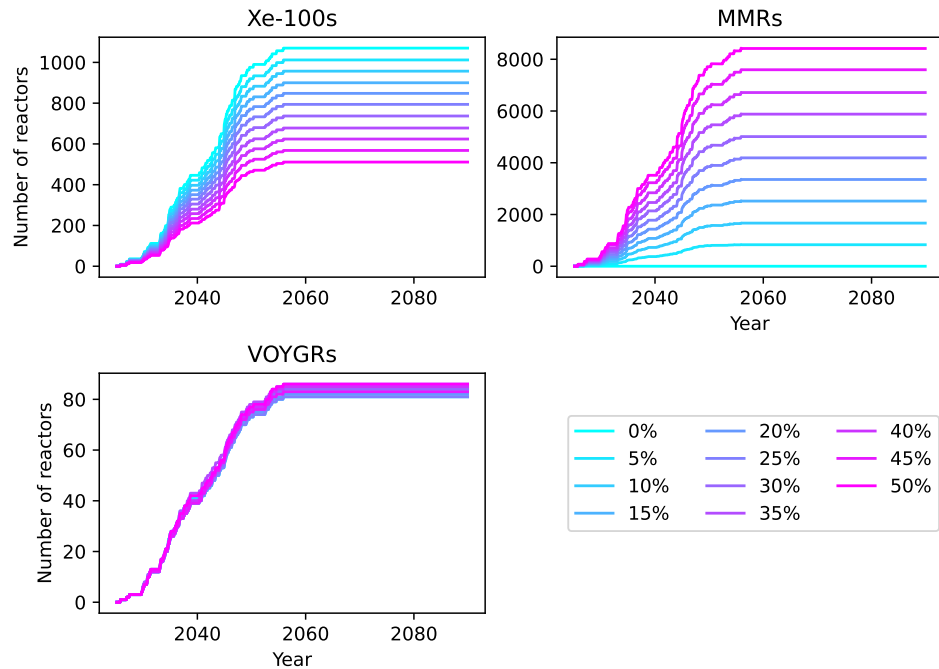


Figure 6.7: Number of Xe-100s (top left), MMRs (top right), and VOYGRs (bottom left) deployed as a function of time and MMR build share.

### 6.2.5 VOYGR build share

Varying the VOYGR build share causes trends that are opposite to the effects observed from varying the Xe-100 build share. (Figure 6.8). The total fuel mass and UNF mass increase, the HALEU-related metrics decrease, and the total SWU capacity remains relatively constant. This reversal of trends occurs because there is a replacement of Xe-100s with VOYGRs with increasing build share (Figure 6.9), the opposite of what happens with an increasing Xe-100 build share.

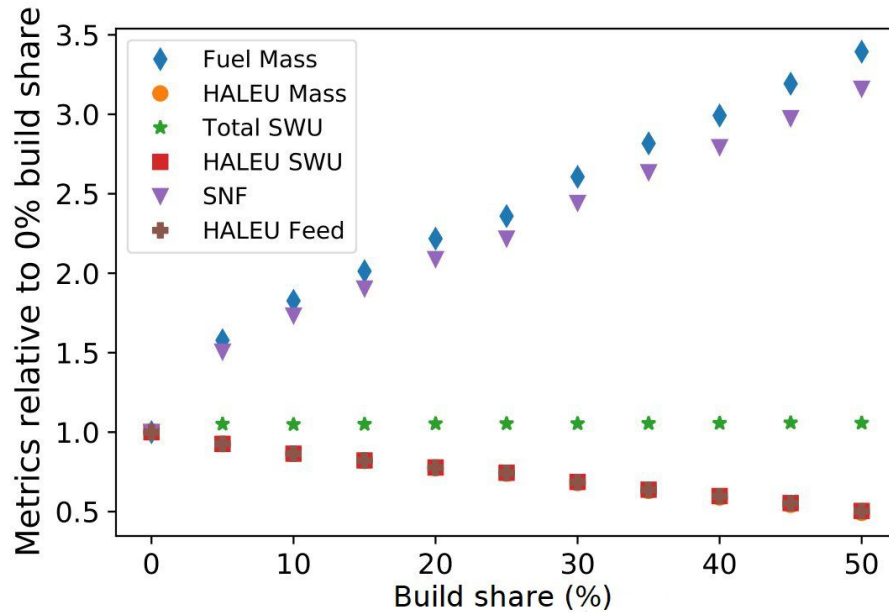


Figure 6.8: Change in each metric as a function of VOYGR build share, relative to a build share of 0%.

The total SWU capacity required varies between 99.6%-101.2% of the SWU capacity needed for a 0% VOYGR build share, a range of  $1.077 \times 10^9$  -  $1.092 \times 10^9$  kg-SWU (Table 6.1). The total fuel mass and UNF mass increase up to 313.9% of the mass required for a 0% VOYGR build share, and the HALEU-related metrics decrease to 49.77% of the mass required for a 0% VOYGR build share. The UNF and total fuel masses increase because the VOYGR requires more fuel than the Xe-100, largely stemming from the difference in discharge burnup of these two reactors. The HALEU-related metrics all decrease because the VOYGR does not require HALEU. As the VOYGR build share increases a smaller portion of the advanced reactor fleet requires HALEU. While the trends from varying the VOYGR build share mirrors the trends from varying the Xe-100 build share, the magnitude of the changes are not the same because these parameter variations cover adjacent but not overlapping design spaces.

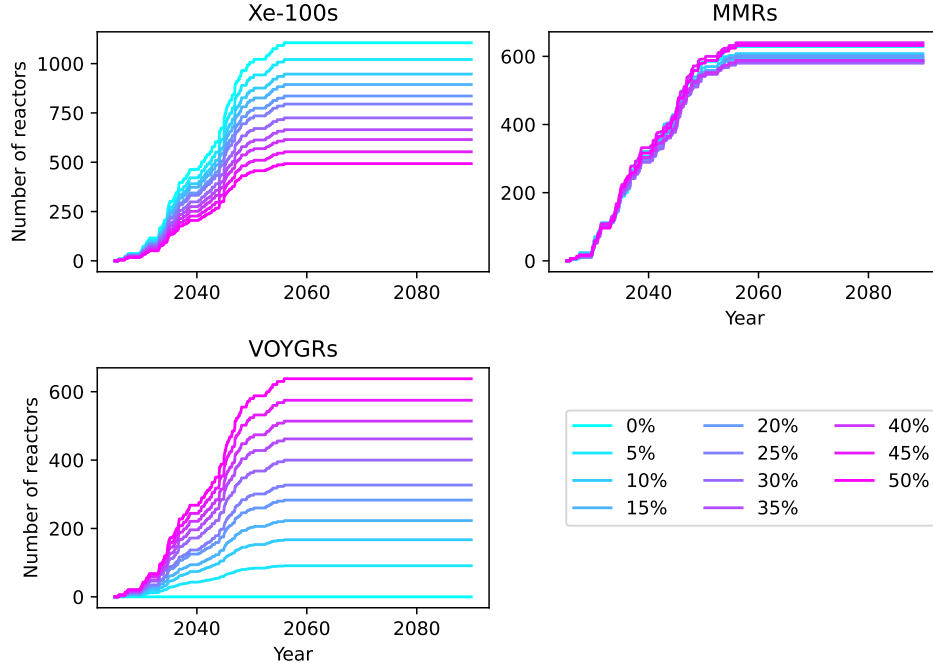


Figure 6.9: Number of Xe-100s (top left), MMRs (top right), and VOYGRs (bottom left) deployed as a function of time and VOYGR build share.

### 6.2.6 Xe-100 burnup

When varying the burnup of fuel discharged from Xe-100s, the metrics decrease as the burnup increases (Figure 6.10). The material requirements decrease with increasing burnup because there are more batches of fuel or the fuel spends more time in the core. Therefore, the Xe-100s in the simulation are receiving less fuel at each refueling or receiving fuel less often as the burnup increases. Varying the burnup of the Xe-100 has a large impact on the metrics; the Xe-100 reaching a burnup of 28 MWd/kg burnup requires up to five times the material requirements compared with the designed burnup of 168 MWd/kgU. When varying this parameter, most of the energy is met through deploying Xe-100s, so their fuel needs drive the total fuel cycle needs. Therefore, changes to the Xe-100 refueling is magnified because of their large deployment.

### 6.2.7 MMR burnup

When varying the MMR discharge burnup, all of the metrics decrease, similar to what was observed by varying the Xe-100 discharge burnup, as shown in Figure 6.11. One difference in the trends observed between varying these two parameters is the magnitude of the relative changes. Varying the MMR burnup has a smaller relative effect on the metrics than varying the Xe-100 burnup because the MMRs meet a much smaller portion of the energy demand than the Xe-100s. Therefore the impact on the cumulative metrics (what is reported here) is smaller. Another

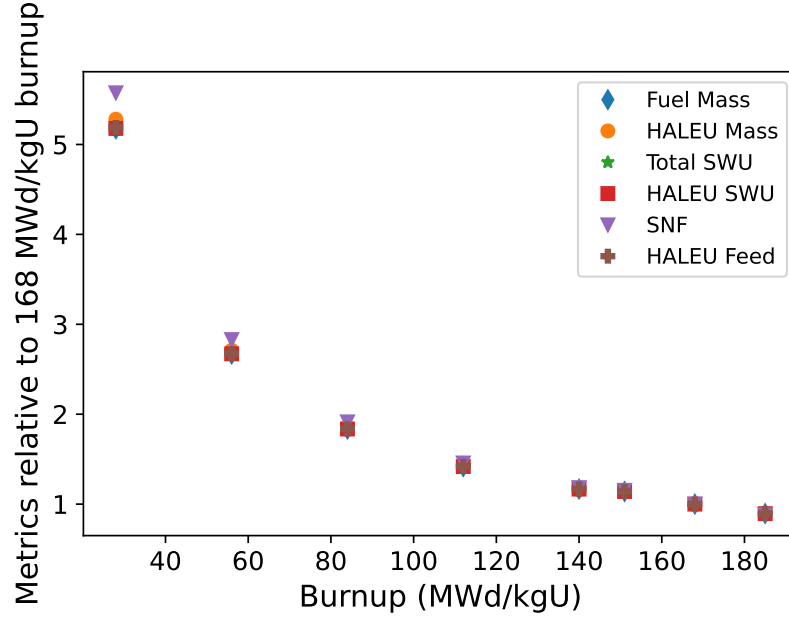


Figure 6.10: Change in metrics from varying the burnup of fuel discharged from Xe-100, relative to a burnup of 168 MWd/kgU.

difference is that the total SWU, HALEU SWU, and HALEU feed increase the most when the MMR burnup is low, compared with the UNF having the greatest relative increase with the Xe-100 burnup is low. The difference in the relative change in UNF is a result of the long cycle time of the MMR and the results not accounting for UNF still in a reactor at the end of the simulation, as previously discussed.

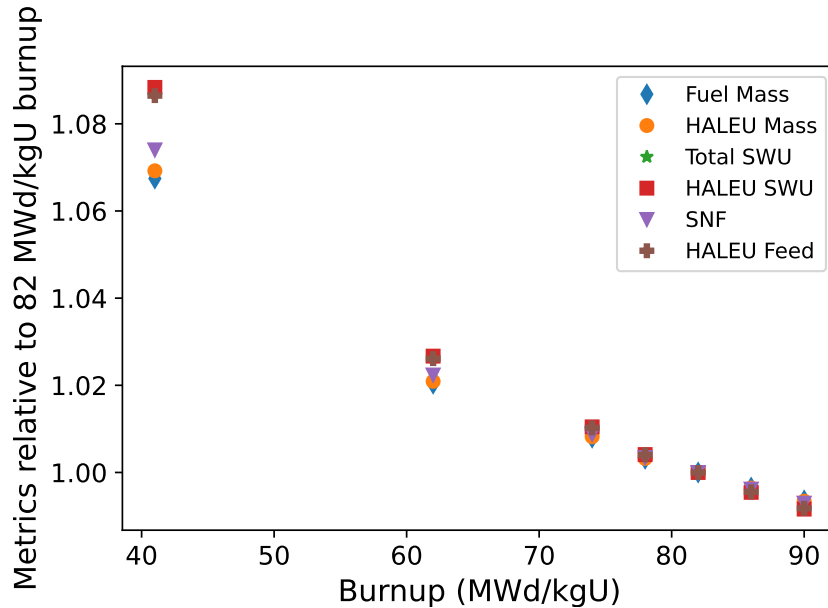


Figure 6.11: Change in metrics from varying the burnup of fuel discharged from the MMR, relative to a burnup of 82 MWd/kgU.

### 6.2.8 Burnup variations with a common build share

To better investigate the effect of varying the discharge burnup of the Xe-100 and MMR without the influence of the deployment scheme preferentially deploying Xe-100s, we repeated each set of analysis using a constant 20% build share for both the Xe-100 and MMR (VOYGRs meet the remaining 60%). Using a constant build share for both reactors means that they each will supply the same fraction of the energy demand. However, because of the different power output for each reactor a constant build share does not mean that the same number of each reactor is built.

Figure 6.12 shows the relative change in each metric as a result of varying the MMR (Figure 6.12a) and Xe-100 (Figure 6.12b) discharge burnup with the constant build share. Changing the MMR burnup has a greater impact with the specified 20% build share than when the build share was not specified. This change is because more MMRs are deployed with a 20% build share than when the build share is not specified. Conversely, the Xe-100 burnup has a smaller impact on the metrics with a 20% build share than when a build share isn't specified because fewer Xe-100s are deployed.

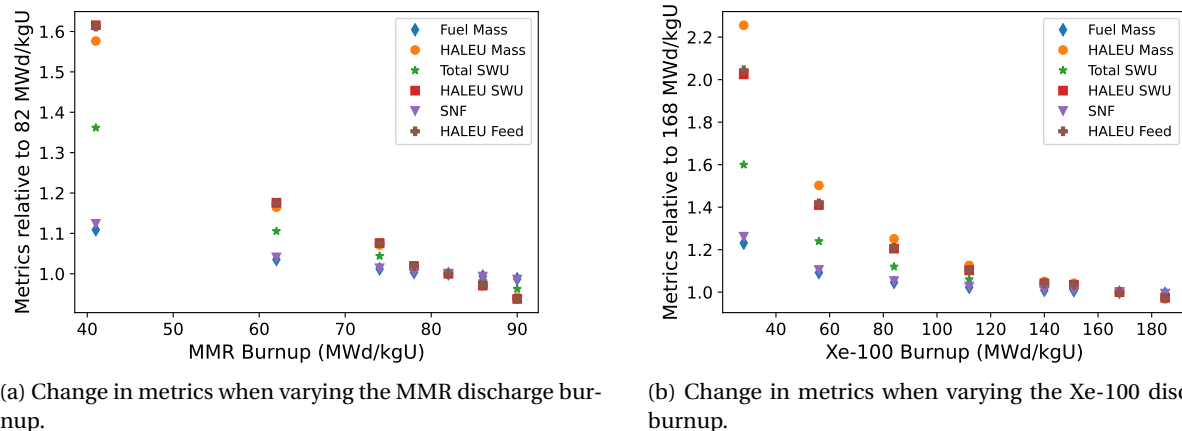


Figure 6.12: Relative changes in the metrics caused by changes in the discharge burnup of the HALEU-fueled advanced reactors, assuming a constant 20% build share for the Xe-100 and MMR.

By applying a constant build share, variations in these parameters lead to more variation in the effect on the metrics than when a build share was not specified. In these scenarios, varying the discharge burnup of either reactor leads to the greatest impact on the HALEU-related metrics while the total fuel mass and UNF mass are affected the least. The HALEU-related metrics are affected the most because most of the energy demand is met through VOYGRs, which do not require HALEU. Small changes in the each of the HALEU-related metrics led to larger relative changes because these two reactors drive the effects on the HALEU-related metrics. Conversely, the total fuel mass and UNF masses are affected less by changes in these parameters because the fuel and UNF for the VOYGRs are

constant and the Xe-100 and MMR have less of an impact on these two metrics.

## 6.3 Synergistic

The synergistic analysis in this work varied two parameters at a time to investigate some of the combined effects of the input parameters. Synergistic sensitivity analysis helps to identify if the combined effect of two parameters has a greater impact on the metrics than when varying a single parameter. It also helps to compare the effect of two different input parameters. We ran synergistic analysis on all combinations of two input parameters studied in the OAT analysis, except combinations of two reactor build shares to limit the scope of this work. The results presented here are only a subset of the analysis performed, with the remaining results in Appendix 9.1.

### 6.3.1 LWR lifetime and VOYGR build share

When the percent of LWRs operating for 80 years and the VOYGR build share are varied, the results are consistent with the results from varying each of the parameters by themselves. The effect on the HALEU mass (Figure 6.14) is fairly uniform across the parameter space. As the VOYGR build share and percent of LWR with extended licenses increase, the HALEU mass required decreases, which is consistent with the results of the OAT analysis for these parameters. By combining these two parameters, there is a greater decrease in the HALEU mass than the decrease observed by just varying a single parameter. However, the linear trend in the metric are consistent with the results of the OAT analysis for each of these parameters, which suggests that these parameters do not interact with each other to cause a greater effect on the metric. The other HALEU metrics, the HALEU SWU and HALEU feed, also decrease in a similar manner as the HALEU mass.

The total enriched uranium mass decreases with increasing LWR lifetimes, but increases with increasing VOYGR build share. There is a greater decrease in the total fuel mass required as the LWR lifetime increases for greater values of VOYGR build share. This suggests some interaction between these two parameters on this output metric because the effects are not uniform across the parameter space.

### 6.3.2 Xe-100 build share and Xe-100 burnup

When the Xe-100 build share and discharge burnup are varied together, there is a strong combined effect on the metrics. The HALEU mass required (Figure 6.15) increases as the burnup decreases and as the Xe-100 share increases. The combined effect of these parameters is pronounced, such that there is a large increase in the HALEU mass as the Xe-100 burnup reaches its minimum and the Xe-100 build share reaches its maximum. This effect stems from a larger portion of the advanced reactor fleet using its fuel less efficiently as this corner of the input

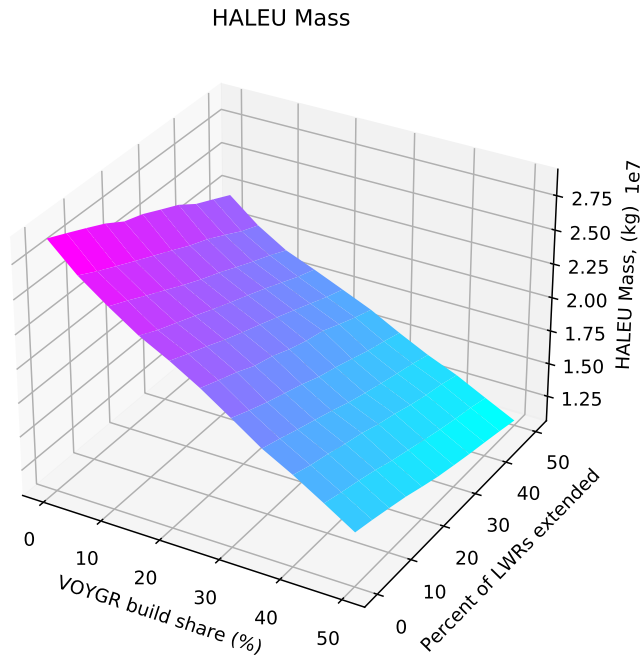


Figure 6.13: Effect of the LWR lifetime and VOYGR build share on the HALEU mass.

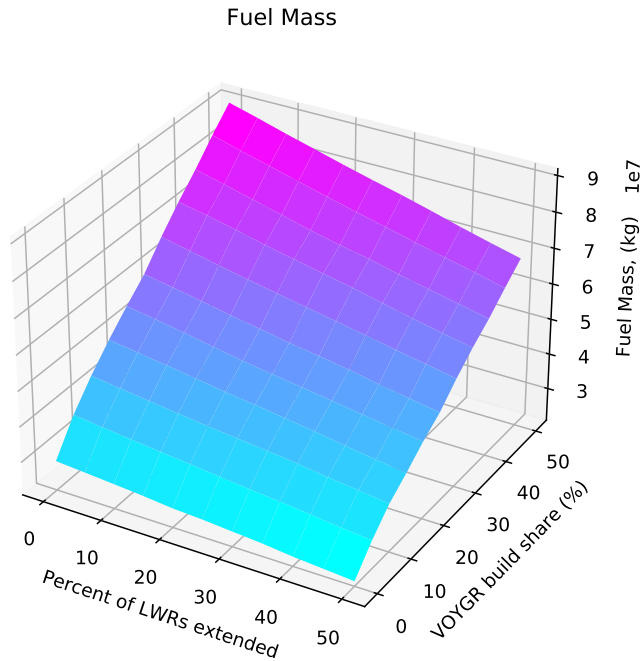


Figure 6.14: Effect of the LWR lifetime and VOYGR build share on the total enriched uranium mass.

space is reached. This result suggests that the discharge burnup of an advanced reactor should be considered when determining the build share of an advanced reactor, if this metric is important.

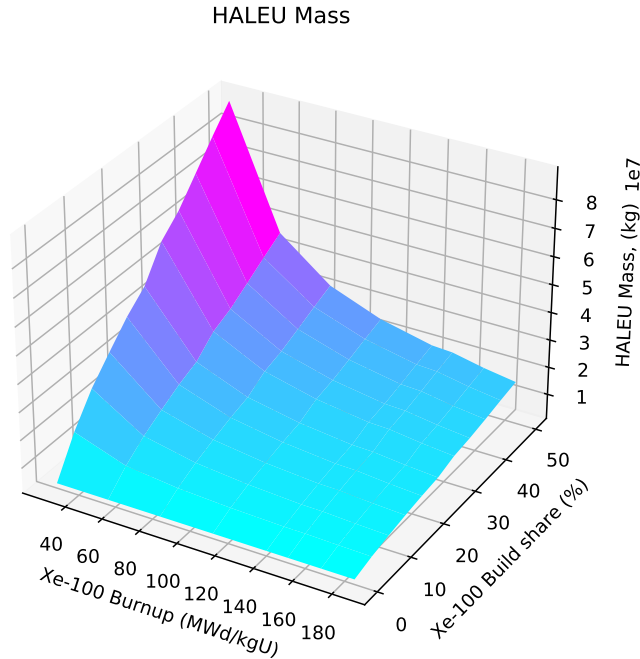


Figure 6.15: Effect of Xe-100 discharge burnup and Xe-100 build share on HALEU mass.

The total fuel mass (shown in Figure 6.16) reaches a minimum with a maximum Xe-100 build share and Xe-100 discharge burnup, which matches the trends observed in the OAT analysis. A minimum is reached in this corner of the parameter space because more of the advanced reactor fleet is getting more energy out of the fuel used, so less fuel is required. Variations in the Xe-100 burnup do not affect the results when there is a 0% Xe-100 build share because no Xe-100s are deployed. The Xe-100 build share does not greatly affect the fuel mass required when the Xe-100 has a discharge burnup of 28 MWd/kgU (the lowest value used in this work) because at this burnup level, the Xe-100 requires a similar amount of enriched uranium as the VOYGR for each 18 month period. Therefore, as the VOYGRs are replaced with Xe-100s as a consequence of increasing the Xe-100 build share, the cumulative total fuel mass required does not change much.

### 6.3.3 MMR build share and Xe-100 burnup

When the MMR build share and Xe-100 burnup are varied together, the effect on the metrics is not as consistent as the results from varying other pairs of parameters, as Figure 6.17 shows. As the Xe-100 burnup increases, the fuel mass required by all of the advanced reactors decreases. However, the effect of increasing the MMR build share is

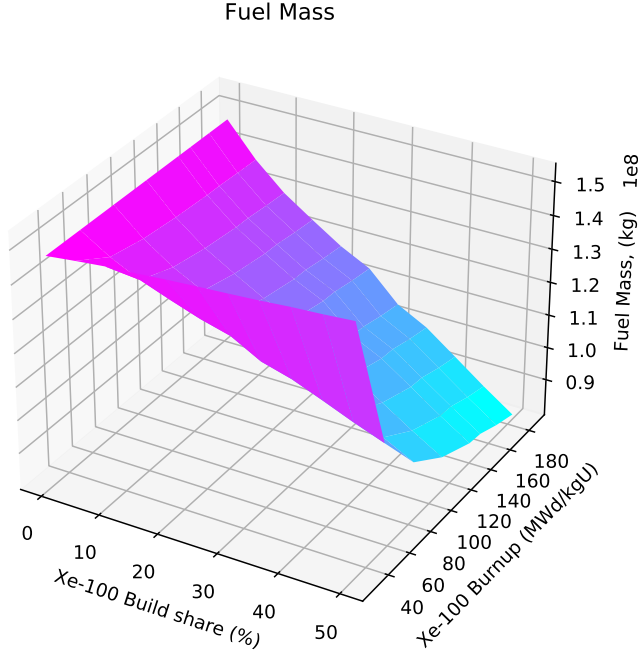


Figure 6.16: Effect of Xe-100 discharge burnup and Xe-100 build share on total fuel mass.

dependent on the Xe-100 discharge burnup. At smaller Xe-100 discharge burnup values, the fuel mass decreases with increasing MMR build share. But at larger Xe-100 discharge burnup values, the fuel mass increases with increasing MMR build share. The different trends result from changes in how much fuel the Xe-100 requires at each refueling and the difference between that and the amount of fuel required by the MMR. At the lowest burnup values, the Xe-100 requires more fuel than the MMR. Therefore, as the Xe-100s are replaced with MMRs from increasing the MMR share, the total mass of fuel required in the transition decreases. However, as the Xe-100 burnup increases, the Xe-100 requires less fuel than the MMR. Therefore, requiring more of the advanced reactor fleet to be MMRs increases the total fuel mass required by advanced reactors in the transition. These results identify how these two input parameters interact to affect the output metrics. We observe the at small Xe-100 burnup values increasing the MMR build share decreases the metric, but at high Xe-100 burnup values increasing the MMR build share increases the metric in all six metrics considered in this work (see Appendix 9.1).

### 6.3.4 Transition start and Xe-100 build share

As Figure 6.18 shows, as the Xe-100 build share increases, the total fuel mass decreases. However, there is little effect in the total fuel mass as the transition start time is delayed. The magnitude of the effect on the fuel mass from varying the Xe-100 build share is greater than the magnitude of the effect from varying the transition start time.

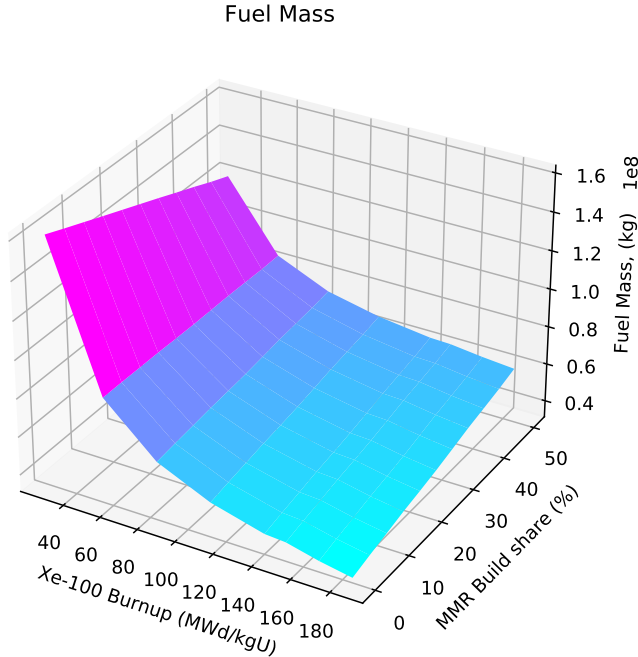


Figure 6.17: Effect of Xe-100 discharge burnup and MMR build share on total fuel mass.

This is consistent with the results from the OAT analysis, and is observed for five of the metrics considered in this work. This result suggests that the transition start time is not as important as the other parameters when trying to minimize or maximize certain metrics.

The effect of varying these two parameters is the opposite when the total SWU capacity is considered: varying the transition start time has a greater impact on the metric than varying the Xe-100 build share as shown in Figure 6.19. This result stems from the similar SWU capacities needed for the Xe-100 and VOYGR and the replacement of VOYGRs with Xe-100s with increasing Xe-100 build share, leading to little change in the total SWU capacity required when varying the Xe-100 build share. Therefore, the transition start time has more impact on this metric than the Xe-100 build share, and there is little of a combined effect observed because of the small impact from each parameter on this metric.

## 6.4 Global

In each calculation of the global sensitivity analysis, we varied the transition start time, percent of LWRs operating for 80 years, the Xe-100 discharge burnup, MMR burnup, and build share of one advanced reactor. We decided to perform this analysis three separate times instead of varying all seven variables to prevent unwanted combinations

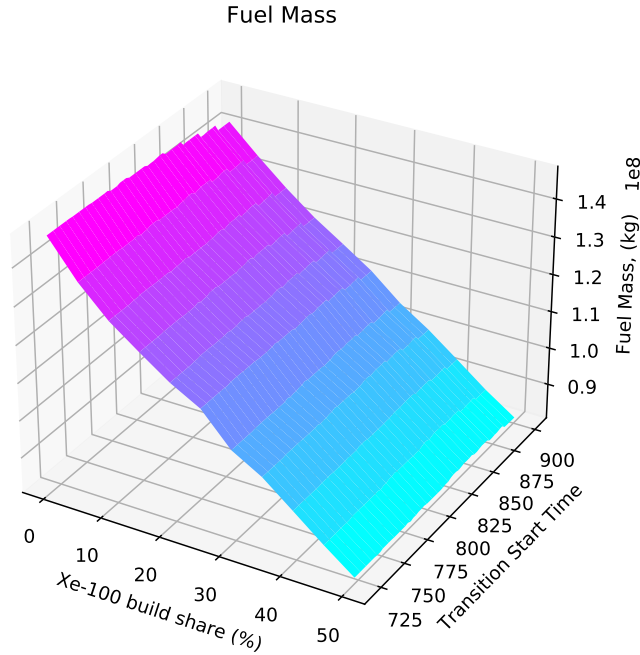


Figure 6.18: Effect of transition start time and Xe-100 build share on total fuel mass.

of the advanced reactor build shares that result in an oversupply or undersupply of power.

Instead of comparing ranges and values of each metric in this analysis, we compared the variance each input parameter causes in the output metrics through the Sobol' indices. To assist in calculating the Sobol' indices, we created surrogate models for each of the iterations. These models are approximations of the relationships between the input and output parameters, are computationally inexpensive [28], and assist in exploring an entire input space, as compared with exploring an input space in a grid search. To generate each of the surrogate models (one for each advanced reactor build share variation), we ran 4000 different fuel cycle transitions based on guidance from the Dakota manual [28] to run

$$100 \times P \times (R + 2) \quad (6.1)$$

number of cases to build the surrogate model In Eq 6.1,  $P$  is the number of input parameters and  $R$  is the number out response metrics.

In each of these transitions, we allowed most of the input parameters vary freely within a given range (defined in Table 6.2), and used Latin Hypercube Sampling (a near-random technique in Dakota) to select parameter values.

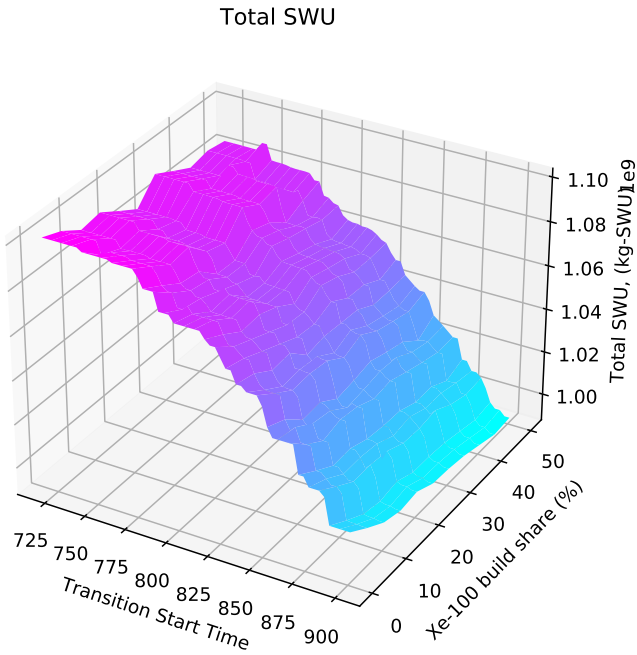


Figure 6.19: Effect of transition start time and Xe-100 build share on total fuel mass.

We did not allow the Xe-100 discharge burnup to vary freely within a range when running the initial transition scenarios. We kept this input parameter constrained to specific values, like in the OAT analysis. The burnup values considered for the sensitivity analysis thus far are based on integer numbers of passes through the core (batches) and integer number of months for the cycle lengths of this reactor. By using Xe-100 burnup values that correspond to integer values, we can adhere to the integer value restrictions in CYCLUS on the number of batches in a core. We expanded the Xe-100 discharge burnup values considered to provide additional data points off of which to generate the surrogate model. We selected additional burnup points to represent between one and six passes for each pebble with a residence time of six, seven, or eight months for each pass. This expansion of the Xe-100 burnup resulted in 16 different burnup values between 28-185 MWd/kgU. We converted the MMR burnup from a discrete variable to a continuous variable by varying the lifetime of the reactor as need to achieve the burnup value. We made this conversion from discrete to continuous for the MMR burnup because the lack of multiple batches in the core means that there are no inherent restrictions to integer numbers.

After explicitly modeling the transition scenarios with different combinations and the specific Xe-100 burnup values, we created surrogate models. When creating the surrogate model, we once again used the Latin Hypercube sampling for all of the variables, but allowed all of the input parameters to be continuous variables. The surrogate

Table 6.2: Ranges of the input parameters considered for generating surrogate models in the global sensitivity analysis. The Xe-100 burnup was constrained to 16 different values within the given range, while the other variables were free to vary within the defined range.

Input parameter	Range	Units
Transition start time	January 2025-January 2040	-
LWR lifetime extensions	0-50	%
Reactor build share	0-50	%
MMR burnup	41-90	MWd/kg
Xe-100 burnup	28-185	MWd/kg

models are not bound by the variable-type restriction in CYCLUS, so we were able to allow the Xe-100 burnup to not be bound by integer numbers of batches. We used both the quadratic and Gaussian fits to the data to create the surrogate models, similar to what Richards and Feng did [54]. The quadratic method defines a second-order response surface based on linear least squares regressions methods [28]. The Gaussian method uses a Gaussian correlation function to define a response surface [28]. We used both methods were used to provide a comparison of the different methods, since they each have limitations. The quadratic method does not implement any forward- or backward-stepping regression methods to remove unnecessary terms in the polynomial fit, and the Gaussian method may discard points if the data points are poorly spaced [28]. These limitations in the methods contributed to the decision to have as many input parameter data points as possible. We also instructed Dakota to perform variance decomposition on both of the surrogate models to calculate the Sobol' indices.

The results presented in this section include the results from the initial transitions modeled, the results from the surrogate models, and the Sobol' indices that describes the impact of each input parameter on each output metric. The results from the modeled transitions and the surrogate models provide information of how well the surrogate models fit some of the trends and relationships between the input parameters and output metrics. The total and the main Sobol' indices reported describe the contribution from each parameter and its interactions with all of the other parameters and the contribution from each individual parameter, respectively.

#### 6.4.1 Xe-100 build share

This section provides the results of the global sensitivity analysis using both a Gaussian and a quadratic surrogate model when varying the Xe-100 build share.

##### Gaussian surrogate model

The Gaussian surrogate model for the variations in the Xe-100 build share results in an  $R^2$  value of 1 for each metric. This value means that the outputs of the surrogate model match perfectly to the data provided from the initial CYCLUS runs. The large  $R^2$  value suggests that this surrogate model type fits to noise in the data provided. Figure

6.20 compares the values of the HALEU mass as a function of the Xe-100 burnup for the Gaussian model and the input data (the explicitly modeled transitions). The results of the Gaussian model follows the input data well, nearly reaching the maximum and minimums of the data. However, closer inspection of the data shows that results of the Gaussian model include non-physical results, such as negative values of HALEU mass. These values suggest that the Gaussian model extrapolates to obtain some of the values, instead of just interpolating. Therefore, the Gaussian model is not a perfect match to the input data, which means that the Sobol' indices are different than if the variance decomposition were performed directly on the input data.

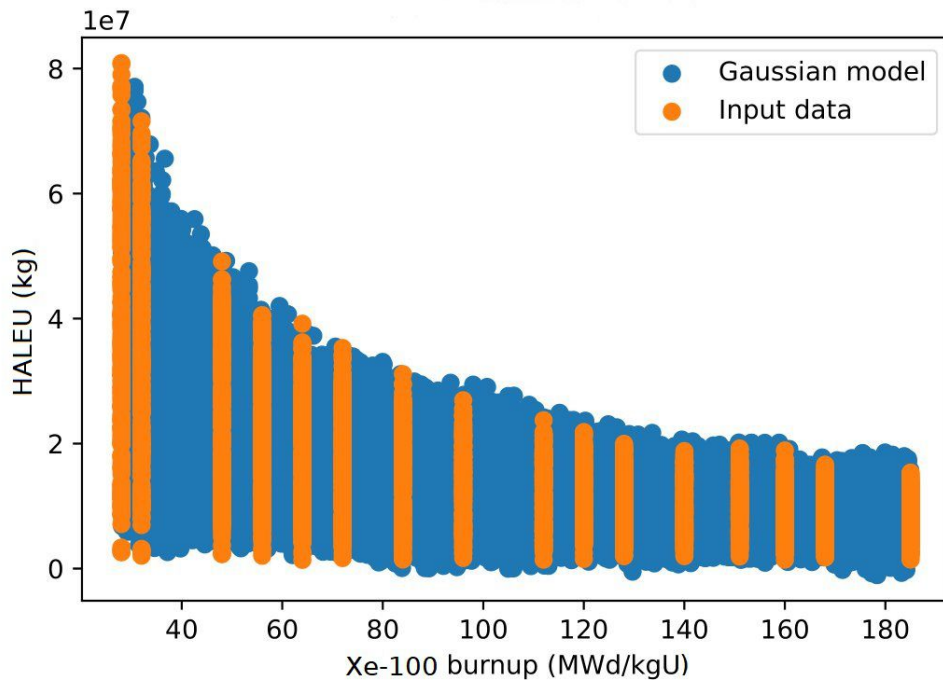


Figure 6.20: Comparison of the input data and the results of the Gaussian surrogate model when varying the Xe-100 build share.

Table 6.3 reports the main and total Sobol' indices for each input parameter on each output metric. The highlighted cells have a total Sobol' index of at least 0.5, to indicate parameters that have a large effect on the metrics. The transition start time has little effect on any of the metrics, which is consistent with the results of the OAT and synergistic analysis. The LWR lifetimes do not greatly affect any of the HALEU-related metrics or the total SWU capacity because this parameter primarily delays when the HALEU-fueled reactors are deployed and not how many are deployed. The LWR lifetimes have some impact on the total fuel mass and the UNF mass, but less of an impact than the Xe-100 build share. The MMR burnup has a small Sobol' index for all of the output metrics because a very small portion of the fleet are MMRs.

The Xe-100 build share and burnup have a large effect (total Sobol' indices more than 0.5) on all three of the HALEU-related metrics because the number of MMRs built in these transitions are relatively constant and the variations in the Xe-100s drive the changes in these metrics. The Xe-100 build share does not have as much of an impact on the total SWU capacity because of the similar SWU capacity required by the Xe-100 and the VOYGR and the replacement of VOYGRs with Xe-100s as the Xe-100 build share increases. The Xe-100 build share has the largest impact on the total fuel mass and the UNF mass because of the replacement of Xe-100s with VOYGRs as the Xe-100 build share decreases and the large difference in fuel mass required by these two reactors. The Xe-100 burnup has the largest impact on the total SWU capacity because as this parameter varies, so does the difference in SWU capacity needed to fuel the Xe-100 and the SWU capacity needed to fuel the VOYGR.

Table 6.3: Sobol' indices for the Gaussian model when varying the Xe-100 build share. The first value is the main index, the second value is the total index. Highlighted values indicate a total Sobol' indices of above 0.5.

Parameter	Output Metric					
	Fuel Mass	HALEU Mass	SWU	HALEU SWU	Feed	UNF Mass
Transition Start	0.003/0.003	0.007/0.007	0.007/0.009	0.009/0.009	0.006/0.009	0.003/0.003
LWR Lifetime	0.268/0.280	0.012/0.021	0.081/0.095	0.013/0.022	0.013/0.022	0.301/0.314
Xe-100 Build Share	0.478/0.533	0.375/0.513	0.099/0.283	0.374/0.511	0.374/0.512	0.411/0.474
Xe-100 Burnup	0.188/0.247	0.465/0.571	0.622/0.775	0.463/0.568	0.463/0.568	0.214/0.280
MMR Burnup	0.002/0.002	0.003/0.004	0.005/0.006	0.004/0.005	0.004/0.005	0.002/0.002

### Quadratic surrogate model

When using a quadratic surrogate model, the  $R^2$  values for the training points on each output metric range between 0.921-0.966. Therefore, these model are expected to fit the input data provided but not be fit to the noise in the input data as much as the Gaussian model. A comparison of the Xe-100 burnup and HALEU mass for the input data and the results of the quadratic model (Figure 6.21) shows that the quadratic model does capture the overall trend of the input data. However, like the Gaussian model, the quadratic model gives the non-physical result of a negative HALEU mass at some points. Additionally, the results of the quadratic model do not meet the maximum of the input data and provide multiple results below the minimum value of the input data. Therefore, the quadratic model is also performing some extrapolation of the data based on the fit placed on the data.

Table 6.4 provides the main and total Sobol' indices for each of the input parameters on each output metric. The green cells identify total Sobol' indices that are at least 0.5. The same patterns observed in the Sobol' indices from the Gaussian model are observed in the values from the quadratic model as well. The Xe-100 build share and Xe-100 burnup affect the metrics the most, the LWR lifetime has some impact, and the MMR burnup and transition start time has the smallest impact on the metrics.

The two surrogate models result in different Sobol' indices for each input parameter/output metric pair. These

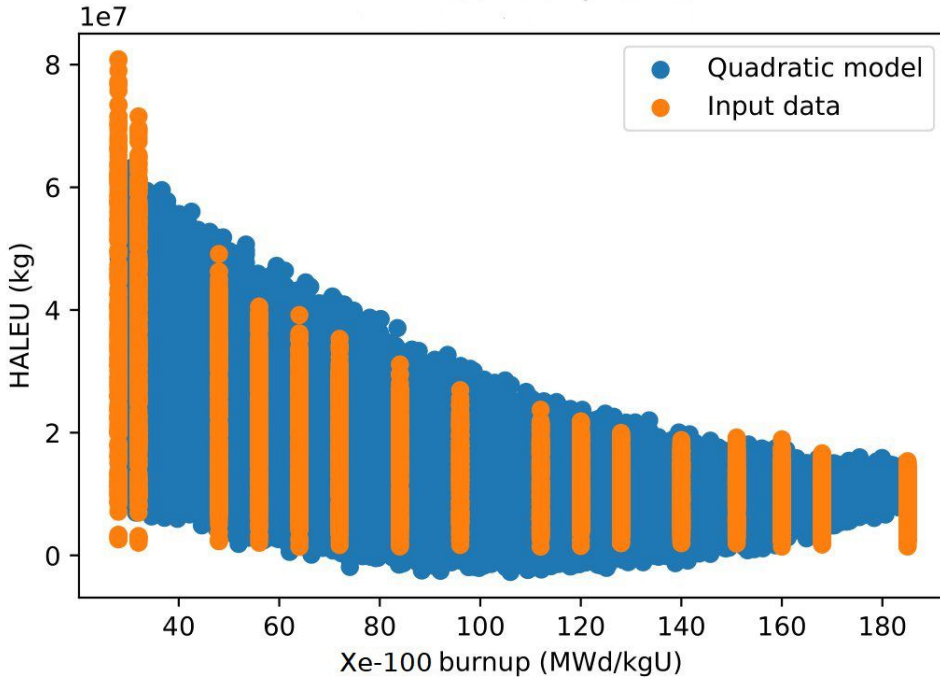


Figure 6.21: Comparison of the input data and the results of the quadratic surrogate model when varying the Xe-100 build share.

Table 6.4: Sobol' indices for the quadratic model when varying the Xe-100 build share. The first number is the main index, the second is the total index. Highlighted values indicate a total Sobol' indices of above 0.5.

Parameter	Output Metric					
	Fuel Mass	HALEU Mass	SWU	HALEU SWU	Feed	UNF Mass
Transition Start	0.000/0.000	0.006/0.005	0.007/0.007	0.008/0.007	0.008/0.007	0.002/0.004
LWR Lifetime	0.278/0.286	0.014/0.021	0.082/0.089	0.015/0.022	0.015/0.022	0.310/0.319
Xe-100 Build Share	0.443/0.501	0.374/0.500	0.115/0.283	0.374/0.499	0.374/0.499	0.375/0.441
Xe-100 Burnup	0.214/0.279	0.472/0.578	0.624/0.773	0.470/0.576	0.430/0.576	0.243/0.315
MMR Burnup	0.001/0.001	0.002/0.002	0.004/0.004	0.003/0.003	0.003/0.003	0.001/0.001

differences are likely a result of how the models fit the data. The Gaussian model fits better the extremes and trends in the input data points and does not assume a specific form for the data, but the quadratic model does not fit to the noise in the input data as much. However, the two models are consistent in their relative comparison of how much each input parameter affects the output metrics, and are consistent with the results from the OAT and synergistic analysis. The two models are also consistent in identifying that the Xe-100 build share and Xe-100 burnup have the largest impact on the metrics.

## 6.4.2 MMR build share

This section provides the results of the global sensitivity analysis using both a Gaussian and a quadratic surrogate model when varying the MMR build share.

### Gaussian surrogate model

The Gaussian model has an  $R^2$  value of 1 with respect to each of the output metrics. This value means that these models are also expected to fit the input data very well, including any noise present in the data. As Figure 6.22 shows, the data from the Gaussian model fits well to the input data provided. Unlike the models predicted based on input data when varying the Xe-100 build share, this model does not result in any negative mass values. However, it still results in mass values lower than what is present in the input data which suggests that this model also extrapolates on some of the data. It also does not fully predict some of the outliers in the data, such as the maximum HALEU mass at a burnup at 128 MWd/kg.

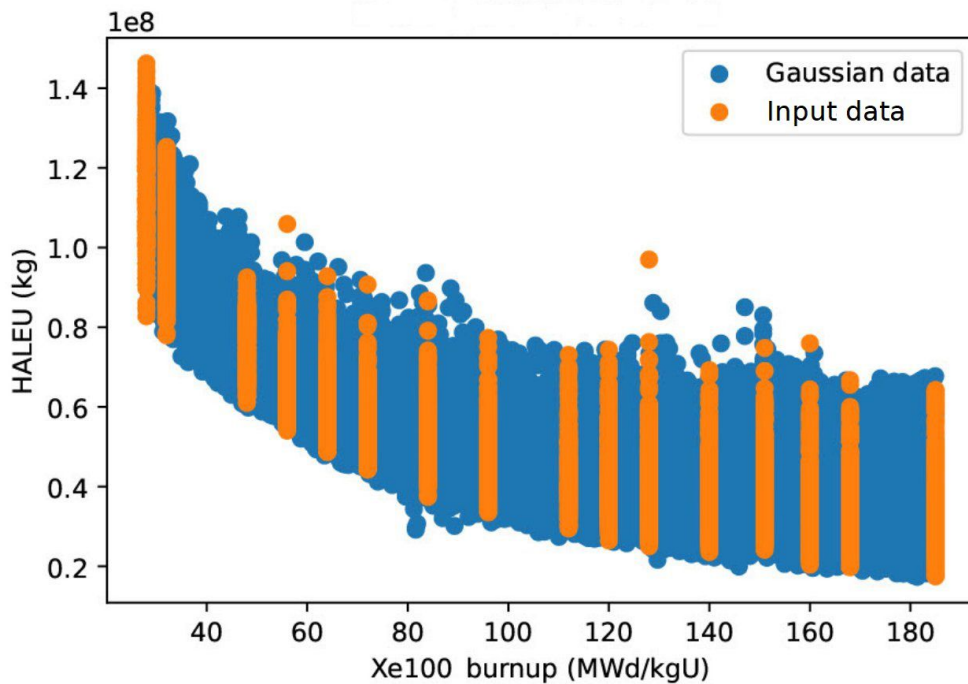


Figure 6.22: Comparison of the input data and the results of the Gaussian surrogate model when varying the MMR build share.

Examination of the Sobol' indices for this model (Table 6.5) shows that the Xe-100 burnup has the largest impact and a significant impact (i.e., total indices greater than 0.5) on all of the output metrics. One may expect the MMR build share and MMR burnup to have a strong combined impact on the results. However, this result is consistent

with the results shown for the synergistic analysis (Figures A.12 and A.13). When the Xe-100 burnup was varied in combination with the MMR share, the range of values for each metric was larger than when the MMR burnup was varied with the MMR build share. Variations in the MMR build share replaces Xe-100s with MMRs. The variations in the Xe-100 burnup lead to greater changes in the metrics than variations in the MMR burnup, as shown in Figure 6.12, because the Xe-100 burnup values span a larger range and the compounding effects of the multiple batches in the Xe-100. Similar to the results from varying the Xe-100 build share, the transition start time has effectively no impact on the results. The LWR lifetime has less of an impact on the metrics than when the Xe-100 build share was varied. The MMR burnup also has little impact on the output metrics.

Table 6.5: Sobol' indices for the Gaussian model when varying the MMR build share. The first number is the main index, the second is the total index. Highlighted values indicate a total Sobol' indices of above 0.5.

Parameter	Output Metric					
	Fuel Mass	HALEU Mass	SWU	HALEU SWU	Feed	UNF Mass
Transition Start	0.001/0.006	0.000/0.004	0.001/0.001	0.001/0.001	0.001/0.001	0.001/0.006
LWR Lifetime	0.054/0.068	0.047/0.063	0.055/0.071	0.054/0.069	0.054/0.069	0.057/0.071
MMR Build Share	0.069/0.107	0.068/0.107	0.162/0.203	0.162/0.204	0.152/0.193	0.015/0.055
Xe-100 Burnup	<b>0.806/0.846</b>	<b>0.819/0.858</b>	<b>0.700/0.732</b>	<b>0.701/0.734</b>	<b>0.713/0.747</b>	<b>0.858/0.900</b>
MMR Burnup	0.035/0.049	0.037/0.050	0.054/0.071	0.054/0.071	0.052/0.069	0.038/0.053

### Quadratic surrogate model

When using the quadratic surrogate model, the model has an  $R^2$  value of 0.94 with respect to each of the output metrics. Therefore, these models also fit the data well without fitting all of the noise present in the input data. As Figure 6.23 shows, the output of the quadratic model fits the input data well, but not perfectly. Similar to the quadratic model created from varying the Xe-100 build share, this model does not perform well in fitting the maximum values and under-predicts some of the minimum values in the input data.

The Sobol' indices from the quadratic model (Table 6.6) are similar to those from the Gaussian model. The Xe-100 burnup has the largest impact on all of the output metrics. The MMR build share has the next largest impact on the metrics, but it is a very small impact. The other model parameters have a negligible effect on the metrics. The Sobol' indices from this model are very similar to those from the Gaussian model.

### 6.4.3 VOYGR build share

This section provides the results of the global sensitivity analysis using both a Gaussian and a quadratic surrogate model when the varying the VOYGR build share.

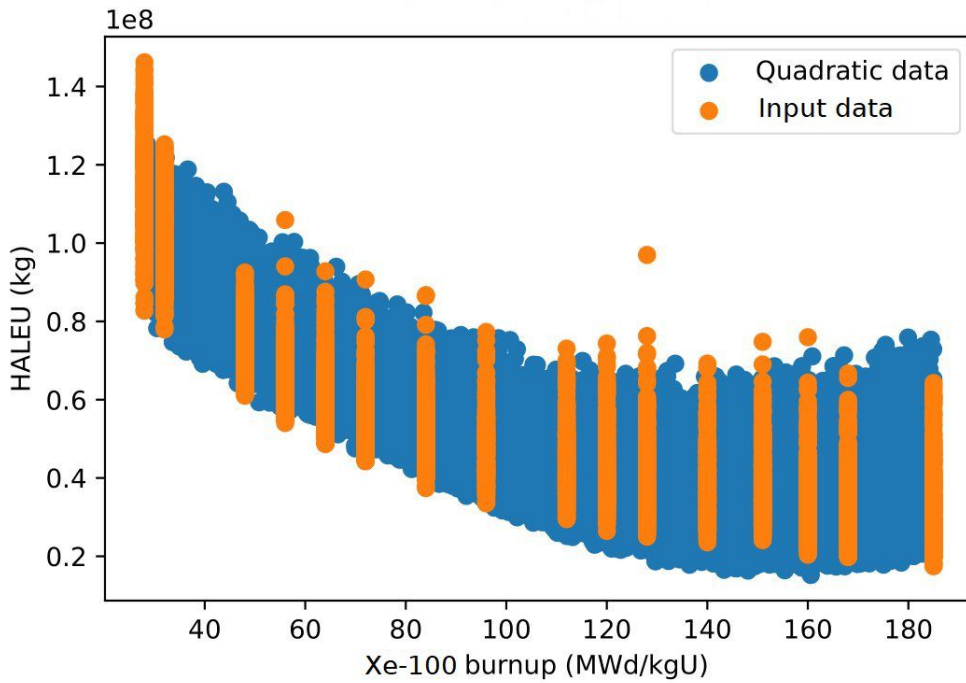


Figure 6.23: Comparison of the input data and the results of the quadratic surrogate model when varying the MMR build share.

Table 6.6: Sobol' indices for the quadratic model when varying the MMR build share. The first number is the main index, the second is the total index. Highlighted values indicate a total Sobol' indices of above 0.5.

Parameter	Output Metric					
	Fuel Mass	HALEU Mass	SWU	HALEU SWU	Feed	UNF Mass
Transition Start	0.002/0.003	0.000/0.000	0.000/0.000	0.000/0.000	0.000/0.000	0.002/0.003
LWR Lifetime	0.023/0.062	0.046/0.054	0.050/0.059	0.049/0.057	0.049/0.057	0.054/0.064
MMR Build Share	0.051/0.087	0.052/0.089	0.133/0.171	0.133/0.171	0.124/0.162	0.008/0.046
Xe-100 Burnup	0.834/0.866	0.846/0.875	0.742/0.764	0.742/0.765	0.753/0.777	0.879/0.909
MMR Burnup	0.034/0.039	0.034/0.040	0.050/0.058	0.050/0.058	0.048/0.056	0.035/0.041

### Gaussian surrogate model

The  $R^2$  values for the Gaussian model with respect to each output metric is 1, similar to each of the other Gaussian models. Comparing the input data and the Gaussian model data (Figure 6.24) shows that the data from the Gaussian model fits very well to the input data provided.

The Sobol' indices from this model, shown in Table 6.7 show a similar trend to the Sobol' indices from varying the MMR build share. The Xe-100 burnup has the largest impact and a large impact (a total Sobol' indices greater than 0.5) on all of the results. The transition start time and MMR burnup have effectively no effect on the metrics, and the LWR lifetimes and VOYGR build share have a very small impact on the metrics. The LWR lifetimes has a smaller effect on the metrics than when varying the Xe-100 build share, but a similar effect on the metrics to when

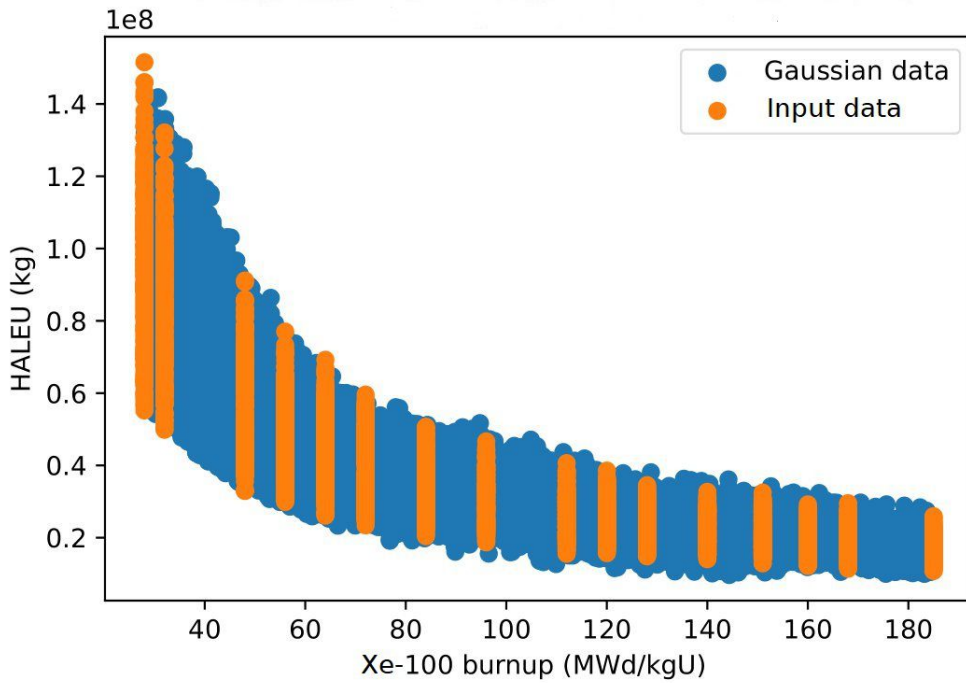


Figure 6.24: Comparison of the input data and the results of the Gaussian surrogate model when varying the VOYGR build share.

varying the MMR build share.

Table 6.7: Sobol' indices for the Gaussian model when varying the VOYGR build share. The first number is the main index, the second is the total index. Highlighted values indicate a total Sobol' indices of above 0.5.

Parameter	Output Metric					
	Fuel Mass	HALEU Mass	SWU	HALEU SWU	Feed	UNF Mass
Transition Start	0.002/0.003	0.000/0.001	0.000/0.002	0.000/0.001	0.000/0.001	0.001/0.003
LWR Lifetime	0.065/0.076	0.020/0.033	0.033/0.045	0.020/0.033	0.020/0.033	0.069/0.081
VOYGR Build Share	0.252/0.284	0.114/0.0151	0.028/0.067	0.114/0.151	0.114/0.151	0.204/0.238
Xe-100 Burnup	0.652/0.683	0.837/0.883	0.910/0.956	0.836/0.881	0.836/0.881	0.696/0.730
MMR Burnup	0.002/0.002	0.000/0.002	0.001/0.001	0.001/0.002	0.001/0.002	0.002/0.002

Based on the results of the OAT analysis, increasing the VOYGR build share replaces Xe-100s with VOYGRs. Therefore, the VOYGR build share implicitly impacts the Xe-100 build share, which leads to this input parameter having a larger impact on most of the metrics than most of the other variables. The VOYGR build share does not have a noticeable impact on the total SWU capacity because of the similar SWU capacities required by the Xe-100 and VOYGR. This result is consistent with the Xe-100 build share having a lesser effect on this metric compared with its effect on the other metrics. The VOYGR build share has a larger impact on the fuel mass and the UNF mass than the other metrics because the VOYGR takes in more and discharges more fuel than the Xe-100 per unit time

and energy. The increased impact of the VOYGR build share on these metrics leads to the decreased impact of the Xe-100 burnup, relative to the HALEU-related metrics.

### Quadratic surrogate model

When using the quadratic fit, the  $R^2$  values range between 0.94-0.95. These values are consistent with the  $R^2$  values for the other quadratic models in this work. The data from this quadratic model, compared with the input data in Figure 6.25, shows that it does not fully reach the maximum of the input data and under-predicts some of the minimum values. These trends have been observed in all of the quadratic models created for this analysis. These trends are a result of the model fitting a second-order polynomial to data that does not follow a second order polynomial. This mis-fit between the data and the model fit leads to the lower  $R^2$  value than the Gaussian surrogate models and the inability to properly fit to the extremes in the data. Therefore, one would expect the Gaussian models to be more accurate in calculating the Sobol' indices. The consistency between the values and trends of the indices from both models suggests that the quadratic models are still sufficient for these purposes.

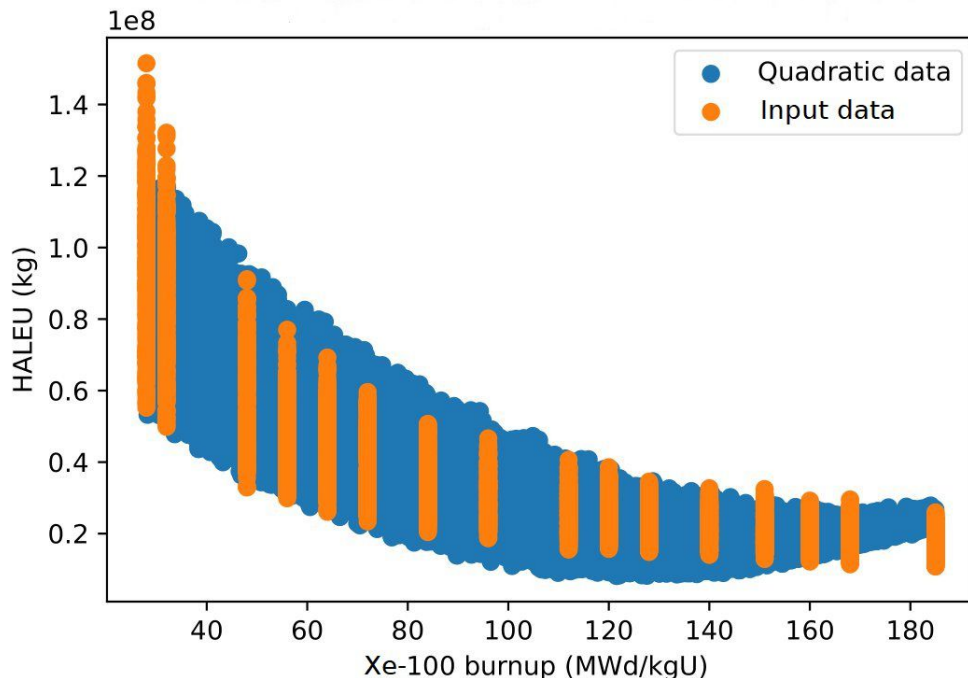


Figure 6.25: Comparison of the input data and the results of the quadratic surrogate model when varying the VOYGR build share.

The Sobol' indices from this model, reported in Table 6.8, have the same pattern as the Sobol' indices from the Gaussian model created. The Xe-100 burnup is the most impactful input parameter on all of the output metrics,

followed by the VOYGR build share and the LWR lifetime. The transition start time and the MMR burnup have a negligible effect on the results of the metrics.

Table 6.8: Sobol' indices for the quadratic model when varying the VOYGR build share. The first number is the main index, the second is the total index. Highlighted values indicate a total Sobol' indices of above 0.5.

Parameter	Output Metric					
	Fuel Mass	HALEU Mass	SWU	HALEU SWU	Feed	UNF Mass
Transition Start	0.002/0.002	0.000/0.000	0.000/0.001	0.000/0.000	0.000/0.000	0.001/0.002
LWR Lifetime	0.063/0.071	0.020/0.031	0.031/0.042	0.051/0.031	0.020/0.031	0.066/0.075
VOYGR Build Share	0.214/0.243	0.108/0.143	0.030/0.066	0.108/0.143	0.108/0.143	0.170/0.200
Xe-100 Burnup	0.700/0.724	0.843/0.884	0.911/0.952	0.842/0.883	0.843/0.883	0.740/0.767
MMR Burnup	0.001/0.001	0.001/0.001	0.001/0.002	0.001/0.002	0.001/0.001	0.001/0.001

# Chapter 7

## Optimization

Optimization of the nuclear fuel cycle aids in developing a fuel cycle based on a specific objective or multiple objectives. Potential objectives include minimizing the amount of a specific resource required to support the fuel cycle. Optimization has previously been applied to the nuclear fuel cycle [23, 119] and other nuclear engineering applications [120]. In this chapter we demonstrate a methodology to identify optimized fuel cycle transitions from LWRs to select advanced reactors. We also provide observations and commentary about the methodology.

### 7.1 Methodology

We developed three different optimization problems to apply to Scenario 7 (no growth, once-through transition to the MMR, Xe-100, and VOYGR): minimizing the SWU capacity to produce HALEU, minimizing the mass of UNF for disposal, and minimizing both the HALEU SWU and the UNF mass. Both the HALEU SWU and UNF mass are important parameters for decision makers. Minimizing the HALEU SWU minimizes the new enrichment infrastructure needed to support the fuel cycle. The US does not have an operating geologic repository for commercial UNF, so minimizing this metric minimizes the amount of commercial UNF kept at reactor sites.

To optimize these transitions, we consider six different variables: percent of LWRs operating for 80 years (the LWR lifetime), the build share of Xe-100s, the build share of MMRs, the build share of VOYGRs, the discharge burnup of the Xe-100, and the discharge burnup of the MMR. The sensitivity analysis in Chapter 6 considered all of these variables and the transition start time. That analysis showed that the transition start time has very little effect on the HALEU SWU and UNF, and delaying the transition can lead to unfulfilled energy demand. Therefore, this parameter is not considered in the optimization of each scenario.

For this work, the percent of LWRs operating for 80 years was constrained to between 0-50% of the current LWR fleet. The build share of each advanced reactor was allowed to range between 0-100%, but the three parameters had to sum to 100%. The discharge burnups are restricted to the values considered in the OAT sensitivity analysis (Section 6.2), which are based on different cycle lengths or the number of passes pebbles go through the core.

We coupled CYCLUS [27] with Dakota [28] to perform this optimization, similar to the coupling used for the

sensitivity analysis (Chapter 6). For the single-objective problems, we used the “soga” solve method in Dakota, which is a single-objective genetic algorithm. For the multi-objective problem, we used the “moga” solve method in Dakota, which is a multi-objective genetic algorithm. The Dakota User’s Manual [28] provides some guidance on selecting the most appropriate optimization method available in Dakota. According to this guide, these two methods are the most appropriate to use, because the problem has bound (variables must be within a given range) and linear constraints (variables must sum to a value). Additionally, genetic algorithms have previously been used to optimize fuel cycle transitions [26], which provides confidence that this optimization method is appropriate for this application. More specifically, the “moga” method in Dakota was found to always lead to a correct and accurate solution set when used with five different benchmark problems [67].

Genetic algorithms are based on the survival of the fittest principle in evolutionary biology [28]. The algorithm randomly selects an initial population of model parameters, with each set of model parameters forming a “genetic string” that is analogous to a DNA string that is unique for each member of a population [28]. Each member of a population is evaluated for its performance on a given problem, and the best performing sets of parameters are passed to the next generations, emulating the breeding of a population. In addition to passing along parameters sets to the next generation, crossovers and mutations occur. Crossovers are when one parameter value is exchanged between two members of the same population, similar to the combination of the genes from a parent to a child [121]. In the crossover, the string of parameters are split at an arbitrary point, and switched to form two different offspring. Mutations are when a parameter value of a population member is replaced with a random value within the parameter space. After mutation, the new population is evaluated for its performance in the defined problem. In the single-objective algorithm, each population is evaluated for its performance with respect to the one objective. In the multi-objective algorithm, the various objectives are combined into a single objective function (such as L-2 norm). This process of crossover, mutation, and evaluation is performed for each population until a convergence criteria is met. Convergence criteria can be based on the convergence of a solution, the number of evaluations, or both.

Genetic algorithms have a variety of hyperparameters (parameters that control the exploration of the genetic algorithm), such as the the mutation rate and crossover rate, that can affect the results of the algorithm and the speed at which a solution is found. Specifically, the crossover and mutation rates of a genetic algorithm control how similar each population is to the one before it, and how much of new space is considered. If the mutation rate is too low, then the genetic algorithm can reach a local minimum instead of a global minimum. If the mutation rate is too high, then the algorithm behaves more like a random search and isn’t able to fully use the information about the previous generation to find a minimum. If the crossover rate is too low, each generation is too similar to the one before it and the algorithm with converge without adequately exploring the parameter space. If the crossover rate

is too high, then the population may not have enough diversity and also lead to convergence without adequately exploring the parameter space. Therefore, before the genetic algorithms in Dakota can be used to optimize the fuel cycle transition, we must tune multiple hyperparameters to determine the best combination for this work and the exact algorithm used by Dakota. We evaluate hyperparameters based on the optimized solution identified with a given set of hyperparameters; the more optimized the solution then the better the hyperparameters.

### 7.1.1 Single-objective hyperparameter tuning

We tuned the hyperparameters by performing a grid search across the possible values for some parameters, a method recommended by Deb [122], and used random search over other parameters. Chee demonstrated this methodology for reactor design optimization [120]. We did not consider all hyperparameters or all possible values of the hyperparameters. We downselected from the possible hyperparameters and values defined in the Dakota Reference Manual [28] based on hyperparameters defined in previous generic algorithms for nuclear energy applications [26, 120], personal intuition, and limitations on time to perform the tuning. We performed the hyperparameter tuning on the single-objective problem to minimize the SWU capacity required to produce HALEU, then used the selected hyperparameters on both single-objective problems.

The first grid search performed 40 total iterations of different hyperparameter values across a coarse grid. We restricted the total number of samples to 500 for each evaluation, which restricts the population size and the number of generations, as the product of these two must equal the total number of samples. Table 7.1 describes the hyperparameters considered in the tuning and the range of possible values considered. The mutation type takes discrete values, so we applied a grid search to this hyperparameter and considered two different mutation types. We also performed a grid search on the population size, because of the evaluation limit, considering the values defined in Table 7.1. We used random sampling for the constraint penalty, crossover rate, and mutation rate, using the ranges defined in Table 7.1 for each hyperparameter. Hyperparameters not varied in the tuning, and held constant for all runs include the convergence type (kept at “best fitness tracker”), the fitness type (kept at “merit function”), and the random seed (kept at the same value for all runs). We did not vary the convergence type or fitness type because of computational resource limitations.

We limited all six of the input parameters considered (the build shares, discharge burnups, and the LWR lifetimes) to integer values by using the “discrete design set” variable definition for the Xe-100 and MMR burnups and the “discrete design range” variable definition for the other four parameters. These variable definitions prevent rounding errors when passing parameters between Dakota and CYCLUS.

Figure 7.1 shows the results of the coarse tuning for the single objective problem, comparing each model parameter (y-axes) selected when using each hyperparameter value (x-axes), and the resulting HALEU SWU when

Table 7.1: Hyperparameters and values considered in tuning. If a range of values is provided, then the hyperparameter a random value in that range was selected.

Hyperparameter	Coarse Search	Fine Search
Experiments [#]	1-40	41-68
Population size [#]	5, 10, 25, 50, 100	50, 100
Constraint penalty	$0.5 \leq x \leq 2$	$0.5 \leq x \leq 2$
Crossover rate	$0.1 \leq x \leq 0.9$	$0.1 \leq x \leq 0.9$
Mutation type	replace uniform, offset normal	replace uniform, offset normal
Mutation rate	$0.01 \leq x \leq 0.2$	$0.01 \leq x \leq 0.19$

using that combination (the color of the data points, dark purple is best). From these results, we observe that a larger population size results in lower HALEU SWU capacity required and performs the best in meeting the build share constraint for this work. These two observations strongly point to the use of a larger population size. From the other hyperparameters, there are no conclusions that can be drawn about a range of values that should be used. Therefore, we performed more tuning cases (the “Fine Search” in Table 7.1) to provide more insight into how the other hyperparameters affect the results with the larger population sizes. In the fine search, we further limited the population size values, based on the results of the coarse tuning, but mostly left the other hyperparameter ranges the same.

The results from the fine tuning, shown in Figure 7.2, are not completely aligned with the results from the coarse tuning. The coarse tuning showed that a population size of 100 consistently performed better than the other population sizes, but the fine tuning showed that a population size of 50 performed better. Both sets of tuning runs suggested a population size to use, albeit suggesting different population sizes, but did not show any strong correlation between the other hyperparameters and the HALEU SWU. Therefore, we compared the hyperparameters and model parameters values in the five best performing tuning cases, based on the HALEU SWU required, shown in Table 7.2.

Four of the five best performing tuning cases are able to find the theoretical minimum for this problem, 0 kg-SWU. However, none of the cases perfectly match the build share target of 100%. Case 38 is the only one that at least meets the target, but it exceeds it by specifying a total build share of 103%. However, this is the only tuning case that does not reach the theoretical minimum.

### Hyperparameter selection

Based on the information in Table 7.2, we selected hyperparameters to use for all single-objective problems in this work. We selected the hyperparameters from tuning case 45, given in Table 7.3, because this tuning case reached the theoretical minimum for the problem and was the closest to meeting the total build share constraint.

The tuning cases each ran a maximum of 500 evaluations to limit the amount of time required for each run.

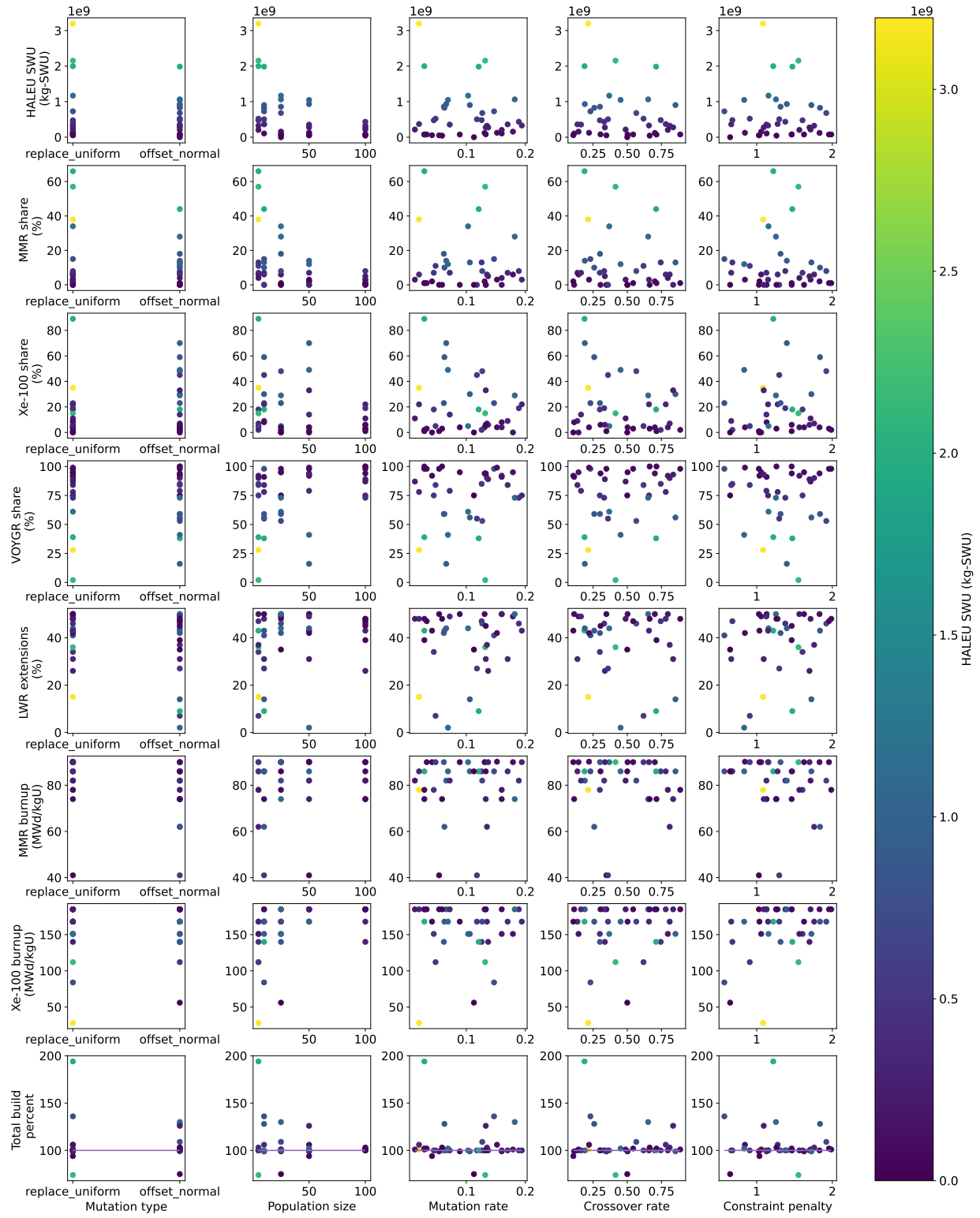


Figure 7.1: Results of coarse tuning for the single-objective optimization. The purple line in the bottom row (total build share at each hyperparameter) identifies a 100% total build share.

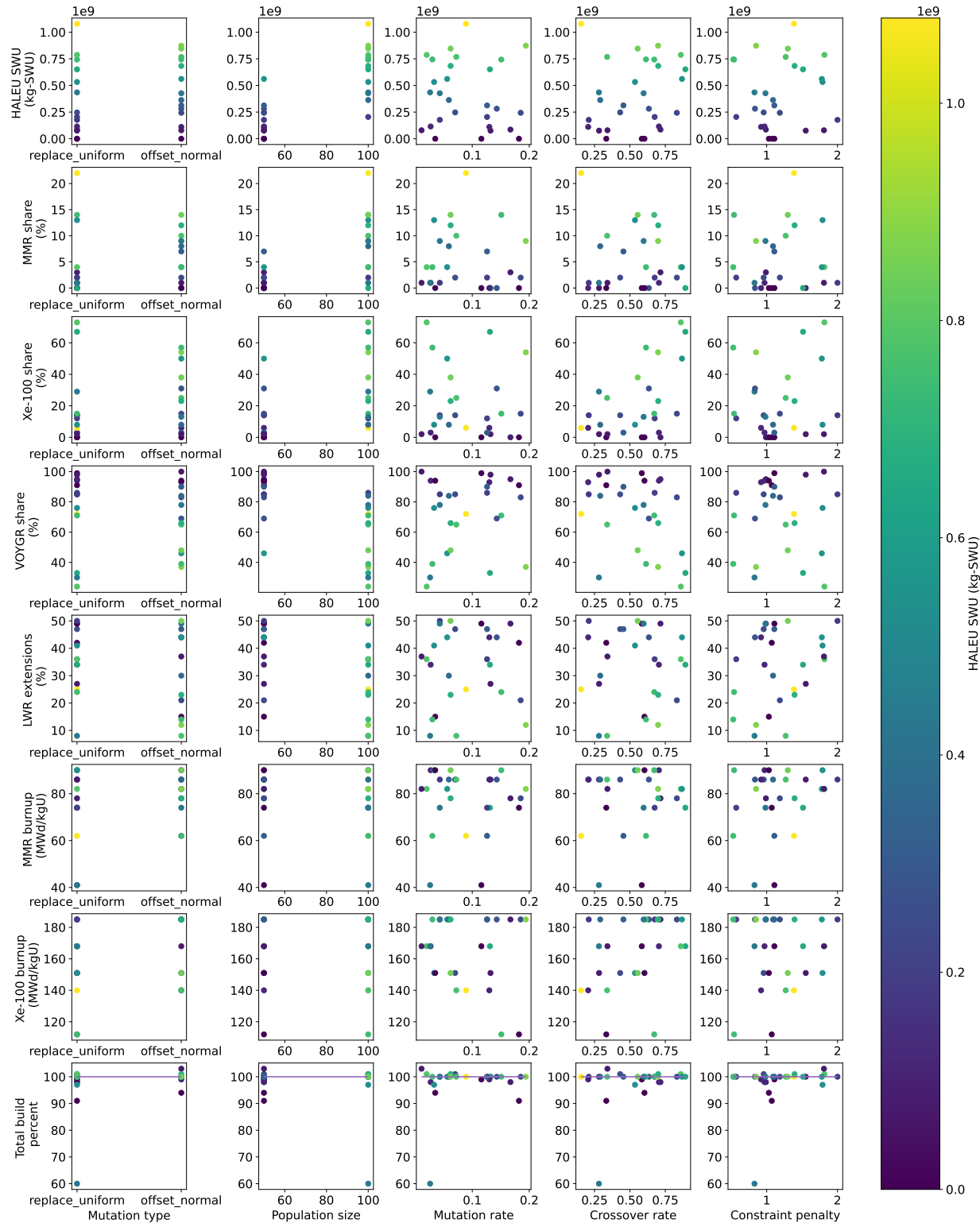


Figure 7.2: Results of fine tuning for the single-objective optimization.

Table 7.2: Hyperparameter and model parameter values from the five best performing tuning cases for the single-objective problems.

<b>Hyperparameter</b>	Tuning case number				
	28	38	43	45	59
Mutation type	offset normal	offset normal	replace uniform	replace uniform	offset normal
Population size	25	100	50	50	50
Mutation rate	0.113	0.059	0.182	0.116	0.035
Crossover rate	0.5	0.664	0.333	0.584	0.603
Constraint penalty	0.648	1.261	1.072	1.109	1.031
<b>Model Parameter</b>					
HALEU SWU (kg-SWU)	0	$4.37 \times 10^7$	0	0	0
VOYGR build share (%)	75	100	91	99	94
MMR build share (%)	0	0	0	0	0
Xe-100 build share (%)	0	3	0	0	0
LWR Lifetime (%)	35	48	42	49	15
MMR burnup (MWd/kgU)	86	74	74	41	90
Xe-100 burnup (MWd/kgU)	56	185	112	168	151

Table 7.3: Hyperparameters selected for single-objective optimization.

Parameter	Value
Population	50
Constraint penalty	1.109
Crossover rate	0.584
Mutation type	replace uniform
Mutation rate	0.116

However, we run each single-objective problem for a maximum of 1000 evaluations. By increasing the maximum number of evaluations, we allow the algorithm to explore the input space and find the minimum objective function for the problem while also meeting the total build share constraint (assuming the convergence criteria is not met first).

### 7.1.2 Multi-objective hyperparameter tuning

Hyperparameter tuning for a multi-objective problem is more complicated than tuning for a single-objective problem. In multi-objective problems, there is no single best solution but rather many solutions that form a Pareto front [28]. The points on a Pareto front are equally optimized, and indicate that further improvement of one objective results in a worsening of another objective. Therefore, to tune the hyperparameters of a multi-objective problem, one tunes base on the hypervolume of the Pareto front [122], because a larger hypervolume indicates a better exploration of the problem space. The hypervolume of a Pareto front is calculated by calculating the area between the Pareto front and a reference point. The reference point must be selected such that all values on the Pareto front are contained in the hypervolume.

We tuned the hyperparameters based on minimizing the SWU capacity to produce HALEU and minimizing

the mass of UNF in Scenario 7. The multi-objective genetic algorithm in Dakota outputs the Pareto front for a problem, which we then use to calculate a hypervolume with a reference point. We selected the reference point after plotting the Pareto fronts and selecting a point that contains all of the points on the front. We applied the same variable definitions from the single objective hyperparameter tuning: bounds, linear constraints, and integers for all variables. We observed that by using a linear equality constraint for the different advanced reactor build shares Dakota only found a single solution, as opposed to a Pareto front, because not all of the samples adhere to linear constraints. By replacing the linear equality constraint with a linear inequality constraint (i.e., defining that the advanced reactor build share is at least 100% instead of equal to 100%), Dakota found multiple solutions to form a Pareto front. Therefore, we used this linear inequality constraint for the tuning cases and the final problem run to ensure that a Pareto front can be found. Therefore, in addition to considering the hypervolumes resulting from each hyperparameter value, we will also consider how close to 100% the total build share is to minimize oversupply of power.

We downselected hyperparameters and hyperparameter values used in this tuning because of computational resource limitations. We tuned the population size, the mutation rate, and the crossover rate, using specific values instead of doing a random search of values. Table 7.4 defines the different values considered, and the default values of each hyperparameter in Dakota. We tuned these hyperparameters because of their observed effect on the single-objective optimization hyperparameter tuning (population size) or intuition (mutation rate and crossover rate). We selected these values based off of the hyper parameters used for the single-objective problem, the default value in Dakota, or intuition. If the value of a hyperparameter is not specified, we used the default value in Dakota (i.e., when using a population size of 25, the mutation rate is 0.08 and the crossover rate is 0.8). We ran each set of hyper parameters 20 times, and compared the statistics of the hypervolumes of the resulting Pareto fronts. From this data, we selected the hyperparameters to use for multi-objective optimization for this work.

Table 7.4: Values of each hyperparameter considered in the multi-objective hyperparameter tuning.

Hyperparameter	Values	Default value
Population size	25, 50, 100	50
Mutation rate	0.08, 0.1, 0.116, 0.15	0.08
Crossover rate	0.3, 0.584, 0.8	0.8
Initialization type	-	unique random
Mutation type	-	replace uniform
Crossover type	-	shuffle random
Fitness type	-	domination count

Figure 7.3 shows box and whisker plots of the hypervolumes resulting from each value of the crossover rate. All three of the crossover rates result in similar median values, and similar statistics. A crossover rate of 0.3 results in the largest median, mean, and maximum for the hypervolumes. A crossover rate of 0.584 results in the smallest

minimum hypervolume. A crossover rate of 0.8 results in the smallest median and mean of the hypervolumes.

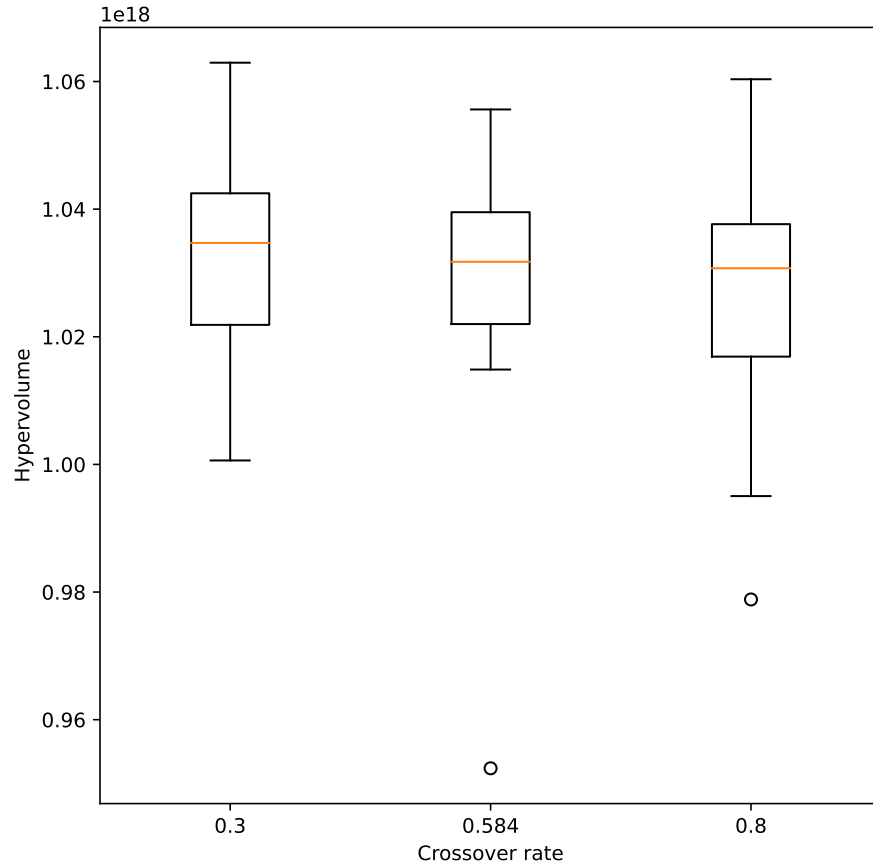


Figure 7.3: Statistics of the hypervolumes resulting from each crossover rate value considered in the MOGA Tuning.

Figure 7.4 shows ox and whisker plots of the hypervolumes resulting from different population sizes. There is more observed variation in the statistics of this hyperparameter than the variation from varying the crossover rate. This observation suggests that the population size has a greater impact on the hypervolume than the crossover rate. A population size of 50 results in the largest median and first quartiles, as well as the smallest minimum. A population of 25 results in the largest mean and maximum hypervolume.

Finally, Figure 7.5 shows ox and whisker plots of the hypervolumes resulting from different values of the mutation rate. A mutation rate of 0.08 resulted in the largest mean and median of the values considered, closely followed by a mutation rate of 0.1, but it also resulted in the largest range of values.

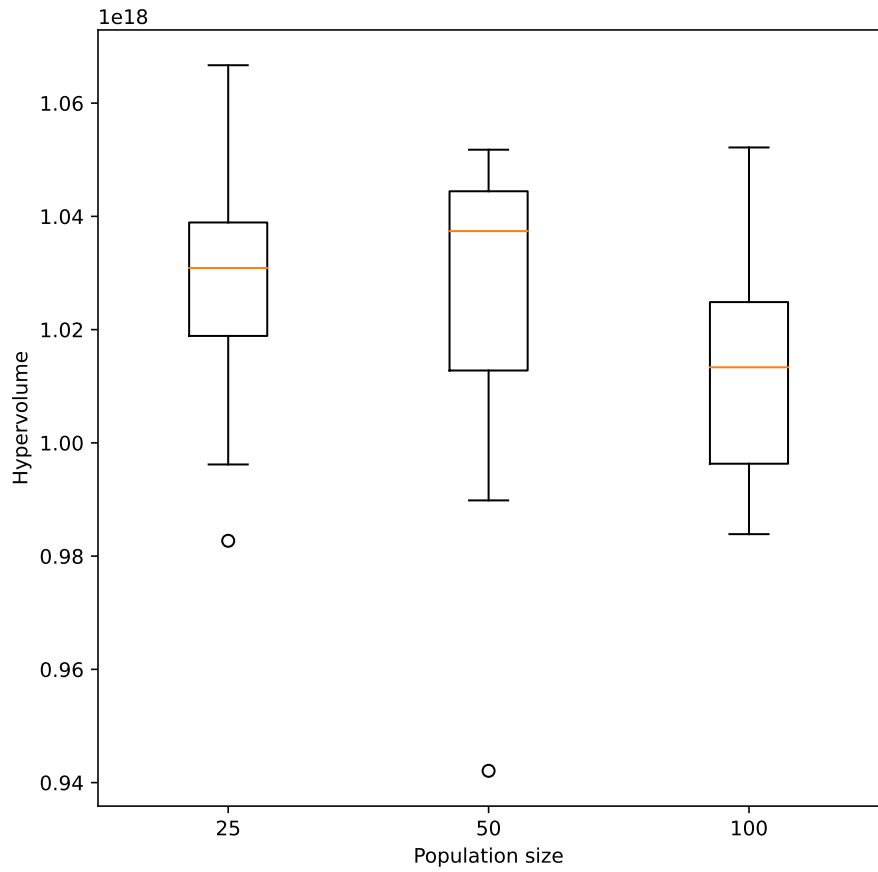


Figure 7.4: Statistics of the hypervolumes resulting from each population size considered in the MOGA Tuning.

### Hyperparameter selection

For the multi-objective problems, we selected the hyperparameter values defined in Table 7.5. We selected a crossover rate of 0.3 because this parameter resulted in the most favorable statistics in the tuning process: the largest median, mean, and maximum of the resulting hypervolumes. We selected a population size of 25 because this population size resulted in the largest mean and maximum hypervolumes in the tuning cases. Additionally, a population size of 25 results in the highest values for the upper quartiles plus or minus 1.5 times the interquartile range (the end of the whiskers), which suggests that when this hyperparameter value is used again the results will continue to be favorable. Finally, we selected a mutation rate of 0.1 because although a mutation rate of 0.08 resulted in a larger mean and median than a rate of 0.1, it also resulted in a smaller minimum hypervolume and more values that are lower than those from a rate of 0.1. Therefore, we selected a mutation rate of 0.1 because the hypervolumes were more consistent than those from a rate of 0.08.

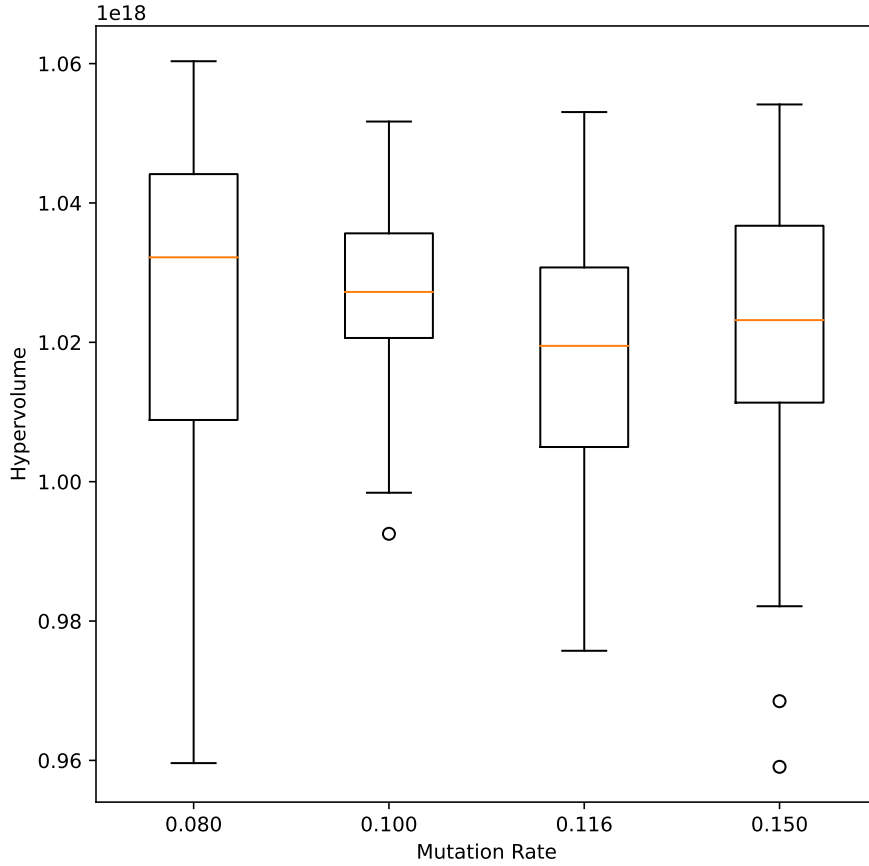


Figure 7.5: Statistics of the hypervolumes resulting from each mutation rate considered in the MOGA Tuning.

Table 7.5: Hyperparameter values selected for multi-objective optimization problems based on tuning.

Hyperparameter	Value
Crossover rate	0.3
Population size	25
Mutation rate	0.1

We applied each of the hyperparameters in Table 7.5 to the multi-objective problem in this work. We also increased the maximum number of evaluations to 1500 to allow for more exploration of the problem space.

## 7.2 Single-objective optimization

This section presents the results of the two single-objective problems: minimizing SWU capacity required to produce HALEU and minimizing the UNF mass. We used the hyperparameters defined in Table 7.2 and a maximum

of 1000 evaluations for both problems.

### 7.2.1 Minimize HALEU SWU

By applying the hyperparameters to an optimization problem to minimize the HALEU SWU capacity needed by this transition scenario, Dakota found a minimum with the values defined in Table 7.6. The SWU capacity required to produce HALEU for these input parameters is  $4.812 \times 10^7$  kg-SWU.

Table 7.6: Values resulting in a minimum HALEU SWU capacity for a once-through transition scenario.

Variable	Value
IWR Lifetime	36%
Xe-100 build share	0%
MMR build share	2%
VOYGR build share	100%
Xe-100 burnup	151 MWd/kgU
MMR burnup	90 MWd/kgU
HALEU SWU	$4.812 \times 10^7$ kg-SWU

The HALEU SWU capacity output from this optimization is not the theoretical minimum for this problem, and is larger than any of the values presented in Table 7.2. This solution results in a larger HALEU SWU capacity required because the parameters selected by Dakota results in a build share greater than 100%, which artificially inflates the material resources needed for the transition. Additionally, Dakota selected a non-zero build share of MMRs which, as the transition analysis (Chapter 4) and sensitivity analysis (Chapter 6) shows, requires more SWU capacity than the Xe-100 and VOYGR.

The inability of the “soga” algorithm to properly meet the build share constraint in the tuning cases and in this problem identifies a significant disadvantage of using this method to optimize the transition. According to the Dakota documentation, the “soga” method provides a feasible solution, but may violate the constraint as it searches the input space [123]. In practice, we observed that the algorithm freely explores the parameter space without regards to the constraint and the final solution provided is the iteration that best meets the constraint and minimizes the objective function. Dakota developers suggest variation of the ‘constraint penalty’ hyperparameter to force the algorithm to more strictly adhere to the constraint [124]. However, Figures 7.1 and 7.2 do not show any strong correlation between the constraint penalty and how well the constraint is met (shown in the purple line in the bottom row of plots) in this problem. This problem ended at 1000 iterations (the maximum allowed) and provided results that met the build share constraint to a similar extent as many of the tuning cases, which only ran a maximum of 500 iterations. Therefore, it is not clear if allowing more iterations will yield results that better meet the constraint. However, if Dakota were allowed to perform as many evaluations as needed to meet the convergence criteria, then it is possible that the constraint would be met. The Dakota manual defines some

optimization methods that will more strictly adhere to linear constraints as they search [123], such as derivative-free pattern searches. Therefore, a future exploration path would include use of these other methods to optimize fuel cycle transitions.

The other model input parameters identified by the optimization of the transition follow the trends identified by the sensitivity analysis to minimize the HALEU SWU. The percent of LWRs receiving license extensions is above 25%, the MMR burnup is at the maximum value considered, and the Xe-100 burnup is near the maximum value considered. There is room for further minimizing the HALEU SWU by increasing the percent of LWRs receiving license extensions. One way to achieve this further improvement is to increase the maximum number of function evaluations. For this specific problem, these three input parameters are not as impactful on the results as the build share of each reactor type. Therefore, it is reasonable that the results provided from Dakota do not place these variables at the very edge of the range of values considered when the algorithm does not converge.

Because the results provided by this algorithm in Dakota do not strictly meet the linear constraint and do not reach the theoretical minimum for this problem, the results should not be accepted at face value. Rather, the results should be taken as guidance on how to implement an optimized solution of this problem with respect to this objective function; maximizing the VOYGR build share in this transition will minimize the SWU capacity required to produce HALEU.

### 7.2.2 Minimize waste mass

By applying the hyperparameters to an optimization problem to minimize the HALEU SWU capacity needed by this transition scenario, Dakota found a minimum with the model input parameters defined in Table 7.7. The minimum waste mass determined through the optimization is 1,736 MT. This UNF mass is smaller than the minimum values presented in the once-through transition analysis (Table 4.15) and the OAT analysis (Table 6.1), suggesting that the algorithm finds a well-optimized solution.

Table 7.7: Values resulting in a minimum waste mass disposed of for a once-through transition scenario.

Variable	Value
LWR Lifetime	50%
Xe-100 build share	100%
MMR build share	7%
VOYGR build share	11%
Xe-100 burnup	185 MWd/kgU
MMR burnup	90 MWd/kgU
UNF mass	1,736 MT

From Table 7.7, it is clear that more than 100% build share is defined, which artificially increases the UNF mass generated from advanced reactors in this fuel cycle. This result is consistent with the results of the other

single-objective problem for this fuel cycle, but suggests that the fuel cycle can be further-optimized for the UNF mass. These results suggest that to minimize the UNF mass, the LWR lifetimes, Xe-100 burnup, and the Xe-100 build share should be maximized. If MMRs are deployed, then maximizing the MMR build share contributes to minimizing the UNF mass. This guidance is consistent with the sensitivity analysis for minimizing this metric. The results of the LWR lifetime, MMR burnup, and Xe-100 burnup demonstrate that this algorithm can perform well with respect to variables that do not have a linear constraint applied.

This optimization problem converged in 590 iterations, and the best objective function found in iteration 437. Therefore, the hyperparameters resulted in a faster convergence for this problem than the previous one, despite the hyperparameters being tuned on the previous problem. The convergence of the algorithm for this problem contributes to the identification of maximizing the the LWR lifetime and Xe-100 burnup parameter in the solution.

### 7.3 Multi-objective optimization

The multi-objective problem in this work minimizes the SWU to produce HALEU and minimizes the UNF mass. In solving this problem, Dakota identified a pareto front of 217 points, shown in Figure 7.6. The points on this figure identify different values of each objective that are equally optimized; in order to improve one objective the other objective becomes worse. There is a linear trade-off between each of the objectives along this pareto front, which is consistent with the the LWR lifetime and each advanced reactor build share having a linear relationship with each of the metrics in the OAT analysis (Section 6.2). The hypervolume of this pareto front is  $1.061 \times 10^{18}$  using a reference point of  $(6 \times 10^9, 2 \times 10^8)$ . This hypervolume is greater than any of the median or mean values in the hyperparameter tuning, using the same reference point. This result suggests that these hyperparameters performed well in this problem.

The points on this pareto front have some similar model parameter values. Every point has a 0% build share of MMRs and an Xe-100 discharge burnup of 185 MWd/kgU. Additionally, the percent LWRs operating for 80 years ranges between 47-50%. Each of these results are very consistent with the results of the sensitivity analysis and the single-objective optimization for each problem. The MMR discharge burnup varies across the range of possible values in this work because the discharge burnup becomes irrelevant if none of these reactors are deployed in the transition. This results identify that maximizing the LWR lifetimes, maximizing the Xe-100 burnup, and minimizing the MMR are all ways to minimize the HALEU SWU capacity and the UNF mass, independent of the weighting of these two objectives.

The Xe-100 and VOYGR build shares vary across the pareto front. The Xe-100 build share varies between 11-100% and the VOYGR build share varies between 10-99%. The total build share varies between 100-191% in these results,

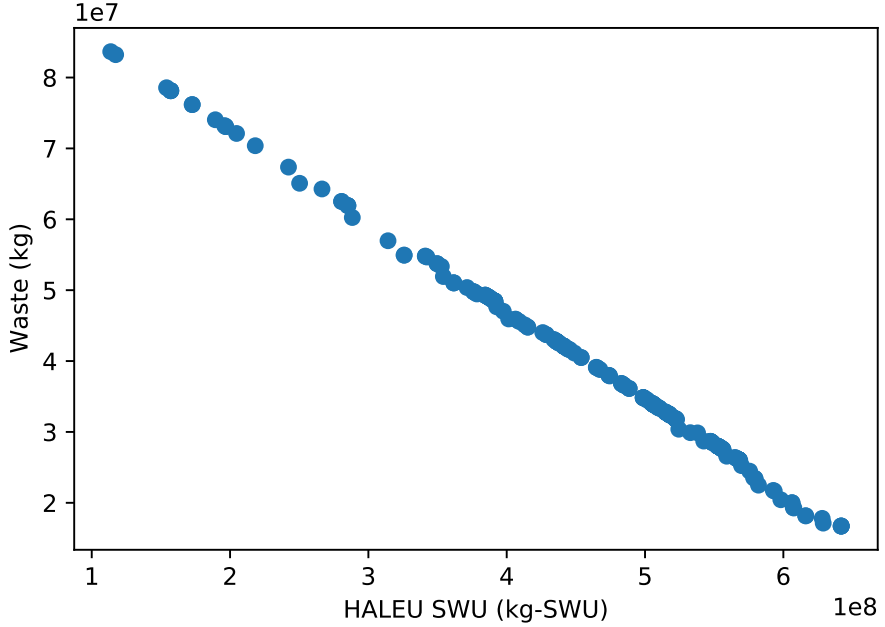


Figure 7.6: Pareto front resulting from the multi-objective optimization of the once-through transition.

with 3 of the results having a total build share of 100%. These two input parameters vary the most in each of the points on the pareto front because they have the most effect on the results. The effect of these parameters explains why the pareto front is linear: each of these build shares has a linear relationship with the objectives (see Section 6.2). Therefore, their combined effect remains linear. The exact balance between the Xe-100 and VOYGR build share to optimize for these metrics will be based on the relative priority of each objective.

Examining the Xe-100, VOYGR, and total build shares also identifies weaknesses in using this tool and methodology. Neither of the two reactor build shares reaches 0%, which suggests that those areas of the parameter space were not fully explored. Additionally, 73 of the 217 (34%) points on the pareto front have a total build share above 150%. Intuition suggests that both objectives would be minimized with a lower total build share. Therefore, the total build shares further suggests that the genetic algorithm, with the selected hyperparameters, does not fully explore the parameter space. However, there is degeneracy in the build share of different reactors. Because the reactors must be built in whole numbers, multiple values of a build share can result in the same number of a reactor type built, suggesting that multiple build share percents will minimize the objectives. Therefore, some variation in the build share of each advanced reactor is a result of the degeneracy of the build shares. The degeneracy of the build shares is why setting a strict linear constraint of the build shares summing to 100% results in so few points on the pareto front. However, the results of this work suggest that a non-infinite upper limit should be applied to the linear constraint.

# Chapter 8

## Effects of uranium impurities

Recovery and downblending of HEU to produce HALEU means that the fuel contains impurities present in the original HEU. Known impurities in potential HEU supplies to create HALEU include  $^{232}\text{U}$  and  $^{236}\text{U}$  [12, 13], which are parasitic neutron absorbers and have the potential to affect reactor physics and reactor operation. To investigate the magnitude of this effect, this chapter presents models of two advanced reactors that use impure HALEU fuel (with compositions based on publicly available information) and compares the performance of the impure fuel to the use of pure HALEU (comprised exclusively of  $^{235}\text{U}$  and  $^{238}\text{U}$ ). This analysis helps in understanding the impacts of the impurities on the performance of the reactor. While the other chapters of this dissertation explore how the reactors affect the fuel cycle this chapter explores how the fuel affects the reactors.

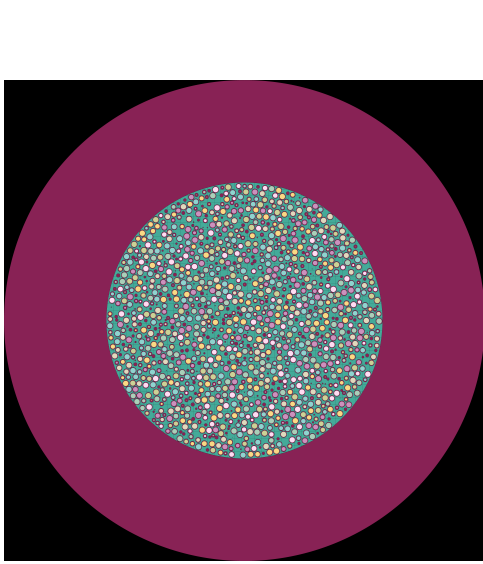
### 8.1 Methodology

For this work we considered the two HALEU-fueled reactors modeled in the transition scenarios described in Chapter 3: the X-energy Xe-100 and the USNC MMR. We created reactor core models that closely resemble these reactors in Serpent [102], modeling the neutronics and fuel depletion in each reactor design. Each model was run using the ENDF VII.1 cross section library [125]. The core geometries used are not the exact geometries designed by X-energy and USNC, respectively, but are replications based on publicly-available information [93, 126, 95, 96]. We used the serpentTools python package [127] to analyze the results from the models.

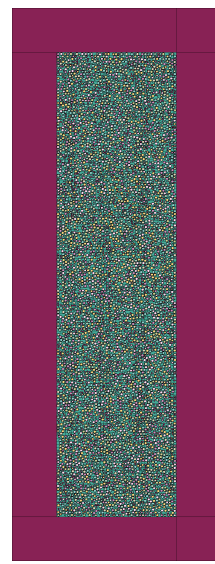
#### 8.1.1 Xe-100-like model

The Xe-100 is a 200 MWth, 80 MWe, Tristructural Isotropic (TRISO)-fueled pebble-bed High Temperature Gas-Cooled Reactor (HTGR) [93]. To model this reactor we used the Sangamon200 model from [128], shown in Figure 8.1, to serve as an Xe-100-like core model. The model itself can be found on GitHub [129]. The Sangamon200 model is a Tristructural Isotropic (TRISO)-fueled, pebble-bed, HTGR-style reactor core model initially created to characterize the isotopic compositions and reactor physics of a 200 MWth pebble-bed HTGR.

While this reactor model is very similar to current published data for the X-energy Xe-100 [93], there are two



(a) Radial view of Xe-100-like core model.



(b) Axial view of Xe-100-like core model.

Figure 8.1: Xe-100-like core model made in Serpent.

notable differences that affect the reactor physics. The first difference is that the TRISO particles in the Sangamon200 are modeled as a blended mix of the TRISO materials and not the explicit layers. Using a homogenized TRISO particle decreases the  $k_{eff}$  of the core by 4.45%, but it does not reduce the thermal and fast neutron fluxes across the reactor outside of error [128]. Despite the effect on  $k_{eff}$  of this modeling decision, we used the homogenized model of the TRISO pebbles to be consistent with the published results of the Sanagamon200 [128] and to be conscious of computational expense. The second notable difference is the reactor vessel shape. The Sanagmon200 is a simple cylinder, while the Xe-100 is a cylinder with a cone at the bottom to funnel the pebbles to a single point as they come out of the core. However, this is a less neutronically important region of the core, and we kept the geometry of the Sangamon200 for consistency with those published results.

In the Xe-100 reactor, each pebble moves down the core while it burns. Each time that a pebbles travels from the top of the core to the bottom is a single pass. Once a pebble reaches the bottom of the core, it is removed, inspected for the burnup level, and placed back in the core for another pass if the pebble has not reached the target burnup. Each pebble is expected to go through multiple passes in the core, an average of six passes per pebble, before reaching the target burnup of 185 MWd/kg. To account for the different burnup of the pebbles in an equilibrium core, six different pebble isotopic compositions were used to approximate the pebble variance in burnup in the core. These isotopic compositions represent burnup from integer numbers of passes through the core. To determine the isotopic composition of the pebbles after each pass we performed the methodology Richter developed for their modeling of the Sangamon200 [128]. We performed depletion on the single pebble model created by Richter [129], with each layer of the TRISO kernel explicitly modeled with depletion steps corresponding to integer numbers of

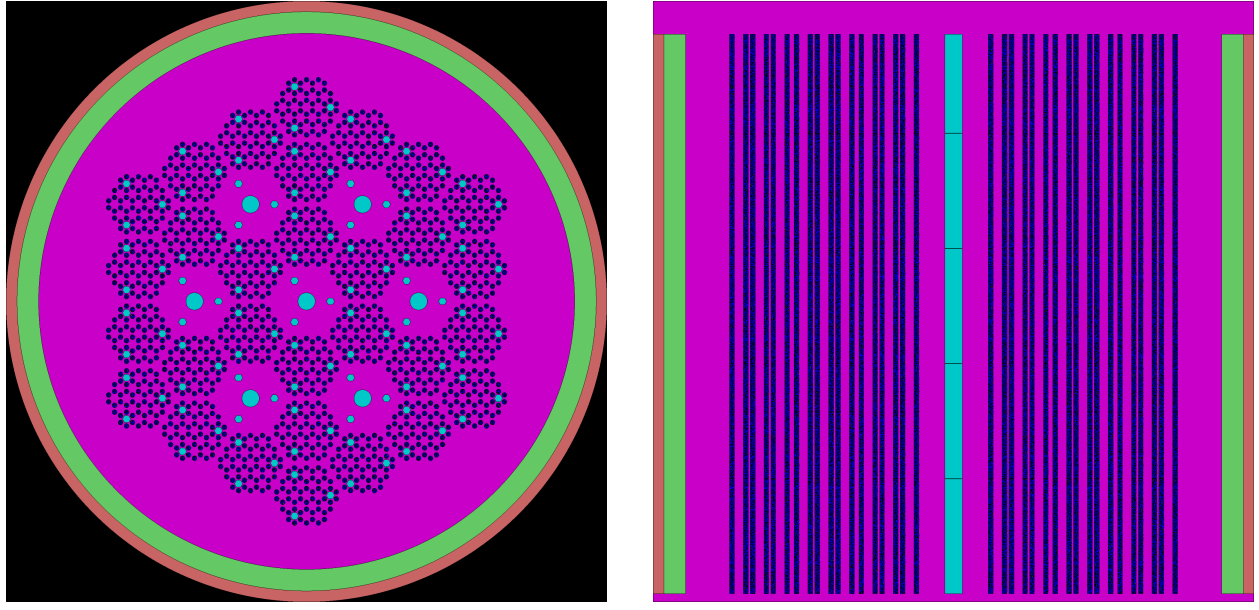
passes. Then we applied the composition corresponding to the burnup step of each pass to 1/6th of the pebbles of the core. The pebbles with different burnups were mixed throughout the core, mimicking the spread of differently burned pebbles throughout a core in the equilibrium state of the reactor. Each pebble at the same burnup level has the same composition in this model.

The Sangamon200 is in an isothermal state at 800 K [128]. We ran this model with 100,000 particles per cycle, 50 inactive cycles, and 200 active cycles without modeling depletion on the Sangamon200 model because our model does not capture pebble movement or the continuous refueling scheme used by the Xe-100. Performing depletion without modeling pebble movement would create non-physical differences from the equilibrium condition of this reactor model. Therefore, we did not model further depletion of the pebbles when comparing the different fuel compositions.

### 8.1.2 MMR-like model

The USNC MMR is a 15 MWth, 5 MWe, prismatic HTGR that uses TRISO fuel in Fully Ceramic Microencapsulated (FCM) pellets inside graphite blocks [92]. We created an MMR-like model primarily based on information in [130], and supplemented or modified based on information published by USNC [92]. Information about the TRISO particle and FCM pellets was found in [92] and information about the graphite block dimensions and configuration was found via visual inspection of figures in [131]. The final core configuration is different than what is modeled by Hawari and Venneri [130] because their model is only meant to operate for 10 years, while the MMR is meant to operate for 20 years [92]. We selected the core configuration shown in Figure 8.2 after modeling some of the other core configurations found in literature [72, 130] and determining that the selected core configuration can operate the longest before going subcritical and achieve a burnup close to the reported 82.6 MWd/kgU reported by USNC [92].

Figure 8.2 shows a radial and axial slice of the MMR model. The fuel channels have a radius of 1.15 cm, the same size as the FCM pellets based on no other available information, the coolant channels have a radius of 3 cm, arbitrarily chosen because no specific information was found, and the control rod channels have a radius of 6 cm, obtained from [130]. These dimensions affect the graphite volume of the core, and thus affect the fuel to moderator ratio of the core. The TRISO particles are modeled with a 40% packing fraction in the FCM particles [132]. Control rods and burnable poisons are not included in this model, or the Sangamon200 model, so the control rod locations are filled with helium. There are five layers of the graphite fuel blocks stacked to form the entire core, to approximate the number of fuel blocks described in [92]. The entire core is assumed to be in an isothermal state at 800 K. There is a 20 cm thick graphite reflector above and below the stacks of graphite, and a 10 cm thick beryllium-oxide reflector on the outside of the graphite blocks of the core, illustrated by the green material in Figure 8.2. While Hawari and



(a) Radial view of the USNC MMR-like model.

(b) Axial view of the USNC MMR-like model.

Figure 8.2: Geometry of USNC MMR-like core model in Serpent. The light blue represents channels helium, dark blue are fuel channels with FCM pellets, and the bright pink is graphite in the core.

Venneri [130] define both of these reflectors in their model, they only define the thickness of the beryllium-oxide reflector. Therefore we assumed a graphite reflector thickness of 20 cm to provide 3-5 mean free paths of material. The input files for this model can be found at [133].

For the MMR-like model, we modeled depletion of the core across the expected 20 year lifetime of the MMR, because the core is not meant to undergo refueling during those 20 years and the lack of fuel movement and replacement in this model aligns with the operational core. Depletion is modeled using burnup steps of 2 years. Each burnup step was run using 140 active cycles, 75 inactive cycles, and 65,000 particles per cycle.

### 8.1.3 Temperature variations and feedbacks

The fuel composition burned will affect the population of fission products, and consequently the delayed neutron precursors. If substantially different, the reactor behavior may not be in a safe regime. Consequently, one of the goals of this work is to compare the temperature feedback coefficients from using the different fuel compositions in each reactor. Therefore we varied the fuel, coolant, and moderator temperatures between 700, 750, 800, 850, and 900 K to calculate the fuel, coolant, moderator, and total temperature feedback coefficients. We assumed a linear relationship between  $k_{eff}$  and temperature to calculate the feedback coefficients. When varying the temperatures of each component, we also varied the corresponding material density. We calculated the density of the UO<sub>2</sub> by using the empirical relationship between density and temperature defined in [134]. The calculated densities were

assumed to hold true for the Sangamon200 fuel. We calculated the graphite density by linearly extrapolating from the data available in [135]. We calculated the density of the helium by interpolating on the data available in [136], assuming the 3 MPa coolant pressure in the MMR-like model as defined by [92] and the 6 MPa inlet pressure in the Xe-100-like model as defined in [93].

### 8.1.4 Fuel compositions

We used three different HALEU compositions for this work: pure HALEU, and HALEU derived from EBR-II and Y-12 HEU stockpiles. The pure fuel composition assumes that all uranium present is either  $^{235}\text{U}$  or  $^{238}\text{U}$ , and at the correct enrichment level for each reactor. The EBR-II composition is based on the estimated uranium isotopic composition from downblending spent fuel from EBR-II, published by INL [12]. The Y-12 composition is based on the estimated uranium isotopic composition from downblending HEU stockpiles at the Y-12 National Security Complex [13]. The published compositions for the EBR-II and Y-12 fuel assume an enrichment of 19.75%, but only the MMR requires this level of enrichment. Therefore, the uranium isotopic ratios published are directly applied for the MMR fuel. For the fuel in the Xe-100, the isotopic fractions had to be adjusted slightly to match the needed enrichment level of 15.5%. The  $^{235}\text{U}$  fraction was set to match the enrichment level required, the non- $^{238}\text{U}$  isotopes were kept in the same weight fraction defined in the publications, and the  $^{238}\text{U}$  was defined to fill the remainder of the fuel. Therefore, all three fuel compositions for each reactor have the same  $^{235}\text{U}$  weight fractions, have non- $^{238}\text{U}$  weight fractions that match the published values, and have varying  $^{238}\text{U}$  weight fractions for each reactor design. Table 8.1 defines the uranium isotopic composition used in each reactor type for each of the HALEU compositions. The standard for uranium enriched to less than 20%  $^{235}\text{U}$ , ASTM C1462-21 [137], sets limits on the mass of  $^{232}\text{U}$  and  $^{234}\text{U}$  relative to the mass of  $^{235}\text{U}$  and the mass of  $^{236}\text{U}$  relative to the total mass of the uranium. The HALEU from both HEU sources is within the standards, using the flexibility of a potential increase in the limit of  $^{236}\text{U}$  in the fuel.

## 8.2 Results

The metrics with which we performed our analysis include:

- $k_{eff}$
- $\beta_{eff}$
- Two-group, spatially dependent neutron flux

Table 8.1: Atom fraction of uranium isotopes in each HALEU composition. Uranium fractions are provided, without the oxygen and/or carbon fractions defined. Therefore, the totals in each column for a reactor model do not sum to one.

Isotope	Pure	EBR-II	Y-12
Xe-100-like reactor			
$^{232}\text{U}$	0	$2.40 \times 10^{-10}$	$7.27 \times 10^{-10}$
$^{233}\text{U}$	0	$1.78 \times 10^{-8}$	0
$^{234}\text{U}$	0	$6.12 \times 10^{-4}$	$9.36 \times 10^{-4}$
$^{235}\text{U}$	$5.56 \times 10^{-2}$	$5.56 \times 10^{-2}$	$5.56 \times 10^{-2}$
$^{236}\text{U}$	0	$2.07 \times 10^{-3}$	$1.64 \times 10^{-3}$
$^{237}\text{U}$	0	$2.14 \times 10^{-14}$	0
$^{238}\text{U}$	$2.99 \times 10^{-1}$	$2.97 \times 10^{-1}$	$2.97 \times 10^{-1}$
MMR-like reactor			
$^{232}\text{U}$	0	$2.25 \times 10^{-10}$	$6.82 \times 10^{-10}$
$^{233}\text{U}$	0	$1.67 \times 10^{-8}$	0
$^{234}\text{U}$	0	$5.73 \times 10^{-4}$	$8.766 \times 10^{-4}$
$^{235}\text{U}$	$6.66 \times 10^{-2}$	$6.67 \times 10^{-2}$	$6.67 \times 10^{-2}$
$^{236}\text{U}$	0	$1.93 \times 10^{-3}$	$1.54 \times 10^{-3}$
$^{237}\text{U}$	0	$2.00 \times 10^{-3}$	0
$^{238}\text{U}$	$2.67 \times 10^{-1}$	$2.64 \times 10^{-1}$	$2.64 \times 10^{-1}$

- Reactivity temperature feedback coefficients for the fuel, coolant, moderator, and the combination of all three.

For the Sangamon200, these metrics are only compared in an equilibrium state of the reactor. For the MMR-like reactor these metrics are compared at Beginning-of-Life (BOL) (0 MWd/kg burnup), Middle-of-Life (MOL) (40.52 MWd/kg burnup), and End-of-life (EOL) (81.04 MWd/kg burnup). The two-group structure for the neutron flux is based on the default two-group structure in Serpent, with the thermal neutrons being between 0-0.625 eV and the fast neutrons being above 0.625 eV. Each metric provides a measurement of the performance of the reactor, such as the materials degradation rate, amount of burnable poisons required, control rod worth, and the cycle time. The neutron flux informs the materials degradation rate, because a larger neutron flux means more damage to the non-fuel materials in the core which may increase the frequency of their replacement. The  $\beta_{eff}$  affects the control rod worth because if too much of the neutron population is born fast then the control rods will have less of an effect on controlling the neutron chain reaction. The  $k_{eff}$  informs the cycle time because the sustainability of the neutron chain reaction controls how long a reactor can operate. Investigating each of these results helps to determine if the impurities present in HALEU will prevent any of the design criteria of the reactors from being met. Results from the simulations are analyzed using the serpentTools python package [127].

### 8.2.1 Xe-100 reactor metric comparisons

The following four sections report and analyze the results of the EBR-II and Y-12 impurities in the Xe-100-like reactor model created. The four different results are presented for an equilibrium state of the reactor.

#### $k_{eff}$ comparison

Table 8.2 reports the  $k_{eff}$  value when using the fuel compositions defined in Table 8.1. The impure fuels result in a  $k_{eff}$  1353-1423 pcm greater than the  $k_{eff}$  from the pure fuel. All three fuel compositions result in a slightly super-critical  $k_{eff}$ . The difference in the  $k_{eff}$  values is more than the error on the values, which means that the different fuel compositions result in statistically different  $k_{eff}$  values for this reactor design.

Table 8.2:  $k_{eff}$  values for the Xe-100-like reactor model for each fuel composition.

Fuel composition	$k_{eff}$
Pure	$1.06663 \pm 0.00016$
EBR-II	$1.08086 \pm 0.00016$
Y-12	$1.08016 \pm 0.00014$

The uranium isotopes mostly present in each of the fuel compositions (weight fraction of at least  $1 \times 10^{-3}$ ) are  $^{234}\text{U}$ ,  $^{235}\text{U}$ ,  $^{236}\text{U}$ , and  $^{238}\text{U}$ . The  $^{235}\text{U}$  weight fraction is the same in each fuel composition, so the impurities are displacing the  $^{238}\text{U}$  in the fuel.  $^{234}\text{U}$  and  $^{236}\text{U}$  have larger thermal total fission cross sections than  $^{238}\text{U}$ , so their displacement of the  $^{238}\text{U}$  in the fuel increases the neutron multiplication of the reactor. This is supported by the impure fuels leading to a slight increase in the thermal fission factor,  $\eta$  (1.737 from EBR-II fuel, 1.735 from Y-12 fuel, and 1.712 from pure fuel), which signifies a greater ratio in the number of neutrons born from fission to the number absorbed in the fuel in the impure fuel compositions. The change in  $\eta$  is relevant because it is fuel specific, but alone it does not define  $k_{eff}$ . Part of the increase in  $k_{eff}$  when using the impure fuels is because the pebbles modeled are at different burnup steps. Therefore, many of the pebbles are already partially burned and the uranium impurities in the fuel have already undergone neutron capture reactions and have been transmuted into other isotopes that are more fissile.

The effect of the impure fuels resulting in increased  $k_{eff}$  is that more control mechanisms may be required to control the chain reaction, or to lower the  $k_{eff}$  and ensure that the targeted discharge burnup and cycle length can be reached.

#### $\beta_{eff}$ comparison

The  $\beta_{eff}$  resulting from the use of each fuel type is reported in Table 8.3. The  $\beta_{eff}$  from using the pure fuel is slightly smaller than the 0.0064  $\beta$  from thermal fissions in  $^{235}\text{U}$  because the depletion of some pebbles in the core

leads to the breeding of  $^{239}\text{Pu}$  from  $^{238}\text{U}$ , which fissions and has a smaller  $\beta_{eff}$  than  $^{235}\text{U}$ . The  $\beta_{eff}$  when using the impure fuels is smaller than when using the pure fuel, a difference that is statistically significant. The pure fuel results in a larger  $\beta_{eff}$  than the impure fuels because the other uranium isotopes present in the impure fuels breed into fissile material that has a smaller  $\beta_{eff}$  than  $^{235}\text{U}$ . The depletion modeled to obtain compositions of pebbles at different numbers of passes captures this breeding of fissile material. The additional fissile material is not present in the pure fuel because it's the material that is bred in from the uranium impurities. The smaller  $\beta_{eff}$  indicates that control mechanisms in the reactor will be less effective because a larger fraction of the neutron population will be prompt neutrons, and there is a smaller time scale on which the neutron population can be impacted.

Table 8.3:  $\beta_{eff}$  value from using each fuel type.

Fuel type	$\beta_{eff}$
Pure	$0.00617 \pm 0.00003$
EBR-II	$0.00604 \pm 0.00003$
Y-12	$0.00598 \pm 0.00003$

### Neutron flux comparison

Figure 8.3 shows the neutron flux in the active region of the core as a function of energy (top) and the difference from the pure fuel flux (bottom). The purple line in both plots shows the delineation between the fast and thermal energy groups in this work (0.625 eV). We used the pre-defined SCALE-238 energy group structure in Serpent. There is a large peak in the thermal flux around 0.01 MeV. The impure HALEU compositions have a smaller thermal flux peak than the pure fuel, differing on the order of  $10^{20} \text{ n/cm}^2/\text{s}$ . However, at high energies (above 10 MeV) the impure fuels result in a larger flux than the pure fuel, differing on the order of  $10^{18} \text{ n/cm}^2/\text{s}$ .

Figures 8.4-8.8 show thermal and fast fluxes in the reactor core axially and radially. The thermal radial flux spectra from all three HALEU compositions (Figure 8.4) show peaks at the edge of the core resulting from the graphite moderator around the core. The middle of the core exhibits a notable difference in the neutron flux between the impure and pure fuel compositions. The impure fuel compositions result in a slightly lower flux than the pure fuel, which is consistent with the results shown in Figure 8.3. However, the smaller thermal flux is in contrast to the larger  $k_{eff}$  from the impure fuels. This difference in trend of the  $k_{eff}$  and the neutron flux suggests that the impurities in the fuel lead to more neutrons born from fissions but the neutrons travel a shorter distance in the core before being absorbed.

$^{238}\text{U}$  has the largest difference between the total and total fission cross sections of the uranium isotopes considered for this model. So by replacing the U-238 with other isotopes the flux should increase from the larger fission to total ratio because the other isotopes are more likely to have fission reactions and produce neutrons. Another factor to consider in this analysis is that this core is not comprised of exclusively fresh fuel. The use of

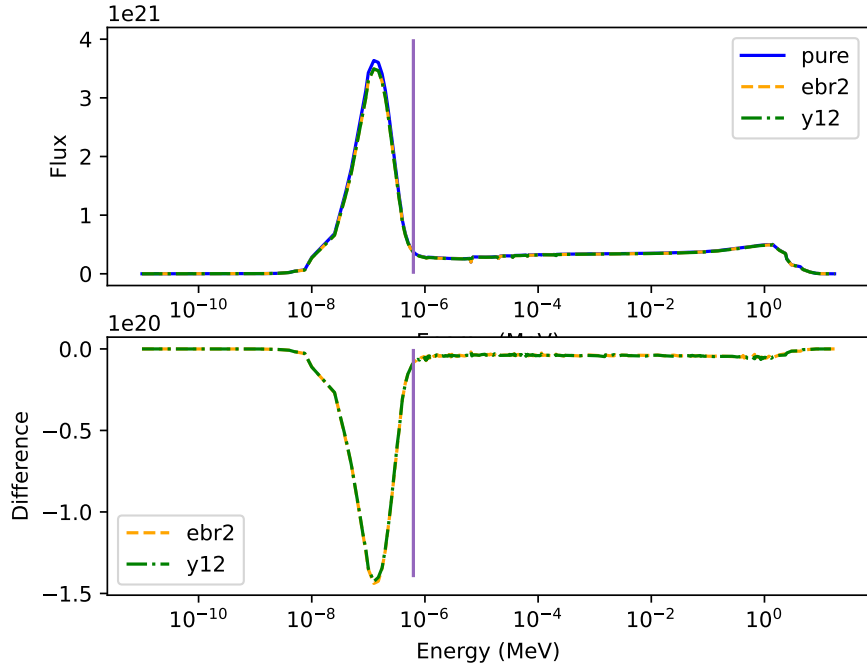


Figure 8.3: 238-group flux in the Xe-100-like reactor model in the active region of the core (top). The absolute difference from the flux from the pure HALEU fuel (bottom). The purple lines denote the delineation of the thermal and fast energy groups used in this work.

burned pebbles in this model affects the flux because the fission yield curves are different for each fissile isotope. If some of the fissions are occurring from reactions in  $^{233}\text{U}$  compared with  $^{235}\text{U}$ , than the fission products present in the partially burned pebbles will be different which affects the neutron reaction rate densities in the core. Also, the even uranium isotopes (e.g.,  $^{234}\text{U}$ ) have relatively small fission cross sections, so they're still more likely to absorb a neutron than to fission.

Figure 8.5 shows the fast radial flux from each HALEU composition in this work. The fast fluxes do not exhibit the same peaks in the reflector as the thermal flux because of the neutron energy difference. The peak magnitude of the fast flux is slightly larger than the thermal flux, indicating that more of the neutrons in the core are at higher energies. The impure fuels also result in a slightly lower flux in the middle of the core, compared with the flux from the pure fuel. The differences in the fast fluxes are on similar order of magnitude to the differences in the thermal fluxes (about  $\pm 2-4 \times 10^{15} \text{ n/cm}^2/\text{s}$ ), but the fast fluxes are larger than the thermal fluxes. Therefore, the impurities result in a smaller overall relative difference in the fast flux than they do in the thermal flux. These results are all consistent with the multi-group flux results. The total area under the curve in the fast region of Figure 8.3 is greater than the area under the curve in the thermal region of that figure, indicating that more neutrons are in the fast energy range. Also, the increase in flux above 10 MeV from the impure fuels is less than the decrease in the flux from

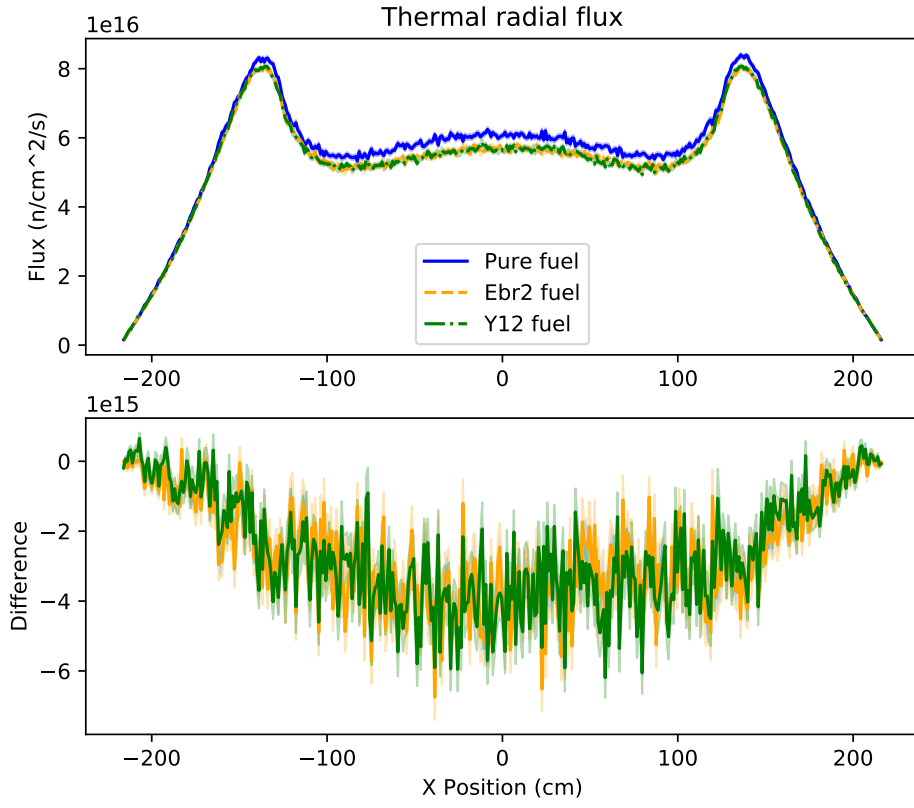


Figure 8.4: Thermal flux (below 0.625 eV) in the Xe-100-like Sangamon200 reactor model in the radial direction, across the x-axis (top). The absolute difference from the flux from the pure HALEU fuel with  $1\sigma$  error shown by the shading (bottom).

the impure fuels between 0.0625 eV–10 MeV, which is why Figure 8.5 shows that the impure fuels result in a smaller flux.

The thermal axial flux (Figure 8.6) shows similar results to the thermal radial flux and the multi-group flux. There is a small bump in the flux at the top and bottom of the core because of the graphite reflector. Additionally, the pure fuel results in a larger flux than the impure fuels. The two impure fuel compositions result in very similar fluxes. The flux differences between the fuel compositions is larger in the bottom of the core, causing flux asymmetry in the core. The pure fuel resulting in a larger thermal flux than the impure fuel is consistent with the larger  $\beta_{eff}$  from the pure fuel. Delayed neutrons are born in the thermal energy range, so a larger  $\beta_{eff}$  means that a larger fraction of the neutrons are born in the thermal energy range.

The asymmetry in the differences in the fluxes is primarily a result of the pebble placement. The pebbles are all evenly spaced around the core, and there are an equal number of pebbles at each integer pass number. However, the pebbles of each pass number are not evenly distributed across the core. This was confirmed by shuffling the

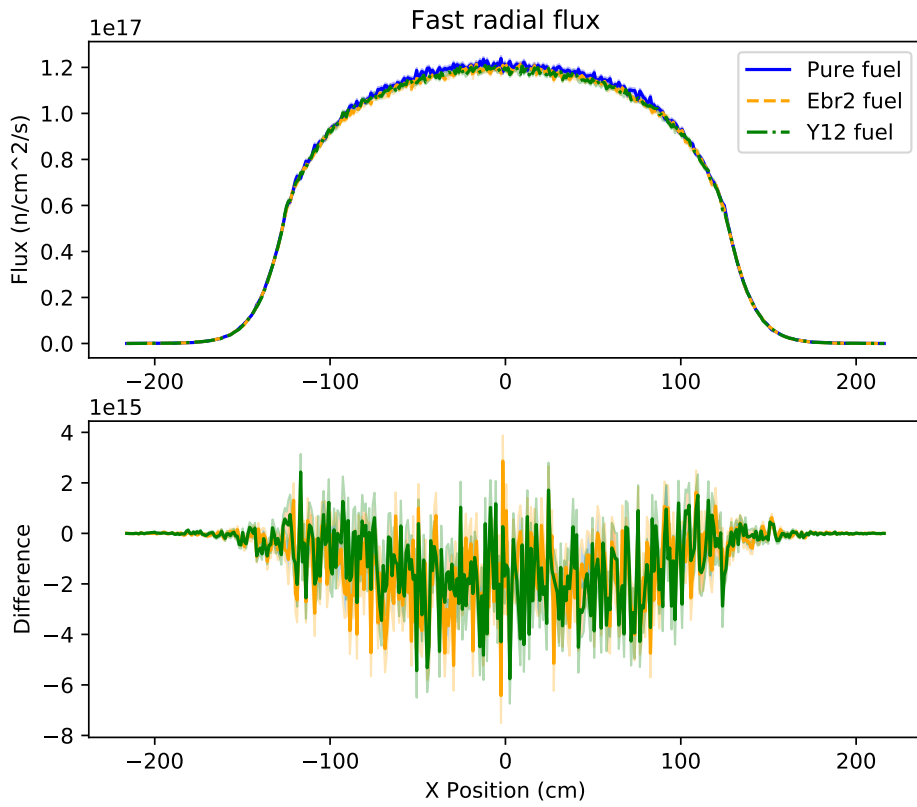


Figure 8.5: Fast flux (above 0.625 eV) in the Xe-100-like Sangamon200 reactor model in the radial direction, across the x-axis (top). The absolute difference from the flux from the pure HALEU fuel with  $1\sigma$  error shown by the shading (bottom).

locations of the pebbles at each pass number when using the Y-12 fuel: fresh pebbles switched with most burnt, single pass pebbles switched with pebbles that have gone through all but one passes, etc. The thermal axial flux when shuffling the Y-12 fuel pebble locations (Figure 8.7) shows that changes the symmetry of the difference. Therefore, some of the difference in the neutron flux is a result of the placement of the pebbles, and the differences in isotopic compositions from burning the different fuel compositions. However, shuffling the pebbles when using the Y-12 HALEU composition still resulted in a smaller flux than the pure fuel. Therefore, the flux depression is a function of the HALEU composition and not the pebble placement.

The fast axial flux (Figure 8.8) shows a smaller difference in the flux magnitudes between the different fuel compositions than the thermal axial fluxes. The impure fuels result in similar fluxes, consistent to observations in the thermal axial flux. The largest flux difference between the pure and impure fuels is also in the bottom of the core. However, unlike in the thermal axial flux, impure fuels result in a slightly larger flux than the pure fuel in the top of the core. The axial asymmetry in the difference between the fluxes is consistent with the differences in the

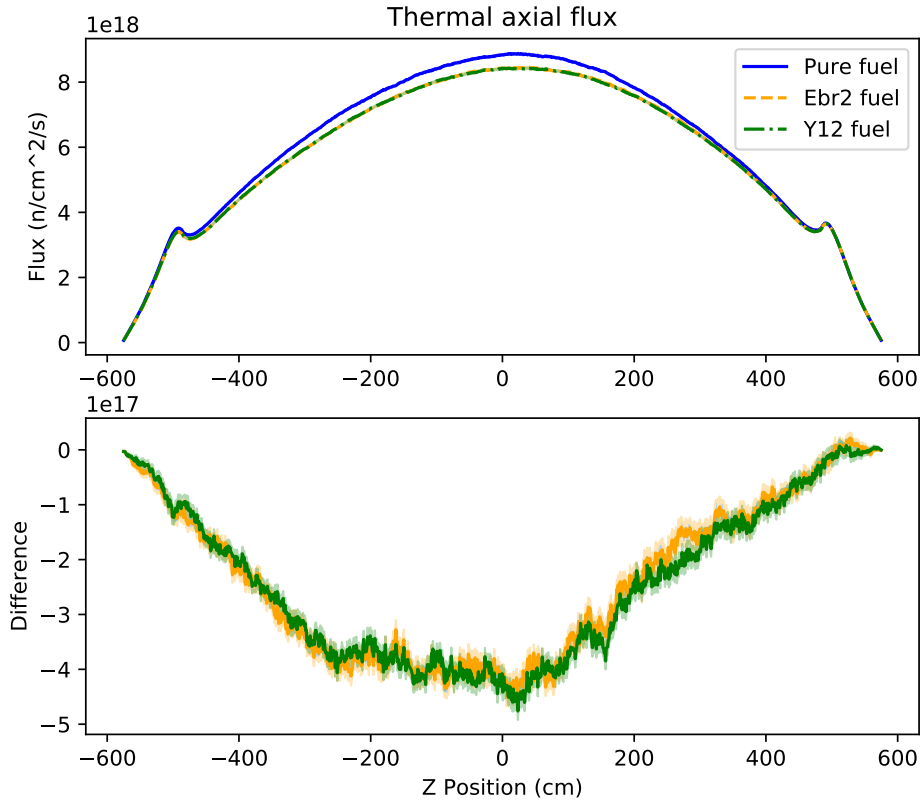


Figure 8.6: Thermal flux (below 0.625 eV) in the Xe-100-like Sangamon200 reactor model in the axial direction (top). The absolute difference from the flux from the pure HALEU fuel with  $1\sigma$  error shown by the shading (bottom). 0 cm is the midpoint of the core.

thermal axial fluxes because of the effect of pebble location and the different compositions in partially burned fuel.

The fluxes from this reactor model are about three orders of magnitudes larger than the results from the modeling of the Xe-100 done by Mulder and Boyes [138]. Part of this difference comes from the ranges used for each energy group. Mulder and Boyes used a definition of greater than 0.1 MeV for the fast energy group and less than 1.86 eV for the thermal energy group. This work applies a definition of greater than 0.625 eV and less than 0.625 eV for fast and thermal neutrons, respectively. Therefore, the definitions used by Mulder and Boyes does not include all possible neutron energies while the definition used in this work does, leading to some of the differences between the fluxes. The other difference comes from the detector definitions in the inputs. For this work, the radial detector was defined across the x- and y-axes and the axial detector was defined across the z-direction. The flux in a detector in Serpent is integrated across the volume of the core [139]. Therefore, the flux across any axes not included in the mesh for a detector is summed across those axes. This is the primary reason why the flux is orders of magnitude different between the two models.

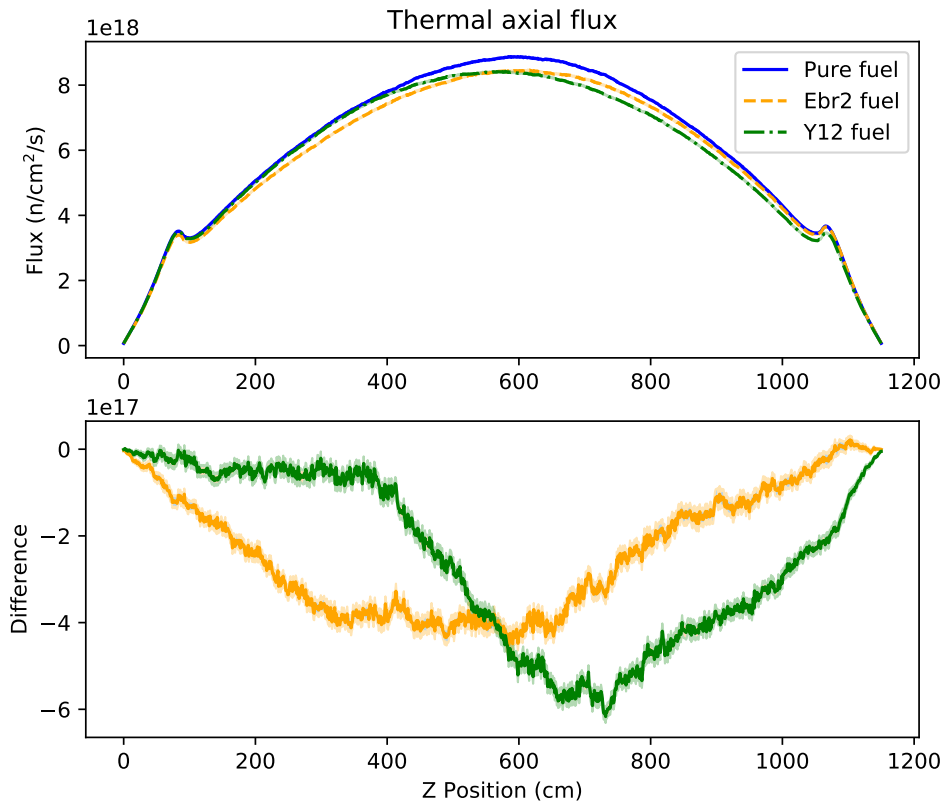


Figure 8.7: Thermal flux (below 0.625 eV) in the Xe-100-like Sangamon200 reactor model in the axial direction when the locations of the pebbles are shuffled when using the Y-12 fuel composition (top). The absolute difference from the flux from the pure HALEU fuel with  $1\sigma$  error shown by the shading (bottom).

#### Reactivity feedback coefficient comparison

Table 8.4 reports the reactivity feedback coefficients for each material type in the Xe-100-like reactor model. All of the coefficients are negative: this is a positive feature of this reactor so that reactivity naturally decreases as temperature increases.

The fuel reactivity feedback coefficient from the pure fuel is more negative than the values from the impure fuels, with the EBR-II fuel resulting in the least negative fuel feedback coefficient. However, all of the values are negative, and are within error of each other. Therefore, one cannot conclude that the fuel composition significantly affects this metric.

For the other three reactivity feedback coefficients, the impure fuels result in coefficients that are more negative than the values from the pure fuel. The coolant feedback coefficient values are outside of the reported error (pure compared with a non-pure fuel), but the values of the other two material coefficients are all within error of each

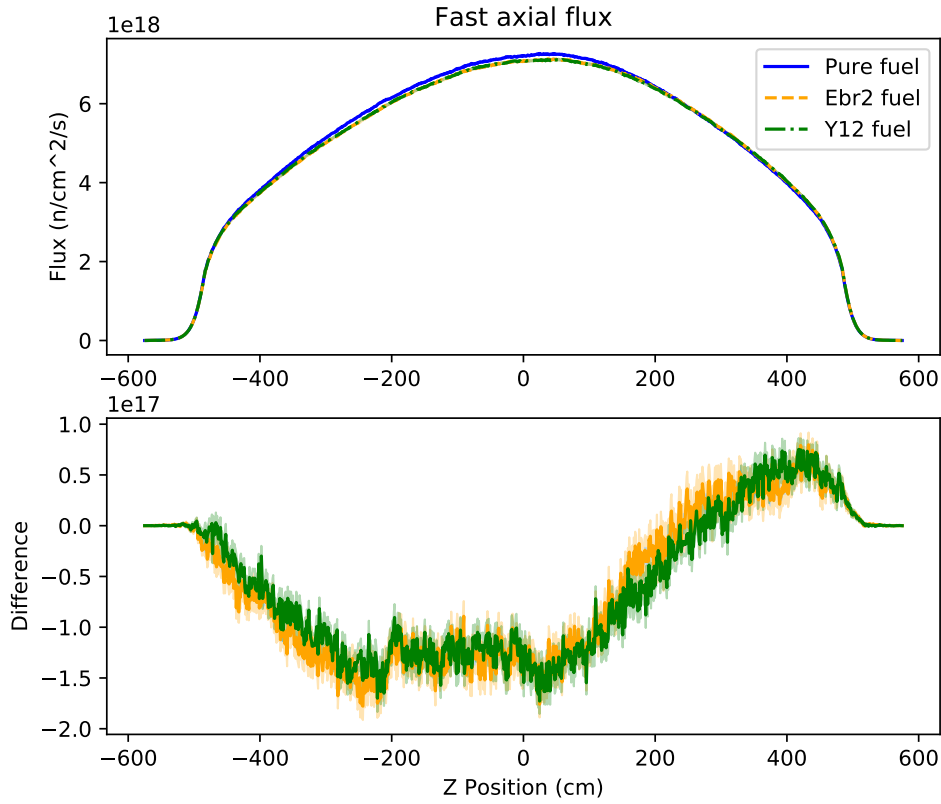


Figure 8.8: Fast flux (above 0.625 eV) in the Xe-100-like Sangamon200 reactor model in the axial direction (top). The absolute difference from the flux from the pure HALEU fuel with  $1\sigma$  error shown by the shading (bottom).

other. The significant impact on the coolant reactivity feedback coefficient suggests that the impurities in the fuel cause a larger flux near the single resonance in the total cross section for helium, resulting in the greater impact from changing this material temperature. However based on the values of each material feedback coefficient, the coolant temperature has a much smaller effect and impact on the total feedback coefficient than the other materials.

The work by Mulder and Boyes [138], reported the reactivity coefficients reported in Table 8.5 for temperatures between 100-900 °C. The feedback coefficients are within the ranges reported by Mulder and Boyes, despite the differences in the reactor models used. The consistency between the feedback coefficient values from the impure fuels in this work and the values reported by Mulder and Boyes suggests that the impurities in the fuel do not greatly impact this reactor operation metric.

Table 8.4: Reactivity temperature feedback coefficients for each material type in the Xe-100-like model for each fuel type.

Fuel Type	Material feedback coefficient (pcm/K)			
	Fuel	Coolant	Moderator	Total
Pure	-3.875 ± 0.094	-0.044 ± 0.112	-0.071 ± 0.459	-4.216 ± 0.502
EBR-II	-3.759 ± 0.138	-0.433 ± 0.048	-0.708 ± 0.404	-4.817 ± 0.438
Y-12	-3.797 ± 0.157	-0.351 ± 0.092	-0.728 ± 0.469	-4.700 ± 0.349

Table 8.5: Reactivity temperature feedback coefficient maximum and minimum values reported by Mulder and Boyes for the Xe-100 between 100-900 °C [138].

Reactivity coefficient	Minimum ( $\Delta k_{eff}$ /°C)	Maximum ( $\Delta k_{eff}$ /°C)
Fuel Doppler	-5.6e-5	-3.2e-5
Moderator	-4.2e-5	-0.4e-5
Total	-6.1e-5	-2.0e-5

### 8.2.2 MMR reactor

The following four sections report and analyze the results of the EBR-II and Y-12 impurities in the MMR-like reactor model created. The four different results are presented for three different burnup steps during the reactor operation: BOL (0 MWd/kgU), MOL (40.52 MWd/kgU), and EOL (81.04 MWd/kgU).

#### $k_{eff}$ comparison

Table 8.6 reports the  $k_{eff}$  value of the MMR at the different burnup steps using each fuel composition. At each burnup step, using the impure fuel compositions results in a  $k_{eff}$  712-1344 pcm smaller than the  $k_{eff}$  when using the pure fuel. The difference in  $k_{eff}$  from the different fuel compositions decreases with burnup because of the depletion of the uranium, which includes burning of the parasitic uranium isotopes. The impure fuel resulting in a lower  $k_{eff}$  than the pure fuel is the opposite effect of that observed in the Xe-100-like model. The change in the trend is because in this reactor the fuel is more homogeneous than in the Xe-100-like model. In the Xe-100-like model, the pebbles are modeled at different burnup stages, while in this model all of the fuel is at the same burnup step. All of the fuel in this model is unburned in the first burnup step, meaning that the impurities have a more significant effect on the neutron population because the impurities are a larger fraction of the uranium in the core than in the Xe-100-like model.

Table 8.6:  $k_{eff}$  in the MMR-like model at select burnup steps and different HALEU compositions.

Fuel Type	Burnup step		
	BOL	MOL	EOL
Pure	1.33797 ± 0.00027	1.18048 ± 0.00025	1.05535±000024
EBR-II	1.32609 ± 0.00028	1.17148 ± 0.00027	1.04792 ± 0.00025
Y-12	1.32453±0.00029	1.17051±0.00027	1.04823±0.0024

The effect of the impurities on this reactor model are significant on the  $k_{eff}$ ; the differences exceed the error on the values. However, even at the last burnup step the  $k_{eff}$  is still above 1. Therefore the effect of the impurities is not great enough to cause the reactor to reach a subcritical state during its operation. The super-critical  $k_{eff}$  throughout the duration of the burn cycle suggests that the lifetime of the reactor will not be affected by the impurities in the fuel.

### $\beta_{eff}$ comparison

Table 8.7 reports the  $\beta_{eff}$  values when using each fuel composition at the different burnup steps. For all three fuel compositions, the  $\beta_{eff}$  decreases with increasing burnup. This is consistent with the depletion of the  $^{235}\text{U}$  in the core and an increase in the number of fissions happening in isotopes that have a lower  $\beta_{eff}$  than  $^{235}\text{U}$ , such as  $^{239}\text{Pu}$ . The  $\beta_{eff}$  values at BOL are slightly larger than the expected 0.0064 value of  $\beta$  for thermal fissions in  $^{235}\text{U}$  or the  $\beta_{eff}$  of a typical PWR. The consistency of the  $\beta_{eff}$  larger than 0.0064 at BOL across the three HALEU compositions is a result of the smaller geometry of this core compared with a PWR core, and not an effect of the fuel compositions. The small size of the core and higher enrichment cause an increase in the probability of non-leakage of fast neutrons to dominate the decrease of the fast fission factor, compared with a PWR.

Table 8.7:  $\beta_{eff}$  value in the MMR-like model at select burnup steps.

Fuel	Burnup step		
	BOL	MOL	EOL
Pure	$0.00669 \pm 0.00004$	$0.00586 \pm 0.00004$	$0.00548 \pm 0.00003$
EBR-II	$0.00663 \pm 0.00003$	$0.00591 \pm 0.00003$	$0.00542 \pm 0.00003$
Y-12	$0.00665 \pm 0.00004$	$0.00598 \pm 0.00004$	$0.00553 \pm 0.00003$

Each of the fuel compositions result in different  $\beta_{eff}$  values at each burnup step. However, almost all of the values from the impure fuels are within error of the value from the pure fuel. Therefore, the fuel impurities do not lead to any significant changes in the  $\beta_{eff}$ . Additionally, the impure fuel compositions do not lead to a consistent change in  $\beta_{eff}$  between burnup steps. Based on these results, the control rod worth and response time will be comparable when using any of these three HALEU compositions.

### Neutron flux comparison

Figure 8.9 shows the flux in the active region of the core as a function of energy (top) and the difference between the flux from the pure fuel and each of the impure fuels (bottom). This data was calculated using the pre-defined SCALE-238 energy group structure in Serpent, with the plotted flux of each group normalized by lethargy. The purple line in both plots in the figure shows the delineation between the fast and thermal energy groups (0.625 eV). This figure shows that the difference between the fluxes is small compared with the magnitude of the flux (two

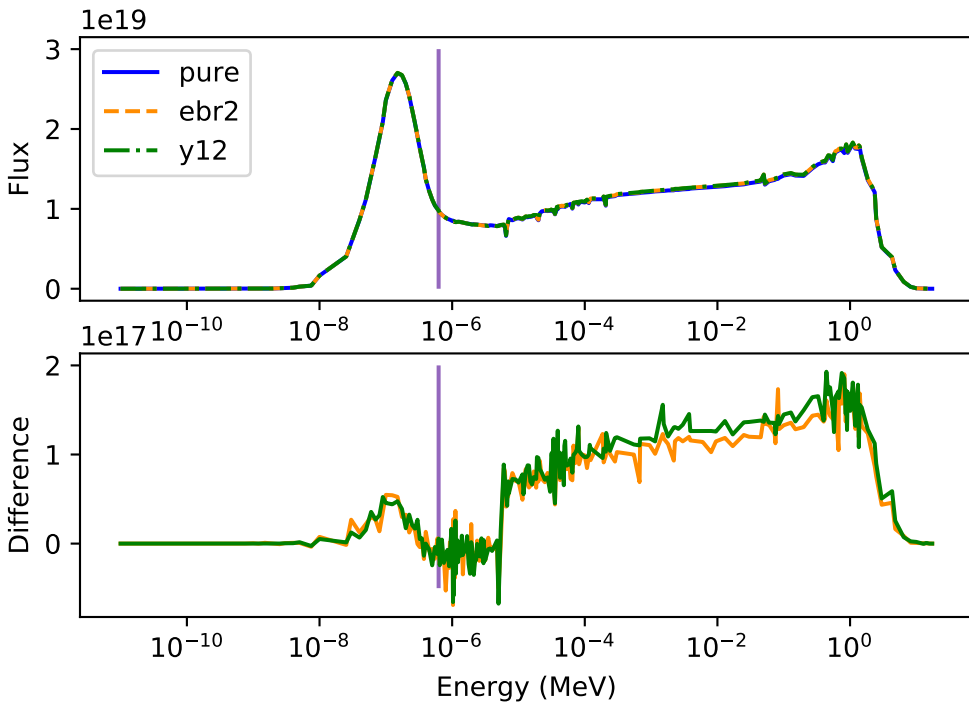


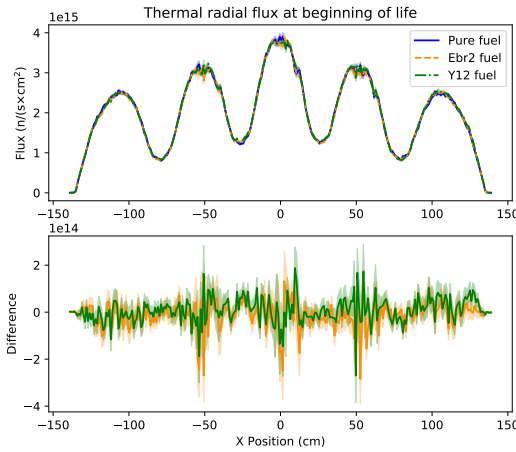
Figure 8.9: Top: Flux energy spectrum for each fuel composition at a burnup of 0 MWd/kgU in the active region of the core. The purple line shows the delineation between the fast and thermal neutron energy groups used in other results of this work. Bottom: Difference between the flux from the pure fuel and each of the impure fuels in each energy group. The purple line shows the delineation between the fast and thermal energy groups (0.625 eV).

orders of magnitude different), especially in the thermal group (left of the purple line). The difference between the fluxes is larger in the epithermal and fast regions, such that the largest difference in the peak around 1 MeV. The differences in the flux from the pure fuel and the flux from each of the impure fuels is larger in the fast energy group than in the thermal energy group.

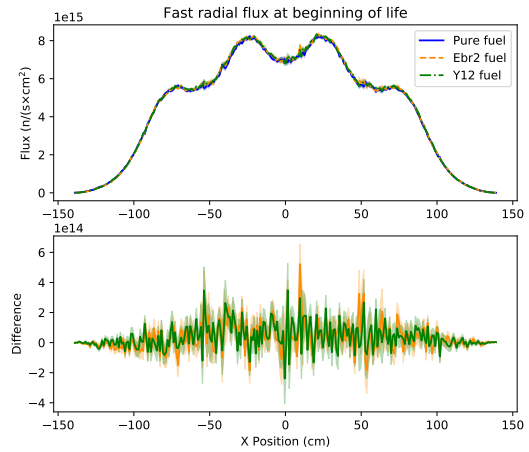
Figures 8.10, 8.11, and 8.12 show the neutron flux in the thermal and fast energy ranges in the radial and axial direction for the BOL, MOL, and EOL burnup steps, respectively. The radial fluxes are taken across the middle of the core in the y-direction, which means the flux is taken across the plane with three coolant channels in Figure 8.2a. The effects of the coolant channels can be observed in the oscillations of the radial fluxes at each burnup step. The axial flux is taken along the z-axis, with the x- and y-directions collapsed. As a result, the axial flux includes radially averaged behavior.

The radial flux at BOL (Figures 8.10a and 8.10b) show that the thermal flux peaks in the control rod channels and the fast flux has a trough in these regions. Conversely, the thermal flux has a trough in the areas closest to the fuel channels and the fast flux has a peak in these areas. These features occur because neutrons from fission in the fuel are born in the fast energy range, but are thermalized as they travel through the graphite towards the

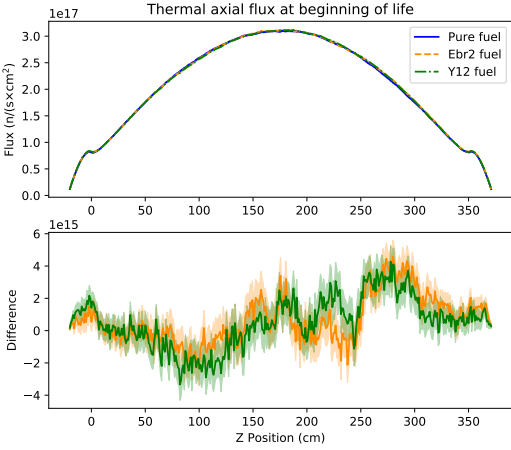
coolant channels. The greatest difference in the fluxes between the fuel compositions is in the areas of the core close to the fuel pellets, where the thermal flux troughs and the fast flux peaks. This result is consistent with only the fuel composition changing between each core model, as the different fuel compositions would lead to different energy spectrums for the neutrons born from fission and thermalizing in the graphite around the fuel channels. The fast flux along this axis is larger than the thermal flux, which is consistent with the observation of the active-core flux as a function of energy. Similar to the neutron flux in the Xe-100-like model, the impure fuels result in similar variations from the flux when using the pure fuel at this burnup step.



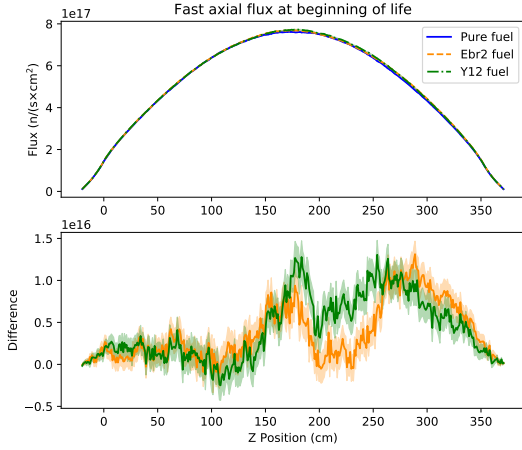
(a) Thermal radial flux in the MMR-like reactor.



(b) Fast radial flux in the MMR-like reactor.



(c) Thermal axial flux in the MMR-like reactor.



(d) Fast axial flux in the MMR-like reactor.

Figure 8.10: Radial and axial flux for each energy group when using each fuel composition in the MMR-like model at the beginning of life. The thermal flux encompasses energies below 0.625 eV, and the fast flux encompasses energies above 0.625 eV.

The axial fluxes at BOL (Figures 8.10c and 8.10d) show the effect of the graphite moderators at the top and

bottom of the core. The thermal flux has a small peak in the moderator while the fast flux has a small exponential decrease in the moderator. The fluxes also show that using the impure fuels results in a slightly smaller flux at the bottom of the core and a slightly higher flux at the top of the core. The differences between the fluxes is 1-2 orders of magnitude smaller than the flux, but is still one order of magnitude larger than the error of the fluxes.

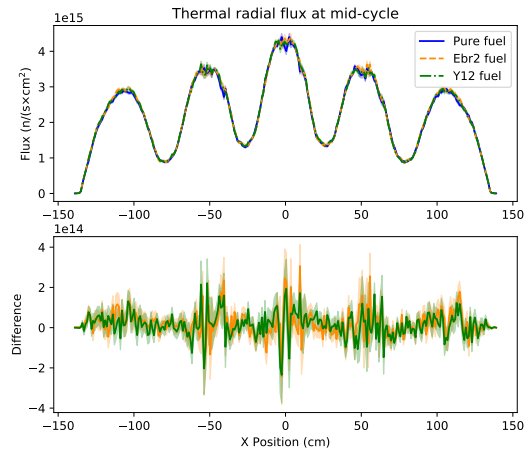
Figure 8.11 shows the different fluxes in the MMR-like reactor at MOL. The trends at mid-cycle in the radial fluxes are similar to those observed at the BOL: the radial fluxes have the greatest difference near the fuel pins in the core. In the axial fluxes however, there is a noticeable difference between the flux from the EBR-II fuel and the other fuels. The EBR-II results in a greater difference from the flux from the pure fuel than the Y-12 fuel, but the shape of the difference is similar to what was observed at BOL; the flux from the EBR-II fuel is less than the flux from the pure fuel in the bottom of the core and greater at the top of the core. For the thermal axial flux, the difference between the flux from the pure and Y-12 fuels decreases compared with the fluxes at BOL, but the difference between the flux from pure and EBR-II fuel increases compared with the flux at BOL. A similar pattern occurs in the fast axial flux. This suggests that as the core burns, the impurities in the Y-12 fuel are burned off sooner than those present in the EBR-II or that the impurities breed material similar to what is present in the pure fuel as it burns.

Finally, Figure 8.12 shows the different fluxes in the MMR-like model at EOL. The radial fluxes continue to show the same trend of the largest differences between the fluxes occurring near the fuel pins. The axial fluxes (Figures 8.12c and 8.12d) show a different trend. Both axial fluxes show that the impure fuels result in a larger flux at the bottom of the core and a smaller flux at the top of the core than the flux from the pure fuel, opposite to what was observed in the BOL and MOL fluxes. The thermal and fast axial fluxes are higher at the EOL than at the other two burnup steps. The difference between the flux from EBR-II fuel and the pure fuel decreases from the difference at MOL, but the difference between the fluxes from the pure and Y-12 fuel increases from the difference at MOL.

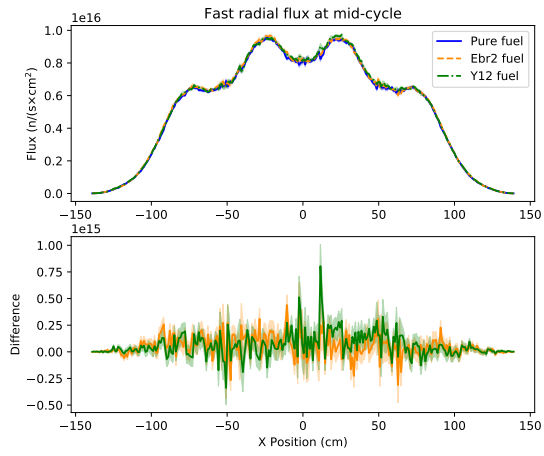
### **Reactivity feedback coefficient comparison**

Finally, the reactivity feedback coefficients of different materials at each burnup step are reported in Table 8.8. The fuel reactivity feedback coefficients become more negative with burnup, because the  $^{235}\text{U}$  in the core depleted with burnup, leaving a larger relative abundance of  $^{238}\text{U}$  and  $^{239}\text{Pu}$  in the core, which both have more resonances than  $^{235}\text{U}$ . The additional resonances of the  $^{238}\text{U}$  and  $^{239}\text{Pu}$  means that the Doppler broadening effect has a more pronounced impact on the reactivity of the core. At each of the burnup steps, the different fuel compositions result in different fuel reactivity coefficients, but each of the values are within error of each other. The values being within error suggests that the fuel composition does not have a significant effect on this parameter.

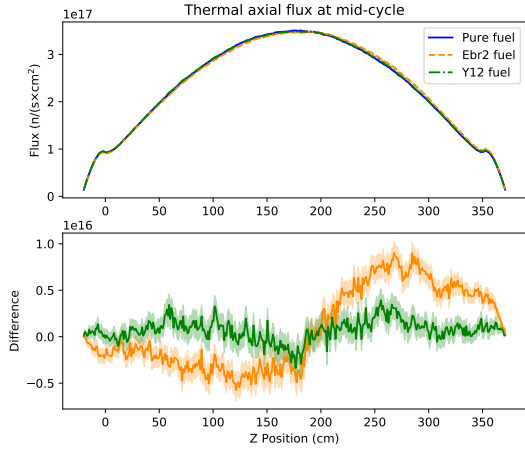
The coolant reactivity feedback coefficients have the smallest absolute value of any of the coefficients considered in this work, which indicates that the helium coolant has the smallest effect on the reactivity of the core as the



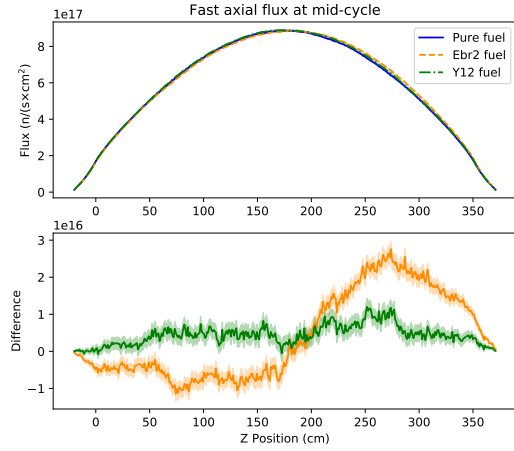
(a) Thermal radial flux in the MMR-like reactor.



(b) Fast radial flux in the MMR-like reactor.



(c) Thermal axial flux in the MMR-like reactor.

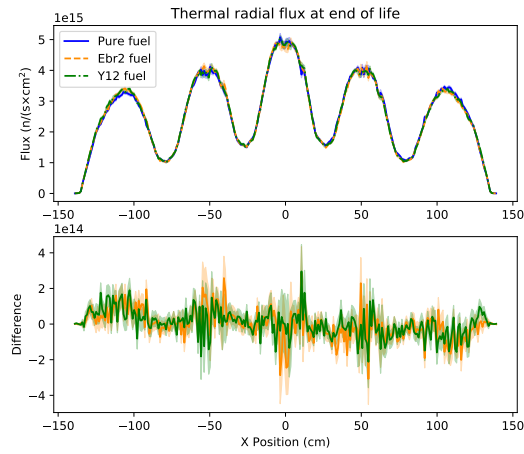


(d) Fast axial flux in the MMR-like reactor.

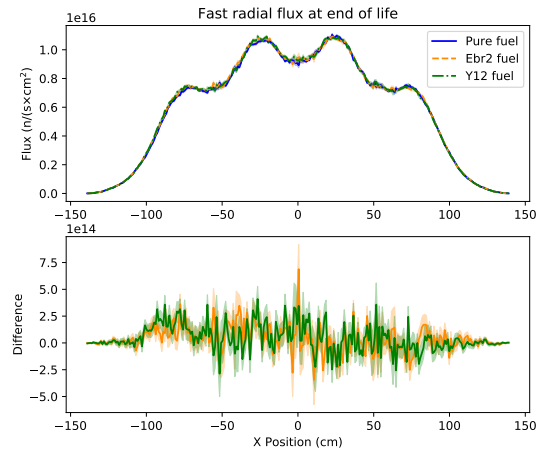
Figure 8.11: Radial and axial flux for each energy group when using each fuel composition in the MMR-like model at middle of the operation cycle. The thermal flux encompasses energies below 0.625 eV, and the fast flux encompasses energies above 0.625 eV.

temperature changes. Additionally, the coolant reactivity feedback coefficient is not as dependent on the burnup of the fuel like the other coefficients, resulting from the density change being the primary temperature-dependent property of the helium coolant instead of widening of cross section resonances. At the BOL, the EBR-II fuel results in a statistically different coolant feedback coefficient, which shows that the fuel composition has some impact on this parameter. However, the coolant reactivity feedback coefficient is small compared to the other feedback coefficients so this change is unlikely to cause significant changes in the operation of the core as a whole.

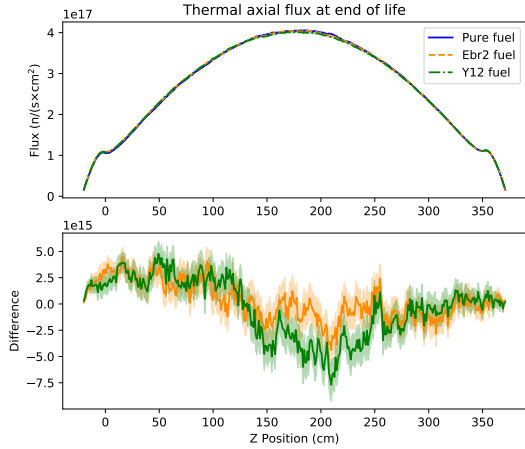
The moderator feedback coefficient is negative for each of the fuel compositions at each burnup step, indicating that this core is undermoderated. This feedback coefficient also becomes more negative with burnup, because the



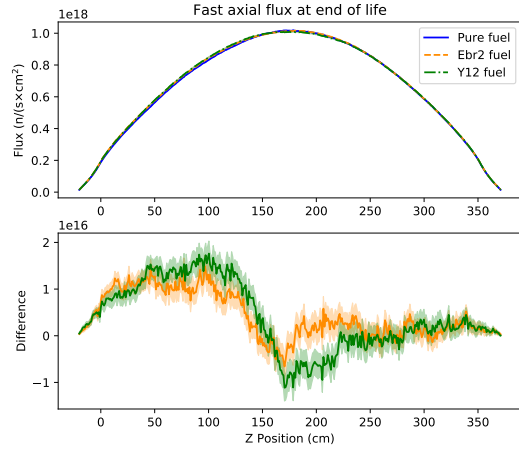
(a) Thermal radial flux in the MMR-like reactor.



(b) Fast radial flux in the MMR-like reactor.



(c) Thermal axial flux in the MMR-like reactor.



(d) Fast axial flux in the MMR-like reactor.

Figure 8.12: Radial and axial flux for each energy group when using each fuel composition in the MMR-like model at the end of life. The thermal flux encompasses energies below 0.625 eV, and the fast flux encompasses energies above 0.625 eV.

flux in the core increases with burnup. The increase in flux could be a result from the resonance broadening having more of an effect on the reactivity of the core, the density change of the graphite, or other effects. At the BOL and MOL steps the pure fuel has the least negative moderator feedback coefficient, but at EOL the pure fuel has the most negative coefficient. However, at each of the burnup steps the moderator feedback coefficient from each of the fuels are within error of each other. This agreement within error suggests that the fuel composition does not have a significant effect on this reactor operation parameter.

Finally, the total reactivity feedback coefficients are also all negative for each fuel composition at each burnup step, and they become more negative with burnup. Based on the values of the feedback coefficients for each

Table 8.8: Reactivity feedback coefficients (pcm/K) for different materials at different burnup steps in the MMR-like reactor model.

Fuel	Burnup step		
	BOL	MOL	EOL
Fuel reactivity feedabck			
Pure	-3.314 ± 0.059	-3.889 ± 0.088	-4.536 ± 0.264
EBR-II	-3.073 ± 0.109	-3.720 ± 0.147	-4.699 ± 0.151
Y-12	-3.233 ± 0.107	-3.704 ± 0.133	-4.168 ± 0.100
Coolant reactivity feedabck			
Pure	-0.211 ± 0.063	0.021 ± 0.169	0.052 ± 0.234
EBR-II	0.007 ± 0.051	-0.165 ± 0.183	0.005 ± 0.085
Y-12	-0.221 ± 0.068	0.197 ± 0.145	-0.0146 ± 0.158
Moderator reactivity feedabck			
Pure	-0.815 ± 0.062	-1.298 ± 0.155	-2.590 ± 0.323
EBR-II	-0.934 ± 0.171	-1.723 ± 0.268	-2.375 ± 0.313
Y-12	-0.950 ± 0.138	-1.333 ± 0.206	-2.432 ± 0.190
Total reactivity feedabck			
Pure	-4.142 ± 0.297	-5.015 ± 0.215	-6.865 ± 0.300
EBR-II	-4.191 ± 0.097	-5.284 ± 0.286	-6.709 ± 0.329
Y-12	-4.037 ± 0.322	-5.410 ± 0.268	-6.689 ± 0.232

individual material, the total feedback coefficient is mostly driven by the fuel feedback coefficient at each burnup step. The different fuel compositions result in total reactivity feedback coefficients that are within error of each other. Therefore, the fuel composition does not significantly affect this reactor parameter either.

At each burnup step, the fuel and total reactivity feedback coefficients are negative for each fuel composition and the values from each fuel composition are within error of each other. These two results suggests that using any of these three fuel composition will not prevent this reactor design from operating in a safe state.

# **Chapter 9**

## **Conclusions**

The US Nuclear Fuel Cycle (NFC) is poised to change as a greater variety of nuclear reactor designs are licensed and deployed. One notable change between currently deployed nuclear reactors and many advanced reactor designs is the enrichment level required; many advanced reactors require fuel at a higher enrichment level (5-20%  $^{235}\text{U}$ , referred to as High Assay Low Enriched Uranium (HALEU)) than current Light Water Reactor (LWR) technology (less than 5%  $^{235}\text{U}$ ). Using a higher enrichment level provides numerous benefits to reactor operation, such as longer cycle times and higher fuel burnup. However, there is currently no domestic way to produce commercial HALEU, which has prompted investigations into how to develop supply chains for HALEU [7, 8]. Potential methods to produce HALEU include the enrichment of natural uranium and the downblending of High Enriched Uranium (HEU), with each method having limitations. Enriching natural uranium is limited by the facilities available to perform the enrichment, and downblending HEU is limited by the amount of material available for downblending. Using either (or both) of these methods will lead to changes in the US NFC.

The goal of this work was to investigate the impacts of deploying reactors fueled by HALEU in the United States. Within this primary goal, there are three specific objectives:

1. Quantify potential material requirements for the transition from LWRs to advanced reactors in open and closed fuel cycles.
2. Understand the impacts of fuel cycle parameters on the material requirements and design optimized transition scenarios.
3. Identify potential limitations in using downblended HEU on reactor performance.

The first objective was met by designing and modeling various transitions to advanced reactors, considering a once-through and a closed fuel cycle (Chapters 3 - 5). The second objective was met by performing sensitivity analysis and optimization to one of the once through fuel cycles (Chapters 6 and 7). Finally, the third objective was met by modeling the two different HALEU-fueled advanced reactors to investigate the impact of different uranium isotopic compositions of the HALEU fuel on reactor performance (Chapter 8).

Chapter 3 provided an overview of the methodology used for the fuel cycle analysis of this work. The methodology includes the advanced reactors, advanced reactor design specifications, fuel cycles considered, and the advanced reactor deployment scheme. This chapter also describes OpenMCyclus, a new archetype that couples CYCLUS with OpenMC to dynamically perform depletion of fuel during a simulation. This archetype extends the depletion capabilities in CYCLUS by providing a coupling to an open-source code, and allowing the depletion to be reactor-agnostic. Benchmarking against the CYCMORE Reactor archetype, a recipe-based archetype, shows generally good agreement with regards to when materials are traded away. There are large differences in the separated plutonium inventory between these two archetypes because of differences in the depletion methodology: CYCMORE Reactor applies the same composition to spent fuel no matter how many cycles the fuel is irradiated while OpenMCyclus performs depletion on a single-cycle basis. This methodology difference leads to different amounts of separated plutonium available, which propagates to different amounts of MOX fuel available for the reactors. The methodology in OpenMCyclus leads to less separated plutonium available than the CYCMORE Reactor methodology.

Chapter 4 presented the results of modeling the transition from LWRs to different combinations of advanced reactors in a once-through fuel cycle. The results identify how the reactors deployed and their relative deployment numbers, obtained through the deployment scheme of this work, drives the enriched uranium mass required by a transition. The discharge burnup of the reactors deployed drives the enriched uranium mass needed by each transition. The SWU capacity and feed uranium requirements are driven by the amount of fuel required by the reactors and the enrichment level of the fuel. The results show how the increased fuel requirements of a reactor demand can be offset by the decrease in the enrichment level, leading to negligible changes in the SWU capacity required.

Chapter 5 presented the results of modeling the transition from LWRs to advanced reactors in different closed fuel cycles. The results of this chapter show how the amount of material available for reprocessing impacts the masses of separated actinide material and the availability of plutonium-based fuels (MOX or U/TRU fuel). The amount of plutonium-based fuels available impacts the mass of enriched uranium, feed uranium, and SWU capacity required, because the plutonium-based fuel displaces uranium-based fuel needed by the advanced reactors. Additionally, the actinide elements separated from UNF impacts the masses of HLW and separated actinide material. The more actinide elements separated out from UNF, the more separated material available and more plutonium-based fuel available. The separation of uranium from the UNF is the primary driver of this impact, as UNF is mostly uranium by mass. Finally, this chapter showed how using a closed fuel cycle can reduce HALEU needs, but the lack of existing reprocessing infrastructure in the US means that using a closed fuel cycle will not help in reducing upfront HALEU needs. These results, combined with the results of Chapter 4, show that potential demand for HALEU and other

resources to support a HALEU-based fuel cycle are dependent on multiple variables and parameters of the fuel cycle.

Chapter 6 examined the effects of different input parameters on different output metrics for the fuel cycle transition from LWRs to different advanced reactors by performing sensitivity analysis. We performed this analysis by coupling CYCLUS with Dakota and perturbing input parameters. We selected input parameters based on the results in Chapter 4, specifically how the relative number of each advanced reactor built and the burnup from each reactor drove many of the transition metrics. The one-at-a-time (OAT) analysis identified the trends from varying each input parameter independently, and how the deployment scheme modeled in this work impacts each of the results. The analysis also highlighted tradeoffs between different reactor designs based on the results of the metrics and the number of each advanced reactor built for a given input parameter. An example of the tradeoffs between advanced reactors is the Xe-100 needing more HALEU than the VOYGR, but a smaller total fuel mass. We identified the transition start time as not as impactful on the results as the other parameters. The synergistic analysis identified how some of the input parameters interact to affect the output metrics. Some of the combinations of input parameters (e.g., varying the LWR lifetime and the VOYGR build share) had trends consistent across the input parameter space and consistent with the results of the OAT analysis. Other combinations (e.g., varying the Xe-100 burnup and the MMR share) varied in their effect across the input parameter space because of interactions between the parameters. Finally, the global sensitivity analysis quantified the effect of different input parameters on the variance of the output metrics. All of the analysis identified the Xe-100 discharge burnup as the most impactful parameter for almost every metric, regardless of which advanced reactor build share was varied. This result stems from the strong relationship between the Xe-100 burnup and the different metrics, as well as the methodology of the deployment scheme. Based on the deployment scheme, the number of Xe-100s deployed varies, no matter which advanced reactor is selected for build share variation. Therefore, the material needs of the Xe-100, which is closely tied to the discharge burnup, always affects the metrics if there is variation in the advanced reactor build shares.

Chapter 7 demonstrated a methodology to optimize the once-through transitions and identified transitions that minimize different fuel cycle metrics. We used the same CYCLUS-Dakota coupling used for the sensitivity analysis, but changed the Dakota inputs to apply the single- and multi-objective genetic algorithms in Dakota to perform optimization. Results from this chapter show that minimizing the SWU capacity to produce HALEU requires maximizing the number of VOYGRs built and minimizing the mass of UNF requires maximizing the number of Xe-100s built. Minimizing both of these fuel cycle metrics is a balance between deploying Xe-100s and VOYGRs. The results of all three optimization problems show agreement in maximizing the number of LWRs operating for 80 years, maximizing the Xe-100 burnup, and minimizing the MMR build share. The MMR burnup becomes irrelevant if no MMRs are built, so the results identified different values for this input parameter. The results

from the optimization work was consistent with the results of the sensitivity analysis, but they did not fully meet expectations. The input parameters identified that were not subject to a linear constraint (i.e., not the advanced reactor build shares) matched expectations based on the trends of the sensitivity analysis and intuition. However, the genetic algorithms we used did not adhere well to the linear constraint of the advanced reactor build shares in all three of the problems. The parameters valued considered in each populations did not always adhere to the constraint, which led to the solution not meeting the constraint. Therefore, the results from the optimization work can not be taken at face value. The results are better used for identifying a relationship between the advanced reactor build shares than a specific set of parameters, because the optimization solutions aligned well with intuition and the sensitivity analysis results even if the linear constraint is not met. Additionally, we limited the number of evaluations for each optimization problem, based on limited computational resources. Allowing the algorithm to run more evaluations may produce results that better meet expectations and the linear constraint.

Finally, Chapter 8 described the analysis of the effects of downblended HEU in the Xe-100 and MMR. This chapter presents the Xe-100-like and MMR-like reactor models developed for this work, which we also used to assist in obtaining spent fuel compositions for the transition analysis. We compared the downblended HEU compositions from EBR-II and Y-12 National Security Complex HEU stockpiles against the performance of HALEU with only  $^{235}\text{U}$  and  $^{238}\text{U}$ , referred to as the “pure” fuel. Performance metrics considered include the  $k_{eff}$ ,  $\beta_{eff}$ , energy- and spatially-dependent flux, and the fuel, coolant, moderator, and total reactivity temperature feedback coefficients. The results of the Xe-100-like reactor in an equilibrium state show that the impurities from the downblended HEU fuel increases the  $k_{eff}$  but decreases the  $\beta_{eff}$ , compared with the results of the pure fuel. The energy-dependent flux shows a decrease in the thermal flux around 0.1 eV and an increase in the fast flux above 20 MeV when using the downblended HEU. The spatially-dependent flux shows a decrease in the thermal (below 0.625 eV) and fast (above 0.625 eV) fluxes when using the impure fuels, across the radial and axial directions. The fluxes also showed an asymmetry in the axial fluxes for both energy groups. This asymmetry is a result of the distribution of pebbles at different burnup steps, but the decrease in the thermal axial flux is a result of the HALEU composition. The reactivity temperature feedback coefficients from each fuel composition are within error of the coefficients from the pure fuel or are consistent with ranges presented by Mulder and Boyes [138].

The results of the MMR-like model at BOL, MOL, and EOL show that the different HALEU compositions result in lower  $k_{eff}$  values than the pure fuel at each burnup step. However, the reactor still has a  $k_{eff}$  above 1 at the EOL with all three HALEU compositions. This result suggests that the change in  $k_{eff}$  would not prevent this reactor from reaching its designed 20 year lifetime. The different HALEU compositions resulted in  $\beta_{eff}$  that are within error of the values from the pure fuel. The energy-dependent flux showed that the downblended HEU mostly affects the fast (above 0.625 eV) flux, causing a small increase in the flux. The spatially-dependent flux showed some asymmetry in

the axial direction from one of the downblended HEU compositions at MOL, but we observed no other large effects. The reactivity temperature feedback coefficients are mostly within error of the coefficients from the pure fuel. The coolant reactivity feedback coefficients from the downblended HEU are outside error from those from the pure fuel, but these values have a much smaller magnitude than the other reactivity feedback coefficients and operate on a much longer time scale. Based on the performance metrics of both reactor designs with the different HALEU compositions, the impurities present in the downblended HEU may lead to small perturbations in performance, but do not lead to large changes in operation or prevent the reactors from operating in a safe state.

## 9.1 Limitations and Future Work

The work performed here provides a foundation for continued analysis and exploration of the fuel cycle impacts of deploying HALEU-fueled reactors. One limitation of this work is that it explores the impacts of deploying HALEU-fueled reactors at a very macroscopic level. We investigated and compared the material requirements across the modeled time period as an aggregate, with an unlimited amount of resources, and without facility constraints. Potential future work to address this limitation would model and explore the impacts of these reactors on a more microscopic level. This includes translating potential demands to facility capacities, numbers, and designs or comparing the material requirements across different time periods. For example, designing and comparing the centrifuge cascades required to produce the enriched uranium for each of the advanced reactors. This work could account for the different NRC facility classifications based on the enrichment level of the handled material. This future work would also explore how to most efficiently develop and use different facilities to produce the enriched uranium. Another example would be comparing the HALEU mass required in the first five years of deploying HALEU-fueled reactors compared with demand after all LWRs decommission. This analysis would provide more detailed information on material requirements during the cycle transition and during equilibrium of the new fuel cycle. A third potential area of work could model the time requirements of different processes (e.g. time to fabricate a fuel assembly). More accurate modeling of the time requirements for each step would provide details of required lead times and how these requirements may impact material availability.

Furthermore, this work also focused on the uranium and heavy metals for the fuel, but these are not the only fuel components or reactor cores. Another area of future work includes modeling non-fuel materials needed to support these transitions, such as the amount of reactor-grade graphite to be the moderators in the Xe-100 and MMR. This analysis would provide insight into other potentially limiting supply chain requirements that are impactful on establishing these fuel cycles. Additionally, this work focused on waste materials that need a repository for disposal. But there are other waste forms, like low level waste (LLW), that also need disposal. The fuel cycle modeling

methodology employed in this work provides a foundation for how to carry out both of these analyses.

A third limitation of this work is the disregard for nonproliferation safeguards in the fuel cycle modeling. Non-proliferation safeguards are an important part of ensuring the peaceful uses of nuclear power, and are implemented across fuel cycle facilities. To address this limitation, one could develop a method to incorporate safeguards into the fuel cycle modeling methodology demonstrated here. Examples of incorporating safeguards into fuel cycle modeling could be to restrict facility throughputs, minimize stockpiles of enriched uranium at a facility, minimize idle SWU capacity, and limit the amount of material that can be transported at once. Each of these restrictions can affect the ability to produce enough fuel for the deployed reactors. Investigating the effects of safeguards on the fuel cycle provides more detailed metrics of how to develop and support a fleet of HALEU-fueled reactors.

A key component of this work is the development of OpenMCyclus to expand the dynamic depletion capabilities in CYCLUS. The continued development of OpenMCyclus would support this expansion. One area of future work is to benchmark this archetype against other fuel cycle simulators that also perform real-time depletion. This additional benchmark would help to identify how differences in material handling and depletion propagate together between the codes, and identify potential areas of improvement for this archetype. Additionally, OpenMCyclus focuses on the back-end of the fuel cycle, but the back-end of the fuel cycle connects to the front-end when modeling reprocessing. Therefore, an extension of this work would be the exploration of how the transport capabilities in OpenMC can be used to determine fresh fuel compositions, such as how DYMOND has a method to perform a criticality search [54], and subsequent development of a fuel fabrication archetype in this library. This capability would prevent the user from having to determine MOX or U/TRU fuel compositions *a priori* while still providing accurate compositions for fresh fuel in a reactor that meets key design criteria.

The optimization methodology demonstrated in this work is limited by the optimization algorithms used. Specifically, the genetic algorithms struggled with adhering to the linear constraint on the advanced reactor build shares we applied. Future work to address this limitation could apply other algorithms in Dakota that strictly adhere to linear constraints, like the derivative-free methods [28], or allow the genetic algorithms to run for more evaluations. Another avenue of future work could also change the input parameters to only consider one advanced reactor build share, which would remove the linear constraint. This avenue would allow the defined advanced reactor build share to vary across integer values in a given range, then deploy the other advanced reactors as needed to meet any remaining energy demand. Removing the linear constraint is expected to yield a solution that does not have unneeded installed capacity from advanced reactors.

Future work can also expand upon the analysis of the downblended HEU on the reactor performance. For example, modeling other HALEU-fueled reactors that have announced an intent to use HALEU created from the identified HEU stockpiles, like the Oklo Aurora, would provide more practical analysis. Additionally, future work

could expand the analysis to include other metrics, such as power peaking factors and power distributions in the core. Expanding the analysis to include these parameters would provide more details on how the impurities from the HEU may affect reactor operation, such as the amount of various reactivity control mechanisms needed. One can also increase the model fidelity by varying temperatures across the core, adding burnable absorbers to the materials, or altering the geometry to better match with vendor information as it is made publicly available. These updates to the models would provide information about how the HALEU composition would affect the reactor performance in a more realistic simulation.

# References

- [1] U.S Energy Information Administration, "Electricity in the U.S. - U.S. Energy Information Administration (EIA)," Apr. 2022. [Online]. Available: <https://www.eia.gov/energyexplained/electricity/electricity-in-the-us.php>
- [2] NEA, "Meeting Climate Change Targets: The Role of Nuclear Energy," OECD Nuclear Energy Agency, Paris, Tech. Rep. NEA 7628, 2022. [Online]. Available: [https://www.oecd-nea.org/jcms/pl\\_69396/meeting-climate-change-targets-the-role-of-nuclear-energy?details=true](https://www.oecd-nea.org/jcms/pl_69396/meeting-climate-change-targets-the-role-of-nuclear-energy?details=true)
- [3] Nuclear Energy Institute, "U.S. Nuclear Plant License Information," May 2021, publication Title: Nuclear Energy Institute. [Online]. Available: <https://www.nei.org/resources/statistics/us-nuclear-plant-license-information>
- [4] World Nuclear Association, "Plans for New Nuclear Reactors Worldwide - World Nuclear Association," May 2022, publication Title: World Nuclear Association. [Online]. Available: <https://world-nuclear.org/information-library/current-and-future-generation/plans-for-new-reactors-worldwide.aspx>
- [5] M. Hussain, F. Reitsma, M. Subki, and H. Kiuchi, "Advances in Small Modular Reactor Technology Developments," Nuclear Power Technology Development Section, Division of Nuclear Power of the IAEA Department of Nuclear Energy, Vienna, Austria, A Supplement to: IAEA Advanced Reactors Information System (ARIS), Sep. 2018. [Online]. Available: <http://aris.iaea.org>
- [6] U.S. Department of Energy Office of Nuclear Energy, "Advanced Reactor Demonstration Program," publication Title: Energy.gov. [Online]. Available: <https://www.energy.gov/ne/advanced-reactor-demonstration-program>
- [7] M. C. Regalbuto, "Addressing HALEU Demand," Apr. 2020. [Online]. Available: [https://inldigitallibrary.inl.gov/sites/sti/sti/Sort\\_24470.pdf](https://inldigitallibrary.inl.gov/sites/sti/sti/Sort_24470.pdf)
- [8] B. Dixon, S. Kim, B. Feng, T. Kim, S. Richards, and J. Bae, "Estimated HALEU Requirements for Advanced Reactors to Support a Net-Zero Emissions Economy by 2050," Tech. Rep. INL/EXT-21-64913-Rev000, 1838156, Jan. 2022. [Online]. Available: <https://www.osti.gov/servlets/purl/1838156/>
- [9] Nuclear Energy Institute, "Addressing the Challenges with Establishing the Infrastructure for the front-end of the Fuel Cycle for Advanced Reactors." Technical Report, Jan. 2018. [Online]. Available: <https://www.nei.org/resources/reports-briefs/infrastructure-for-the-front-end-fuel-cycle>
- [10] M. N. O. Patterson, B. R. Westphal, D. D. Tolman, and J. C. Price, "HALEU Decontamination Investigations for EBR-II Recovered Uranium. HALEU Drip Casting Results in the Fuel Conditioning Facility Cathode Processor," Idaho National Lab. (INL), Idaho Falls, ID (United States), Tech. Rep. INL/EXT-19-53191-Rev000, Mar. 2019. [Online]. Available: <https://www.osti.gov/biblio/1503291>
- [11] R. C. Robinson and L. Jollay, "Establishment of a HALEU Advanced Rx Strategic Reserve (Y/PM-20-042)," Apr. 2020, place: Virtual Meeting Type: Webinar. [Online]. Available: [https://gain.inl.gov/HALEU\\_Webinar\\_Presentations/23-24-Robinson-Jollay\\_Y-12\\_Brief-29Apr2020.pdf](https://gain.inl.gov/HALEU_Webinar_Presentations/23-24-Robinson-Jollay_Y-12_Brief-29Apr2020.pdf)
- [12] D. Vaden, "Isotopic Characterization of HALEU from EBR-II Driver Fuel Processing," Tech. Rep. INL/EXT-18-51906-Rev000, 1484450, Nov. 2018. [Online]. Available: <http://www.osti.gov/servlets/purl/1484450/>

- [13] T. Nelson and B. Eddy, "Foreign research reactor uranium supply program: The Y-12 national security complex process," Belgium, Tech. Rep. 978-92-95064-10-2, 2010.
- [14] S. Nagley, "HA-LEU Supply (Enrichment, De-conversion, Fuel Fab & Transportation)," Apr. 2020, place: GAIN/NEI/EPRI Webinar. [Online]. Available: [https://gain.inl.gov/HALEU\\_Webinar\\_Presentations/12-Nagley,BWXT-28Apr2020.pdf](https://gain.inl.gov/HALEU_Webinar_Presentations/12-Nagley,BWXT-28Apr2020.pdf)
- [15] E. Sunny, A. Worrall, J. Peterson, J. Powers, J. Gehin, and R. Gregg, "Transition Analysis of Promising U.S. Future Fuel Cycles Using ORION," in *Proceedings of Global 2015*, Paris, France, Sep. 2015, p. 10.
- [16] J. W. Bae, "Fuel cycle transition simulation capabilities in CYCLUS," Master's thesis, University of Illinois at Urbana-Champaign, Urbana, IL, Dec. 2018. [Online]. Available: <https://www.ideals.illinois.edu/handle/2142/102517>
- [17] S. J. Piet, B. W. Dixon, J. J. Jacobson, G. E. Matthern, and D. E. Shropshire, "Dynamic Simulations of Advanced Fuel Cycles," *Nuclear Technology*, vol. 173, no. 3, pp. 227–238, Mar. 2011. [Online]. Available: <http://epubs.ans.org/?a=11658>
- [18] A. M. Bachmann, R. Fairhurst-Agosta, Z. Richter, N. Ryan, and M. Munk, "Enrichment dynamics for advanced reactor HALEU support," *EPJ Nuclear Sciences & Technologies*, vol. 7, p. 22, 2021. [Online]. Available: <https://www.epj-n.org/articles/epjn/abs/2021/01/epjn210024/epjn210024.html>
- [19] D. Djokic, A. M. Scopatz, H. R. Greenberg, K. D. Huff, R. P. Nibbelink, and M. Fratoni, "The Application of CYCLUS to Fuel Cycle Transition Analysis," in *Proceedings of Global 2015*, ser. LLNL-CONF-669315, Paris, France, Sep. 2015. [Online]. Available: <https://www.osti.gov/biblio/1241931-application-cyclus-fuel-cycle-transition-analysis>
- [20] G. J. Chee, "Sensitivity Analysis of Nuclear Fuel Cycle Transitions," Master's thesis, University of Illinois at Urbana-Champaign, Urbana, IL, 2019. [Online]. Available: <https://www.ideals.illinois.edu/handle/2142/106272>
- [21] B. Feng, S. Richards, J. Bae, E. Davidson, A. Worrall, and R. Hays, "Sensitivity and Uncertainty Quantification of Transition Scenario Simulations," Argonne National Lab. (ANL), Argonne, IL (United States), Tech. Rep. ANL/NSE-20/38, Sep. 2020, published: = <https://www.osti.gov/biblio/1670703>.
- [22] N. Thiollière, J.-B. Clavel, F. Courtin, X. Doligez, M. Ernoult, Z. Issoufou, G. Krivtchik, B. Leniau, B. Mouginot, A. Bidaud, S. David, V. Lebrin, C. Perigois, Y. Richet, and A. Somaini, "A methodology for performing sensitivity analysis in dynamic fuel cycle simulation studies applied to a PWR fleet simulated with the CLASS tool," *EPJ Nuclear Sciences & Technologies*, vol. 4, p. 13, 2018. [Online]. Available: <https://www.epj-n.org/articles/epjn/abs/2018/01/epjn170042/epjn170042.html>
- [23] S. Passerini, "Sensitivity Analysis and Optimization of the Nuclear Fuel Cycle: A Systematic Approach," PhD Thesis, Jan. 2012. [Online]. Available: <https://ui.adsabs.harvard.edu/abs/2012PhDT.....216P>
- [24] P. O. Kim, K. J. Lee, and B. W. Lee, "Selection of an optimal nuclear fuel cycle scenario by goal programming and the analytic hierarchy process," *Annals of Nuclear Energy*, vol. 26, no. 5, pp. 449–460, Mar. 1999. [Online]. Available: <http://www.sciencedirect.com/science/article/pii/S0306454998000814>
- [25] E. Shwageraus, P. Hejzlar, and M. S. Kazimi, "Optimization of the LWR Nuclear Fuel Cycle for Minimum Waste Production," Massachusetts Institute of Technology. Center for Advanced Nuclear Energy Systems. Nuclear Fuel Cycle Program, Technical Report, Oct. 2003. [Online]. Available: <https://dspace.mit.edu/handle/1721.1/75166>
- [26] S. Passerini, M. S. Kazimi, and E. Shwageraus, "A Systematic Approach to Nuclear Fuel Cycle Analysis and Optimization," *Nuclear Science and Engineering*, vol. 178, no. 2, pp. 186–201, Oct. 2014. [Online]. Available: <https://doi.org/10.13182/NSE13-20>

- [27] K. D. Huff, M. J. Gidden, R. W. Carlsen, R. R. Flanagan, M. B. McGarry, A. C. Opotowsky, E. A. Schneider, A. M. Scopatz, and P. P. H. Wilson, "Fundamental concepts in the Cyclus nuclear fuel cycle simulation framework," *Advances in Engineering Software*, vol. 94, pp. 46–59, Apr. 2016. [Online]. Available: <http://www.sciencedirect.com/science/article/pii/S0965997816300229>
- [28] B. M. Adams, M. S. Eldred, G. Geraci, and W. J. Bohnhoff, "Dakota, A Multilevel Parallel Object-Oriented Framework for Design Optimization, Parameter Estimation, Uncertainty Quantification, and Sensitivity Analysis: Version 6.15 User's Manual," Nov. 2021.
- [29] P. K. Romano, N. E. Horelik, B. R. Herman, A. G. Nelson, B. Forget, and K. Smith, "OpenMC: A state-of-the-art Monte Carlo code for research and development," *Annals of Nuclear Energy*, vol. 82, no. Supplement C, pp. 90–97, Aug. 2015. [Online]. Available: <http://www.sciencedirect.com/science/article/pii/S030645491400379X>
- [30] N. Tsoulfanidis, *The Nuclear Fuel Cycle*. La Grange Park, Illinois, USA: American Nuclear Society, 2013.
- [31] U.S. Nuclear Regulatory Commission, "Stages of the Nuclear Fuel Cycle," Dec. 2020, publication Title: NRC Web Published: <https://www.nrc.gov/materials/fuel-cycle-fac/stages-fuel-cycle.html>.
- [32] L. Rodríguez-Penalonga and B. Y. Moratilla Soria, "A Review of the Nuclear Fuel Cycle Strategies and the Spent Nuclear Fuel Management Technologies," *Energies*, vol. 10, no. 8, p. 1235, Aug. 2017. [Online]. Available: <https://www.mdpi.com/1996-1073/10/8/1235>
- [33] R. Wigeland, T. Taiwo, H. Ludewig, M. Todosow, W. Halsey, J. Gehin, R. Jubin, J. Buelt, S. Stockinger, and K. Jenni, "Nuclear Fuel Cycle Evaluation and Screening – Final Report," Tech. Rep. INL/EXT-14-21465, Oct. 2014, publication Title: Final Report. [Online]. Available: <https://fuelcycleevaluation.inl.gov/SitePages/Home.aspx>
- [34] R. Wigeland, B. Dixon, and J. Gehin, "Identification, Description, and Characterization of Existing and Alternative Nuclear Energy Systems," Tech. Rep., May 2011.
- [35] *Status and Trends in Pyroprocessing of Spent Nuclear Fuels*, ser. TECDOC Series. Vienna: INTERNATIONAL ATOMIC ENERGY AGENCY, 2021, no. 1967. [Online]. Available: <https://www.iaea.org/publications/11062/status-and-trends-in-pyroprocessing-of-spent-nuclear-fuels>
- [36] S. Widder, "Benefits and concerns of a closed nuclear fuel cycle," *Journal of Renewable and Sustainable Energy*, vol. 2, no. 6, p. 062801, Nov. 2010. [Online]. Available: <https://aip.scitation.org/doi/abs/10.1063/1.3506839>
- [37] B. H. Park, F. Gao, E.-h. Kwon, and W. I. Ko, "Comparative study of different nuclear fuel cycle options: Quantitative analysis on material flow," *Energy Policy*, vol. 39, no. 11, pp. 6916–6924, Nov. 2011. [Online]. Available: <https://www.sciencedirect.com/science/article/pii/S0301421511002801>
- [38] U.S. Nuclear Regulatory Commission, "Louisiana Energy Services (LES)," Jan. 2022, publication Title: NRC Web. [Online]. Available: <https://www.nrc.gov/info-finder/fc/urencu-enrichment-fac-nm-lc.html>
- [39] ——, "Centrus Energy Corp. (formerly USEC Inc.) Gas Centrifuge Enrichment Facility Licensing," May 2021, publication Title: NRC Web.
- [40] S. Villani, *Uranium enrichment*, ser. Topics in applied physics; v. 35. Springer-Verlag, New York, NY, Jan. 1979. [Online]. Available: <https://www.osti.gov/biblio/5449407>
- [41] J. Whitaker, N. McGirl, D. Tucker, and A. Kapsimalis, "Uranium Enrichment Plant Characteristics - A Training Manual for the IAEA," Oak Ridge National Lab, Tech. Rep. ORNL/TM-2019/1311, 1606938, Oct. 2019. [Online]. Available: <https://www.osti.gov/servlets/purl/1606938/>
- [42] N. R. Brown, B. W. Carlsen, B. W. Dixon, B. Feng, H. R. Greenberg, R. D. Hays, S. Passerini, M. Todosow, and A. Worrall, "Identification of fuel cycle simulator functionalities for analysis of transition to a new fuel cycle," *Annals of Nuclear Energy*, vol. 96, pp. 88–95, Oct. 2016. [Online]. Available: <http://www.sciencedirect.com/science/article/pii/S0306454916303383>
- [43] K. Huff and B. Dixon, "Next Generation Fuel Cycle Simulator Functions and Requirements Document," Idaho National Laboratory, Tech. Rep. fcrd-sysa-2010-000110, Jul. 2010.

- [44] B. Feng, B. Dixon, E. Sunny, A. Cuadra, J. Jacobson, N. R. Brown, J. Powers, A. Worrall, S. Passerini, and R. Gregg, "Standardized verification of fuel cycle modeling," *Annals of Nuclear Energy*, vol. 94, pp. 300–312, Aug. 2016. [Online]. Available: <http://www.sciencedirect.com/science/article/pii/S0306454916301098>
- [45] A. Yacout, J. Jacobson, G. Matthern, S. Piet, D. Shropshire, and C. Laws, "VISION–Verifiable Fuel Cycle Simulation of Nuclear Fuel Cycle Dynamics," *Waste Management*, 2006.
- [46] R. Gregg and C. Grove, "Analysis of the UK Nuclear Fission Roadmap using the ORION fuel cycle modelling code," in *Proc of the IChemE nuclear fuel cycle conference, Manchester, United Kingdom*, Manchester, United Kingdom, 2012. [Online]. Available: <http://www.iceme.org/events/conferences/nuclear%20fuel%20cycle%20conference//media/2255BD59DEAC4D6D9C2C78032E995B5A.pdf>
- [47] C. Coquelet-Pascal, M. Tiphine, G. Krivtchik, D. Freynet, C. Cany, R. Eschbach, and C. Chabert, "COSI6: A Tool for Nuclear Transition Scenario Studies and Application to SFR Deployment Scenarios with Minor Actinide Transmutation," *Nuclear Technology*, vol. 192, no. 2, pp. 91–110, Nov. 2015. [Online]. Available: <https://www.tandfonline.com/doi/full/10.13182/NT15-20>
- [48] E. A. Schneider, C. G. Bathke, and M. R. James, "NFCsim: A Dynamic Fuel Burnup and Fuel Cycle Simulation Tool," *Nuclear Technology*, vol. 151, no. 1, pp. 35–50, Jul. 2005.
- [49] R. W. Carlsen, M. Gidden, K. Huff, A. C. Opotowsky, O. Rakimov, A. M. Scopatz, and P. Wilson, "Cycamore v1.0.0," *Figshare*, Jun. 2014. [Online]. Available: [http://figshare.com/articles/Cycamore\\_v1\\_0\\_0/1041829](http://figshare.com/articles/Cycamore_v1_0_0/1041829)
- [50] M. J. Gidden, "An Agent-Based Modeling Framework and Application for the Generic Nuclear Fuel Cycle," PhD Thesis, University of Wisconsin, Madison, WI, United States, Mar. 2015.
- [51] M. J. Gidden and P. P. H. Wilson, "A methodology for determining the dynamic exchange of resources in nuclear fuel cycle simulation," *Nuclear Engineering and Design*, vol. 310, pp. 378–394, Dec. 2016. [Online]. Available: <https://www.sciencedirect.com/science/article/pii/S0029549316304101>
- [52] A. M. Yacout, J. J. Jacobson, G. E. Matthern, S. J. Piet, D. E. Shropshire, and C. Laws, "VISION – Verifiable Fuel Cycle Simulation of Nuclear Fuel Cycle Dynamics," in *Waste Management Symposium*, 2006. [Online]. Available: <http://www.inl.gov/technicalpublications/Documents/3394908.pdf>
- [53] J. W. Bae, J. L. Peterson-Droogh, and K. D. Huff, "Standardized verification of the Cyclus fuel cycle simulator," *Annals of Nuclear Energy*, vol. 128, pp. 288–291, Jun. 2019. [Online]. Available: <http://www.sciencedirect.com/science/article/pii/S0306454919300179>
- [54] S. Richards and B. Feng, "Application of sensitivity analysis in DYMOND/Dakota to fuel cycle transition scenarios," *EPJ Nuclear Sciences & Technologies*, vol. 7, p. 26, 2021, published: = <https://www.epjn.org/articles/epjn/abs/2021/01/epjn210022/epjn210022.html>.
- [55] S. E. Skutnik, N. C. Sly, and J. L. Littell, "CyBORG: An ORIGEN-Based Reactor Analysis Capability for Cyclus," in *Transactions of the American Nuclear Society*, ser. Fuel Cycle and Waste Management: General—II, vol. 115. Las Vegas, Nevada, United States: American Nuclear Society, Nov. 2016, pp. 299–301.
- [56] E. Schneider and A. Scopatz, "An Integrated Fuel Depletion Calculator for Fuel Cycle Options Analysis," battelle Energy Alliance, LLC, Tech. Rep. 12-4065, 1258475, Apr. 2016. [Online]. Available: <http://www.osti.gov/servlets/purl/1258475/>
- [57] J. W. Bae, A. Rykhlevskii, G. Chee, and K. D. Huff, "Deep learning approach to nuclear fuel transmutation in a fuel cycle simulator," *Annals of Nuclear Energy*, vol. 139, p. 107230, May 2020. [Online]. Available: <http://www.sciencedirect.com/science/article/pii/S0306454919307406>
- [58] B. Leniau, B. Mouginot, N. Thiolliere, X. Doligez, A. Bidaud, F. Courtin, M. Ernoult, and S. David, "A neural network approach for burn-up calculation and its application to the dynamic fuel cycle code CLASS," *Annals of Nuclear Energy*, vol. 81, pp. 125–133, Jul. 2015. [Online]. Available: <https://www.sciencedirect.com/science/article/pii/S0306454915001693>

- [59] J. Peterson, R. Lefebvre, H. Smith, D. Ilas, K. Robb, T. Michener, H. Adkins, and J. Scaglione, "Used Nuclear Fuel Storage Transportation & Disposal Analysis Resource and Data System (UNF-ST&DARDS)," FCRD-NFST-2013-000117 Rev. 0, US Department of Energy Nuclear Fuels Storage and Transportation Planning Project, Tech. Rep., 2013.
- [60] A. M. Yacout, R. N. Hill, and J. S. Herring, "Dynamic Analysis of the AFCI Scenarios," in *PHYSOR 2004 -The Physics of Fuel Cycles and Advanced Nuclear Systems: Global Developments*. Chicago, IL: American Nuclear Society, Apr. 2004, p. 10.
- [61] S. J. Piet and N. R. Soelberg, "Assessment of Tools and Data for System-Level Dynamic Analyses," Idaho National Lab. (INL), Idaho Falls, ID (United States), Tech. Rep. INL/EXT-11-22588, Jun. 2011, published: <https://www.osti.gov/biblio/1031709>.
- [62] G. D. Del Cul, B. Spencer, R. Hunt, R. Jubin, and E. Collins, "Advanced head-end for the treatment of used LWR fuel," in *Actinide and Fission Product Partitioning and Transmutation: Eleventh Information Exchange Meeting*, ser. NEA. San Francisco, CA: OECD, Nov. 2010, no. 6996, pp. 265–268. [Online]. Available: [https://www.oecd-ilibrary.org/nuclear-energy/actinide-and-fission-product-partitioning-and-transmutation\\_9789264991743-en](https://www.oecd-ilibrary.org/nuclear-energy/actinide-and-fission-product-partitioning-and-transmutation_9789264991743-en)
- [63] J. L. Littell, "Development and Application of Nuclear Fuel Cycle Simulators for Evaluating Potential Fuel Cycle Options," Master's thesis, University of Tennessee - Knoxville, Knoxville, TN, May 2016. [Online]. Available: [http://trace.tennessee.edu/utk\\_gradthes/3783/](http://trace.tennessee.edu/utk_gradthes/3783/)
- [64] "The Effects of the Uncertainty of Input Parameters on Nuclear Fuel Cycle Scenario Studies," OECD, Nuclear Energy Agency, Tech. Rep. NEA/NSC/R(2016)4, Mar. 2017. [Online]. Available: <https://www.oecd-nea.org/science/docs/2016/nsr-r2016-4.pdf>
- [65] P. L. Kunsch and J. Teghem, "Nuclear fuel cycle optimization using multi-objective stochastic linear programming," *European Journal of Operational Research*, vol. 31, no. 2, pp. 240–249, Aug. 1987. [Online]. Available: <https://www.sciencedirect.com/science/article/pii/0377221787900282>
- [66] A. Skulborstad and S. Nelson, "Multi-Objective Optimization for Coupled Mechanics-Dynamics Analyses of Composite Structures," in *American Society for Composites 2018*. DEStech Publications, Inc., Nov. 2018. [Online]. Available: <http://www.dpi-proceedings.com/index.php/asc33/article/view/26122>
- [67] G. Chiandussi, M. Codegone, S. Ferrero, and E. E. Varesio, "Comparison of multi-objective optimization methodologies for engineering applications," *Computers & Mathematics with Applications*, vol. 63, no. 5, pp. 912–942, Mar. 2012. [Online]. Available: <https://www.sciencedirect.com/science/article/pii/S0898122111010406>
- [68] "10 CFR 50.68 Criticality accident requirements." Nov. 2006. [Online]. Available: <https://www.nrc.gov/reading-rm/doc-collections/cfr/part050/part050-0068.html>
- [69] Nuclear Energy Institute, "Establishing a HALEU Infrastructure for Advanced Reactors," Nuclear Energy Institute, Tech. Rep., Jan. 2022. [Online]. Available: <https://www.nei.org/resources/reports-briefs/establishing-a-haleu-infrastructure-for-advanced-r>
- [70] J. W. Herczeg, "High-Assay Low Enriched Uranium (HALEU)," Mar. 2019. [Online]. Available: <https://www.energy.gov/sites/prod/files/2019/04/f61/HALEU%20Report%20to%20NEAC%20Committee%203-28-19%20FINAL%29.pdf>
- [71] B. Harlan, "X-energy Xe-100 Reactor initial NRC meeting," Sep. 2018, place: Rockville, MD. [Online]. Available: <https://www.nrc.gov/docs/ML1825/ML18253A109.pdf>
- [72] M. Mitchell, "USNC Micro Modular Reactor – Project and Fuel," Apr. 2020, place: Virtual Meeting Type: Webinar. [Online]. Available: [https://gain.inl.gov/HALEU\\_Webinar\\_Presentations/33-Mitchell\\_Ultrasafe\\_Rev02-29apr2020.pdf](https://gain.inl.gov/HALEU_Webinar_Presentations/33-Mitchell_Ultrasafe_Rev02-29apr2020.pdf)

- [73] P. A. Demkowicz, B. Liu, and J. D. Hunn, "Coated particle fuel: Historical perspectives and current progress," *Journal of Nuclear Materials*, vol. 515, pp. 434–450, Mar. 2019. [Online]. Available: <https://www.sciencedirect.com/science/article/pii/S0022311518310213>
- [74] S. Shiozawa, S. Fujikawa, T. Iyoku, K. Kunitomi, and Y. Tachibana, "Overview of HTTR design features," *Nuclear Engineering and Design*, vol. 233, no. 1, pp. 11–21, Oct. 2004. [Online]. Available: <https://www.sciencedirect.com/science/article/pii/S0029549304002341>
- [75] H. Gottaut and K. Krüger, "Results of experiments at the AVR reactor," *Nuclear Engineering and Design*, vol. 121, no. 2, pp. 143–153, Jul. 1990. [Online]. Available: <https://linkinghub.elsevier.com/retrieve/pii/002954939090099J>
- [76] L. L. Snead, F. Venneri, Y. Kim, K. A. Terrani, J. E. Tulenko, C. W. Forsberg, P. F. Peterson, and E. J. Lahoda, "Fully Ceramic Microencapsulated Fuels: A Transformational Technology for Present and Next Generation Reactors," in *Transactions of the American Nuclear Society*, vol. 104, 2011, pp. 668–674.
- [77] F. Venneri, Y. Kim, L. L. Snead, K. A. Terrani, A. Ougouag, J. E. Tulenko, C. W. Forsberg, P. F. Peterson, and E. J. Lahoda, "Fully Ceramic Microencapsulated Fuels: A Transformational Technology for Present and Next Generation Reactors - Preliminary analysis of FCM fuel reactor operation," in *Transactions of the American Nuclear Soceity Annual Meeting*, vol. 104, Hollywood, FL, Jun. 2011, pp. 671–674. [Online]. Available: [https://epubs.ans.org/?a=12071&\\_ga=2.107688578.1679227796.1646919142-287406757.1598467895](https://epubs.ans.org/?a=12071&_ga=2.107688578.1679227796.1646919142-287406757.1598467895)
- [78] X-energy, "TRISO-X Submits First Ever High-Assay Low-Enriched Uranium Fuel Fabrication Facility License Application to the Nuclear Regulatory Commission," Apr. 2022. [Online]. Available: <https://x-energy.com/media/news-releases/triso-x-submits-first-ever-high-assay-low-enriched-uranium-fuel-fabrication-facility-license-application-to-the-nuclear-regulatory-commission>
- [79] D. C. Crawford, C. E. Baily, C. R. Clark, R. S. Fielding, and S. C. Marschman, "Fuel Fabrication Facility Study for FCF HALEU," Idaho National Lab. (INL), Idaho Falls, ID (United States), Tech. Rep. INL/EXT-19-52614-Rev000, Mar. 2019. [Online]. Available: <https://www.osti.gov/biblio/1504421>
- [80] M. Korsnick, "Need for High-Assay Low Enriched Uranium," Jul. 2018. [Online]. Available: <https://www.nei.org/resources/letters-filings-comments/nei-letter-perry-need-haleu>
- [81] ——, "Updated Need for High-Assay Low Enriched Uranium," Jul. 2020. [Online]. Available: <https://www.nei.org/resources/letters-filings-comments/updated-need-for-haleu>
- [82] ——, "Updated Need for High-Assay Low Enriched Uranium," Dec. 2021. [Online]. Available: [https://www.nei.org/CorporateSite/media/filefolder/resources/letters-filings-comments/NEI-Letter-for-Secretary-Granholm\\_HALEU-2021.pdf](https://www.nei.org/CorporateSite/media/filefolder/resources/letters-filings-comments/NEI-Letter-for-Secretary-Granholm_HALEU-2021.pdf)
- [83] J. R. Burns, R. Hernandez, K. A. Terrani, A. T. Nelson, and N. R. Brown, "Reactor and fuel cycle performance of light water reactor fuel with 235U enrichments above 5%," *Annals of Nuclear Energy*, vol. 142, p. 107423, Jul. 2020. [Online]. Available: <https://www.sciencedirect.com/science/article/pii/S0306454920301213>
- [84] L. Carlson, J. Miller, and Z. Wu, "Implications of HALEU fuel on the design of SMRs and micro-reactors," *Nuclear Engineering and Design*, vol. 389, p. 111648, Apr. 2022. [Online]. Available: <https://www.sciencedirect.com/science/article/pii/S0029549322000024>
- [85] L. Carlson, Z. Wu, J. Olson, and L. E. Liu, "An Economic Cost Assessment on HALEU Fuels for Small Modular Reactors," *Science and Technology of Nuclear Installations*, vol. 2020, p. e8815715, Dec. 2020. [Online]. Available: <https://www.hindawi.com/journals/stni/2020/8815715/>
- [86] V. Mascolino, L. M. Jamison, W. Cowherd, K. E. Anderson, J. A. Stillman, L.-W. Hu, and E. H. Wilson, "Impact of LEU U-10Mo Fuel Impurities on the Massachusetts Institute of Technology Reactor's Neutronics Performance," in *Transactions of the American Nuclear Soceity Annual Meeting*, vol. 126, Anaheim, CA, United States, Jun. 2022.

- [87] O. S. Celikten and D. Sahin, "The Effects of Impurities in Down-Blending Highly Enriched Uranium on the Reactor Neutronics and Cycle Length," in *Transactions of the American Nuclear Society Winter Meeting*, vol. 125, Washington D.C., Dec. 2021, pp. 165–167. [Online]. Available: [https://epubs.ans.org/?a=50496&\\_ga=2.168282849.1300862486.1643044250-1896939585.1615568796](https://epubs.ans.org/?a=50496&_ga=2.168282849.1300862486.1643044250-1896939585.1615568796)
- [88] M. Nichol, "Current Status of Advanced Nuclear Reactors," Aug. 2021. [Online]. Available: [https://files.nc.gov/ncdeq/energy-policy-council/August\\_18\\_2021\\_EPC\\_Meeting.pdf](https://files.nc.gov/ncdeq/energy-policy-council/August_18_2021_EPC_Meeting.pdf)
- [89] "Power Reactor Information System (PRIS): Reference and On-line Access Manual," INTERNATIONAL ATOMIC ENERGY AGENCY, Vienna, Technical Report, 1989. [Online]. Available: <https://www.iaea.org/publications/762/power-reactor-information-system-pris-reference-and-on-line-access-manual>
- [90] N. E. Todreas, *Nuclear systems*, 2nd ed. Boca Raton, FL: Taylor & Francis, 2012.
- [91] D. G. Cacuci, Ed., *Handbook of nuclear engineering*. New York: Springer, 2010, vol. 4: Reactors of Generations III and IV.
- [92] "USNC Micro Modular Reactor (MMR Block 1) Technical Information," 2021. [Online]. Available: [https://usnc.com/assets/media-kit/\[022989\]\[01\]%20MMR%20Technical%20Information%20Document.pdf?v=30823a846f](https://usnc.com/assets/media-kit/[022989][01]%20MMR%20Technical%20Information%20Document.pdf?v=30823a846f)
- [93] E. J. Mulder, "Overview of X-Energy's 200 MWth Xe-100 Reactor," Jan. 2021. [Online]. Available: <https://www.nationalacademies.org/documents/embed/link/LF2255DA3DD1C41C0A42D3BEF0989ACAECE3053A6A9B/file/DCB77DCC95AEF75D0CA6FE9C717CAA34436F7817D15A>
- [94] NuScale, "Chapter One Introduction and General Description of the Plant," Jul. 2020. [Online]. Available: <https://www.nrc.gov/reactors/new-reactors/design-cert/nuscale.html>
- [95] J. Reyes, "NuScale Power - A Scalable Clean Energy Solution," Jan. 2021.
- [96] J. N. Reyes, "Correction of Factual Error in PNAS Paper titled "Nuclear waste from small modular reactors"," May 2022. [Online]. Available: <https://newsroom.nuscalepower.com/news/>
- [97] World Nuclear News, "NuScale SMR plants become VOYGR : New Nuclear - World Nuclear News," Dec. 2021, publication Title: World Nuclear News. [Online]. Available: <https://www.world-nuclear-news.org/Articles/NuScale-SMR-plants-become-VOYGR>
- [98] NuScale, "NuScale Small Modular Reactor," 2022. [Online]. Available: [https://s24.q4cdn.com/104943030/files/doc\\_downloads/factsheet/nuscale-smr-fact-sheet.pdf](https://s24.q4cdn.com/104943030/files/doc_downloads/factsheet/nuscale-smr-fact-sheet.pdf)
- [99] U.S. Energy Information Administration, "Electric Power Monthly," Tech. Rep., May 2022. [Online]. Available: <https://www.eia.gov/electricity/monthly/>
- [100] ——, "Annual Energy Outlook 2022 - U.S. Energy Information Administration (EIA)," Mar. 2022, publication Title: U.S. Energy Information Administration. [Online]. Available: <https://www.eia.gov/outlooks/aoe/narrative/electricity/sub-topic-01.php>
- [101] J. Jacobson, A. Yacout, G. Matthern, S. Piet, D. Shropshire, R. Jeffers, and T. Schweitzer, "Verifiable fuel cycle simulation model (VISION): a tool for analyzing nuclear fuel cycle futures," *Nuclear Technology*, vol. 172, no. 2, pp. 157–178, Nov. 2010.
- [102] J. Leppanen, M. Pusa, T. Viitanen, V. Valtavirta, and T. Kaltiaisenaho, "The Serpent Monte Carlo code: Status, development and applications in 2013," *Annals of Nuclear Energy*, vol. 82, pp. 142–150, Aug. 2014.
- [103] S. T. Arm, G. B. Hall, G. J. Lumetta, and B. E. Wells, "Plan for Developing TRISO Fuel Processing Technologies," Pacific Northwest National Laboratory (PNNL), Richland, WA (United States), Tech. Rep. PNNL-32969, Jun. 2022. [Online]. Available: <https://www.osti.gov/biblio/1874375>

- [104] K. Kiegiel, I. Herdzik-Koniecko, L. Fuks, and G. Zakrzewska-Kołtuniewicz, “Management of Radioactive Waste from HTGR Reactors including Spent TRISO Fuel—State of the Art,” *Energies*, vol. 15, no. 3, p. 1099, Jan. 2022. [Online]. Available: <https://www.mdpi.com/1996-1073/15/3/1099>
- [105] P. K. Romano, “Depletion capabilities in the OpenMC Monte Carlo particle transport code,” *Annals of Nuclear Energy*, p. 15, 2021.
- [106] R. S. Herbst, P. Baron, and M. Nilsson, “6 - Standard and advanced separation: PUREX processes for nuclear fuel reprocessing,” in *Advanced Separation Techniques for Nuclear Fuel Reprocessing and Radioactive Waste Treatment*, ser. Woodhead Publishing Series in Energy, K. L. Nash and G. J. Lumetta, Eds. Woodhead Publishing, Jan. 2011, pp. 141–175. [Online]. Available: <https://www.sciencedirect.com/science/article/pii/B9781845695019500062>
- [107] A. R. Baker and R. W. Ross, “Comparison of the value of plutonium and uranium isotopes in fast reactors,” in *PROCEEDINGS OF THE CONFERENCE ON BREEDING, ECONOMICS AND SAFETY IN LARGE FAST POWER REACTORS*, Argonne National Laboratory, Oct. 1963.
- [108] B. S. Triplett, E. P. Loewen, and B. J. Dooies, “PRISM: A Competitive Small Modular Sodium-Cooled Reactor,” *Nuclear Technology*, vol. 178, no. 2, pp. 186–200, May 2012. [Online]. Available: <https://www.tandfonline.com/doi/full/10.13182/NT178-186>
- [109] C. Fichtlscherer, F. Friess, and M. Kütt, “Assessing the PRISM reactor as a disposition option for the British plutonium stockpile,” *Science & Global Security*, vol. 27, no. 2-3, pp. 124–149, Sep. 2019, publisher: Routledge \_eprint: <https://doi.org/10.1080/08929882.2019.1681736>. [Online]. Available: <https://doi.org/10.1080/08929882.2019.1681736>
- [110] T. Sumner, “Effects of fuel type on the safety characteristics of a sodium-cooled fast reactor,” Ph.D. dissertation, Georgia Institute of Technology, Jul. 2011. [Online]. Available: <https://linkinghub.elsevier.com/retrieve/pii/S0306454911001010>
- [111] A. M. Bachmann, O. Yardas, and M. Munk, “OpenMCyclus v0.1.0,” Sep. 2023. [Online]. Available: <https://zenodo.org/record/8349474>
- [112] “Modeling a Pin-Cell.” [Online]. Available: <https://nbviewer.org/github/openmc-dev/openmc-notebooks/blob/main/pincell.ipynb>
- [113] “Total Energy Monthly Data,” U.S. Energy Information Administration, Technical Report, Jun. 2022. [Online]. Available: <https://www.eia.gov/totalenergy/data/monthly/>
- [114] U.S. Energy Information Administration, “2020 Domestic Uranium Production Report,” U.S. Energy Information Administration, Tech. Rep., May 2021. [Online]. Available: <https://www.eia.gov//uranium-production/annual/index.php>
- [115] “Nuclear Waste Policy Act of 1982,” Jan. 1983. [Online]. Available: <http://www.congress.gov/>
- [116] G. Chee, G. Westphal, and K. Huff, “arfc/dcwrapper : Gwen’s MS Thesis Release,” 2019, published: <https://doi.org/10.5281/zenodo.3530964>.
- [117] “Higher Burnup,” Jul. 2023. [Online]. Available: <https://www.nrc.gov/reactors/power/atf/technologies/burnup.html>
- [118] A. M. Bachmann, S. Richards, M. Munk, and B. Feng, “Sensitivity analysis of fuel cycle transitions using Cyclus-Dakota,” in *Proceedings of the International High Level Radioactive Waste Management Conference*, Phoenix, AZ, Nov. 2022.
- [119] A. A. Andrianov, I. S. Kuptsov, T. A. Osipova, O. N. Andrianova, and T. V. Utyanskaya, “Optimization models of a two-component nuclear energy system with thermal and fast reactors in a closed nuclear fuel cycle,” *Nuclear Energy and Technology*, vol. 5(1), pp. 39–45, Mar. 2019. [Online]. Available: <https://nucet.pensoft.net/article/33981/>

- [120] G. J. Y. Chee, “Fluoride-Salt-Cooled High Temperature Reactor Design Optimization with Evolutionary Algorithms,” Dissertation, University of Illinois at Urbana-Champaign, Urbana, IL, Aug. 2022. [Online]. Available: <https://github.com/arfc/2022-chee-dissertation>
- [121] O. Kramer, “Genetic Algorithms,” in *Genetic Algorithm Essentials*, ser. Studies in Computational Intelligence, O. Kramer, Ed. Cham: Springer International Publishing, 2017, pp. 11–19. [Online]. Available: [https://doi.org/10.1007/978-3-319-52156-5\\_2](https://doi.org/10.1007/978-3-319-52156-5_2)
- [122] K. Deb, *Multi-objective optimization using evolutionary algorithms*. John Wiley & Sons, 2001, vol. 16.
- [123] “Dakota Reference Manual: moga,” Nov. 2021. [Online]. Available: <https://dakota.sandia.gov/sites/default/files/docs/6.15/html-ref/method-moga.html>
- [124] “Optimization with constraints · snl-dakota · Discussion #29,” Mar. 2023. [Online]. Available: <https://github.com/orgs/snl-dakota/discussions/29>
- [125] M. B. Chadwick, M. Herman, P. Obložinský, M. E. Dunn, Y. Danon, A. C. Kahler, D. L. Smith, B. Pritychenko, G. Arbanas, R. Arcilla, R. Brewer, D. A. Brown, R. Capote, A. D. Carlson, Y. S. Cho, H. Derrien, K. Guber, G. M. Hale, S. Hoblit, S. Holloway, T. D. Johnson, T. Kawano, B. C. Kiedrowski, H. Kim, S. Kunieda, N. M. Larson, L. Leal, J. P. Lestone, R. C. Little, E. A. McCutchan, R. E. MacFarlane, M. MacInnes, C. M. Mattoon, R. D. McKnight, S. F. Mughabghab, G. P. A. Nobre, G. Palmiotti, A. Palumbo, M. T. Pigni, V. G. Pronyaev, R. O. Sayer, A. A. Sonzogni, N. C. Summers, P. Talou, I. J. Thompson, A. Trkov, R. L. Vogt, S. C. van der Marck, A. Wallner, M. C. White, D. Wiarda, and P. G. Young, “ENDF/B-VII.1 Nuclear Data for Science and Technology: Cross Sections, Covariances, Fission Product Yields and Decay Data,” *Nuclear Data Sheets*, vol. 112, no. 12, pp. 2887–2996, Dec. 2011. [Online]. Available: <https://www.sciencedirect.com/science/article/pii/S009037521100113X>
- [126] NuScale, “Chapter Four Reactor,” Jul. 2020. [Online]. Available: <https://www.nrc.gov/reactors/new-reactors/design-cert/nuscale.html>
- [127] A. E. Johnson, D. Kotlyar, S. Terlizzi, and G. Ridley, “serpentTools: A Python Package for Expediting Analysis with Serpent,” *Nuclear Science and Engineering*, vol. 194, no. 11, pp. 1016–1024, Nov. 2020, publisher: Taylor & Francis \_eprint: <https://doi.org/10.1080/00295639.2020.1723992>. [Online]. Available: <https://doi.org/10.1080/00295639.2020.1723992>
- [128] Z. Richter, “Isotopic Fuel Compositions in the Sangamon200 Model,” Apr. 2022. [Online]. Available: <https://zenodo.org/record/6426312>
- [129] Z. Richter, R. Fairhurst, M. Türkmen, K. Huff, and S. Dotson, “ZoeRichter/phlox: Version 1.1,” Apr. 2022. [Online]. Available: <https://zenodo.org/record/6451576>
- [130] A. I. Hawari and F. Venneri, “Development and Deployment Assessment of a Melt-Down Proof Modular Micro Reactor (MDP-MMR),” North Carolina State University, Tech. Rep. 14–6782, 1431209, Apr. 2018. [Online]. Available: <http://www.osti.gov/servlets/purl/1431209/>
- [131] F. Venneri, “Micro Modular Reactor (MMR) Energy Systems,” Warsaw, Poland, Sep. 2019. [Online]. Available: [https://www.ifnec.org/ifnec/upload/docs/application/pdf/2019-09/3-4.\\_usnc\\_mmr.pdf](https://www.ifnec.org/ifnec/upload/docs/application/pdf/2019-09/3-4._usnc_mmr.pdf)
- [132] J. J. Powers, A. Worrall, K. A. Terrani, J. C. Gehin, and L. L. Snead, “FULLY CERAMIC MICROENCAPSULATED FUELS: CHARACTERISTICS AND POTENTIAL LWR APPLICATIONS,” Kyoto, Japan, 2014, p. 16.
- [133] Bachmann, “MMR-like Serpent Model,” Sep. 2023. [Online]. Available: <https://zenodo.org/record/8349385>
- [134] J. K. Fink, “Thermophysical properties of uranium dioxide,” *Journal of Nuclear Materials*, vol. 279, no. 1, pp. 1–18, Mar. 2000. [Online]. Available: <https://www.sciencedirect.com/science/article/pii/S0022311599002731>
- [135] D. M. McEligot, W. D. Swank, D. L. Cottle, and F. I. Valentin, “Thermal Properties of G-348 Graphite,” p. 23.
- [136] H. Petersen, “The Properties of Helium: Density, Specific Heats, Viscosity, and Thermal Conductivity at Pressures from 1 to 100 bar and from Room Temperature to about 1800 K,” p. 46.

- [137] "Standard Specification for Nuclear-Grade, Sinterable Uranium Dioxide Powder," Oct. 2021. [Online]. Available: <https://compass.astm.org/document/?contentCode=ASTM%7CC0753-16AR21%7Cen-US&proxycl=https%3A%2F%2Fsecure.astm.org&fromLogin=true>
- [138] E. J. Mulder and W. A. Boyes, "Neutronics characteristics of a 165 MWth Xe-100 reactor," *Nuclear Engineering and Design*, vol. 357, p. 110415, Feb. 2020. [Online]. Available: <https://www.sciencedirect.com/science/article/pii/S0029549319304467>
- [139] J. Leppanen, "Serpent – a Continuous-energy Monte Carlo Reactor Physics Burnup Calculation Code," *VTT Technical Research Centre of Finland, Espoo, Finland*, vol. 4, 2013.

# Appendix A: Synergistic sensitivity analysis

This appendix contains the plots with results for the synergistic sensitivity analysis of Scenario 7. Any plots shown in Section 6.3 are not duplicated here.

Figure A.1 shows the trends in each of the metrics as a result of varying the transition start time and the percent of LWRs operating for 80 years. The transition starts later and the percent of LWRs increases all of the metrics decrease, which is consistent with the results of the OAT analysis. Increasing the percent of LWRs has a greater effect than delaying the transition start time, which is consistent with the OAT analysis results. Additionally, these results show that the combined effect of varying these parameters together is minimal. This result is because increasing the number of LWRs that operate for 80 years inherently delays the transition start time because the LWRs continue to supply the power needed and advanced reactors are not needed until a later time. Therefore, these results suggest that extending LWR lifetimes is a more effective method than only delaying the transition start time to change the material requirements of this transition scenario.

Figure A.2 shows the results of varying the transition start time and Xe-100 build share on the HALEU mass, SWU to produce HALEU, waste mass discharged, and feed to produce HALEU. This figure shows that increasing the Xe-100 build share has a greater impact on the metrics than changing the transition start time, which is consistent with the OAT results. There is no clear combined effect from varying these parameters together.

Figure A.3 shows the results of varying the transition start time and the MMR build share on all six of the metrics. The HALEU-related metrics and the total SWU capacity show a much stronger effect from the MMR build share than the transition start time. The total fuel mass and UNF mass show an effect from varying both parameters, but they do not compound on each other (result in a non-linear trend in the metric).

Figure A.4 shows the effects of varying the transition start time and the VOYGR build share on all six of the metrics. Except for the total SWU capacity, the metrics exhibit more impact from the VOYGR build share than the transition start time. The total SWU capacity is impacted more by the transition start time than the VOYGR build share. This different trend is because the Xe-100 and VOYGR require similar SWU capacity, so this parameter has almost no impact on this metric.

Figure A.5 shows the effects of varying the transition start time and the Xe-100 discharge burnup on all six

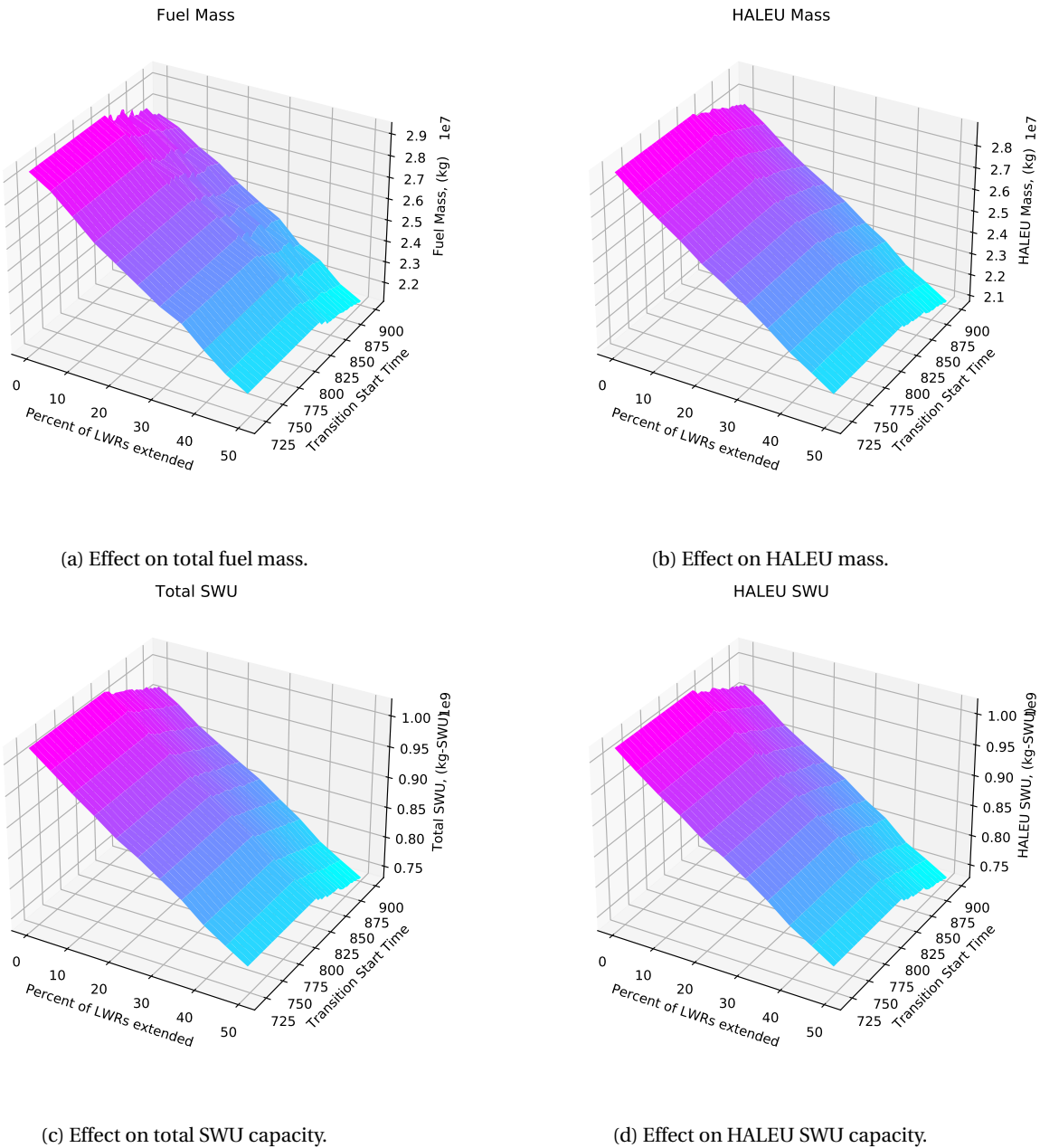


Figure A.1: Change in metrics resulting from variations in the transition start time and LWR lifetimes.

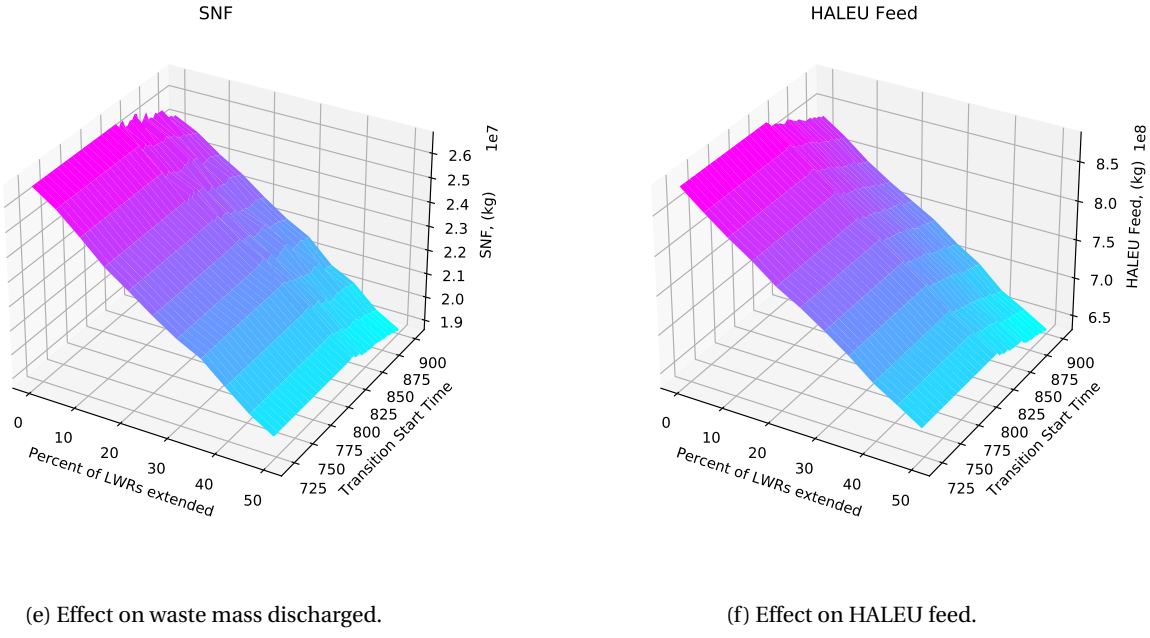


Figure A.1: (cont.) Change in metrics resulting from variations in the transition start time and LWR lifetimes.

metrics. These two parameters impact all six of the metrics in a similar manner: the metrics decrease as the Xe-100 burnup increases and are not greatly impacted by the transition start time. The Xe-100 burnup has a more pronounced effect on the metrics because Xe-100s comprise most of the advanced reactors.

Figure A.6 shows the effects of varying the transition start time and the MMR discharge burnup on all six metrics. All of the metrics exhibit the same trends as the parameters vary: the metrics decrease as the transition start time is later and as the MMR burnup increases. The two parameters have impacts on similar magnitudes, which is in contrast to the impact from the Xe-100 burnup. The MMR burnup has a smaller impact on the metrics because MMRs make up a smaller fraction of the advanced reactor fleet than Xe-100s.

Figure A.7 shows the effects of varying the percent of LWRs operating for 80 years and the Xe-100 build share on all six metrics. The trends observed in the OAT can also be observed here, such as how increasing the Xe-100 share increases the HALEU mass required but increasing the percent of LWRs decreases this metric. However, these results show that there is a combined effect from varying these parameters together that is not captured in the OAT analysis. For example, the HALEU mass (Figure A.7b) decreases by a greater fraction as the percent of LWRs and Xe-100 build shares increase than when only the percent of LWRs extended increases. This combined effect is a result of more of the advanced reactor fleet being fueled by HALEU-fueled reactors. However, these results also show that despite this combined effect, not deploying Xe-100s will still result in a minimum in the HALEU mass required. This trend is also observed in the other HALEU-related metrics (Figures A.7d, and A.7f).

The total fuel (Figure A.7a) and used fuel mass (Figure A.7e) both exhibit a different trend than the HALEU-

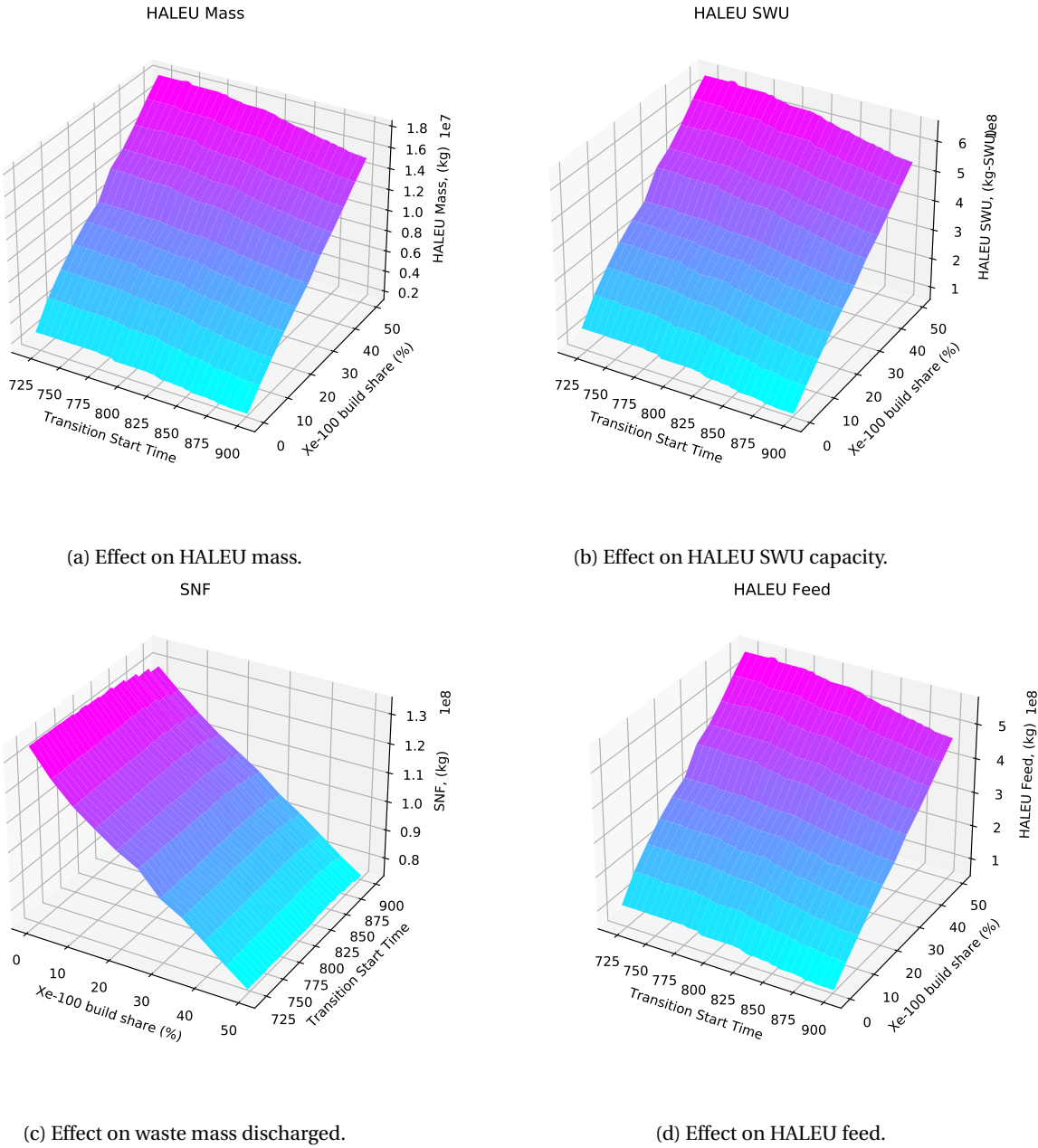


Figure A.2: Change in metrics resulting from variations in the transition start time and  $\chi_{\text{-}100}$  build share.

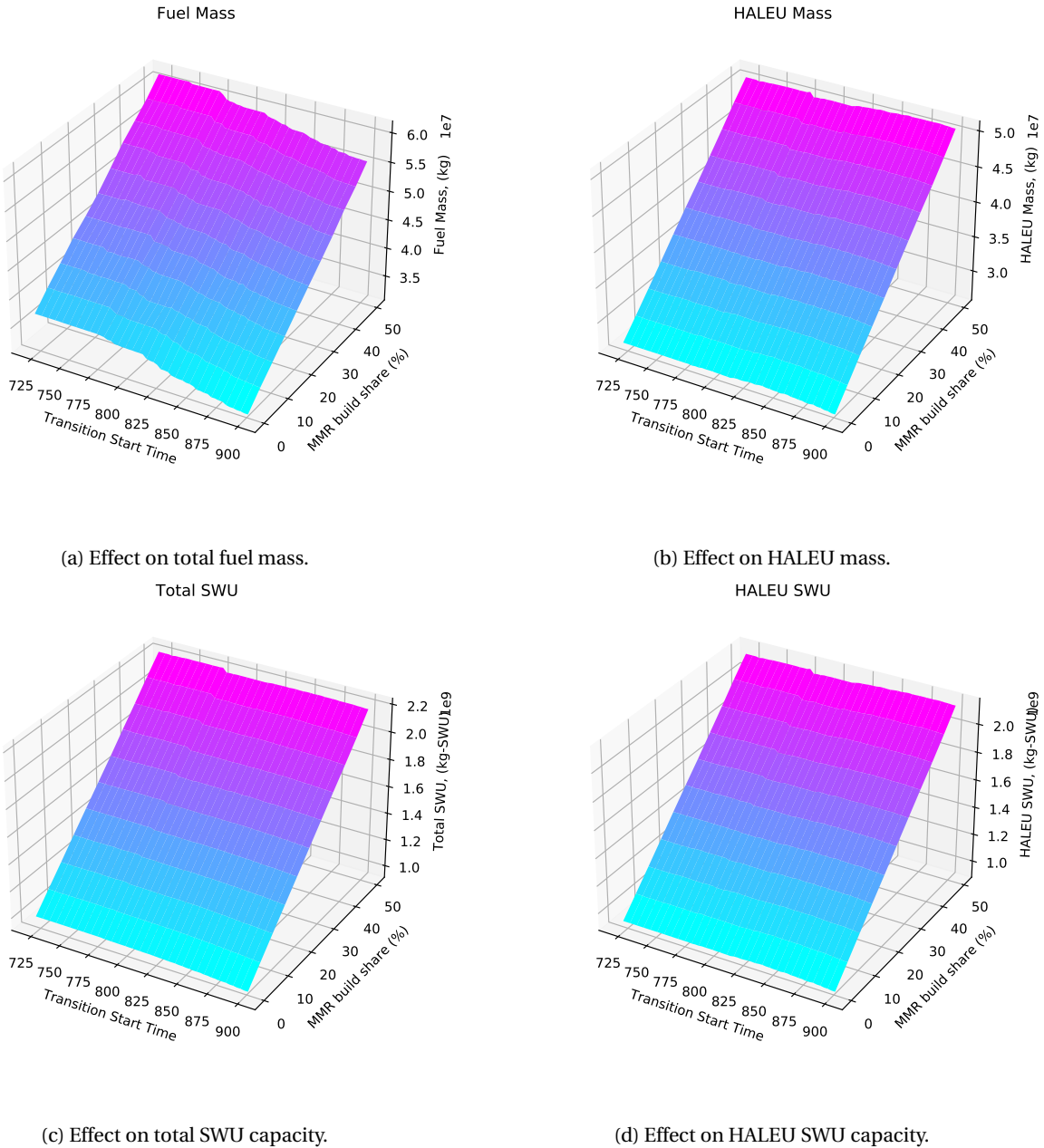
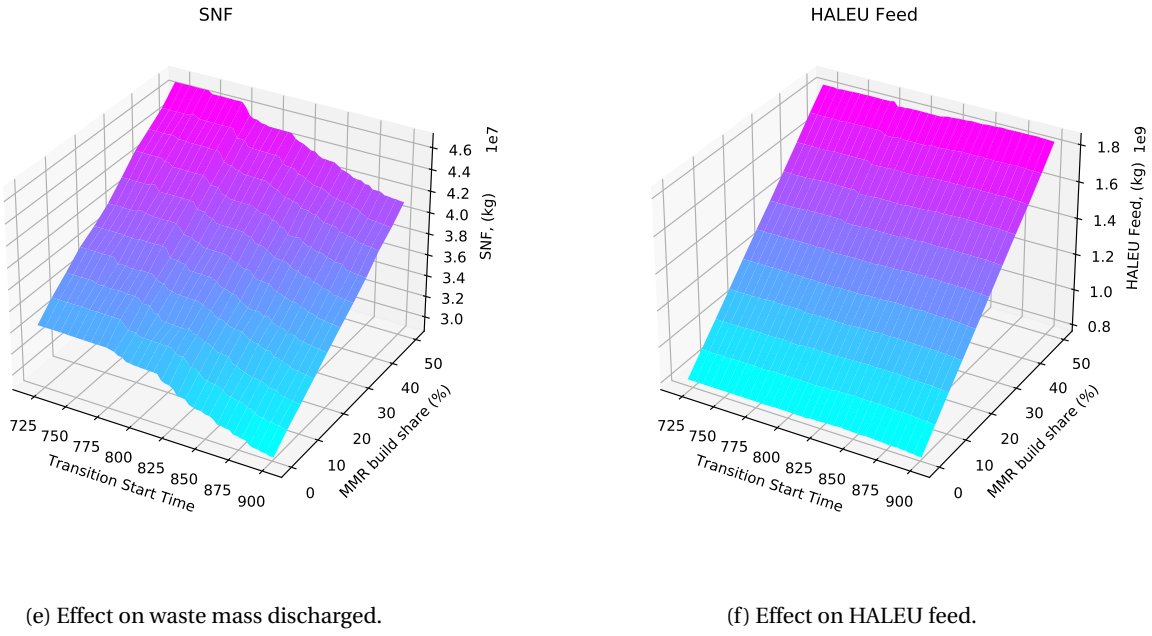


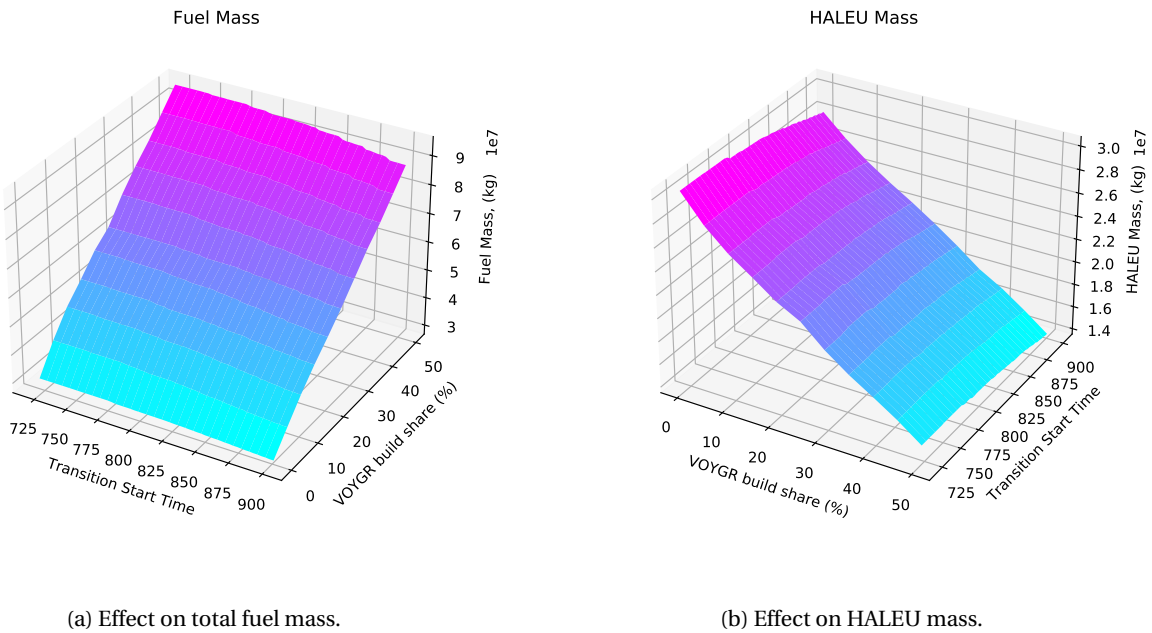
Figure A.3: Change in metrics resulting from variations in the transition start time and MMR build share.



(e) Effect on waste mass discharged.

(f) Effect on HALEU feed.

Figure A.3: (cont.) Change in metrics resulting from variations in the transition start time and MMR build share.



(a) Effect on total fuel mass.

(b) Effect on HALEU mass.

Figure A.4: Change in metrics resulting from variations in the transition start time and VOYGR build share.

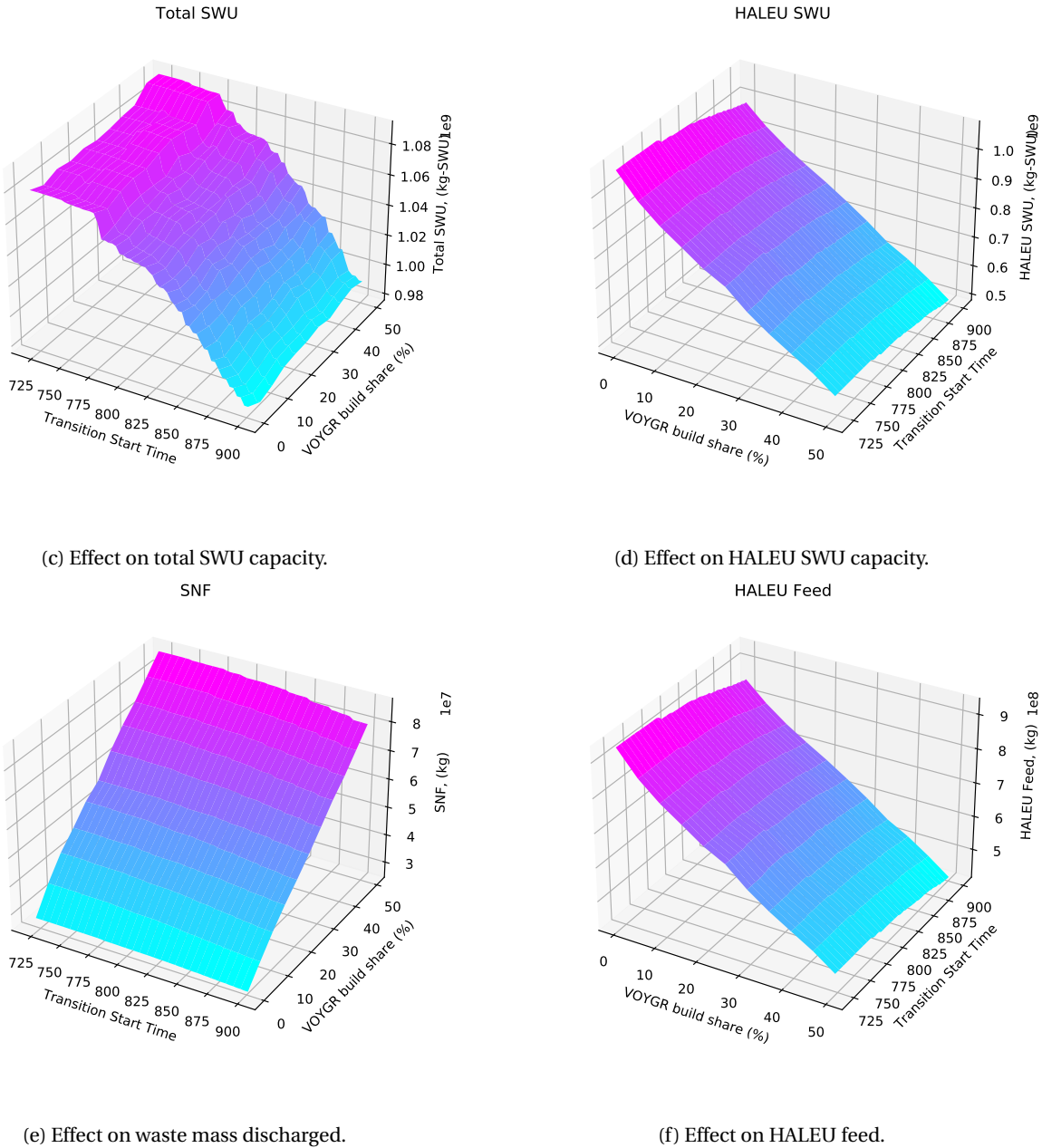


Figure A.4: (cont.) Change in metrics resulting from variations in the transition start time and VOYGR build share.

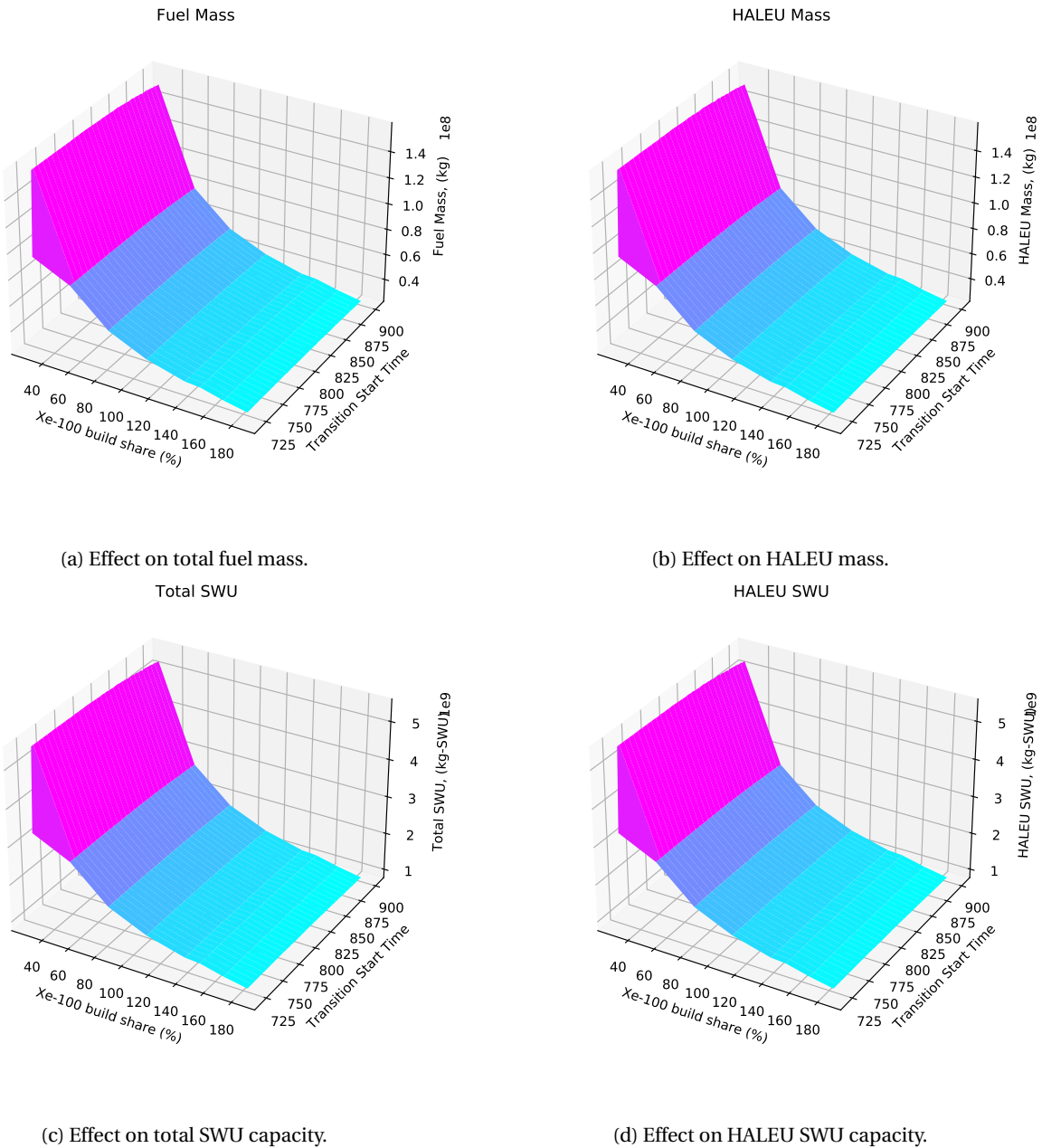
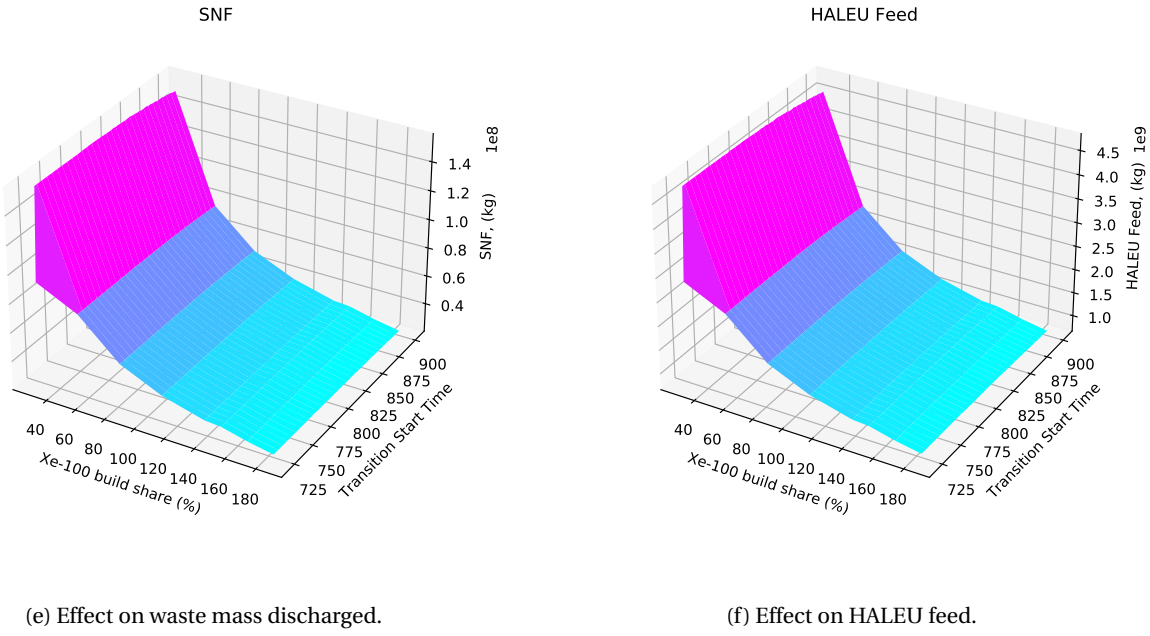


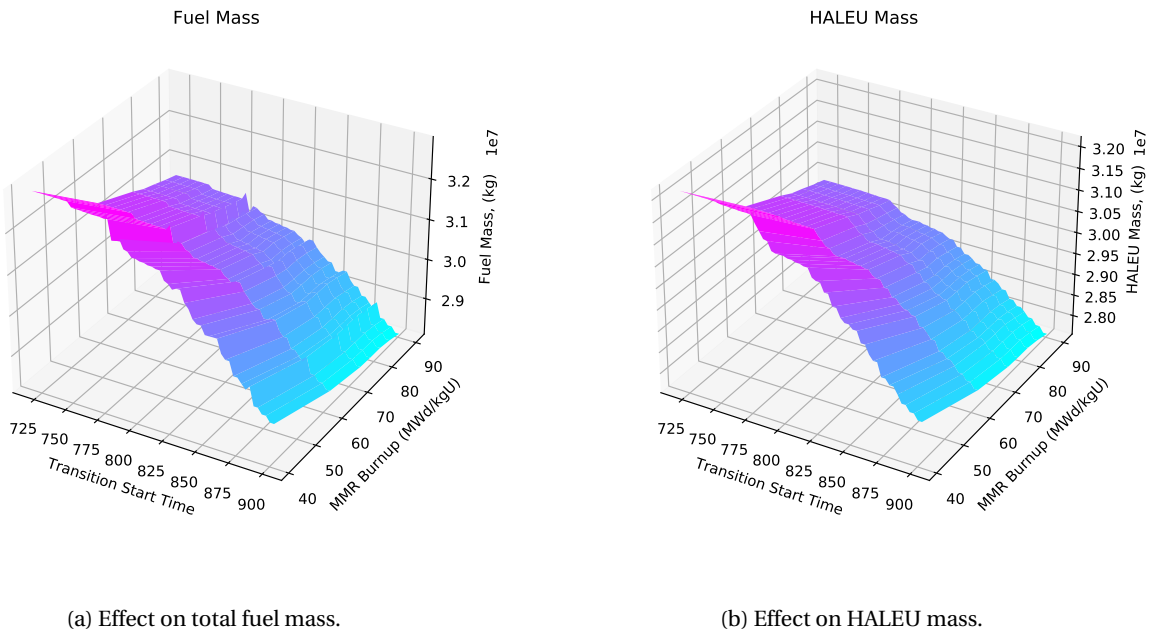
Figure A.5: Change in metrics resulting from variations in the transition start time and Xe-100 burnup.



(e) Effect on waste mass discharged.

(f) Effect on HALEU feed.

Figure A.5: (cont.) Change in metrics resulting from variations in the transition start time and Xe-100 burnup.



(a) Effect on total fuel mass.

(b) Effect on HALEU mass.

Figure A.6: Change in metrics resulting from variations in the transition start time and MMR burnup.

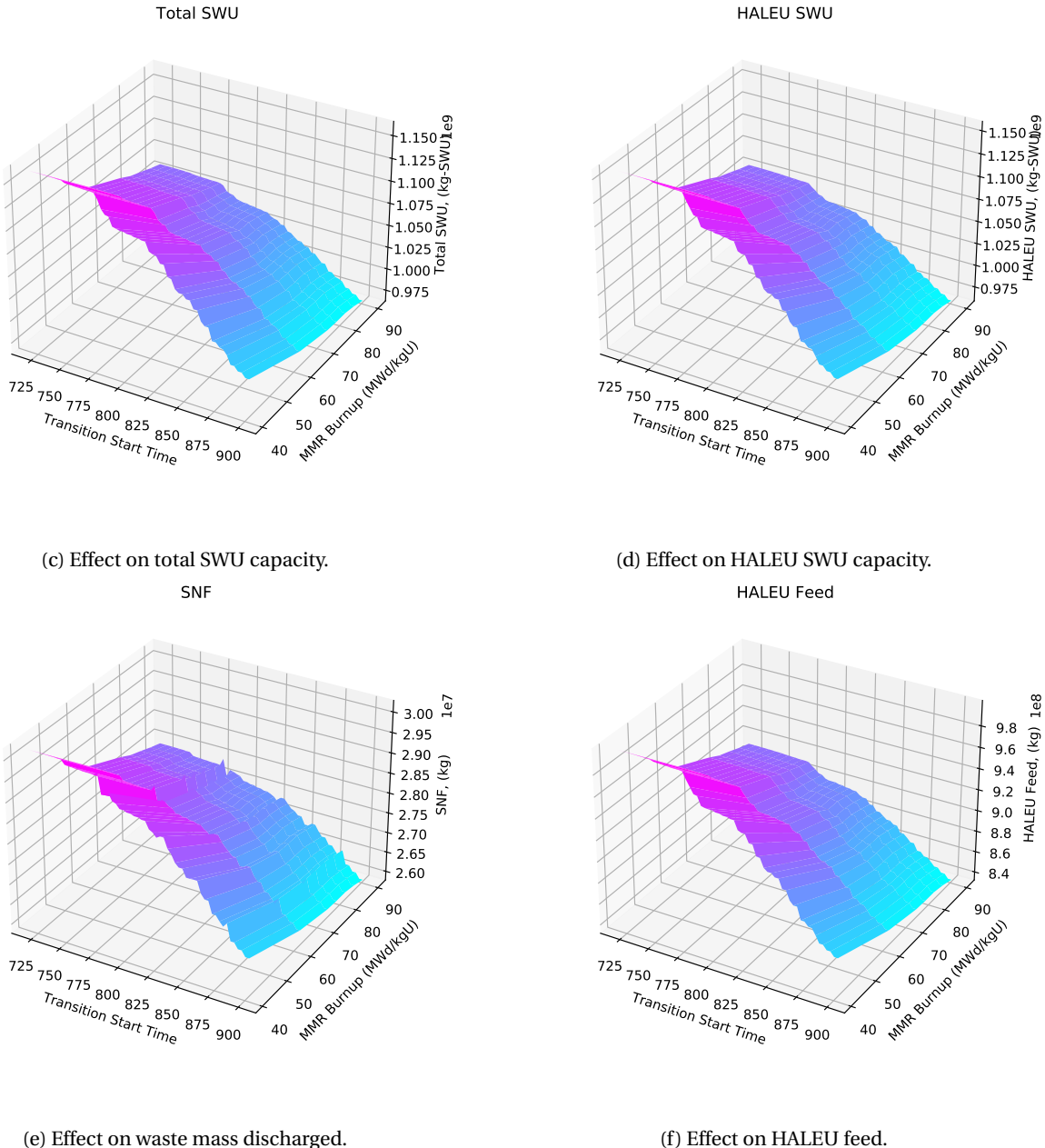


Figure A.6: (cont.) Change in metrics resulting from variations in the transition start time and MMR burnup.

related metrics. These two parameters have a similar effect on these metrics: as the parameter values increase, the metric value decreases. Therefore, by increasing both of these parameters, there is a larger effect on the total and used fuel masses than varying each on separately.

Figure A.8 shows the effects of varying the percent of LWRs operating for 80 years and the MMR build share on all of the metrics. The metrics have the same trends as the parameters are varied: they increase as the MMR build share increases and as the percent of LWRs extended decreases. Therefore, all six metrics reach a minimum with 50% of the LWRs operating for 80 years and a 0% MMR build share.

Figure A.9 shows the effects of varying the percent of LWRs operating for 80 years and the VOYGR build share on the total SWU capacity, HALEU SWU capacity, UNF mass, and feed mass to produce HALEU. The total SWU capacity, HALEU SWU, and feed mass exhibit the same trend of decreasing with increased LWR percent. The HALEU SWU and feed mass decrease with increase VOYGR build share, while the total SWU capacity is constant. The UNF mass also decreases with increasing LWR percent, but increases with the VOYGR build share.

Figure A.10 shows the effects of varying the LWR lifetime extension percent and the Xe-100 discharge burnup. All of the output metrics exhibit the same trends as these parameters are varied, which is consistent with these parameters having the same effect on the metrics in the OAT analysis. The metrics decrease with increasing Xe-100 discharge burnup and increasing number of LWRs that receive lifetime extensions. The effect of the LWR lifetime extensions diminishes as the Xe-100 burnup increases, indicating that the Xe-100 discharge burnup has a greater influence on the metrics of this transition. This result is consistent with most of the advanced reactors deployed in this work being Xe-100s and the global analysis performed, showing that the Xe-100 discharge burnup consistently had one of the highest Sobol' indices.

Figure A.11 shows the effects of varying the percent of LWR operating for 80 years and the MMR discharge burnup. Varying these parameters has the same effect on all of the metrics: increasing these parameters decreases the metrics. The LWR lifetime has a greater effect on the metrics than the MMR burnup because MMRs supply a small share of the energy demand, compared with the other advanced reactors.

Figure A.12 shows the effects from varying the MMR build share and the Xe-100 discharge burnup on the HALEU mass, total SWU capacity, HALEU SWU capacity, UNF mass discharged, and the feed mass to produce HALEU. The effects on each of these metrics are consistent with the effects on the total enriched uranium mass, presented in Section 6.3. Increasing both of the parameters has contradictory effects. Increasing the Xe-100 burnup decreases all of the metrics while increasing the MMR build share increases all of the metrics. As the MMR build share increases, the Xe-100 burnup has a smaller impact on the metrics because fewer of the advanced reactors deployed are Xe-100s.

Figure A.13 shows the effects of varying the MMR share and MMR burnup on all of the metrics. All of the metrics

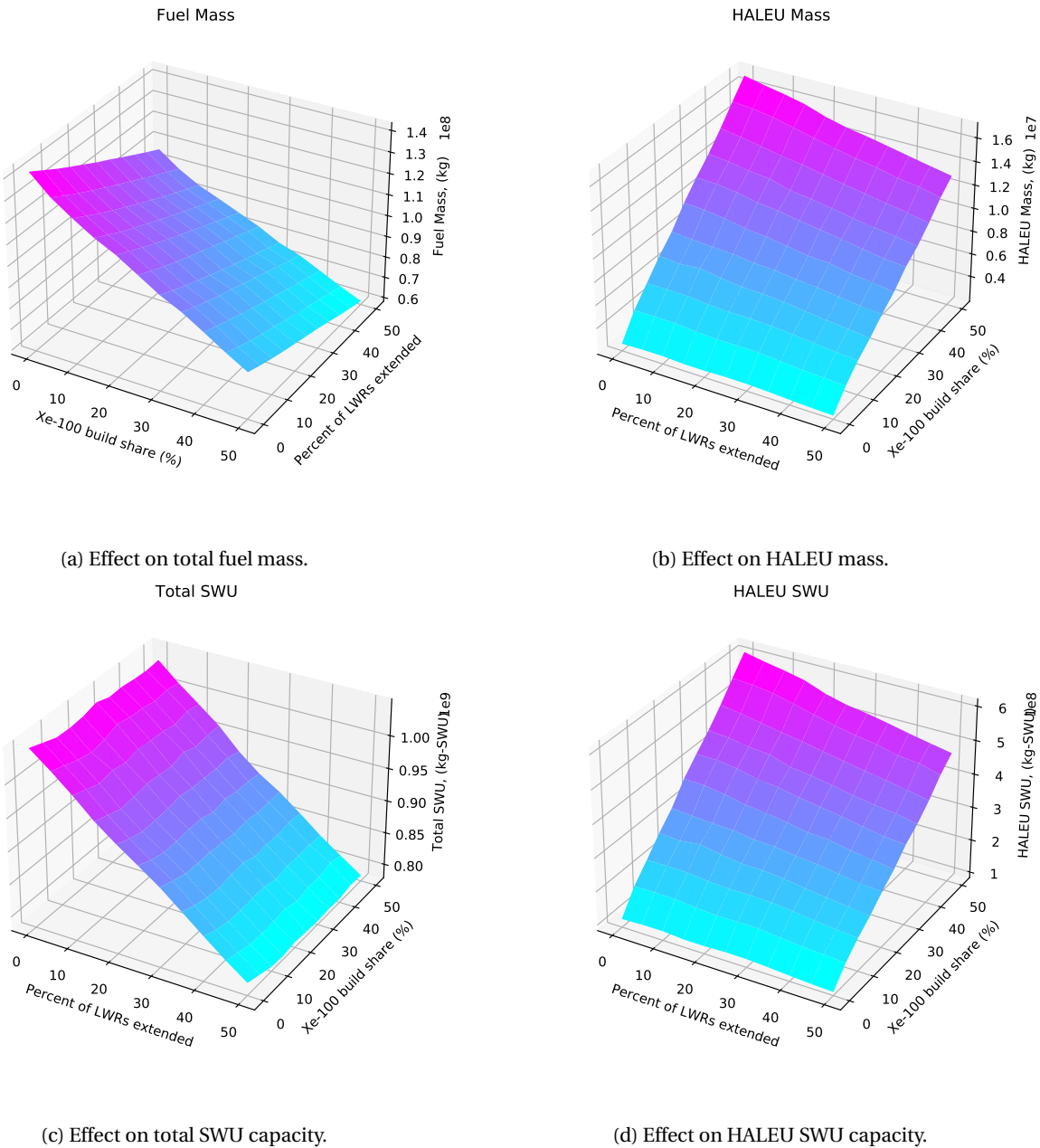


Figure A.7: Change in metrics resulting from variations in the LWR lifetimes and Xe-100 build share.

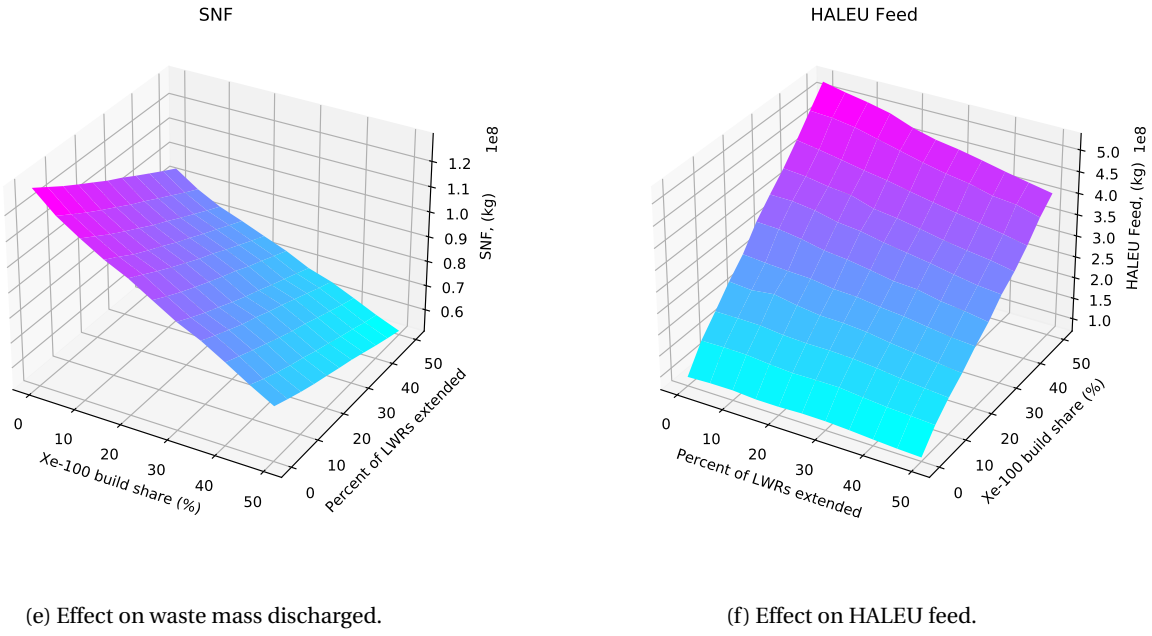


Figure A.7: (cont.) Change in metrics resulting from variations in the LWR lifetimes and Xe-100 build share.

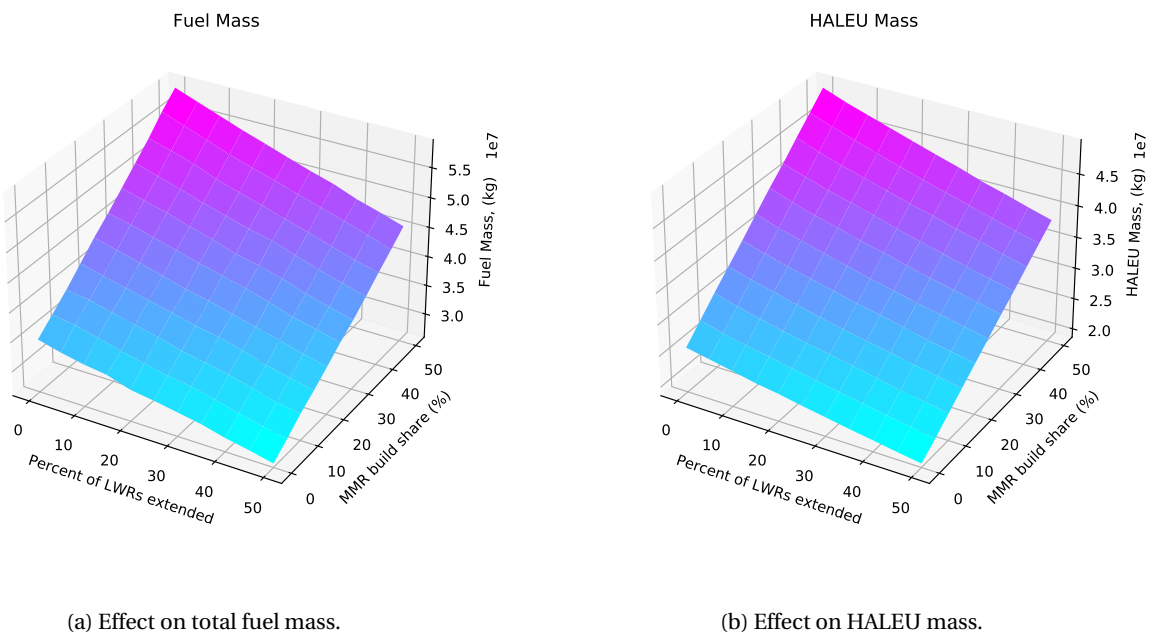


Figure A.8: Change in metrics resulting from variations in the LWR lifetimes and MMR build share.

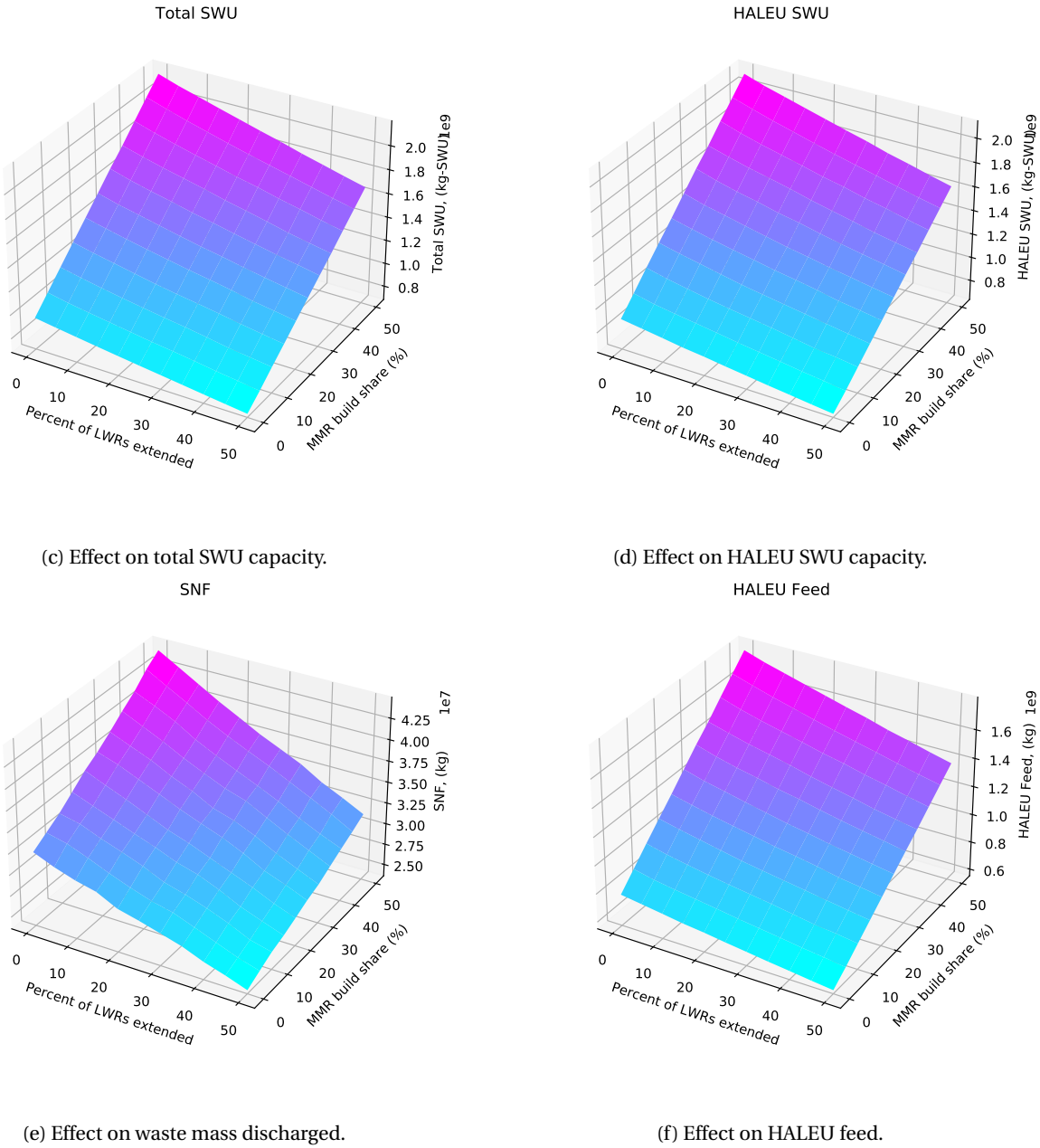


Figure A.8: (cont.) Change in metrics resulting from variations in the LWR lifetimes and MMR build share.

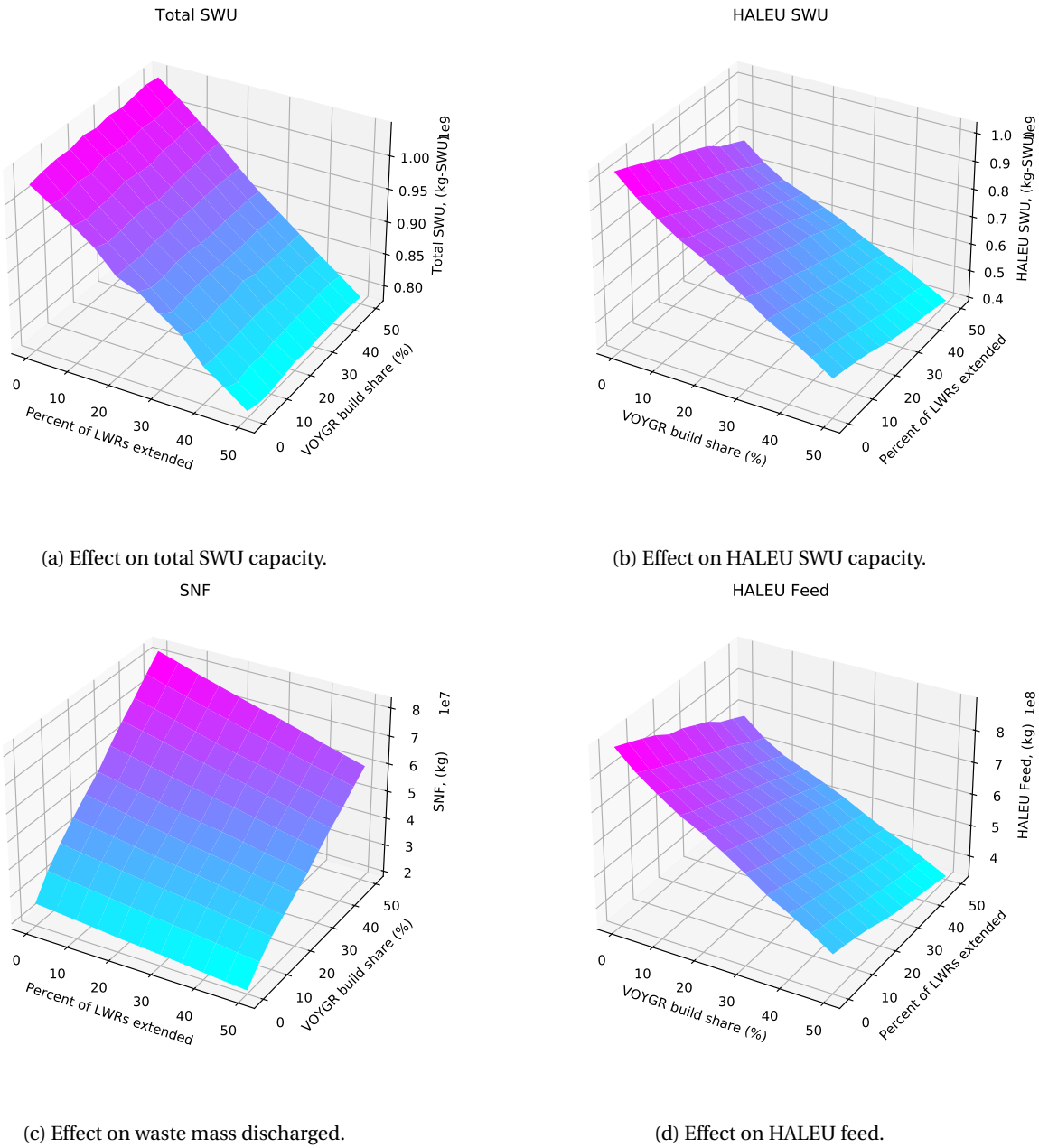


Figure A.9: Change in metrics resulting from variations in the LWR lifetimes and VOYGR build share.

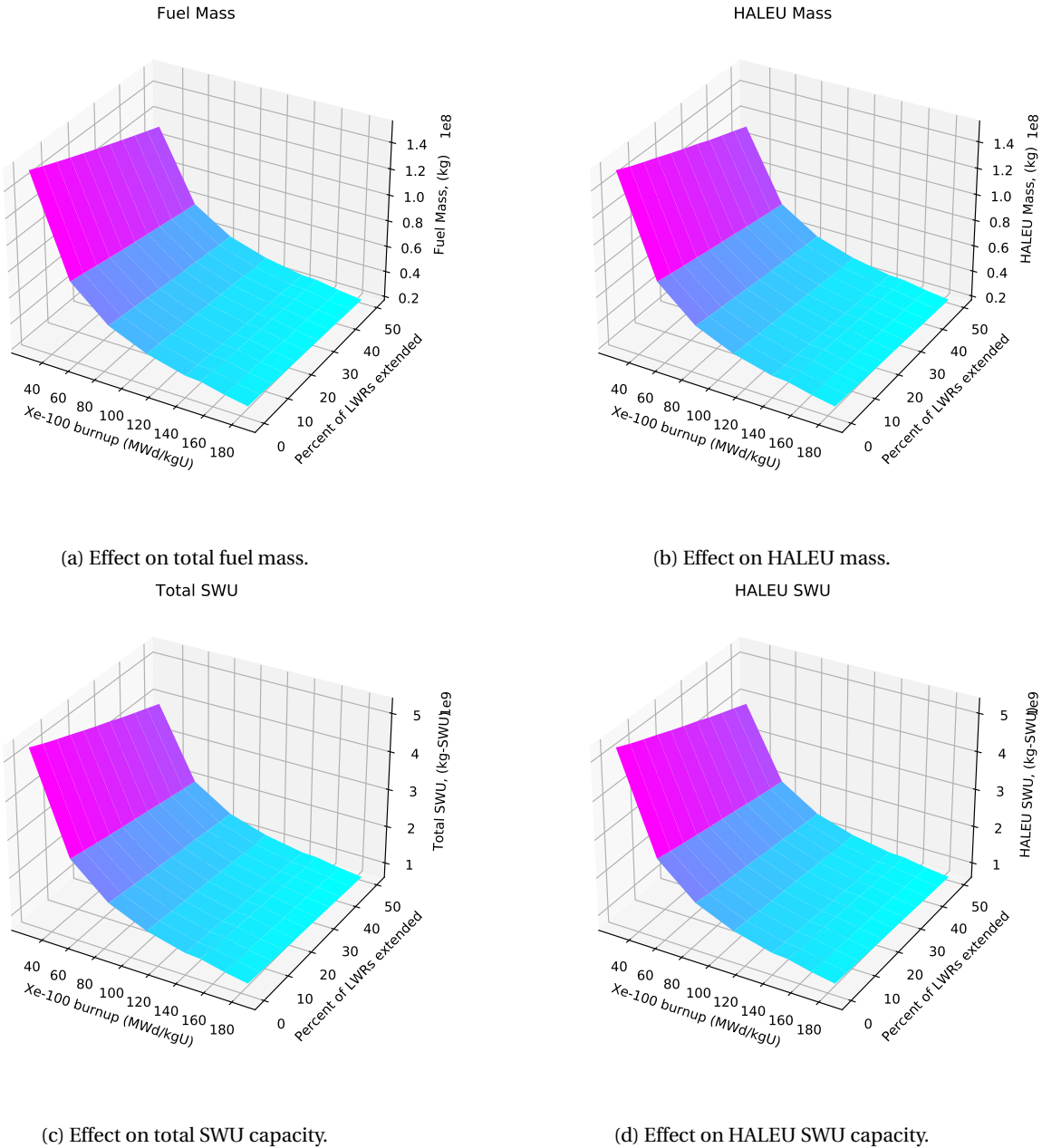
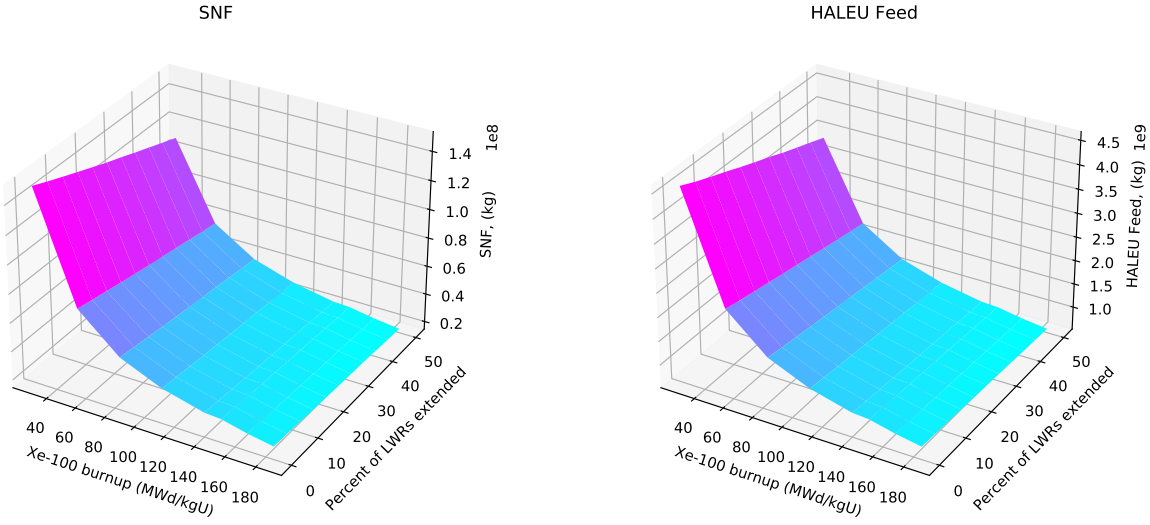


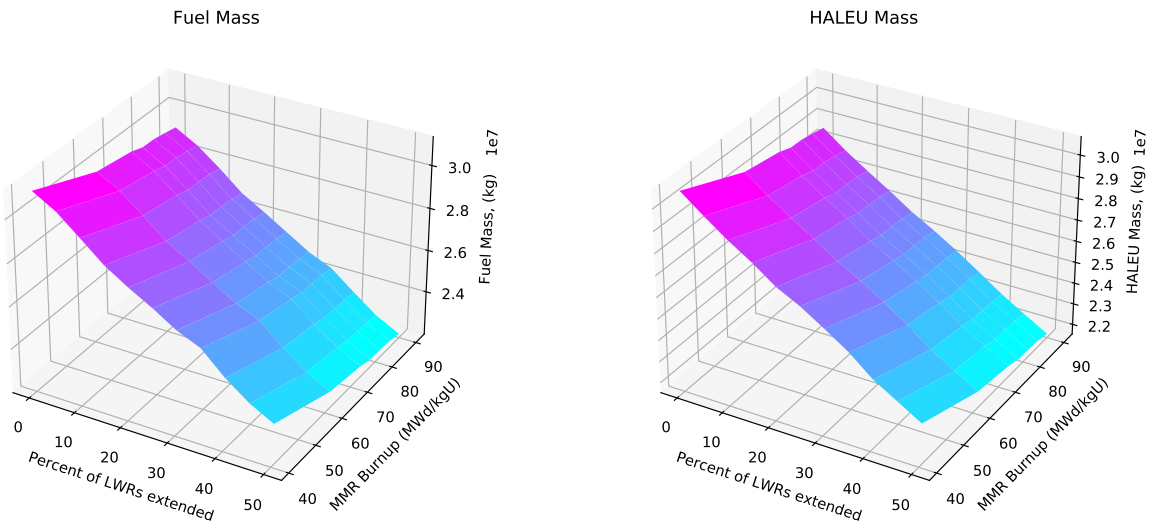
Figure A.10: Change in metrics resulting from variations in the LWR lifetimes and the Xe-100 discharge burnup



(e) Effect on waste mass discharged.

(f) Effect on HALEU feed.

Figure A.10: (cont.) Change in metrics resulting from variations in the LWR lifetimes and the Xe-100 discharge burnup



(a) Effect on total fuel mass.

(b) Effect on HALEU mass.

Figure A.11: Change in metrics resulting from variations in the LWR lifetimes and MMR discharge burnup.

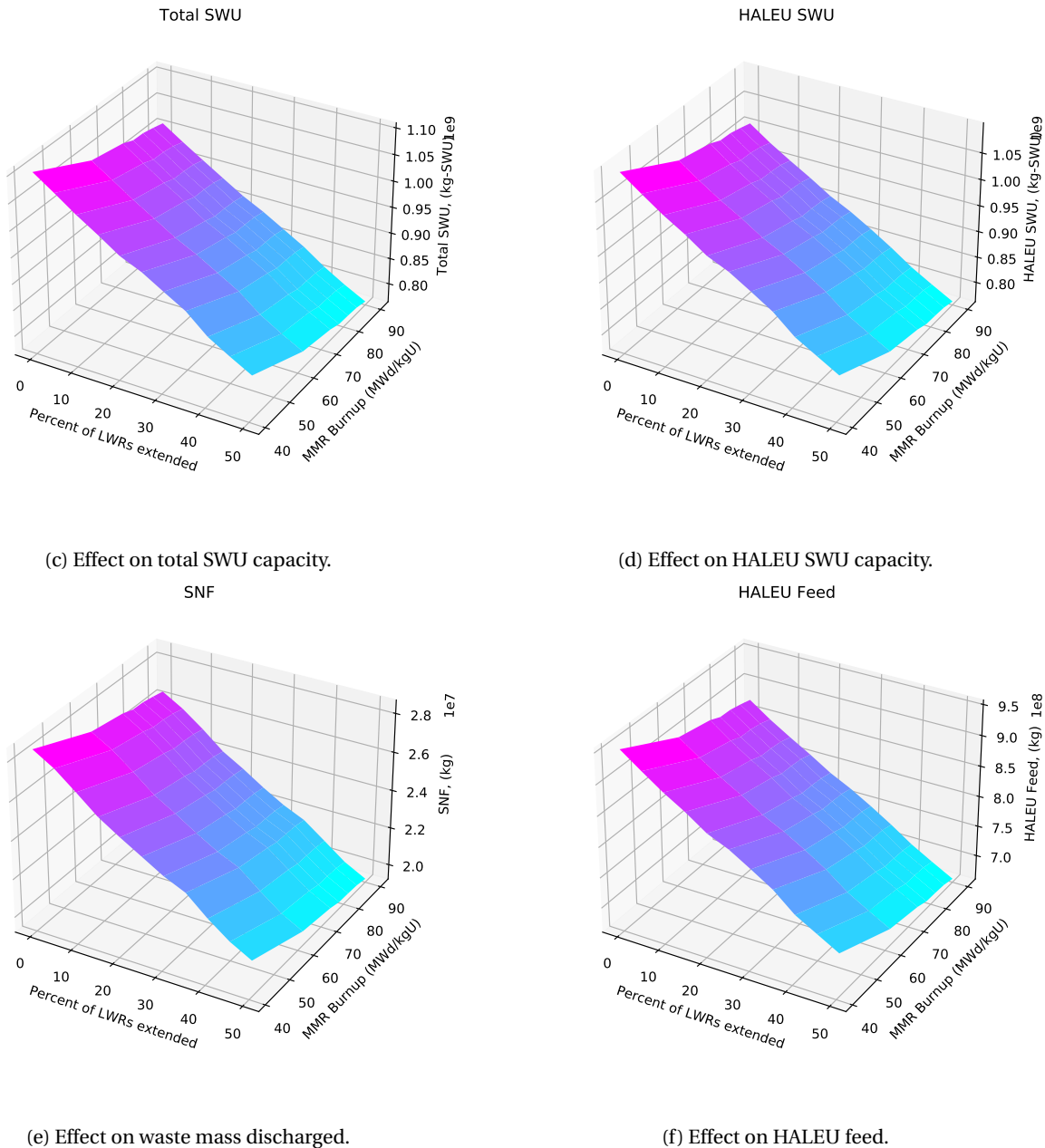


Figure A.11: (cont.) Change in metrics resulting from variations in the LWR lifetimes and MMR discharge burnup.

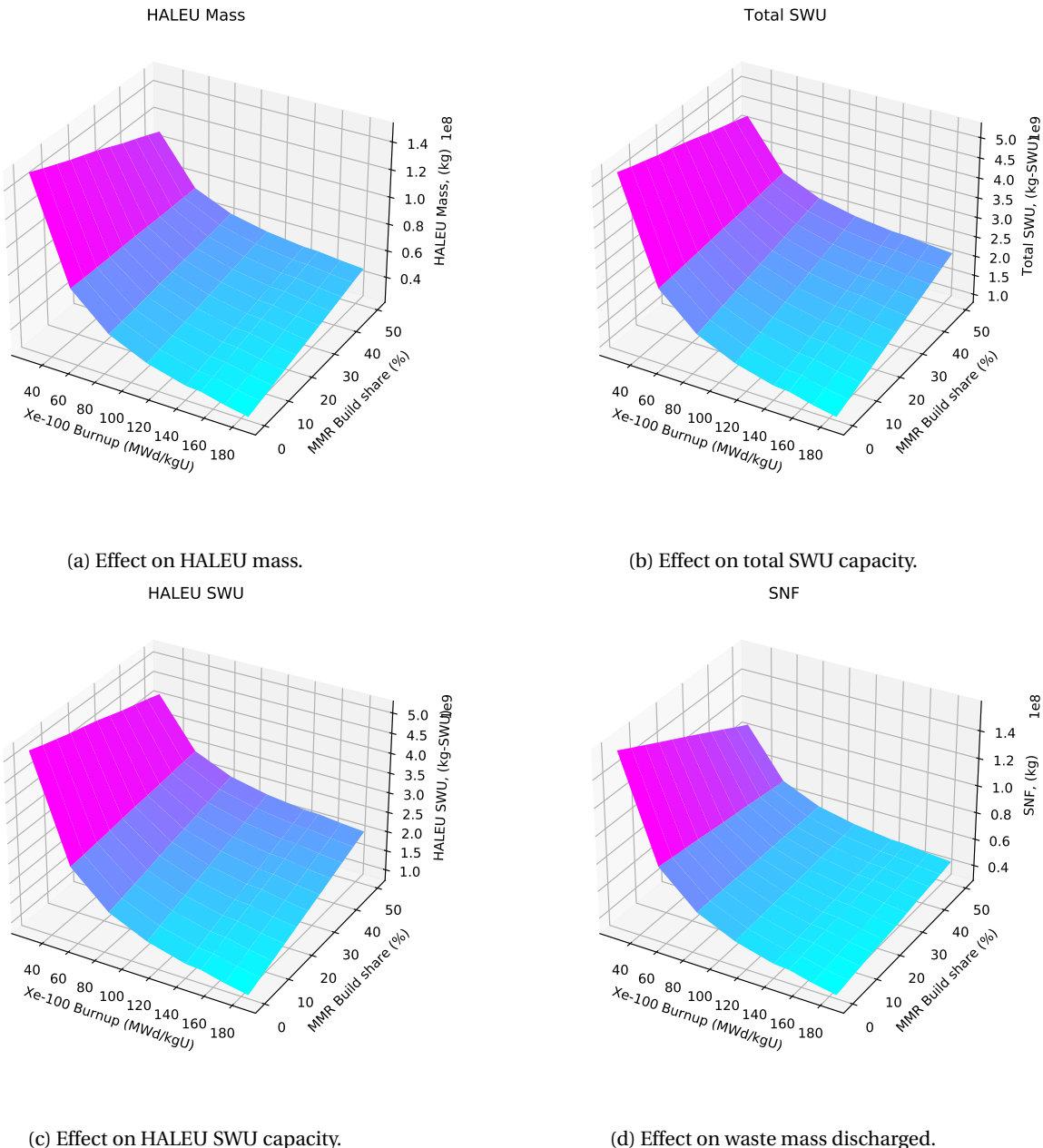
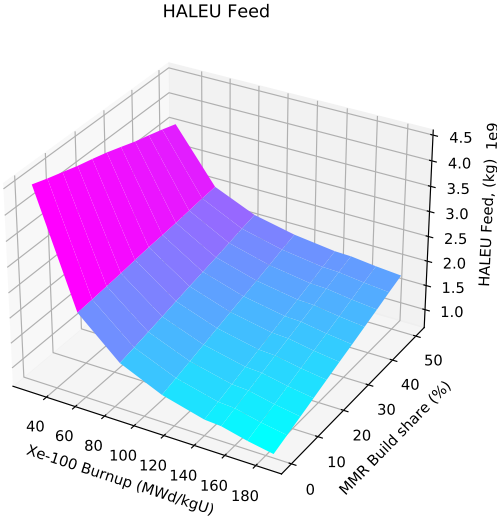


Figure A.12: Change in metrics resulting from variations in the MMR build share and Xe-100 discharge burnup.



(e) Effect on HALEU feed.

Figure A.12: (cont.) Change in metrics resulting from variations in the MMR build share and Xe-100 discharge burnup.

exhibit the same trends as each parameter is varied: the metrics decrease with increasing MMR burnup and increase with increasing MMR build share. These trends are a result of less fuel and materials produced by the MMR as the MMR burnup increases, but the MMR requiring more materials than Xe-100 to meet the same energy demand. These two parameters have a compounding effect, such that as the MMR build share increases the variations in the burnup have a greater impact on the metrics because MMRs comprise more of the advanced reactor fleet. All of the metrics are at a minimum when the MMR build share is 0%, independent of the MMR burnup. This result is because if there are no MMRs deployed in the transition, then the discharge burnup of the fuel that goes into these reactors has no effect on the transition.

Figure A.14 shows the effects of varying the Xe-100 build share and Xe-100 discharge burnup on total SWU capacity, HALEU SWU capacity, UNF mass discharged, and the feed mass to produce HALEU. The UNF exhibits a different trend than the other three metrics. As the Xe-100 build share and burnup increase the UNF mass decreases. The other metrics generally increase with increasing Xe-100 build share and decreasing burnup. As identified in the OAT analysis, the effects in the metrics from varying the Xe-100 build share is a result of design and material requirement differences between the Xe-100 and VOYGR. Therefore, the different trends in each of the metrics as the Xe-100 build share increases is a result of the difference in the two reactor designs. In each of the metrics, the impact of the Xe-100 burnup increases as the Xe-100 build share increases because Xe-100s comprise more of the advanced reactor fleet. Additionally, the metrics have a constant value as a function of Xe-100 burnup when the build share is 0% because none of the advanced reactors deployed are Xe-100s.

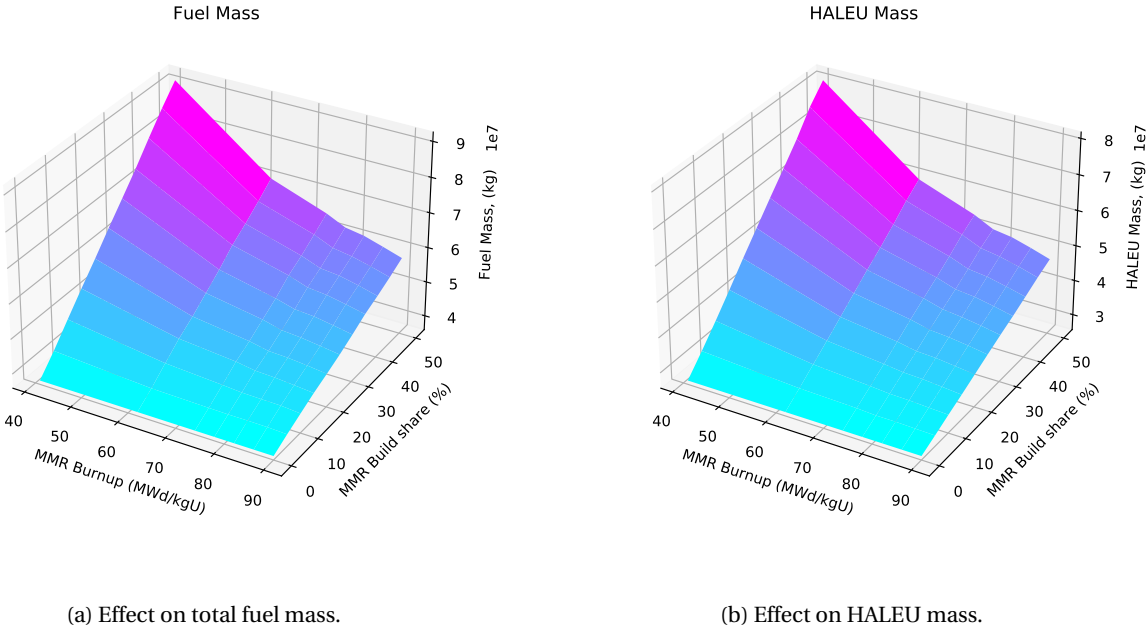


Figure A.13: Change in metrics resulting from variations in the MMR build share and MMR discharge burnup.

The OAT showed that as the Xe-100 build share increases, the total SWU capacity remained constant for a given burnup because of the trade-off in enrichment level and mass of fuel between the Xe-100 and VOYGR. The results of the synergistic analysis show that this metric only remains relatively constant for high burnup values. At low burnup values (below about 140 MWd/kgU), the Xe-100 requires more fuel mass than the VOYGR, which means that more SWU capacity is needed to fuel the reactors.

Figure A.15 shows the effects of varying the Xe-100 build share and the MMR burnup on each of the metrics. The total fuel mass and UNF mass decrease with increasing Xe-100 build share and are affected little by the MMR burnup. The HALEU mass, HALEU SWU, and feed mass to produce HALEU the Xe-100 build share increase with increasing Xe-100 build share and are affected little by the MMR burnup. The total SWU capacity decreases with increasing MMR burnup and is affected little by the Xe-100 build share. All of the metrics are only strongly influenced by one of the parameters varied, which indicates that these two parameters do not interact. Variations in the Xe-100 build share primarily impacts the number of Xe-100s and VOYGRs built, as shown in the OAT analysis. Because this parameter does not greatly affect the number of MMRs deployed, these two parameters do not have any combined effects on the metrics. The total SWU capacity is most affected by the MMR burnup because the Xe-100 build share primarily affects the deployment of Xe-100s and VOYGRs, and these two reactors require similar SWU capacity. Therefore, the changes in fuel requirements and SWU capacity from varying the MMR burnup is greater than the change in the change in SWU capacity from varying the Xe-100 build share.

Figure A.17 shows the results of varying the VOYGR build share and the Xe-100 burnup on all of the metrics. All

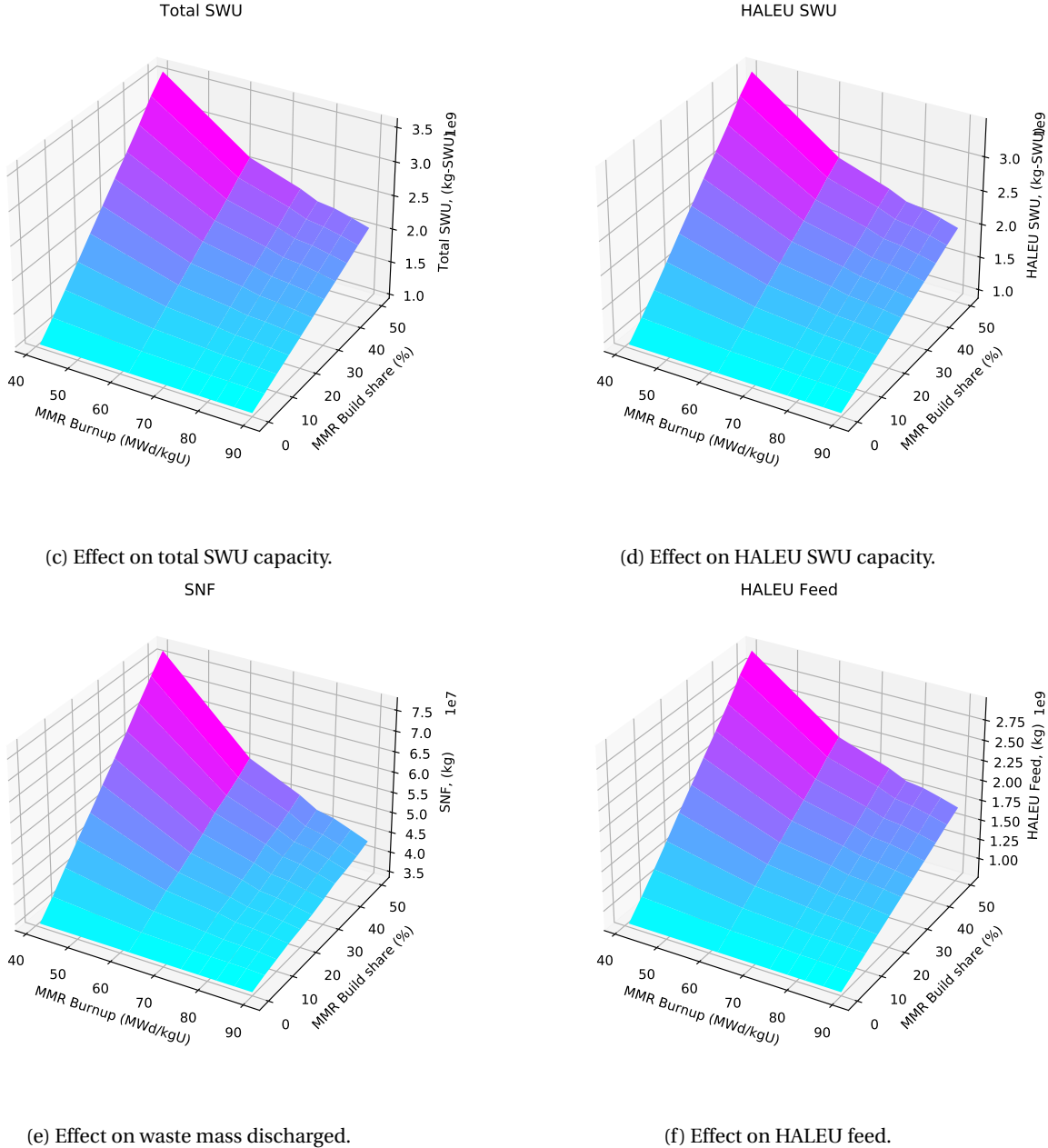


Figure A.13: (cont.) Change in metrics resulting from variations in the MMR build share and MMR discharge burnup.

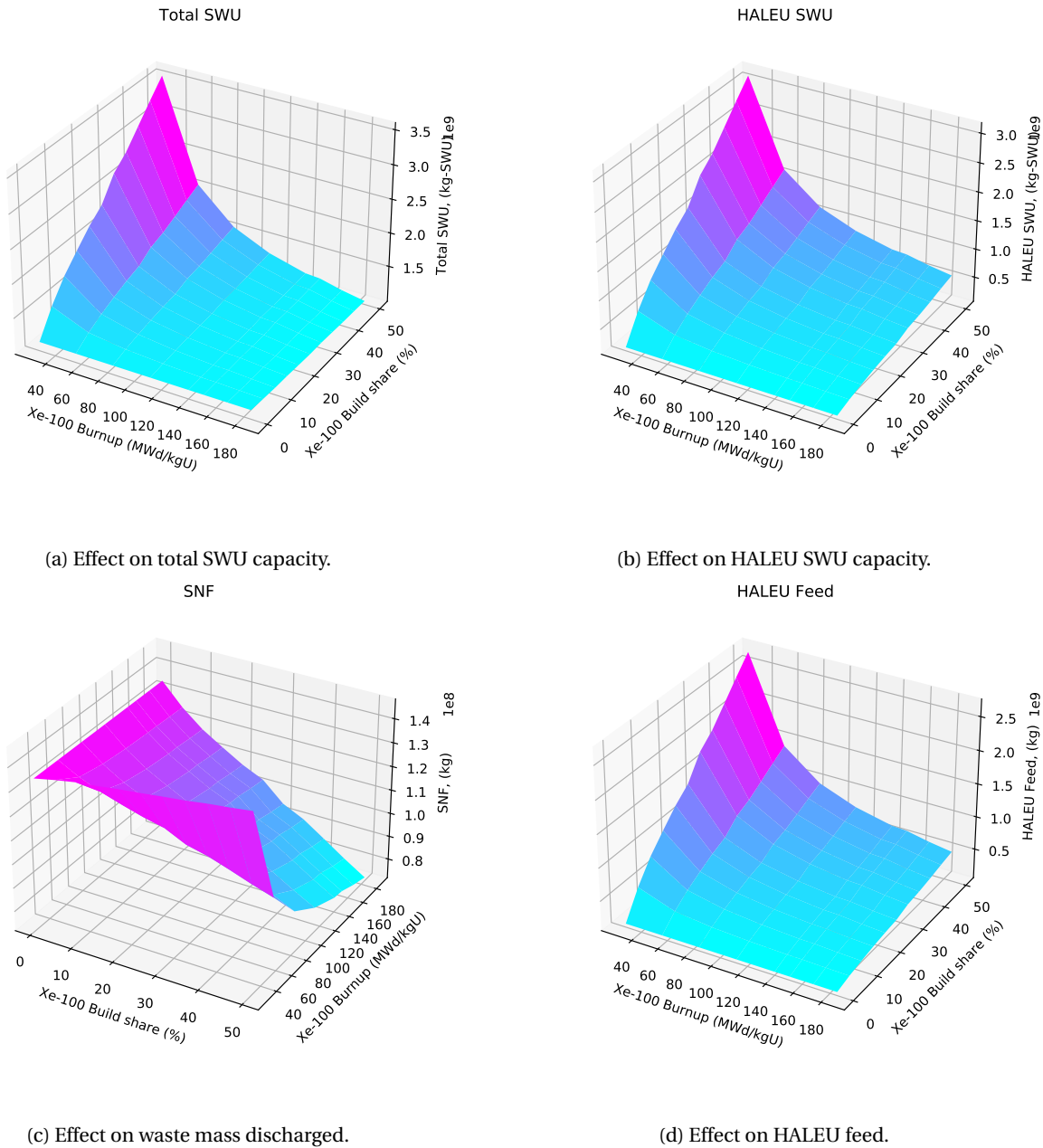


Figure A.14: Change in metrics resulting from variations in the Xe-100 build share and Xe-100 discharge burnup.

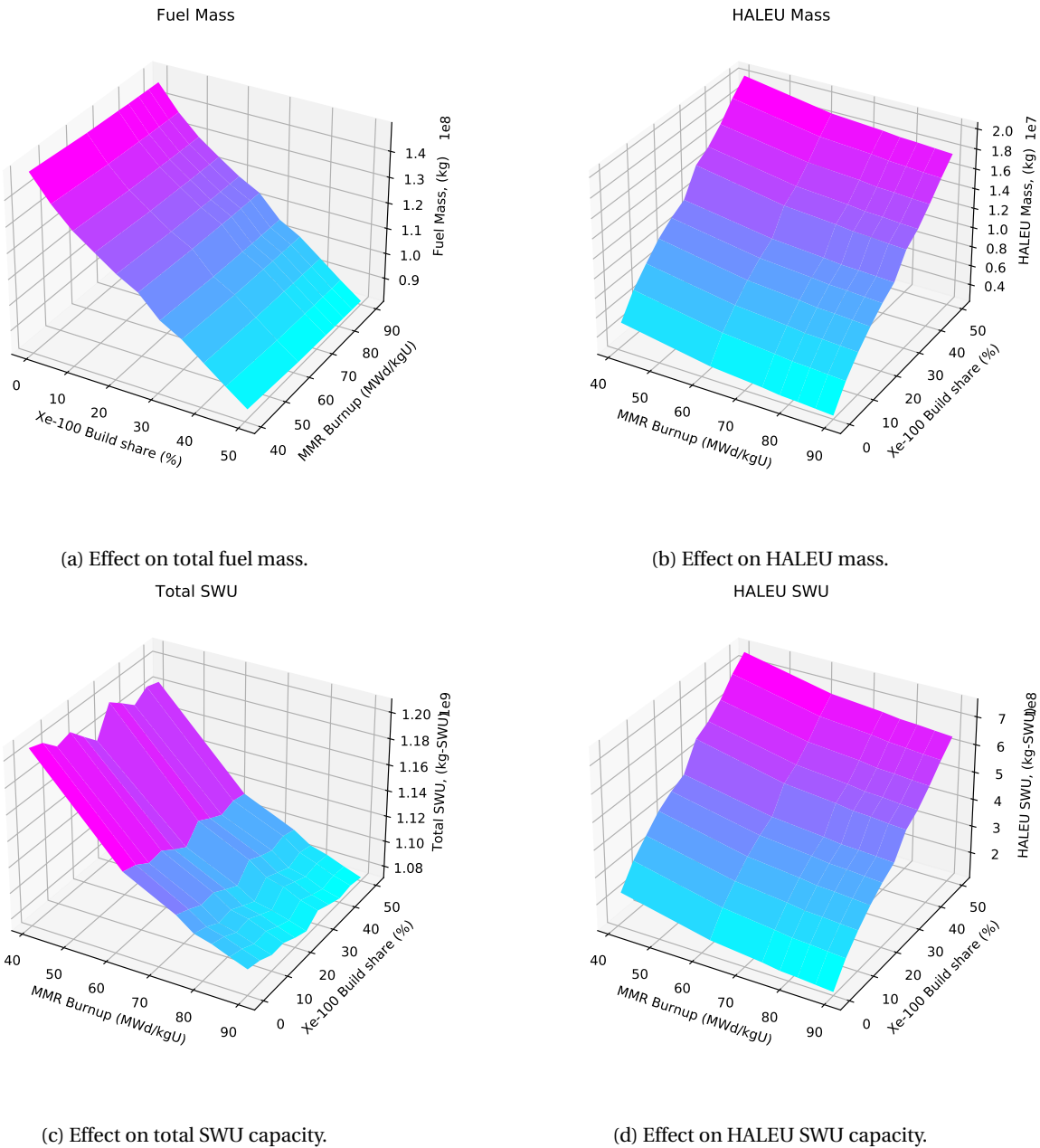
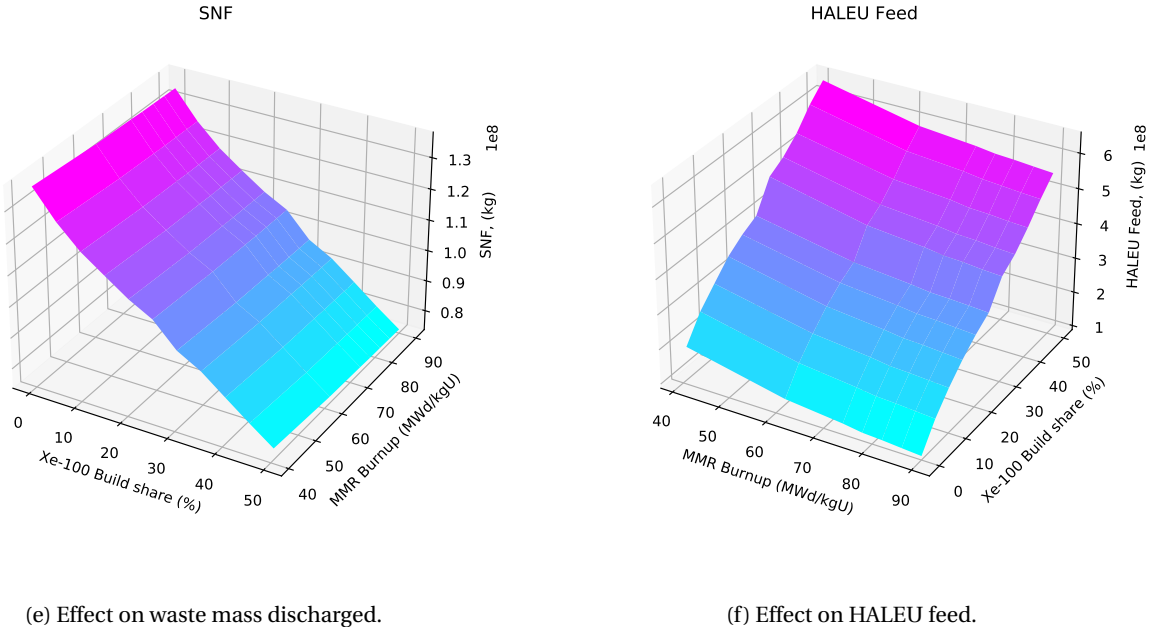


Figure A.15: Change in metrics resulting from variations in the Xe-100 build share and MMR discharge burnup



(e) Effect on waste mass discharged.

(f) Effect on HALEU feed.

Figure A.15: (cont.) Change in metrics resulting from variations in the Xe-100 build share and MMR discharge burnup

six metrics decrease as a function of the Xe-100 burnup. The total fuel mass and UNF generally decrease with the VOYGR build share while the HALEU-related metrics and total SWU capacity decrease with increasing build share. The results indicate that there is interaction between these two parameters. As the VOYGR build share increases, the number of Xe-100s deployed decreases. This effect is the opposite of the result of increasing the Xe-100 build share. Therefore, the VOYGR build share and Xe-100 burnup interact in opposite ways as the Xe-100 build share and the Xe-100 burnup. As the VOYGR build share increases, the Xe-100 burnup has less impact on the metrics. Additionally, as the Xe-100 burnup increases, the VOYGR build share has less impact on the metrics.

Figure A.17 shows the effects of varying the VOYGR build share and MMR burnup on all of the metrics. The results of varying these two parameters is similar, but opposite in direction, to the results of varying the Xe-100 build share and MMR burnup. The total fuel mass and UNF mass increase with increasing VOYGR build share and are not impacted greatly by the MMR burnup. The HALEU-related metrics decrease with increasing VOYGR build share and are not greatly affected by the MMR burnup. The total SWU capacity decreases with increasing MMR burnup and is not greatly affected by the VOYGR build share. These results identify that these two parameters do not interact with each other. The VOYGR build share affects the number of VOYGRs and Xe-100s deployed, while the MMR burnup affects the fuel requirements of the the MMRs that are deployed.

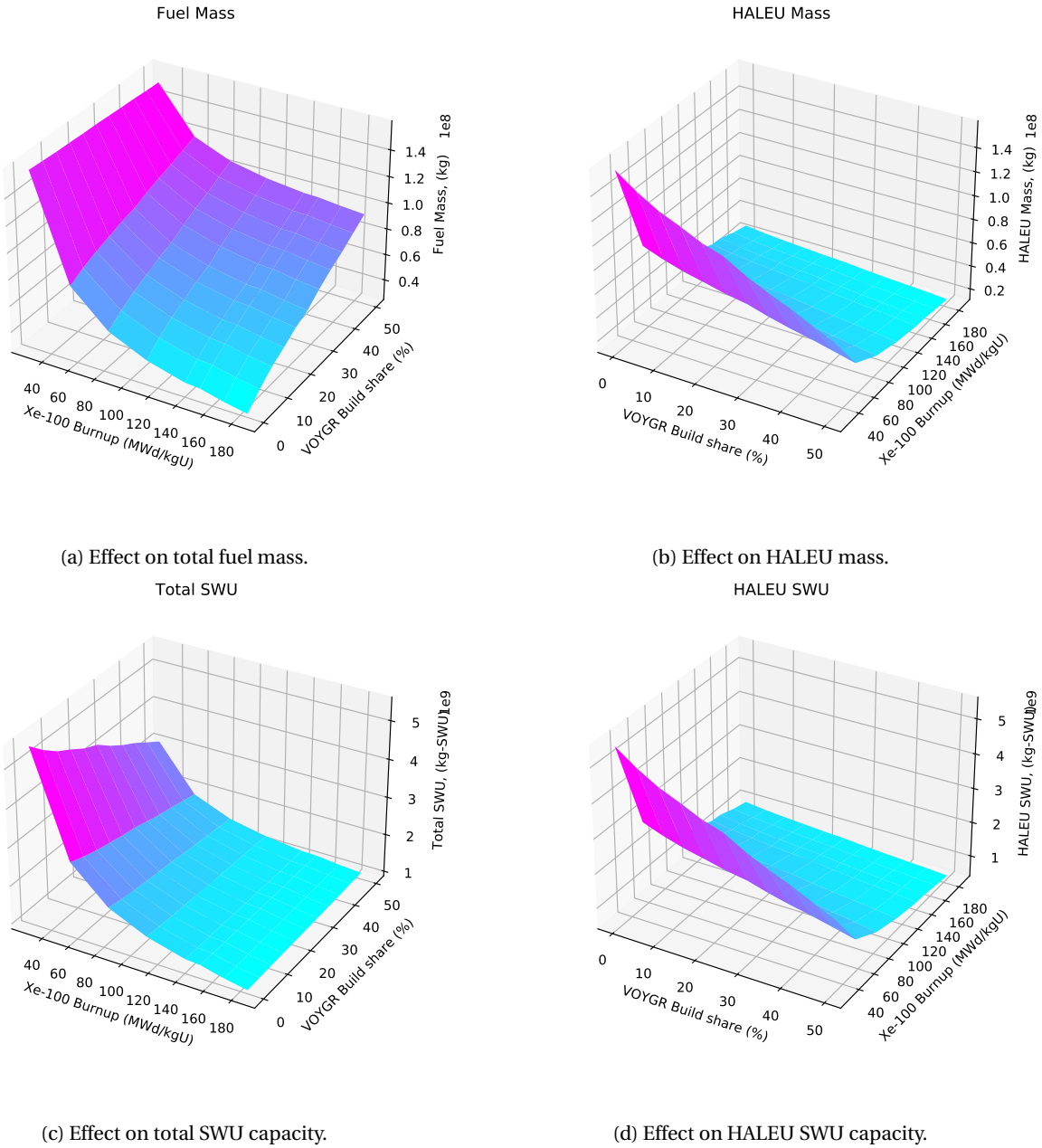
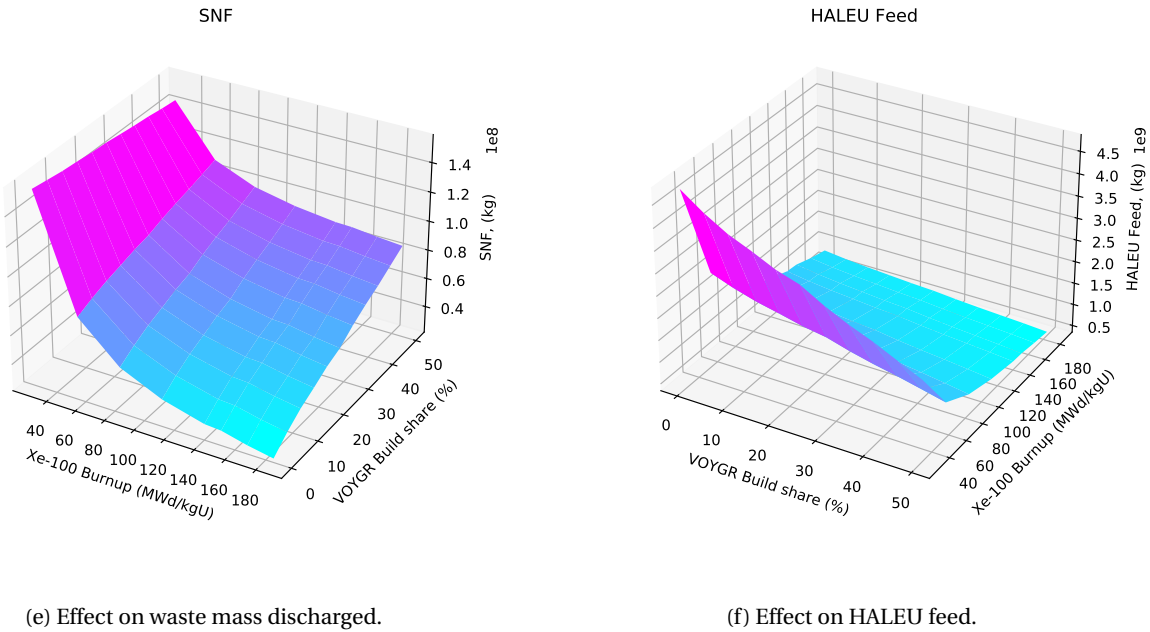


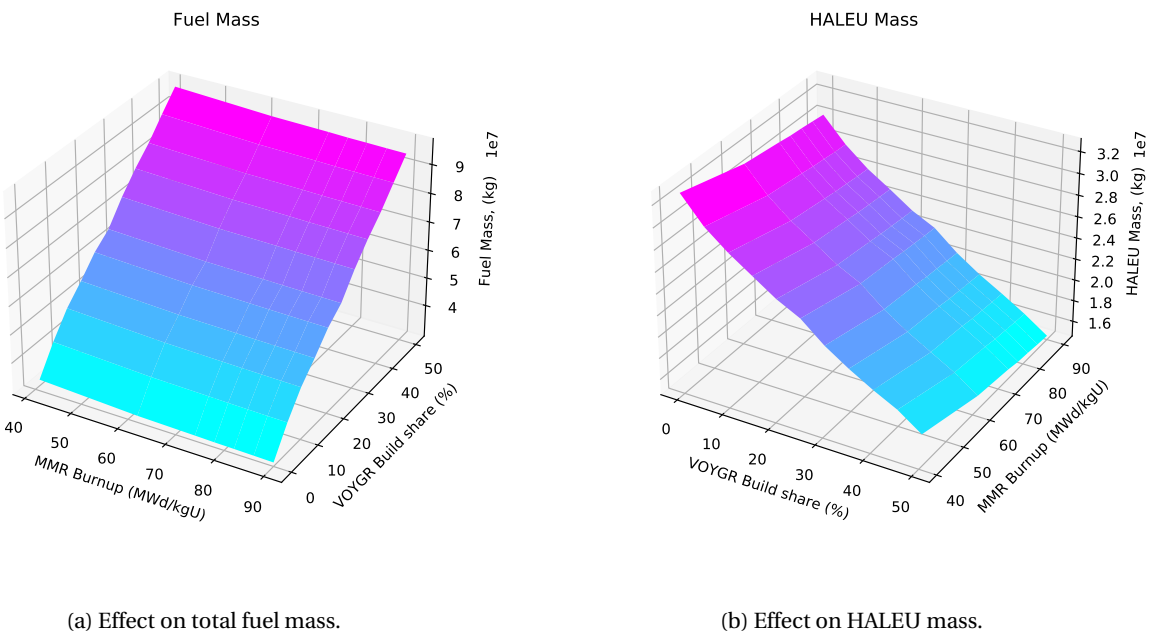
Figure A.16: Change in metrics resulting from variations in the VOYGR build share and Xe-100 discharge burnup.



(e) Effect on waste mass discharged.

(f) Effect on HALEU feed.

Figure A.16: (cont.) Change in metrics resulting from variations in the VOYGR build share and Xe-100 discharge burnup.



(a) Effect on total fuel mass.

(b) Effect on HALEU mass.

Figure A.17: Change in metrics resulting from variations in the VOYGR build share and MMR discharge burnup.

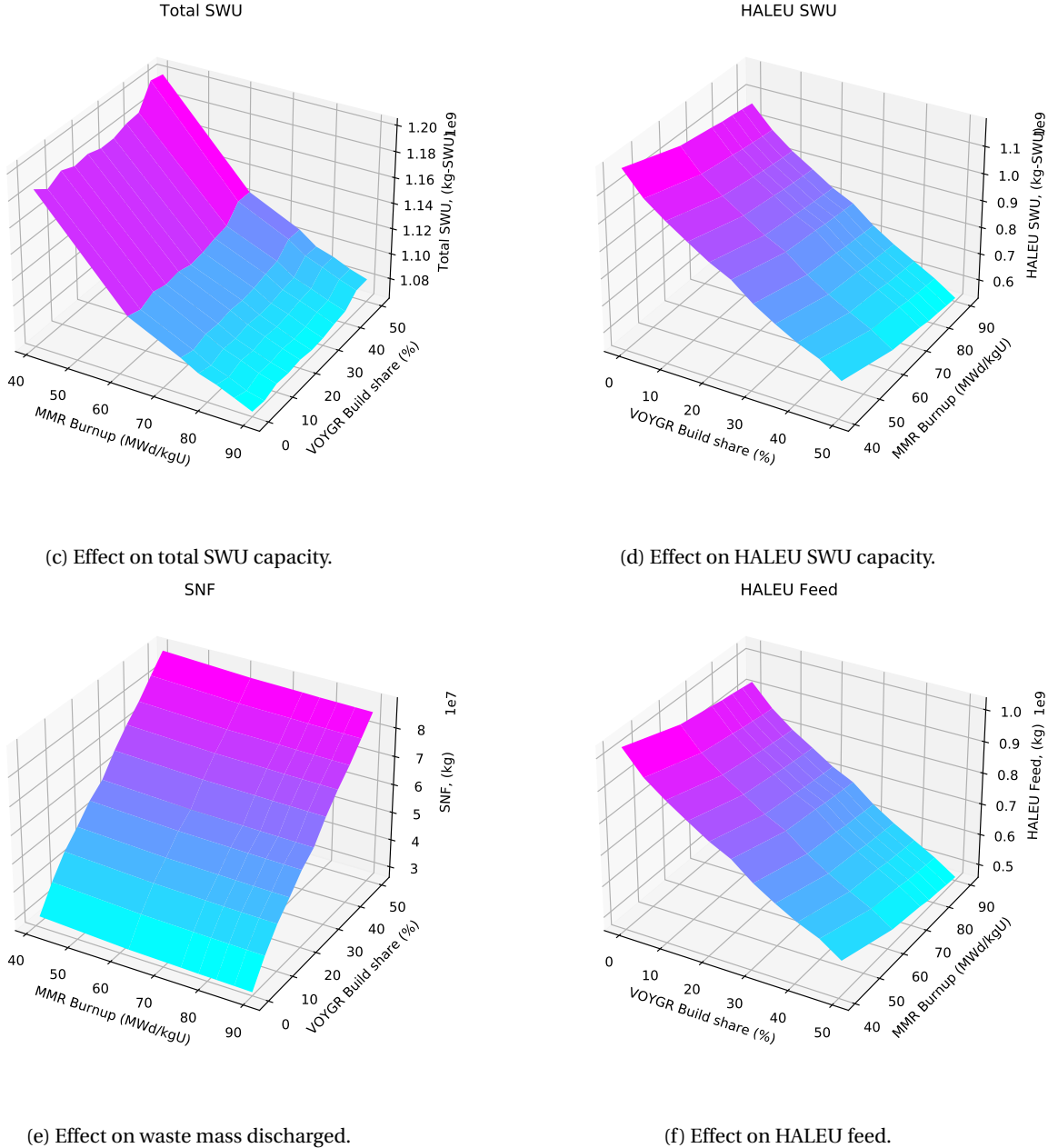


Figure A.17: (cont.) Change in metrics resulting from variations in the VOYGR build share and MMR discharge burnup.